

Diffusion-Weighted Magnetic Resonance Imaging (DW-MRI) of the normal bone marrow in children and effects of local and systemic cancer therapies

Dr Erika Pace

A thesis submitted in conformity with the requirements for the degree of

Doctor of Medicine (Research)

The Institute of Cancer Research


University of London

September 2019

Declaration

I certify that this thesis is the product of my own research and any material that does not belong to my own research has been appropriately cited or acknowledged. No part of this thesis has been or is currently being submitted for any other degree.

Dr Erika Pace

A handwritten signature in black ink that reads "Erika Pace". The signature is written in a cursive style with a large initial 'E'.

London, 9th September 2019

*To David
(Dr MacVicar)*

*Lifelong grateful to a superb, thoughtful, wise, and witty mentor and father figure
who, with his daily advice, shaped me into the radiologist and girl I am today.*

Grand thank you for always being there, inspiring me, and guiding me.

I will forever treasure every moment spent together.



Success is not final, failure is not fatal: it is the courage to continue that counts.

Acknowledgements

My heartfelt thanks to my supervisor **Professor Nandita deSouza** for her guidance, critical insight, and patience: this work would have not been possible without her constant dedication.

I am hugely thankful to **Dr Andy MacKinnon** — Consultant Neuroradiologist at St George's University Hospital and The Royal Marsden — who have played a pivotal role during the collection of the data for the non-oncological cohort and **Dr Christina Messiou** — Consultant Radiologist at The Royal Marsden — who constantly provided me with valuable analytical advice and suggestions, especially during the period before the mid-term viva.

Dr Henry Mandeville and **Dr Enrico Clarke** — Consultant and Fellow Clinical Oncologist, respectively — made invaluable contribution to this thesis supplying dose data for the radiotherapy chapter, including retrieving information from the archive of their department and liaising with both proton therapy centres in Jacksonville and Oklahoma City. Thank you!

I am very grateful to the scientific officers **Simon Doran**, **James d'Arcy**, and **Matthew Orton** who have been pivotal in the anonymisation of the MR images and regular support with unexpected technical issues during the whole process of the data analysis.

My warm thanks go also to the radiographers of The Royal Marsden — **Karl Spolander**, **Vonnie Morgan**, **Julie Hughes**, **Alison MacDonald**, and **Sharon Giles** — and of the Neuroradiology Department of St George's Hospital — **Jonathan Rhodes** — for their prompt help with the selection of patients and the transfer of MR images from the scanners to the Research PACS.

I thank **Professor John Yarnold** for his discreet and meticulous advice and the statistician **Karen Thomas** for her regular skillful suggestions.

Many thanks to the clerical team including **Ms Sue Reader** (Professor deSouza's personal assistant), **Mrs Caroline Eley** (Dr Andy MacKinnon's personal assistant), **Mrs Nadia Azzouzi** (Joint Research and Enterprise Office

at St George's University Hospital), and **Mrs Joanna Fearn** (Registry Office of The Institute of Cancer Research), who played a significant role in different stages of this long journey.

Thank you also to the Paediatric Oncology Consultants with expertise in Haematology — **Drs Sucheta Vajda, Caroline Furness, Robin Dowse, Sanjay Tewari, Toni Petterson** — and **Mrs Innie Johnson** — Paediatric Bone Marrow Transplant Coordinator — for their unceasing help with the PUMA study recruitment.

Furthermore, I am immensely glad for the daily abundant moral support I freely received over the past four years from my past and current colleagues (**consultants and fellows**), both in the **Departments of Radiology and Paediatrics** of The Royal Marsden and St Mary's Hospital.

Last but not least, I profoundly thank my beloved **parents, brothers,** and **friends** for their constant encouragement and endless patience.

Abstract

Bone marrow, one of the largest organs in the body, is a highly proliferative tissue because of its dynamic function in providing the cellular elements of blood. In a paediatric population, the proportion of red marrow (cellular compartment) and yellow marrow (fatty stroma) vary with age and with location within the skeleton. The cellular component may be imaged with diffusion-weighted imaging: the sensitivity of the technique to tissue cellularity and its integral fat suppression mean that haematopoietic cellular marrow is differentiated from yellow marrow with high contrast.

As prospective studies in children to investigate normal bone marrow are ethically difficult, the work in this thesis is largely retrospective. In the first instance, I undertook to establish the variation of the apparent diffusion coefficient (ADC) quantified from diffusion-weighted MRI of the skull with child's age and gender. The work in Chapter 2 shows a significant reduction in ADC at puberty, likely due to a replacement of red with yellow marrow, without gender related differences.

Chapter 3 examines the effects of local cancer treatments (radiation therapy and proton therapy to brain tumours) on normal marrow in the clivus and interprets these changes in the context of the reproducibility of the measurement. An early (within 3 months of treatment) increase in ADC with both techniques (reflecting oedema) was followed by a decrease between 3 and 6 months. With systemic treatment, (described in Chapter 4), there was a reduction in lumbar vertebral ADC at 3 months, which stabilised or continued to fall by 6 months. The oedematous response seen with local treatment was absent, but replacement of haematopoietic tissue with fat still resulted.

Finally, I designed a protocol investigating the effects of bone marrow transplantation on the ADC during engraftment. This prospective study currently open to recruitment will accrue patients over the next 12 months.

Table of Contents

CHAPTER 1 – INTRODUCTION	21
1.1 HISTOLOGY OF NORMAL BONE MARROW	21
1.2 RATIONALE TO INVESTIGATE BONE MARROW	23
1.3 BONE MARROW VARIATIONS WITH AGE	24
1.4 TREATMENTS WITH POTENTIAL EFFECT ON BONE MARROW	27
1.4.1 Photon radiotherapy (RT)	28
1.4.2 Proton beam therapy (PTB)	29
1.4.3 Chemotherapy	32
1.4.3.1 Chemotherapy regimens commonly used in paediatric malignancies and their mechanism of action	33
1.4.4 Marrow transplantation	33
1.5 DIAGNOSTIC BONE MARROW INVESTIGATION	35
1.5.1 Tissue sampling	35
1.5.2 Role of imaging	37
1.5.2.1 Methods using ionising radiation for bone marrow assessment	37
1.5.2.2 Methods using non-ionising radiation for bone marrow assessment - Magnetic Resonance Imaging	34
1.5.2.2.1 Estimating marrow fat-derivation of fat fraction	39
1.5.2.2.2 Diffusion-weighted MRI	41
1.6 IDENTIFIED GAPS IN KNOWLEDGE	44
1.7 AIMS	45
REFERENCES	46

CHAPTER 2 – NORMAL BONE MARROW APPARENT DIFFUSION COEFFICIENT VALUES AND THEIR VARIATION WITH AGE, PUBERTAL STATUS, AND GENDER	51
2.1 INTRODUCTION	51
2.1.1 Normal bone marrow	51
2.1.1.1 Composition with age and hormonal status	51
2.1.1.2 Regional variation by skeletal area	53
2.2 AIM	54
2.3 METHODS	54
2.3.1 Patient selection	54
2.3.1.1 Inclusion criteria	56
2.3.1.2 Exclusion criteria	56
2.3.2 Image acquisition	57
2.3.3 Image analysis	57
2.3.3.1 Method of region of interest delineation	57
2.3.3.2 Apparent Diffusion Coefficient (ADC) calculation	58
2.3.3.3 Derivation of centile values	59
2.3.3.4 Recognition of pubertal status	59
2.3.3.5 Statistical analysis	62
2.4 RESULTS	63
2.4.1 Patients' characteristics	63
2.4.2 Region of interest size	63
2.4.3 Normal Apparent Diffusion Coefficient values	64
2.4.3.1 Median and mean Apparent Diffusion Coefficient values in the population	64
2.4.3.2 Comparison of centile Apparent Diffusion Coefficient values	

in the population	67
2.4.4 Variation with age	68
2.4.5 Variation with pubertal status	71
2.4.6 Variation with gender	73
2.5 DISCUSSION	76
2.5.1 Relationship with age and pubertal status	76
2.5.2 Region of interest sizes	78
2.5.3 Significance of measurements in the clivus	79
2.5.4 Relationship of Apparent Diffusion Coefficient with cellularity	79
2.5.5 Technical factors and study limitations	80
2.6 SUMMARY	82
2.7 KEY POINTS	82
REFERENCES	82

CHAPTER 3 – INVESTIGATING THE EFFECTS OF RADIATION AND PROTON BEAM THERAPY ON BONE MARROW: CRANIAL APPARENT DIFFUSION COEFFICIENT STUDIES	86
3.1 INTRODUCTION	86
3.1.1 Paediatric brain tumours	87
3.1.2 Variations in treatment schedules	88
3.1.3 Treatment-related toxicity in photon versus proton beam therapy	88
3.1.3.1 Toxicity and bone marrow effects	88
3.1.3.2 Other common toxicities of cranial irradiation	89
3.1.3.2.1 Endocrine	89

3.1.3.2.2 Neurocognitive	89
3.1.3.2.2 Lifetime risk of new cancers	90
3.2 AIM	91
3.2.1 Objectives	91
3.3 METHODS	91
3.3.1 Measurement reproducibility cohort	91
3.3.2 Photon therapy cohort	92
3.3.2.1 Patient selection	92
3.3.2.1.1 Inclusion criteria	92
3.3.2.1.2 Exclusion criteria	92
3.3.2.2 Dose evaluation	93
3.3.2 Proton beam therapy cohort	94
3.3.3.1 Patient selection	94
3.3.3.1.1 Inclusion criteria	94
3.3.3.1.2 Exclusion criteria	95
3.3.3.2 Dose evaluation	96
3.3.4 Image acquisition	96
3.3.5 Image analysis	100
3.3.5.1 Method of region of interest delineation	100
3.3.5.2 Apparent Diffusion Coefficient calculation	100
3.3.5.3 Statistical analysis	102
3.4 RESULTS	102
3.4.1 Measurement reproducibility	102
3.4.2 Photon therapy cohort	103
3.4.2.1 Patients' characteristics	103
3.4.2.2 Region of interest size	103

3.4.2.3 Dose	104
3.4.2.4 Longitudinal treatment effects with photon therapy on Apparent Diffusion Coefficient of clivus	105
3.4.3 Proton beam therapy cohort	111
3.4.3.1 Patients' characteristics	111
3.4.3.2 Region of interest size	111
3.4.3.3 Dose	111
3.4.3.4 Longitudinal treatment effects with proton beam therapy on Apparent Diffusion Coefficient of clivus	112
3.4.4 Comparison photon (RT) and proton beam therapy (PBT) cohorts	118
3.4.4.1 Timing of follow-up scans	118
3.4.4.2 Dose delivered	118
3.4.4.3 Longitudinal Apparent Diffusion Coefficient changes with treatment	120
3.5 DISCUSSION	122
3.5.1 Nature of the Apparent Diffusion Coefficient changes post treatment	123
3.5.2 Longitudinal evolution of the Apparent Diffusion Coefficient changes post treatment	124
3.5.3 Clinical impact of the findings	125
3.5.4 Limitations of the measurements and measurement variability	127
3.6 SUMMARY	128
3.7 KEY POINTS	128
REFERENCES	128

CHAPTER 4 – INVESTIGATING THE EFFECTS OF CHEMOTHERAPY ON BONE MARROW: LUMBOSACRAL APPARENT DIFFUSION COEFFICIENT STUDIES	132
4.1 INTRODUCTION	132
4.1.1 Paediatric abdominopelvic tumours	132
4.1.2 Toxicity induced by chemotherapy	136
4.1.2.1 Acute toxicity induced by chemotherapy	136
4.1.2.2 Late effects induced by chemotherapy	136
4.1.2.2.1 Effects of chemotherapy on bone	136
4.1.2.2.2 Effects of chemotherapy on other tissues	137
4.2 AIM	138
4.2.1 Objectives	138
4.3 METHODS	138
4.3.1 Measurement reproducibility	138
4.3.2 Chemotherapy cohort	139
4.3.2.1 Patient selection	139
4.3.2.1.1 Inclusion criteria	139
4.3.2.1.2 Exclusion criteria	139
4.3.3 Derivation of patients for chemotherapy cohort	141
4.3.3.1 Combination of drug evaluation	141
4.3.4 Imaging analysis	142
4.3.4.1 Method of region of interest delineation	144
4.3.4.2 Apparent Diffusion Coefficient calculation	144
4.3.4.3 Statistical analysis	144
4.4 RESULTS	146
4.4.1 Measurement reproducibility	146

4.4.2 Chemotherapy cohort	148
4.4.2.1 Patients' characteristics	148
4.4.2.2 Combination of agents	149
4.4.2.3 Region of interest size	149
4.4.2.4 Longitudinal Apparent Diffusion Coefficient changes with treatment	149
4.4.2.5 Changes in peripheral blood post chemotherapy	158
4.5 DISCUSSION	159
4.5.1 Nature of the Apparent Diffusion Coefficient changes post treatment	159
4.5.2 Longitudinal evolution of the Apparent Diffusion Coefficient changes post treatment	160
4.5.3 Clinical impact of the findings	162
4.5.4 Limitations of the measurements and measurement variability	163
4.6 SUMMARY	164
4.7 KEY POINTS	165
REFERENCES	166
CHAPTER 5 – SUMMARY AND FUTURE WORK	169
5.1 HOW TO MEASURE THE BONE MARROW IN CHILDREN:	
Challenges in assessing variability and need for multicentre trials	169
5.2 WHEN TO MEASURE THE BONE MARROW IN CHILDREN:	
Response assessments and their timing in the face of multimodality treatment	171

5.3 WHERE TO MEASURE THE BONE MARROW IN CHILDREN:	
Regional variations in response in the maturing skeleton – local versus whole skeleton measurements	174
5.4 POTENTIAL UTILITY OF APPARENT DIFFUSION COEFFICIENT IN BONE TRANSPLANTATION	175
5.5 FUTURE POTENTIAL FOR WHOLE BODY DIFFUSION-WEIGHTED FOR ASSESSING CHILDHOOD LEUKAEMIA	176
5.1 Preliminary work	177
5.6 PUMA STUDY	177
5.6.1 Recruitment status	180
5.6.2 Future	180
REFERENCES	181
APPENDIX 1 – Service Evaluation 662 proposal form	183
APPENDIX 2 – Erika Pace, Andrew D. MacKinnon, Nandita M. deSouza Variation of the apparent diffusion coefficient of skull marrow by age group, pubertal status, and gender in a paediatric population	
Acta Radiologica, 2020 Sep; 61 (9): 1240-1248	190
APPENDIX 3 – PUMA research study	199

List of Figures

Figure 1.1: Red and yellow marrow	21
Figure 1.2: Marrow anatomy in long bones	22
Figure 1.3: Histological component of bone marrow	23
Figure 1.4: Normal marrow conversion	25
Figure 1.5: Marrow conversion	26
Figure 1.6: Differences between photon and proton therapy	28
Figure 1.7: Bragg peak and the proton difference	30
Figure 1.8: Indications for proton beam therapy in paediatric oncology	31
Figure 1.9: Trephine biopsy	36
Figure 1.10: Reproduced from Charles-Edwards E. and deSouza NM; Cancer Imaging, 2006; 6: 135-143	41
Figure 1.11: Signal intensity versus b-value plot showing derivation of fast and slow (D^*) components of the Apparent Diffusion Coefficient	43
Figure 2.1: Percentage bone marrow occupied by haematopoietic tissue and fat with age	53
Figure 2.2: Four stages of spheno-occipital synchondrosis closure	60
Figure 2.3: Axial photograph of the central skull base showing ridges indicative of vascular bed and fossa navicularis	61
Figure 2.4: T1-weighted sagittal images in a 7-year-old female and a 14-year female	62
Figure 2.5 a: Boxplots of median ADC by age group	65
Figure 2.5 b: Scattered plot of median ADC by age group	66

Figure 2.6: Correlation of ADC with age	68
Figure 2.7: Histogram plots for the whole population pre- and post-puberty	72
Figure 2.8: Axial T2-weighted, diffusion-weighted, and ADC map in a 5.5 year-old pre-pubertal male	72
Figure 2.9: Axial T2-weighted, diffusion-weighted, and ADC map in a 16.8 year-old pre-pubertal male	73
Figure 2.10: Boxplots of pre- and post-pubertal median ADC values in females and males	74
Figure 2.11: Histogram plots for post-pubertal females alone versus pre-pubertal subjects and males alone versus all pre-pubertal subjects	75
Figure 3.1: Adapted from 'Principles and Practice of Pediatric Oncology' Philip A. Pizzo and David G. Poplak, Lippincott Williams and Wilkins, 6 th edition, 2011 – chapter 26 A, pg. 718	87
Figure 3.2: Derivation of patients for radiation therapy cohort	93
Figure 3.3: Derivation of patients for proton beam therapy cohort	95
Figure 3.4: Protocol parameters of the DW of the head	97
Figure 3.5: Bland-Altman plot showing reproducibility of bone marrow ADC from the clivus in children	103
Figure 3.6: Longitudinal patterns of ADC change in skull marrow in children who received RT	108
Figure 3.7: Histogram distribution of ADC values before and after RT	109
Figure 3.8: Longitudinal patterns of ADC change in skull marrow in children who received PBT	115
Figure 3.9: Histogram distribution of ADC values before and 1-3 and 3-6 months after PBT	116

Figure 3.10: Comparison of RT and PBT doses delivered to each of the cohorts	120
Figure 3.11: Box and whisker plots showing absolute increases in mean ADC for the whole RT and PBT cohorts and percentage changes from baseline at the early and late time points	121
Figure 4.1: Main types of childhood cancer based on data provided by the National Registry of Childhood Tumours	133
Figure 4.2: Derivations of patients for retrospective analysis of effects of chemotherapy on lumbosacral marrow	140
Figure 4.3: Diffusion-weighted axial through the lumbar spine of a 14-year-old female with corresponding T2-weighted images showing circular region-of-interest outlined in vertebral marrow	146
Figure 4.4: Bland-Altman plots showing variability of marrow median and mean ADC values from the lumbosacral spine in children	147
Figure 4.5: Longitudinal patterns of ADC change in lumbar vertebral marrow in children treated with chemotherapy	152
Figure 4.6 a: Scattered plot illustrating mean ADC values pre-treatment, at early, and late post-treatment follow-up	154
Figure 4.6 b: Box and whisker plots showing median, quartiles, and ranges of ADC values pre-chemotherapy and post-treatment	155
Figure 4.7: Longitudinal ADC changes during chemotherapy in two individuals over time	155
Figure 4.8: Histograms distributions of ADC values pre- and post-chemotherapy	156
Figure 5.1: Types of leukaemia from Medicine.Net.com and the American Society of Hematology	176

List of Tables

Table 2.1: Search criteria to develop a database of children not on medication, free of treatment, and without a suspected oncological diagnosis	55
Table 2.2: Staging system for pubertal status based on spheno-occipital synchondrosis closure on imaging (adapted from Alhazmi A. 2017)	60
Table 2.3: Number of voxels in the clival ROI by age group	64
Table 2.4: Median and mean ADC by age	64
Table 2.5: Pre- and post-pubertal median, mean, and centile ADC	67
Table 2.6: Distribution of histogram parameters by age group	67
Table 2.7: Pre- and post-pubertal median, mean, and centile ADC value	71
Table 2.8: Mean, median and centile vales in female and male subjects showing significant differences before and after puberty	74
Table 3.1: Relationship of scan timings to end of treatment and scanner used for assessment at each time-point	99
Table 3.2: Diffusion-weighted image acquisition protocol for the different scanners used in this study	101
Table 3.3: RT dose to the clivus colour coded by tumour type	104
Table 3.4: Longitudinal changes in ADC at baseline and at subsequent follow-up after RT	107
Table 3.5: Centile values for individual patients before, 1-3 months and 3-6 months after RT	110
Table 3.6: PBT dose to the clivus colour coded by tumour type	113
Table 3.7: Longitudinal changes in ADC at baseline and at subsequent follow-up after PTB	114
Table 3.8: Centile values for individual patients before, 1-3 months and 3-6 months after PBT	117

Table 3.9 a: Dose delivered to the clivus in patients receiving RT	119
Table 3.9 b: Dose delivered to the clivus in patients receiving PBT	119
Table 4.1: Paediatric abdominopelvic tumour types treated with chemotherapy	135
Table 4.2: Relation of scan timings to treatment and scanner used for assessment at each time-point	141
Table 4.3: Diffusion-weighted protocols on different scanners at different locations	143
Table 4.4: ADC values at 2 time points in 10 patients imaged twice at the beginning and end of the same examination and in 4 patients imaged on separate occasions at a median of 10 weeks apart	145
Table 4.5: Patient characteristics and combination of anticancer drug received conjointly with the duration of the whole treatment	148
Table 4.6: Longitudinal changes in ADC at baseline and at subsequent follow-up after chemotherapy	151
Table 4.7: Median and centile values for individual patients before, 1-3 months and 4-12 months after the completion of chemotherapy	157
Table 4.8: Peripheral blood haemoglobin and white cells for individual patients at equivalent time-points to imaging data	158
Table 5.1: Recruitment status of PUMA study	179

List of Abbreviations

ADC	Apparent Diffusion Coefficient
ALL	Acute Lymphoblastic Leukaemia
CCR	Committee for Clinical Research
CHESS	Chemical Shift Selective
CNS	Central Nervous System
CT	Computerised Tomography
DICOM	Digital Imaging and Communications in Medicine
DNA	Deoxy Ribose Nucleic Acid
DW-	Diffusion weighted
EPI	Echo Planar Imaging
FLAIR	Fluid Attenuated Inversion Recovery
FSE	Fast Spin echo
GCSF	Granulocyte Colony Stimulating Factor
Gd	Gadolinium
GRE	Gradient Recalled Echo
Gy	Gray
HRQOL	Health Related Quality of Life
ICR	The Institute of Cancer Research
IQR	Inter Quartile Range
LQ	Lower Quartile
MRI	Magnetic Resonance Imaging
MRS	Magnetic Resonance Spectroscopy
NICE	National Institute for Clinical Excellence
PACS	Picture Archiving and Communication System
PBT	Proton Beam Therapy
PET	Positron Emission Tomography
ROI	Region of Interest
RT	Photon Radiotherapy
SE	Spin Echo
SPAIR	Spectral Attenuated Inversion Recovery
STIR	Short Tau Inversion Recovery
T1-W	T1-weighted
T2-W	T2-weighted
TE	Echo time
TR	Repetition Time
TSE	Turbo Spin Echo
TRUFI	True Fast Imaging with Steady Precession
XNAT	X- Neuroimaging Archive Toolkit
UQ	Upper Quartile
WB-DW-MRI	Whole Body Diffusion Weighted Magnetic Resonance Imaging
WHO	World Health Organisation

CHAPTER 1 – INTRODUCTION

Composition of paediatric bone marrow, effects of treatment and methods of assessment

1.1 HISTOLOGY OF NORMAL BONE MARROW

Bone marrow is a functionally dynamic structure with a primary haematopoietic function. Its cellularity and composition vary with age and with changing needs for oxygenation and immune response of the growing organism.¹

Healthy bone marrow consists of:

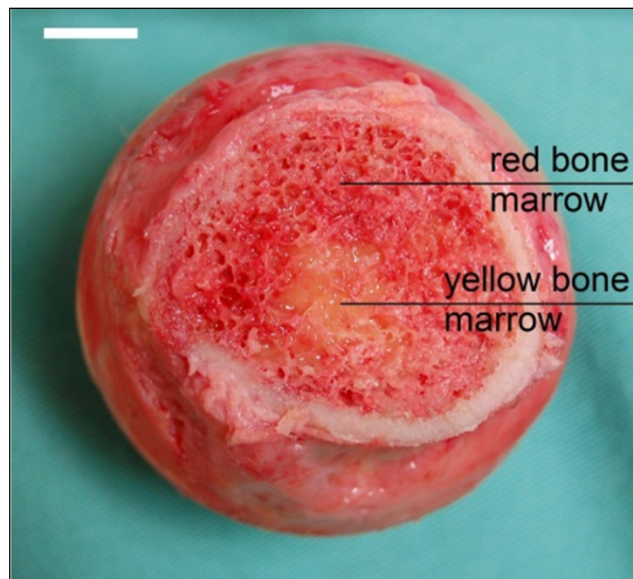


Figure 1.1: Red and yellow marrow.

- a cellular component:
 - red marrow: haematopoietically active part; composed of platelets, red (haemoglobin is responsible for the colour of this fraction) and white cells; contains approximately 40% water, 40% fat, and 20% proteins;

- yellow marrow: the inactive portion; mainly contains fat cells (carotenoids within the adipocytes account for the colour of this component), a smaller fraction of red marrow elements. It comprises approximately 15% water, 80% fat, and 5% proteins (**Figure 1.1**);²
- an osseous component: trabeculae – within the medulla – providing architectural support for the cells and mineral depot; the number of trabeculae diminish with age (**Figure 1.2**);
- a supporting system:
 - stroma (or reticulum, which predominates in red marrow and is sparse in yellow marrow);
 - a vascular supply (sinusoidal, more generous in red marrow, and poorly represented in yellow marrow – **Figure 1.3**);
 - neural and lymphatic elements.

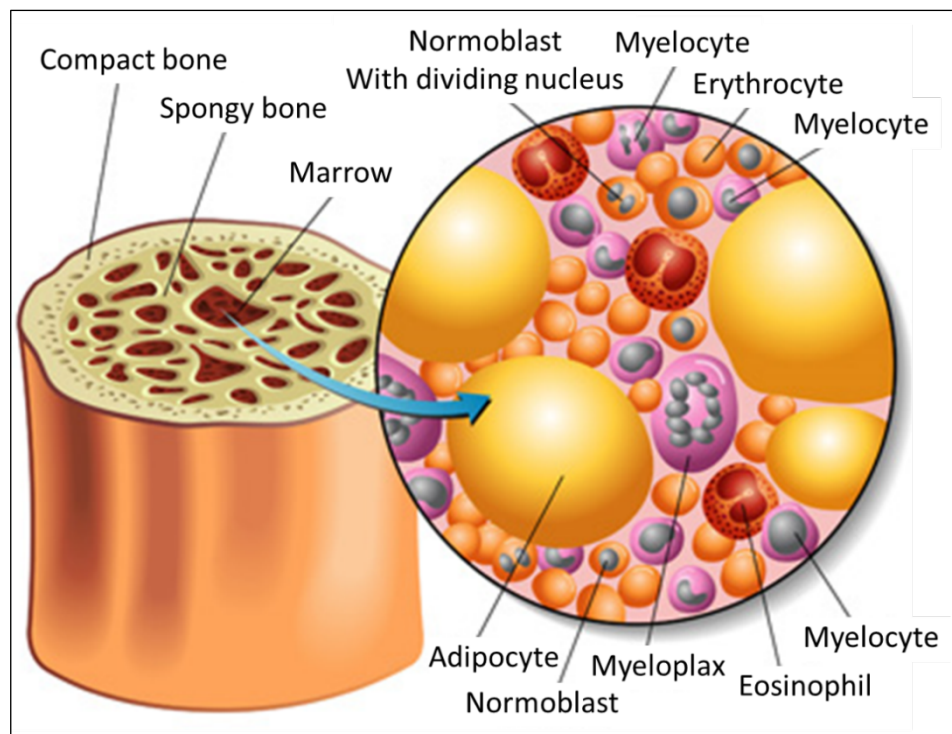


Figure 1.2: Marrow anatomy in long bones.

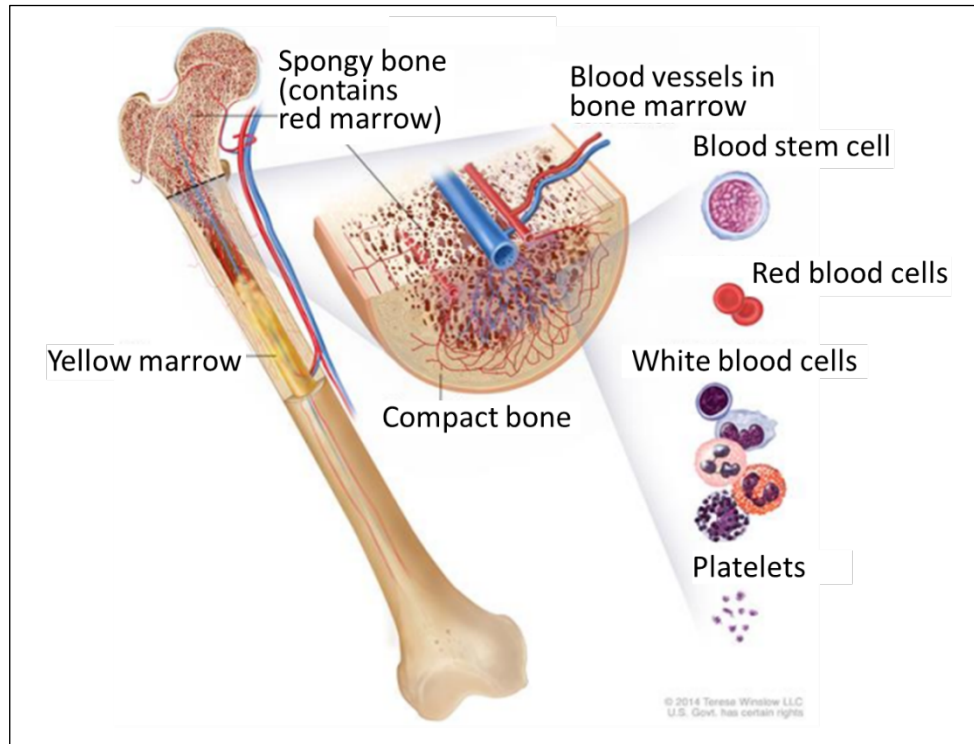


Figure 1.3: Histological component of bone marrow.

1.2 RATIONALE TO INVESTIGATE BONE MARROW

Being the bone marrow a highly dynamic tissue it is challenging to study its changes, especially related to physiological factors such as gender, age, and hormonal influence. Initial reports are now available in the literature, with the vast majority focussing on data obtained in mice and adults but mainly investigating the biological effects of drugs (such as chemotherapy, immunotherapy, and hormonotherapy), changes in relation to diseases, among which cardiometabolic pathology and implication of bone marrow adiposity. Consequently, imaging-based studies are paying particular attention to the same areas of research.

It is a matter of fact that knowing what is physiological undoubtedly contributes to better understand what is pathological. Therefore, to fully

comprehend the aetiopathogenesis of many haematological illnesses, both oncological and non, it is crucial to examine what is behind the differences between female and male marrow, which role is played by puberty, and the physiological maturation of the marrow from the foetal life until the adult stage. Much needs to be done in terms of biological and molecular research, both in vitro and in vivo, considering that only initial results are available. Imaging, including MR, can definitely supply further helpful information, especially by virtue of advanced techniques, such as diffusion-weighted imaging, spectroscopy, and perfusion.

This study wants to be one of the first reports exploring how apparent diffusion coefficient (ADC) values of bone marrow is affected by age, gender, and puberty.

1.3 BONE MARROW VARIATION WITH AGE

The amount of bone marrow and its distribution vary throughout life in response to normal maturation and physiological stress conditions. Differences between children and adults may be ascribed to the immaturity of the haematopoietic system at birth and the increased oxygen requirement during normal tissue growth.

Conversion of red to yellow marrow occurs in a predictable and progressive fashion (**Figure 1.4**). At birth, haematopoietic or red marrow is present in the whole skeleton. Conversion starts during the neonatal period in the periphery of the skeleton and continues from the appendicular and later to the axial skeleton, bilaterally in a symmetric and centripetal manner. In the

second decade of life, the marrow of long bones becomes predominantly fatty and, by the age of 25 years, the adult allocation of bone marrow is accomplished with normal persistence of red component within the axial skeleton, both proximal humeri and femora.³

Normal variation may be represented by residual islands of red marrow within the long bones or focal areas of fatty marrow in the spine.⁴

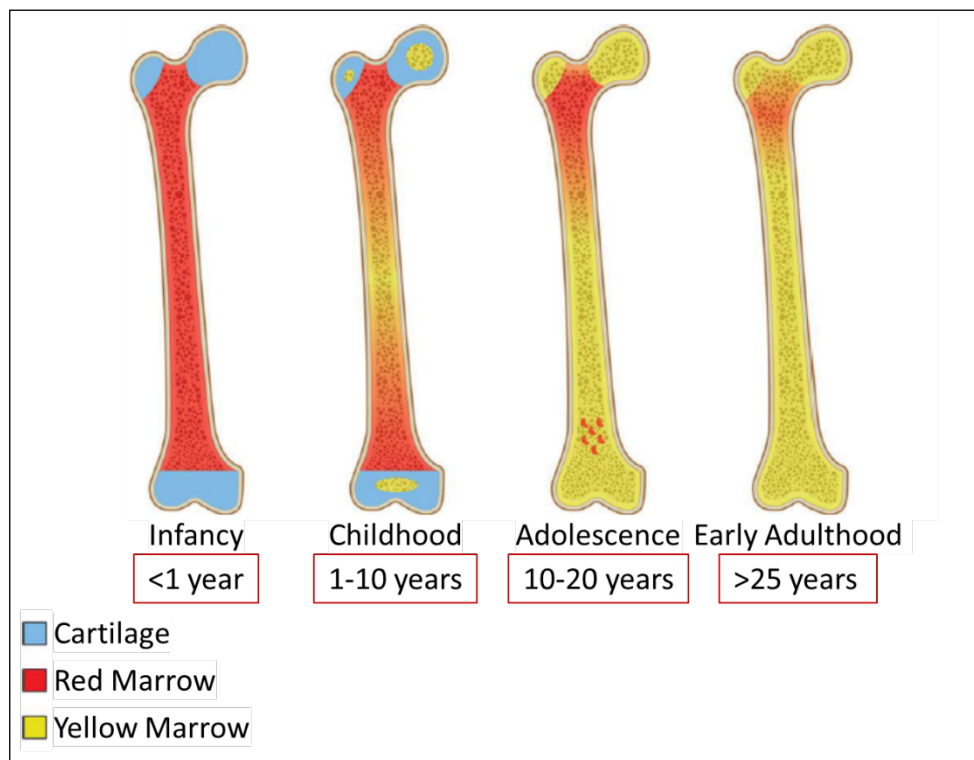


Figure 1.4: Normal marrow conversion.

In adults, yellow fraction may revert to red marrow (**Figure 1.5**) following triggering conditions, such as chronic anaemia (sickle cell disease and thalassemia), heavy smoking, long distance/endurance running, stress, chemotherapy with granulocyte colony-stimulating factor, marrow proliferative or replacement disorders. This process starts from central regions of the skeleton

(spine) and moves to include the peripheral skeleton in the long bones as needed, and from bone metaphysis to the diaphysis.⁵

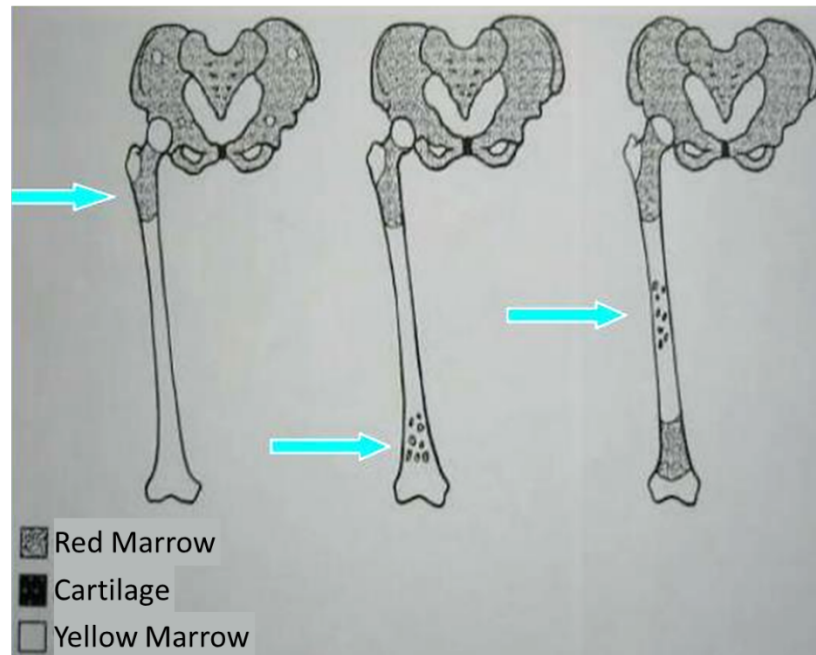


Figure 1.5: Marrow conversion.

The amount of fatty marrow present thus depends on the need for haematopoietic marrow. In periods of decreased haematopoiesis, fat cells increase in number and size. They may actively contribute to haematopoiesis by supplying metabolic or nutritional support, possibly along with growth factors. Conversely, when severe blood loss occurs, fatty adventitial cells lose fat and increase the space available for haematopoiesis.⁶

The factors governing the relative amounts of haematopoietic and fatty components was elegantly hypothesised by Gurevitch et al.,⁷ where a dependence on the number of mesenchymal stem cells that are pluripotent (as they differentiate to support both osteogenesis and haematopoiesis) was recognised. They speculated that as these cells are bound to endosteal and trabecular surfaces, they were numerous in growing tubular and cancellous

bone, but once maturity was reached, they were far less numerous in tubular bones than in cancellous bone, because of the smaller internal osseous surface area in the former. Post-maturity, therefore, there is exhaustion of the mesenchymal stem cell pool; those that remain favour support of a critical osteogenic function. In cancellous bone, they are more numerous and remain pluripotent.⁷

Regulation of conversion of red to yellow marrow and vice versa also has been ascribed to hormonal influences. However, although, there is evidence in adults linking corticosteroid use to the increase in marrow fat,⁸ there is surprisingly no evidence linking the sex steroid hormone surges at puberty to this process. Recent evidence in a murine model has linked leutinizing hormone signalling to restriction of stem cell expansion in puberty.⁹

1.4 TREATMENTS WITH POTENTIAL EFFECT ON BONE MARROW

X-ray and proton therapy are radiotherapy techniques employing different particles to irradiate malignant tissues, have very diverse physical properties.¹⁰ Before reaching the tumour, both radiation types must pass through the patient's skin and surrounding tissues (**Figure 1.6**) with the potential for harm to the tissues through which they pass.

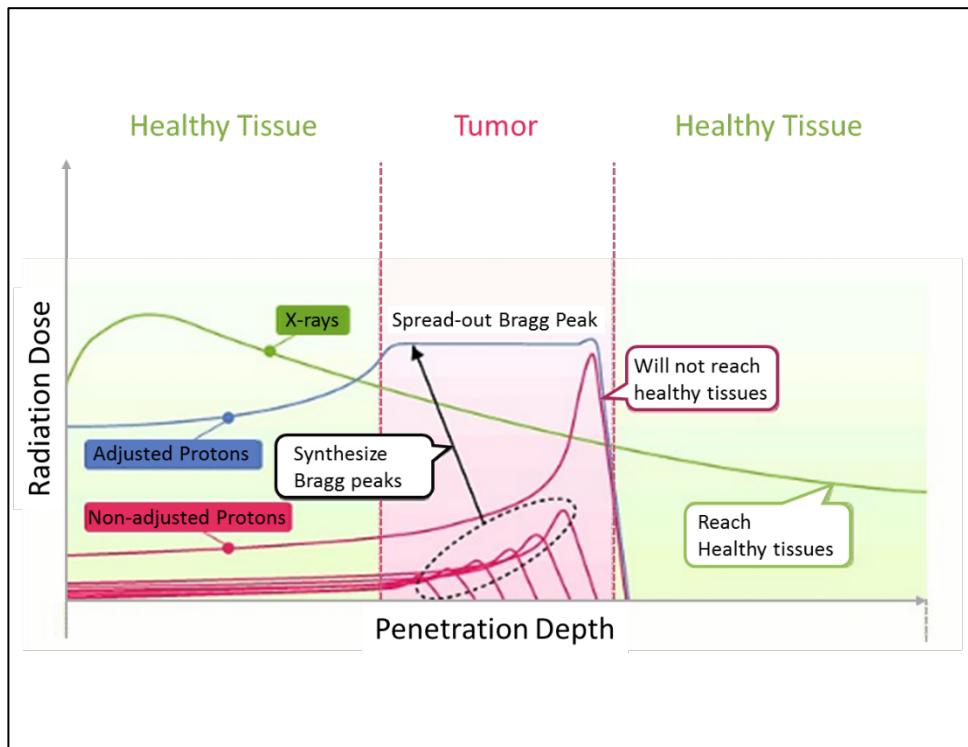


Figure 1.6: Differences between photon and proton therapy.

<https://www.aamg.co/aaro/comprehensive-cancer-service/proton-therapy>

1.4.1 Photon radiotherapy (RT)

Photons, with no mass and no charge, are highly penetrating and deliver a dose throughout any volume of tissue irradiated. However, depending on their initial energy, most of the radiation is delivered only 0.5 to 3 cm from the patient's skin, with progressive reduction in energy as photons travel towards a tumour target at depth within the body. Multiple beams delivered from different angles that intersect at the target are, therefore, used to achieve a therapeutic dose at the target. As photons traverse normal healthy tissue in their path, they actively interact with these healthy cells. Photons that are not attenuated by human tissue leave the patient's body and continue to emit radiation (exit dose).¹¹

Brain tumours, the most frequent paediatric solid neoplasms in children,^{12, 13} are routinely treated with conventional radiotherapy (RT) in

conjunction with surgery and chemotherapy. Over the past 75 years, RT has been incorporated into the upfront treatment of many paediatric brain neoplasms either as adjuvant therapy for resected lesions, definitive treatment for unresectable malignancies or as prophylactic therapy for occult microscopic disease.¹⁴ In children treated for brain tumours, irradiation of the skull, a major site of haematopoiesis, is unavoidable. This results in apoptosis or mitotic catastrophe in bone marrow haematopoietic stem cells. The mechanism by which this occurs is now well understood to be due to direct damage to DNA.¹⁵ High linear energy transfer causes DNA to cluster and break: these breaks are inefficiently repaired.¹⁵

Furthermore, there is formation of reactive oxygen species, that participate in altered cell signalling and results in tissue injury over time.¹⁵ The overall effect of radiation, therefore, is suppression of the haematopoietic system, leading to a reduction in red marrow and an increase in yellow marrow. As a result of this compositional change, neutropenia and thrombocytopenia may occur.^{16, 17}

1.4.2 Proton beam therapy (PBT)

Unlike photons, protons are heavy charged particles that gradually lose their speed while interacting with human tissue.¹⁰ They are easily controlled and deliver their maximum dose at a precise depth, which is determined by the amount of energy generated by the cyclotron (via acceleration), and can reach distances up to 32 cm. At the entry point, protons travel quickly depositing only a small dose on their way.¹¹ The absorbed dose increases gradually with

greater depth and lower speed, suddenly rising to a sharp energy peak (Bragg peak – **Figure 1.7**) which spreads out to cover the tumour volume before the proton is ultimately stopped. The energy before the peak is suppressed and that behind the peak is almost zero.¹⁸ Hence, the dose to normal tissue surrounding a target is lower in proton beam therapy when compared with RT. This substantially reduces the low and intermediate (0-40 Gy) dose areas, so that there is a low rate of late toxicity, and of second malignancy.¹⁷ In adults, several studies have documented the reduction in bone marrow toxicity of proton (PBT) compared to RT as a result of better avoidance of organs-at-risk when making dose plans for PBT: this has been demonstrated in lung¹⁹, gynaecological²⁰, and oesophageal²¹ cancers. PBT is, therefore, particularly attractive in a paediatric population, where dose to sensitive adjacent critical structures is of crucial importance, and where the long-term toxicity of therapy is a major consideration.¹⁸

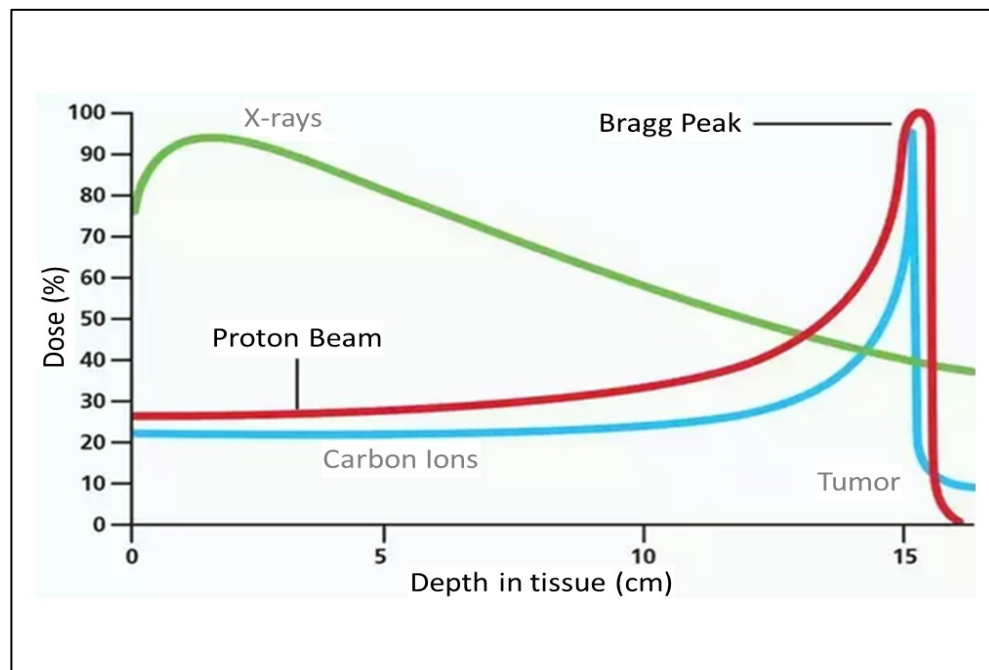


Figure 1.7: Bragg peak and the proton difference.

<https://www.scripps.org/services/cancer-care>

Age, anatomy of tumour location, neoplasm distance from critical structures, and comorbidities are all crucial factors when considering a referral for PBT. Skull base tumours, retinoblastoma, majority of central nervous system tumours (low-grade glioma, optic pathway glioma, medulloblastoma, craniopharyngioma, ependymoma, germ cell tumour) and nephroblastoma represent the most common paediatric indications for PBT (**Figure 1.8**).^{22, 23}

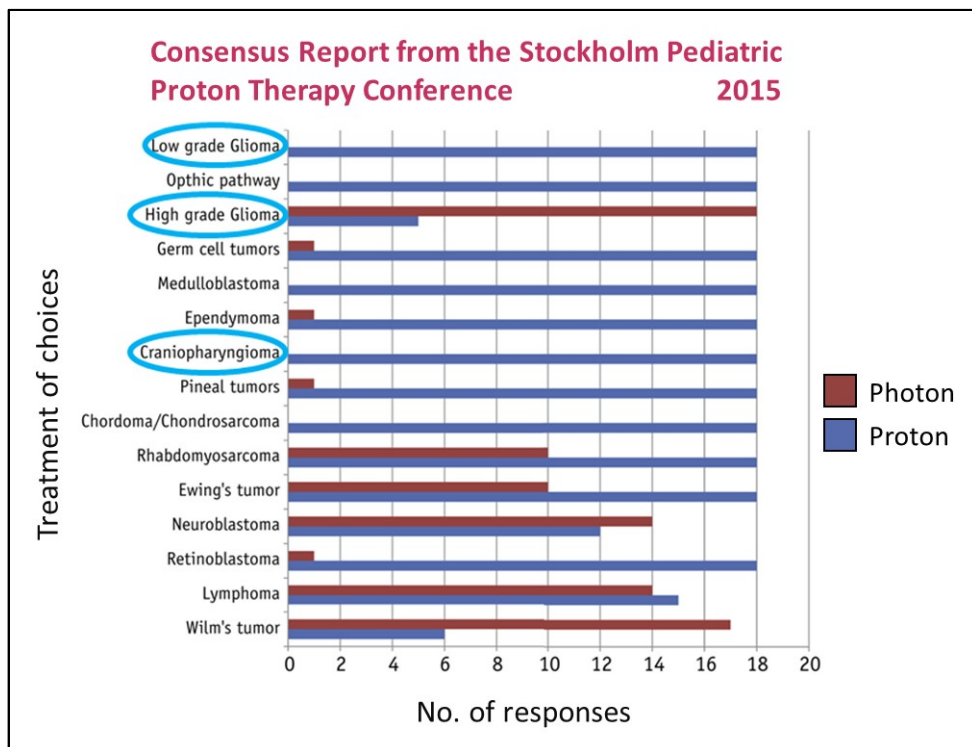


Figure 1.8: Indications for proton beam therapy in paediatric oncology.

Since 2012 children affected by brain tumours referred to The Royal Marsden have started benefitting from PBT when clinically indicated. Once the diagnosis is made by imaging and/or histology (when the neoplasm is amenable to biopsy) the case is discussed at the weekly South Thames Paediatric Neuro-oncology Multidisciplinary Team Meeting. Whether the collegial recommendation is to treat the tumour with PBT, the case is brought to the attention of the UK Proton Clinical Reference Panel. If this is approved, the

clinical oncologist will meet the family to communicate which American Centre (the UF Health Proton Therapy in Jacksonville or the ProCure Proton Therapy Centre in Oklahoma City) has been chosen for their child. The Proton Overseas Programme is currently centrally funded by National Health Service.

1.4.3 Chemotherapy

In solid childhood tumours, chemotherapy is used frequently as a neoadjuvant or adjuvant treatment. National/international guidelines have been developed and published by multidisciplinary committees of experts in the field as to the optimal regimens to be delivered. The combination of drugs, dose and number of cycles differ by tumour type, but the effects of these treatments are ultimately to cause necrosis of cancer cells through their cytotoxic effect on cell proliferation. Highly proliferative normal tissues, such as paediatric bone marrow, are highly sensitive to these toxic effects, and marrow suppression with anaemia and neutropenia are common side-effects of chemotherapy. Human-derived hematopoietic cells of all lineages (progenitor, lymphoid, and myeloid) have been shown to be sensitive to chemotherapy; for example, a temozolomide-based regimen that inhibits tumour xenograft growth also adversely affects normal haematopoietic proliferation.²⁴ In the clinic, high-dose chemotherapy administered for non-haematological malignancies causes marrow suppression²⁵ and may require support with granulocyte colony stimulating factor therapy (G-CSF) to restore marrow function.²⁶ Although it is simple to monitor these effects globally through blood counts, regional variations in effect, or the secondment of haematopoietically inactive site to a

functionally more active region and the ability of regions of bone marrow to recover remains unknown.

1.4.3.1 Chemotherapy regimens commonly used in paediatric malignancies and their mechanism of action

Cancer chemotherapeutic agents used in children are largely the same as those used in adults, albeit at a reduced dose commensurate with the child's age and weight. The commonly used classes of drugs used are the alkaloids, alkylating agents, antimetabolites, and antitumour antibiotics. The alkaloids (etoposide, vincristine, vinblastine and paclitaxel) exert their effects on microtubules within the cell (antimicrotubule agents) to halt cell division at specific points in the cell cycle. Alkylating agents, such as carboplatin and cyclophosphamide, are cell cycle non-specific and damage DNA at any point in the cell cycle. Methotrexate, an antimetabolite, competes with folic acid during cell division. Antitumour antibiotics, such as bleomycin and doxorubicin, halt DNA replication by altering enzyme activity required for this process. All these agents, therefore, also have profound effects on normally dividing cells within bone marrow, so that bone marrow suppression with resulting anaemia, myelosuppression, and subsequent susceptibility to infection and bleeding disorders due to platelet dysfunction are extremely common side-effects of cancer chemotherapy.

1.4.4 Marrow transplantation

Bone marrow transplant involves the transfer of donor bone marrow to an immunosuppressed recipient in whom a process of engraftment occurs. This process involves the establishment of the donor cells and their replication within

the recipient marrow. White cells usually engraft first, followed by red cells and platelets.²⁷ Stable engraftment of donor is essential for a successful outcome of bone marrow transplantation.

The physiological processes involved in successful engraftment are measured by the outcome of rising cell counts in peripheral blood. It is not usually necessary to monitor changes within the marrow itself. However, an understanding of the molecular processes behind successful versus slow engraftment would enable modification of processes to optimise engraftment. For instance, it may be useful to identify unfavourable conditions for engraftment; in vitro studies have demonstrated that several intrinsic and extrinsic factors influence the typical competence of the stem cells to self-renew maintaining their potentiality to differentiate. Particularly, it has been postulated that oxygen concentration is associated with the conservation of stemness.²⁸ Since in bone marrow haematopoietic stem cells lie along the endosteum, in proximity to both osteoblastic cells and blood vessels, changes in partial oxygen tension are key to start their replication — they remain quiescent or divide at slower rate in hypoxia²⁹ — and to favour or to hamper their terminal differentiation into one cell type or another before they exit the marrow into the systemic bloodstream.

Increasingly, these functional parameters can be mapped within tissue using imaging (cf section 1.4.2), which is non-invasive and potentially can interrogate the entire skeleton.

1.5 DIAGNOSTIC BONE MARROW INVESTIGATION

1.5.1 Tissue sampling

Bone marrow aspiration or biopsy is required for diagnosis. Aspiration involves sucking bone marrow cells up into a syringe for analysis that includes microscopy and differential cell counts. In paediatric oncology aspiration is mainly performed for investigation of abnormal peripheral blood findings (eg, atypical cells or blasts, pancytopenia, unexplained anaemia, leukopenia or thrombocytopenia) and diagnosis of malignant haematological disorders, hypoplastic anaemia, inherited bone marrow failure syndromes, and metastatic spread.³⁰⁻³² Results from an aspirate may be available within hours. Conversely, tests such as flow cytometry, molecular and cytogenetic analyses take longer. Trepine biopsy (**Figure 1.9**) involves removal of 1 or 2 cm core of bone marrow in one piece. An adequate biopsy in children should contain at least 0.5 cm of well-preserved tissue. The advantage of this exam is displaying the structure of the marrow inside the bone. However, this requires decalcification, and results are available after two or more days. Trepine is performed if marrow aspiration has failed, there is suspected bone marrow fibrosis, aplastic anaemia, myelodysplastic syndromes, and acute megakaryoblastic leukemia (AML-M7)³³ or sometimes for investigation and staging of Hodgkin's and non-Hodgkin's lymphoma, and small blue round cell tumours of childhood (neuroblastoma, rhabdomyosarcoma, and Ewing's sarcoma). The preferred site for obtaining bone marrow in children is the posterior superior iliac crest due to higher cellularity. Furthermore, no vital organs are adjacent to this location and it is a non-weight-bearing structure.⁶ The posterior superior iliac crest is therefore selected in all children, including small infants; the anterior iliac crest

is chosen only in markedly obese patients. In patients younger than 18 months, the anteromedial face of the tibia also may be suitable; however, this site may fail to yield adequate samples whether the procedure is performed by an inexperienced technician and the risk of bone fracture is higher.

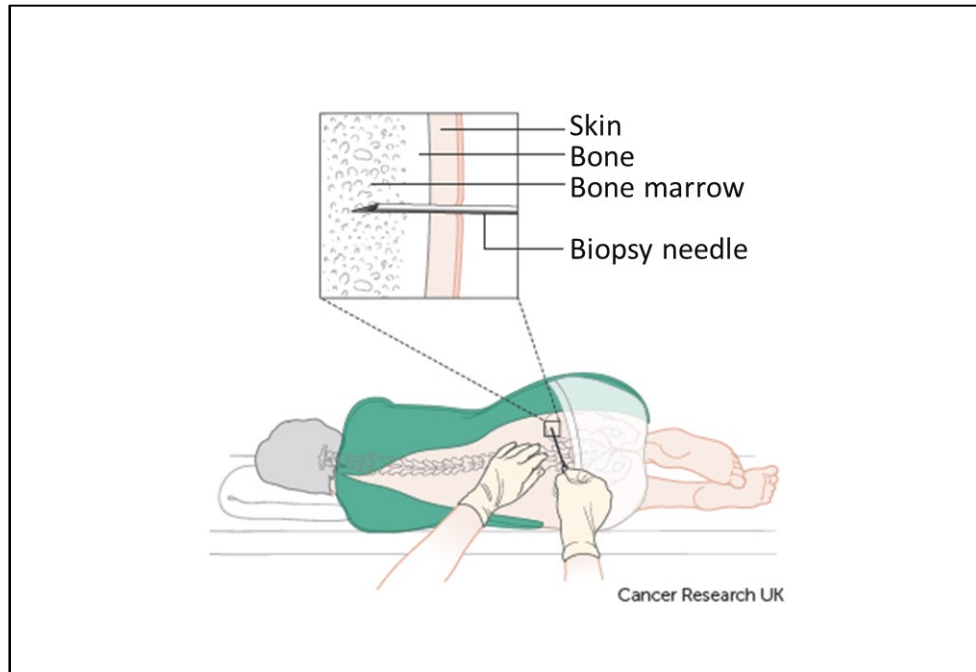


Figure 1.9: Trephine biopsy.

Although both aspiration and trephine biopsy are generally safe procedures with a low risk of morbidity, adverse events secondary has been showed an incidence of 0.08% in a recent review.³⁴ The most frequent adverse events were haemorrhage, infection and persistent pain at the marrow site. The bleeding episodes occurred mainly in the buttocks, thighs and retroperitoneum. Bone marrow trephine is painful, requires general anaesthesia and is contraindicated in haemophilia, disseminated intravascular coagulation, concomitant use of anticoagulants, skin infection or recent radiation therapy at the sampling site and osteomyelitis.

1.5.2 Role of Imaging

1.5.2.1 Methods using ionizing radiation for bone marrow assessment

Imaging with ionizing radiation exploits contrast that is based on differences in tissue density. Radiographs and computed tomographic (CT) imaging, therefore, mainly show detail of cortical bone and are not used to image marrow abnormalities. In case of soft tissue masses arising from bone or cartilage, the invasion of bone marrow may occur, but it is the cortical bone destruction that is depicted with these techniques. Similarly, with bone metastases, where bone marrow is invaded, it is the destruction of the bone trabeculation and cortex that is demonstrated; infiltration of the marrow itself is not visualised. In haematological malignancy, plain radiographs and CT have no role in assessing the bone marrow. In adults, conditions such as myeloma, where marrow involvement causing trabecular destruction was previously assessed on x-ray skeletal survey, magnetic resonance imaging is currently the modality of choice because of its high soft-tissue contrast.

1.5.2.2 Methods using non-ionizing radiation for bone marrow assessment - Magnetic Resonance Imaging

Magnetic resonance is currently the pivotal radiological modality for the evaluation of bone marrow.⁴ The use of this radiation-free cross-sectional imaging provides high spatial and temporal resolution and has improved diagnostic accuracy. Appearances of bone marrow on MRI are influenced by the choice of sequence, cellularity, lipid content, and surrounding trabecular bone (little direct signal, but contributes to T2 shortening, producing local magnetic field gradients), iron content of the marrow, and haematopoietic component.³⁵ An early study of the cadavers of 70 children (aged 1 day to 24

years) without history of bone marrow disease showed that regional and age-related differences in the signal intensity of pelvic marrow taken from six anatomic regions correlated with the percentage of fat seen on microscopic examination of anatomically matched bone marrow biopsy specimens.³⁶

Conventional spin-echo sequences represent the mainstay for evaluation of bone marrow. Differences in appearances on T1- and T2-W sequences potentially can distinguish normal red and yellow components from pathological marrow.^{37, 38} On T1-W images the intensity of yellow marrow is higher than red marrow. Red marrow in turn is hyperintense compared to skeletal muscle or to intervertebral discs. Conversely, on T2-W images, red and yellow marrow return similar signal; both appear hyperintense when compared to skeletal muscles and intervertebral discs. Fast spin echo sequences provide more conspicuity of both yellow and red marrow.³⁹

Another useful sequence is the Gradient-recalled echo sequence (GRE) which is sensitive to susceptibility differences and signal loss such as the effects induced by marrow and trabecular bone heterogeneity or sclerosis within the marrow.³⁵ Unfortunately, MR imaging findings are often nonspecific and there is an overlap between appearances from a variety of causes. Therefore, a definitive diagnosis is reliant on a combination of imaging findings, clinical evaluation, laboratory assessment, and occasionally tissue analysis.⁶ Imaging bone marrow requires fat suppression techniques to reveal abnormality within the water compartment. To suppress the fat-signal contribution for any given MR imaging sequence, a fat-suppression module is inserted into the sequence, usually at the beginning or as a replacement for the excitation pulse, or, with

Dixon techniques, at the time of signal acquisition after the excitation pulse. The main categories (families) of fat-suppression pulse sequences are Chemical shift Selective (CHESS), short inversion time inversion recovery (STIR), hybrid techniques, water excitation, and Dixon techniques. The CHESS works on the basis of the chemical shift difference between water and fat. An excitation pulse with a narrow bandwidth centred on the resonance frequency of fat (chemically selective RF pulse) and a flip angle of 90° tips the magnetic vector of fat in the transverse plane. This process is immediately followed by a “homogeneity” spoiler gradient that is applied to dephase the protons and, thus, suppress the fat signal.⁴⁰ In the STIR technique, the fat signal is inverted with a nonselective 180° pulse, and acquisition is begun after the inversion time (TI) that nulls the fat signal, resulting in a water signal with reduced magnitude. The SPAIR technique is similar, where the fat signal is inverted with an adiabatic spectrally selective pulse, and acquisition is begun after the inversion time that nulls the fat signal. Finally, in the Dixon technique, both water and fat are excited, with the first echo (TE1) is acquired when the two magnetization vectors in the transverse plane are out of phase, and the second echo (TE2) is acquired when the two vectors are in phase.⁴¹

1.5.2.2.1 Estimating marrow fat-derivation of fat fraction

Bone marrow that fills the cavities of trabecular bone primarily consists of adipocytes (yellow marrow regions) or adipocytes and hematopoietic red blood cells (red marrow regions). MRI allows non-invasive derivation of a fat-fraction within bone marrow. This is a key indicator of bone health and is potentially altered following treatment with radiotherapy or chemotherapy as these

treatments are likely to suppress red marrow function to a greater extent. T1-W imaging (T1WI), magnetic resonance spectroscopy (MRS), and chemical shift encoding-based water–fat imaging have been previously used to assess bone marrow fat fraction. T1-W imaging is not technically demanding and has been mostly applied on the pelvis, hip, and spine of adults.⁴² Measurements of bone marrow fat volume have been proposed by applying thresholds on T1WI to extract bone marrow fat voxels.⁴³ The applied threshold was usually set at the same gray-scale level as subcutaneous adipose tissue. The intra- and interobserver reproducibility for the assessment of bone marrow fat volume in T1WI images expressed as coefficient of variation (CV) amounted 0.9% (intraobserver) and 2.2% (interobserver) (for the post-processing).⁴⁴ The main source of error for the calculation of bone marrow fat volume based on T1WI occurs as a result of partial volume effects and threshold selection, especially in regions with red marrow.

Although fat-fraction can be estimated from single-voxel MRS, this technique lacks spatial resolution and has been superseded by Chemical shift encoding-based methods. Multi-echo GRE pulse sequences with an echo time step that maximises the water–fat phase difference is achieved by acquiring all echoes in a single TR. Phase errors and multiple confounding factors have to be addressed when measuring bone marrow proton density fat fraction with water–fat imaging, including the presence of multiple peaks in the fat spectrum,⁴⁵ T1-bias⁴⁶, and T2* decay.⁴⁵ As the work in this thesis used retrospective data in children, formal fat quantification was not available in any

of the studies and further discussion on these methods is outside the scope of this work.

1.5.2.2.2 Diffusion-weighted MRI

Diffusion-weighted (DW) MRI has emerged as a potential novel biomarker in oncological imaging.⁴⁷ By quantifying the diffusivity of water molecules within a tumour (**Figure 1.10**), this technique improves lesion detection and the assessment of treatment response.⁴⁸⁻⁵⁰ Changes in the apparent diffusion coefficient (ADC) values are inversely correlated with tumour cellularity.⁵¹ Because it avoids radiation exposure and intravenous contrast agents,⁵² DW-MRI is appealing in the field of paediatric imaging, but more work is needed to determine its utility in paediatric bone marrow disease.⁵³

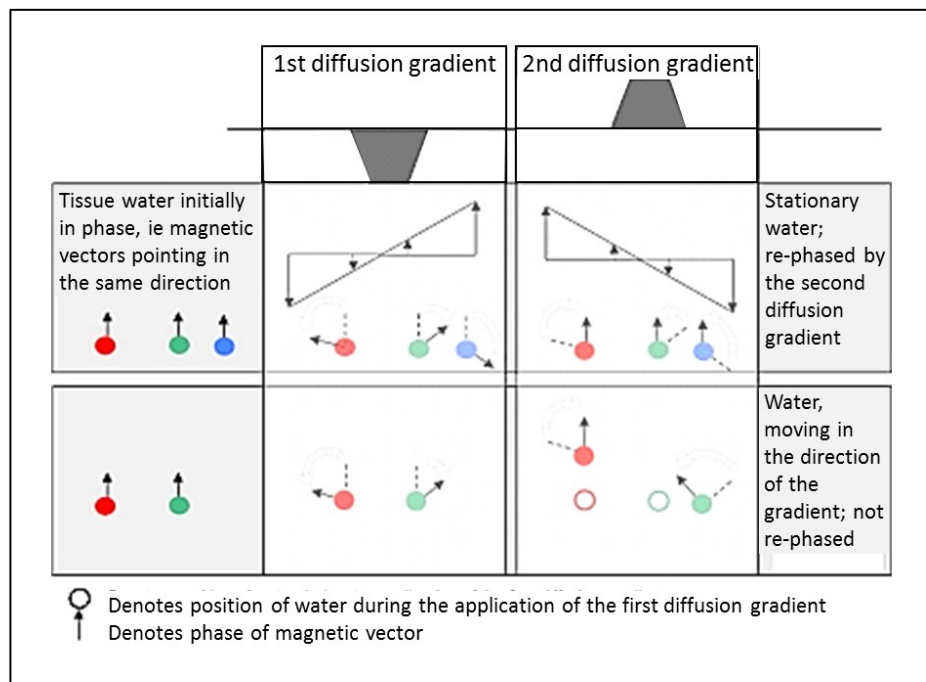


Figure 1.10: Reproduced from Charles-Edwards E and deSouza NM, *Cancer Imaging*, 2006; 6: 135-143

The advent of whole body DW-MRI (WB DW-MRI) has been one of the most useful advances in imaging of oncology patients over the last decade. The high sensitivity, speed, and quantitative capability have addressed an unmet need in imaging assessment of these patients. Combined with anatomical imaging WB DW-MRI now provides a tool that enables detection of both focal and diffuse skeletal disease, to quantify burden and response and to assess the complications of therapy.⁵⁴ This blend of anatomical and functional imaging has recently been recommended by the International Myeloma Working Group for work-up of solitary bone Plasmacytoma or Smoldering multiple myeloma.⁵⁵ It is now recognized that in adults WB DWI can provide information on differences between normal and diseased bone marrow architecture for the entire skeleton in a 25 minute time frame.⁵⁶ This has led to exploratory and feasibility studies for staging and follow-up of solid malignancies in children. However, there is no data on its utility in the context of bone marrow disease.^{57, 58}

Quantification of DW-MRI images to obtain the biomarker known as the Apparent Diffusion Coefficient (ADC) is done from fitting a signal decay curve to data acquired using multiple b values. The b-values are representative of the diffusion-weighting of the sequence and use the amplitude, duration and spacing of the diffusion-weighted gradients in their derivation. The equation describing this is given by:

$$\text{➤ } b = \gamma^2 G^2 \delta^2 (\Delta - \delta / 3)$$

Where

γ = gyromagnetic ratio

G = gradient amplitude

δ = Duration of diffusion gradients

Δ = Spacing of the pulsed gradients

A plot of signal-intensity versus b-value may be fitted with a variety of functions. If only two b-values are acquired, the fit is monoexponential. Data acquisition at a larger number of b-values increases imaging time but allows more complex and accurate fitting of the data (bi-exponential, stretched exponential, intravoxel incoherent motion, IVIM, models).⁵⁹ The derived ADC values are often described in terms of “fast” perfusion dependent and “slow” tissue dependent components. The latter are denoted by D^* and are representative of the true diffusion within tissue extracellular and intracellular water, depending on the length scale of the diffusion being probed.

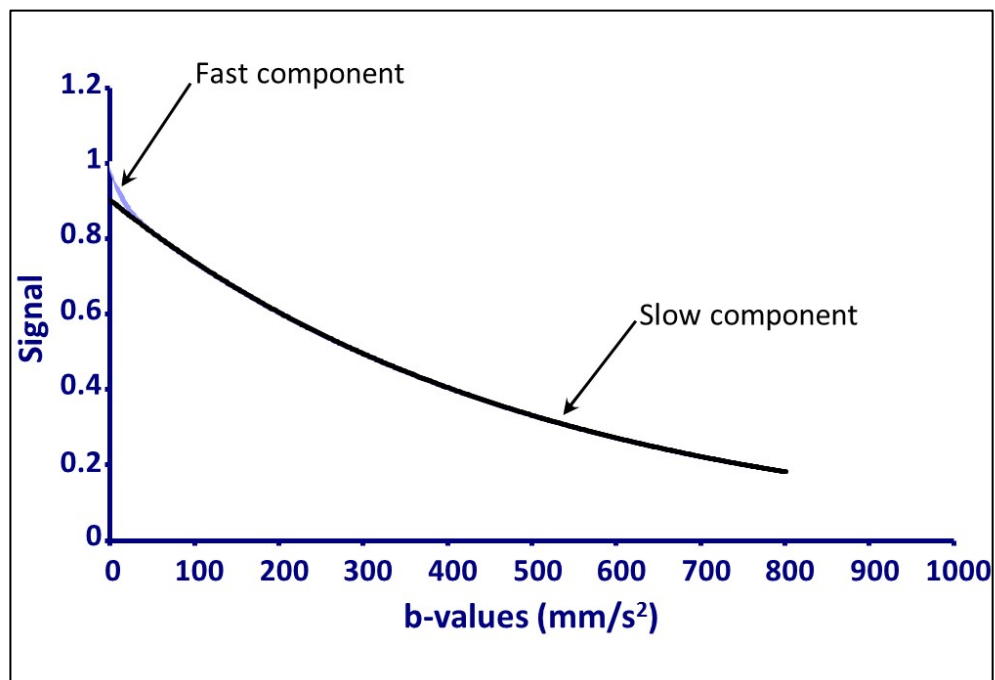


Figure 1.11: Signal Intensity versus b-value plot showing derivation of fast and slow (D^*) components of the Apparent Diffusion Coefficient.

Currently paediatric brain MR scans routinely include DW images as part of the standard protocol (different b values may be applied in each different MRI unit, however, images with $b=1,000 \text{ s/mm}^2$ are usually universally accepted and implemented as the norm).^{60, 61} The availability of this data is a rich source of interrogating normal skull bone marrow or the changes that may occur within it following PBT or RT.

1.6 IDENTIFIED GAPS IN KNOWLEDGE

Despite its advantages, (non-ionizing radiation, intrinsic contrast mechanisms that do not require external agents), WB-DW-MRI is not used routinely in paediatrics for assessing bone marrow. In adults, the technique has been approved for assessing haematological conditions (NICE guidelines for assessment of myeloma). As a first step to getting this technique into the repertoire of paediatric bone marrow imaging, I identified the following gaps in knowledge that would need addressing:

Establishing the normal values for bone marrow in children, and their variation with age gender and pubertal status.

Establishing the reproducibility of the derived measurements;

Documenting the effects of treatments such as conventional radiotherapy (RT), proton therapy (PTB), and chemotherapy on normal bone marrow;

Describing longitudinal changes in the bone marrow following bone marrow transplantation.

My hypothesis was:

In paediatric bone marrow, the apparent diffusion coefficient (ADC) derived from diffusion-weighted MRI does not vary with age, puberty, or gender in a non-oncological population.

1.7 AIMS

To establish the ADC values for normal bone marrow and their variation with age, gender and pubertal status using measurements from the skull in normal children undergoing brain MR studies.

To establish the changes in ADC in the skull following RT and PBT of brain tumours and compare them to variation in the measurement from reproducibility studies.

To establish the changes in ADC in the lumbar spine following chemotherapy for solid abdominal tumours and compare them to variation in the measurement from reproducibility studies.

To develop a longitudinal study to prospectively assess changes in the marrow after bone marrow transplantation.

REFERENCES

1. Proytcheva M. Bone marrow evaluation for pediatric patients. *International journal of laboratory hematology*. 2013; 35: 283-289.
2. Feller J. MRI of bone marrow. 2011 Advance MRI – From head to toe.
3. Hwang S and Panicek DM. Magnetic resonance imaging of bone marrow in oncology, Part 2. *Skeletal radiology*. 2007; 36: 1017-1027.
4. Blebea JS, Houseni M, Torigian DA, et al. Structural and functional imaging of normal bone marrow and evaluation of its age-related changes. *Seminars in nuclear medicine*. 2007; 37: 185-194.
5. Malkiewicz A and Dzedzic M. Bone marrow reconversion - imaging of physiological changes in bone marrow. *Polish journal of radiology*. 2012; 77: 45-50.
6. Chan BY, Gill KG, Rebsamen SL and Nguyen JC. MR Imaging of Pediatric Bone Marrow. *Radiographics: a review publication of the Radiological Society of North America, Inc.* 2016; 36: 1911-1930.
7. Gurevitch O, Slavin S and Feldman AG. Conversion of red bone marrow into yellow - Cause and mechanisms. *Medical hypotheses*. 2007; 69: 531-536.
8. Vande Berg BC, Gilon R, Malghem J, Lecouvet F, Depresseux G and Houssiau FA. Correlation between baseline femoral neck marrow status and the development of femoral head osteonecrosis in corticosteroid-treated patients: a longitudinal study by MR imaging. *European journal of radiology*. 2006; 58: 444-449.
9. Peng YJ, Yu H, Hao X, et al. Luteinizing hormone signaling restricts hematopoietic stem cell expansion during puberty. 2018; 37.
10. Paediatric PTB Guidelines – NHS 2013.
11. Metz J. Proton Therapy. *Demos Medical, Radiation Medicine Rounds*. 2010; vol. I: 415.
12. Knab B and Connell PP. Radiotherapy for pediatric brain tumors: when and how. *Expert review of anticancer therapy*. 2007; 7: S69-77.

13. Main types of childhood cancer: children aged 0-14 years. United Kingdom 2001 to 2010. *Based on data provided by National Registry of childhood Tumours*
14. Children's cancers incidence by type.
15. O'Neill P and Wardman P. Radiation chemistry comes before radiation biology. *International journal of radiation biology*. 2009; 85: 9-25.
16. Carmona R, Pritz J, Bydder M, et al. Fat composition changes in bone marrow during chemotherapy and radiation therapy. *International journal of radiation oncology, biology, physics*. 2014; 90: 155-163.
17. Kirsch DG, Diehn M, Kesarwala AH, et al. The Future of Radiobiology. *Journal of the National Cancer Institute*. 2018; 110: 329-340.
18. Gilbert ES. Ionising radiation and cancer risks: what have we learned from epidemiology? *International journal of radiation biology*. 2009; 85: 467-482.
19. Schild SE, Rule WG, Ashman JB, et al. Proton beam therapy for locally advanced lung cancer: A review. *World journal of clinical oncology*. 2014; 5: 568-575.
20. Verma V, Simone CB, 2nd, Wahl AO, Beriwal S and Mehta MP. Proton radiotherapy for gynecologic neoplasms. *Acta oncologica (Stockholm, Sweden)*. 2016; 55: 1257-1265.
21. Warren S, Hurt CN, Crosby T, Partridge M and Hawkins MA. Potential of Proton Therapy to Reduce Acute Hematologic Toxicity in Concurrent Chemoradiation Therapy for Esophageal Cancer. *International journal of radiation oncology, biology, physics*. 2017; 99: 729-737.
22. Mizumoto M, Oshiro Y, Yamamoto T, Kohzuki H and Sakurai H. Proton Beam Therapy for Pediatric Brain Tumor. *Neurologia medico-chirurgica*. 2017; 57: 343-355.
23. Indelicato DJ, Merchant T, Laperriere N, et al. Consensus Report From the Stockholm Pediatric Proton Therapy Conference. *International journal of radiation oncology, biology, physics*. 2016; 96: 387-392.
24. Cai S, Wang H, Bailey B, et al. Humanized bone marrow mouse model as a preclinical tool to assess therapy-mediated hematotoxicity. *Clinical cancer research : an official journal of the American Association for Cancer Research*. 2011; 17: 2195-2206.
25. Ilari I, De Ioris MA, Milano GM, et al. Toxicity of high-dose chemotherapy with etoposide, thiotepa and CY in treating poor-prognosis Ewing's sarcoma family tumors: the experience of the Bambino Gesù Children's Hospital. *Bone marrow transplantation*. 2010; 45: 1274-1280.

26. Goldman SC, Bracho F, Davenport V, et al. Feasibility study of IL-11 and granulocyte colony-stimulating factor after myelosuppressive chemotherapy to mobilize peripheral blood stem cells from heavily pretreated patients. *Journal of pediatric hematology/oncology*. 2001; 23: 300-305.
27. Greinix HT, Linkesch W, Keil F, et al. Early detection of hematopoietic engraftment after bone marrow and peripheral blood stem cell transplantation by highly fluorescent reticulocyte counts. *Bone marrow transplantation*. 1994; 14: 307-313.
28. Mas-Bargues C, Sanz-Ros J, Román-Domínguez A. et al. Relevance of oxygen concentration in stem cell culture for regenerative medicine. *Int J Mol Sci*. 2019; 20, 1195 (1-27).
29. Eliasson P, Rehn M, Hammar P, et al. Hypoxia mediates low cell-cycle activity and increases the proportion of long-term-reconstituting hematopoietic stem cells during in vitro culture. *Experimental hematology*. 2010; 38: 301-10.e2.
30. Abla O, Friedman J and Doyle J. Performing bone marrow aspiration and biopsy in children: Recommended guidelines. *Paediatrics & child health*. 2008; 13: 499-501.
31. Rahim F, Ahmad I, Islam S, Hussain M, Khattak T and Bano Q. Spectrum of hematological disorders in children observed in 424 consecutive bone marrow aspirations/biopsies. *Pakistan Journal of Medical Sciences*. 21: 433-436.
32. Bashawri LA. Bone marrow examination. Indications and diagnostic value. *Saudi medical journal*. 2002; 23: 191-6.
33. Riley RS, Hogan TF, Pavot DR, et al. A pathologist's perspective on bone marrow aspiration and biopsy: I. Performing a bone marrow examination. *Journal of clinical laboratory analysis*. 2004; 18: 70-90.
34. Bain BJ. Bone marrow trephine biopsy. *Journal of clinical pathology*. 2001; 54: 737-742.
35. Shah LM and Hanrahan CJ. MRI of spinal bone marrow: part I, techniques and normal age-related appearances. *AJR American journal of roentgenology*. 2011; 197: 1298-1308.
36. Dawson KL, Moore SG and Rowland JM. Age-related marrow changes in the pelvis: MR and anatomic findings. *Radiology*. 1992; 183: 47-51.
37. Swartz PG and Roberts CC. Radiological reasoning: bone marrow changes on MRI. *AJR American journal of roentgenology*. 2009; 193: S1-4, Quiz S5-9.
38. Herrmann J, Krstin N, Schoennagel BP, et al. Age-related distribution of vertebral bone-marrow diffusivity. *European journal of radiology*. 2012; 81: 4046-4049.
39. Burdiles A and Babyn PS. Pediatric bone marrow MR imaging. *Magnetic resonance imaging clinics of North America*. 2009; 17: 391-409, v.

40. Keller PJ, Hunter WW, Jr. and Schmalbrock P. Multisection fat-water imaging with chemical shift selective presaturation. *Radiology*. 1987; 164: 539-541.
41. Del Grande F, Santini F, Herzka DA, et al. Fat-suppression techniques for 3-T MR imaging of the musculoskeletal system. *Radiographics: a review publication of the Radiological Society of North America, Inc.* 2014; 34: 217-233.
42. Bandirali M, Di Leo G, Papini GD, et al. A new diagnostic score to detect osteoporosis in patients undergoing lumbar spine MRI. *European radiology*. 2015; 25: 2951-2959.
43. Shen W, Scherzer R, Gantz M, et al. Relationship between MRI-measured bone marrow adipose tissue and hip and spine bone mineral density in African-American and Caucasian participants: the CARDIA study. *The Journal of clinical endocrinology and metabolism*. 2012; 97: 1337-1346.
44. Shen W, Gong X, Weiss J and Jin Y. Comparison among T1-weighted magnetic resonance imaging, modified dixon method, and magnetic resonance spectroscopy in measuring bone marrow fat. *Journal of obesity*. 2013; 2013: 298675.
45. Bydder M, Yokoo T, Hamilton G, et al. Relaxation effects in the quantification of fat using gradient echo imaging. *Magnetic resonance imaging*. 2008; 26: 347-359.
46. Liu CY, McKenzie CA, Yu H, Brittain JH and Reeder SB. Fat quantification with IDEAL gradient echo imaging: correction of bias from T(1) and noise. *Magnetic resonance in medicine*. 2007; 58: 354-364.
47. O'Connor JP, Aboagye EO, Adams JE, et al. Imaging biomarker roadmap for cancer studies. *Nature reviews Clinical oncology*. 2017; 14: 169-186.
48. Dietrich O, Biffar A, Reiser MF and Baur-Melnyk A. Diffusion-weighted imaging of bone marrow. *Seminars in musculoskeletal radiology*. 2009; 13: 134-144.
49. Padhani AR, Liu G, Koh DM, et al. Diffusion-weighted magnetic resonance imaging as a cancer biomarker: consensus and recommendations. *Neoplasia (New York, NY)*. 2009; 11: 102-125.
50. Afaq A, Andreou A and Koh DM. Diffusion-weighted magnetic resonance imaging for tumour response assessment: why, when and how? *Cancer imaging : the official publication of the International Cancer Imaging Society*. 2010; 10 Spec no A: S179-188.
51. Koh DM and Collins DJ. Diffusion-weighted MRI in the body: applications and challenges in oncology. *AJR American journal of roentgenology*. 2007; 188: 1622-1635.

52. Kyriazi S, Morgan V, Collins D and deSouza N. Echo planar diffusion-weighted MRI of the abdomen and pelvis: comparison of free-breathing monopolar and bipolar spin-echo sequences in assesng image quality and apparent diffusion coefficients. *International Society for Magnetic Resonance in Medicine*. 17: 4066.
53. Voss SD. Pediatric oncology and the future of oncological imaging. *Pediatric radiology*. 2011; 41 Suppl 1: S172-185.
54. Messiou C and Kaiser M. Whole body diffusion weighted MRI--a new view of myeloma. *British journal of haematology*. 2015; 171: 29-37.
55. Dimopoulos MA, Hillengass J, Usmani S, et al. Role of magnetic resonance imaging in the management of patients with multiple myeloma: a consensus statement. *Journal of clinical oncology : official journal of the American Society of Clinical Oncology*. 2015; 33: 657-664.
56. Giles SL, deSouza NM, Collins DJ, et al. Assessing myeloma bone disease with whole-body diffusion-weighted imaging: comparison with x-ray skeletal survey by region and relationship with laboratory estimates of disease burden. *Clinical radiology*. 2015; 70: 614-621.
57. Siegel MJ, Acharyya S, Hoffer FA, et al. Whole-body MR imaging for staging of malignant tumors in pediatric patients: results of the American College of Radiology Imaging Network 6660 Trial. *Radiology*. 2013; 266: 599-609.
58. Nievelstein RA and Littooi AS. Whole-body MRI in paediatric oncology. *La Radiologia medica*. 2016; 121: 442-453.
59. Le Bihan D, Breton E, Lallemand D, Aubin ML, Vignaud J and Laval-Jeantet M. Separation of diffusion and perfusion in intravoxel incoherent motion MR imaging. *Radiology*. 1988; 168: 497-505.
60. Cui FZ, Cui JL, Wang SL, et al. Signal characteristics of normal adult bone marrow in whole-body diffusion-weighted imaging. *Acta radiologica (Stockholm, Sweden : 1987)*. 2016; 57: 1230-1237.
61. Saunders DE, Thompson C, Gunny R, Jones R, Cox T and Chong WK. Magnetic resonance imaging protocols for paediatric neuroradiology. *Pediatric radiology*. 2007; 37: 789-797.

CHAPTER 2 – Normal Bone Marrow ADC Values and their variation with age, pubertal status and gender

The purpose of this chapter is to explore the influence of age, puberty, and gender on ADC values in the marrow of the clivus in a non-oncological paediatric population based on retrospective data so that the results can be used as a benchmark when monitoring effects induced by local and systemic cancer treatments.

2.1 INTRODUCTION

2.1.1 Normal Bone Marrow

2.1.1.1 Composition with age and hormonal status

Bone marrow is a dynamic tissue comprising different type of cells.¹ Its composition varies across the lifespan of an individual based on the requirements of a healthy body and is related to various developmental stages and different physiological needs. For its function, it comprises pluripotent haematopoietic stem cells that self-renew, proliferate and differentiate into every lineage of mature blood cells. These broadly fall into two categories, the multi-potential myeloid progenitor cells (which are precursors of granulocytes, monocytes, erythrocytes, and platelets) and the lymphoid stem cells (which give rise to lymphocytes, and plasma cells). The latter provide immunological protection: B lymphocytes (B-cell) maturation commences in the bone marrow where precursor cells acquire surface immunoglobulin, while precursor T-cells

complete their programmed maturation once these migrate to the thymus. Bone marrow-derived T-cell precursors drop in number with advancing age. Haematopoietic cells are first appreciable within the medullary cavities of bones at around 14 weeks of gestation.² By birth the bone marrow represents the principal anatomical location of haematopoiesis and under normal circumstances the bone marrow is the only site of haematopoiesis. Extramedullary haematopoiesis may occur in the liver, spleen and lymph nodes in pathological states when the marrow compensatory mechanisms are surpassed. Growth hormone production declines with age and this, too, has been linked with deposition of fat within the bone marrow.³ Administration of growth hormone to preclinical models reduces marrow fat and increases hematopoietic tissue.³

The marrow space occupied by the haematopoietic cells diminishes from 90% at birth to approximately 50% at 30 years old and 30% at age 70.^{4, 5} The same involution occurs in the thymus resulting in shrinkage of the lymphoid mass and replacement with adipocytes. Fat infiltration into the bone marrow and thymus leads to a reduced volume of haematopoietic tissue. Nevertheless, physiological effects throughout life result in activation of the haematopoietic and immunological functions of the marrow. Male sex hormones affect erythrocyte production, stimulating the synthesis of renal erythropoietic factor (indirect) and of DNA and heme (direct) in the bone marrow cells.⁶ Certain sex steroid metabolites are capable of significantly stimulating the synthesis of both heme and globin in cultured human bone marrow cells.⁷ There is, therefore, good evidence to indicate that the relative proportions of different

components of the bone marrow is in part hormonally driven and is potentially changing substantially around the time of puberty.

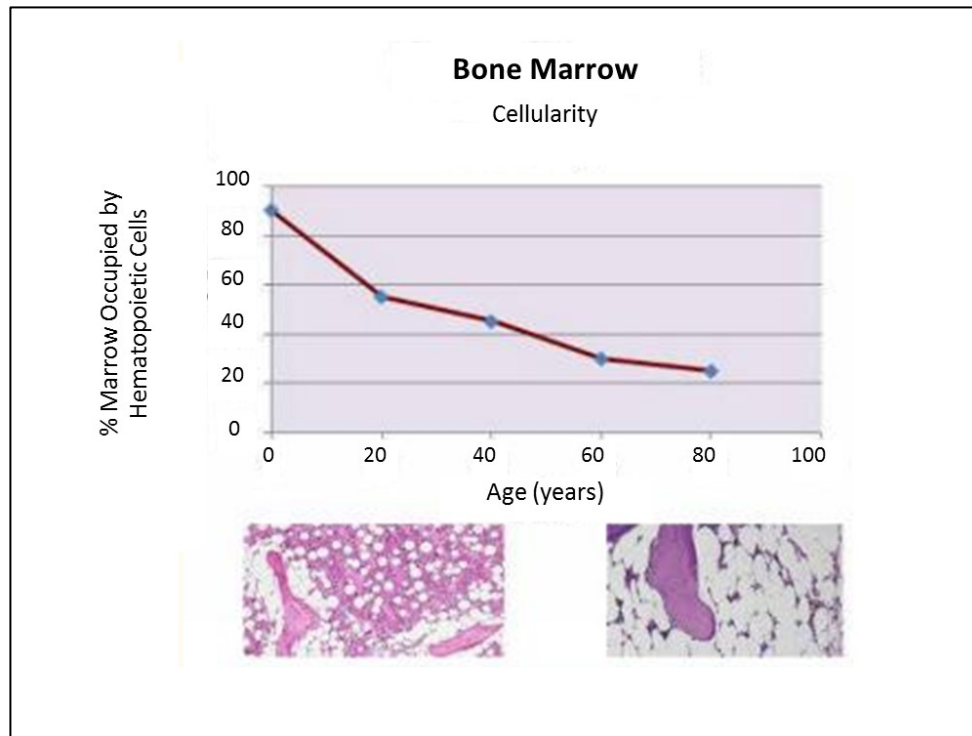


Figure 2.1: Percentage bone marrow occupied by haematopoietic tissue and fat with age.

2.1.1.2 Regional variation by skeletal area

The relative proportion of different components of the bone marrow depends on the type of bone (long, short, flat, and irregular). Until puberty the entire skeleton remains hematopoietically active but by age 18 only the production of blood cells persists only in the vertebrae, ribs, sternum, skull, pelvis, proximal humeral and femoral epiphyses, whilst the other osseous locations bones undergo a fatty infiltration process.⁸

In this retrospective study, I limited my investigation to study of bone marrow in the skull as DW-MRI forms a routine part of brain imaging in children. The flat shape of the skull bones means that region-of-interest (ROI)

delineation, particularly in a paediatric population where unfused sutures may inadvertently be included, is unsuitable. The clivus was therefore selected as a suitable region for measurement. This area of the skull base represents one of the thickest bones within the cranium, making ROI in multiple adjacent slices with an interval of 5 mm feasible and obtaining a volume was easier when compared with other thinner areas of the skull vault or calvarial bones. Additionally, its midline location meant that the clivus is routinely included in the field of irradiation as a treatment for brain tumour, making it ideally placed for measurement of post-treatment ADC changes.

2.2 AIM

To assess the absence of variability of ADC in a paediatric population by age, gender, and pubertal status in a retrospective analysis of the marrow within the clivus.

2.3 METHODS

2.3.1 Patient selection

Non-oncological subjects who had previously had brain MRI for clinical purposes and in whom DW-MRI was routinely performed as part of the examination were selected. This study was approved as a Service Evaluation (662) by The Royal Marsden (Appendix 1) and included scans carried out at St. George's Hospital with approval from the Joint Research Committee. The data

collection was supported by Dr Andrew MacKinnon (Consultant Neuroradiologist). Search criteria for identifying patients are shown in **Table 2.1** with those highlighted in green representing the options selected on the Radiology Information System Soliton®.

Start date	
End date	
Exam type	MRI head
Visit type	all (day, inpatients, outpatients)
Category	both (NHS and private)
Site	Neuroradiology AMV
Status	authorised
Reason	all
Referred by	all
Specialty	all
Source	all
Room	AMW MRI
Practice	all
Assigned to	all
Patient Age	paediatric
Priority	all
Flag	all
Medication	no
Treatment (RT, PBT,...)	no
Neoplasm	no

Table 2.1: Search criteria to develop a database of children not on medication, free of treatment, and without a suspected oncological diagnosis.

The following inclusion and exclusion criteria were then applied to achieve a cohort of children with benign pathology, free from medications that could potentially influence the result, and whose images were artefact free:

2.3.1.1 Inclusion Criteria

- age between 5-17 years old
- iso DW-MRI ISO performed
- indications for MRI: headaches, seizures (first episode but medications not started and electroencephalogram within normal limits), assessment of anatomical normal variants (Chiari malformation, cavum septi pellucidi)

2.3.1.2 Exclusion criteria

- Dental brace
- Artefacts on DW-MRI and/or other main sequences
- Oncological patients at any stage
- Patients on any type of medication (including chemotherapy)
- Positive neurological symptoms (usually associated with brain abnormalities)
- Psychosis (as usually medicated)
- Systemic diseases (anaemia, sickle cells, hypoglycaemia, muscular dystrophy)
- Bony lesions or illness
- Colloid cysts
- Space-occupying lesions
- Empyema
- Abnormal electroencephalogram findings (as they may be associated with brain abnormalities)

1,140 children were identified by the search criteria. Their MRI scans reviewed on Picture Archiving and Communication System (PACS). Application of the inclusion and exclusion criteria resulted in the identification of 60 individuals who met these criteria.

2.3.2 Image acquisition

All children had been scanned on a 1.5T Philips Achieva-Ingenua upgraded to d-stream (digital rf) platform. Their examinations were anonymised and transferred to the Institute of Cancer Research through a secure web-based data analysis platform (XNAT_Collaborations). Axial DW images (b-values = 0 and 1000 s/mm²) were routinely acquired as part of the standard MRI brain scan. The voxel resolution was 0.9375 x 0.9375 x 4 mm. Axial T2-W spin-echo (SE) and Fluid-Attenuated Inversion Recovery (FLAIR), as well as sagittal T1-W SE and coronal T2-W SE images were acquired in each case. In individuals older than 16 years, the sagittal T1-W SE was replaced by T2-W SE. These images were part of a standard anatomical protocol for brain imaging and were not optimised for bone marrow study; they were not utilised in this study.

2.3.3 Image analysis

2.3.3.1 Method of region of interest delineation

Both coronal and axial T2-W images were used to identify the exact location of the clivus. Specifically, I simultaneously used an ICR desktop

computer and a PACS work station so that the DW images uploaded onto the software Adept® (in-house, The Institute of Cancer Research, ICR) could be accurately correlated with morphological axial T2-W images — and any coronal or sagittal images, when available — on the original MR examinations launched on PACS, in order to meticulously assess where on a midline slice of the axial DW images exactly select a region of interest of approximately 4-6 mm in diameter within the clivus and draw a circle using Adept®. Both .xroi and .txt files for each slice containing the drawn ROI were saved on Adept® an ICR computer. Using the software CombineAdeptResultsFiles® data from the entire volume of the region of interest were obtained merging the .txt files of all the ROIs drawn on DW images in the clivus on different slices.

2.3.3.2 ADC calculation

As data was acquired with 2 b-values (0 and 1000 s/mm², as these are routinely acquired in a standard MRI brain scan), ADC was calculated through a monoexponential fit of the data, creating the relative ADC maps.

The formula applied to obtain the ADC values voxel by voxel and create the map was as follows:

$$S(b)/S_0 = \exp(-b \times \text{ADC}), \quad [1]$$

where S(b) is the signal magnitude with diffusion weighting b, S₀ is the signal magnitude without diffusion weighting, and b is the b-value, which is calculated for a standard square-shaped gradient pulse pair as follows:

$$b = \gamma^2 \times G^2 \times \delta^2(\Delta - \delta/3). \quad [2]$$

γ is the gyromagnetic ratio (42.58 MHz/T for hydrogen), G is the strength of the motion probing gradients (MPGs), δ is the duration of one rf pulse, and Δ is the interval between the leading edges of the rf pulses.

2.3.3.3 Derivation of centile values

The generated Multislices derived using the software CombineAdeptResultsFiles[®] was opened on Excel[®] and the consequent file saved in .xlsx. This resulted in a final spreadsheet containing information regarding the following values of ADC: median, mean, 10th, 25th, 75th, and 90th percentile.

2.3.3.4 Recognition of pubertal status

This was done from the imaging appearances. Assessment of the pituitary gland on sagittal images (T1-W if younger than 16 years and T2-W if older as per adult MR routine protocol) and coronal T2-W was made. Physiological hypertrophy of the gland was demonstrated in both genders at puberty, although this was more prominent in girls in whom convex upper margins and spherical shape were also noted. At puberty, the plump gland completely fills the pituitary fossa, and a convex upper border appears; a posterior hyperintense spot is often identifiable in the posterior portion of the gland on T1- W sequences thought to be caused by the storage of vasopressin, which has a T1-shortening effect. On coronal view a hat shape of the gland characterises a pubertal appearance⁹ (**Figure 2.4**).

A further assessment was utilized that considers spheno-occipital synchondrosis closure. Its relationship to puberty has been described in a recent study (n=741 subjects between 6 and 20 years old, 380 girls and 361 boys). I used the staging system they proposed on CT and applied it to the MRI exams. Stages 0 and 1 were considered pre-pubertal and stages 2 and 3 post-pubertal (**Table 2.2, Figure 2.2**).¹⁰

Stage		
0	UNFUSED	Completely open with no evidence of fusion between the basilar portion of the occipital and the sphenoid, no bone present in the gap
1	FUSING ENDOCRANIALY	<50% the length of the synchondrosis is fused proceeding endo- to ectocranially
2	FUSING ECTOCRANIALY	>50% the length of the synchondrosis is fused, the ectocranial (inferior) border remains unfused
3	COMPLETE FUSION	Completely fused with the appearances of normal bone throughout, a fusion scar may be present.

Table 2.2: Staging system for pubertal status based on spheno-occipital synchondrosis closure on imaging (adopted from Alhazmi A et al. 2017 Timing and rate of spheno-occipital synchondrosis closure and its relationship to puberty PLoS One Aug 21; 12 PLoS One Aug 21; 12 (8):e0183305.

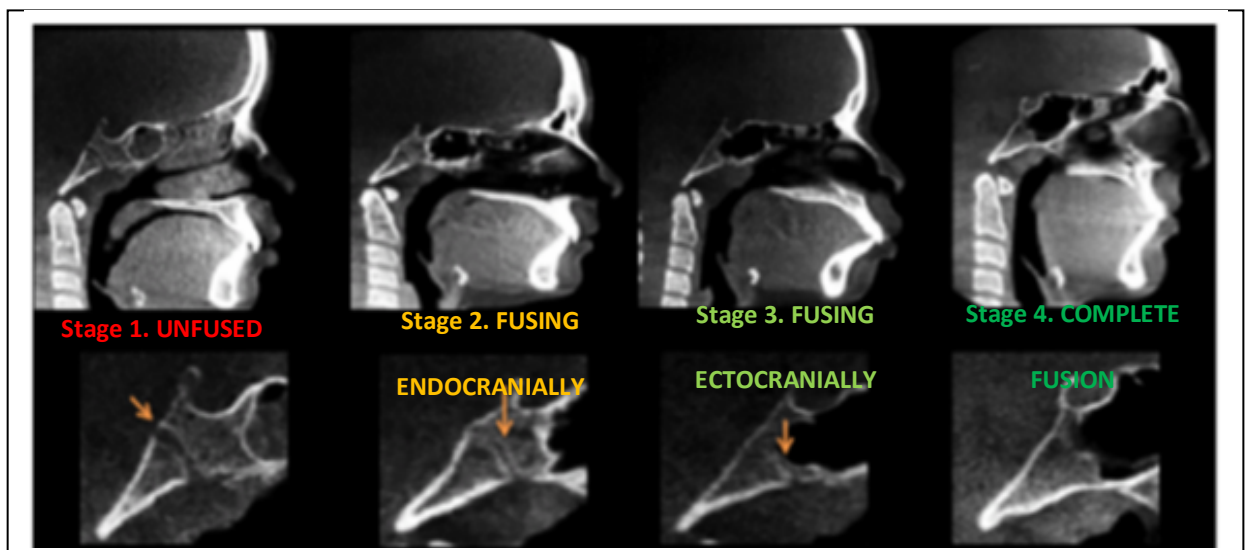


Figure 2.2: Four stages of spheno-occipital synchondrosis closure.

To avoid including artefacts consisting of punctiform foci with low signal-to-noise ratio on diffusion-weighted images, the region-of-interest was drawn as a circle of approximately 6-mm within the clivus at the level of the fossa navicularis (indicated by a white star in **Figure 2.3**).

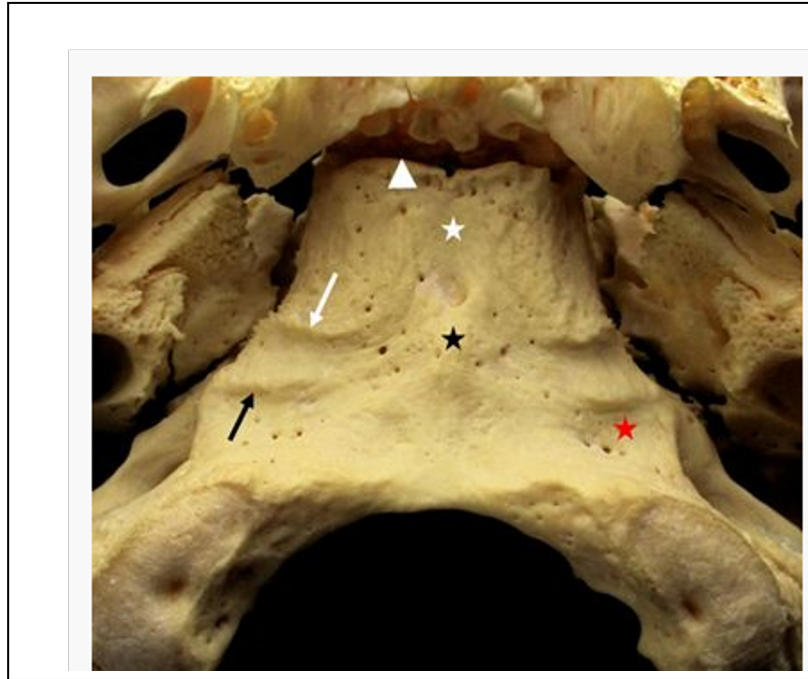


Figure 2.3: Axial photograph of the central skull base showing ridges indicative of vascular bed (arrows) and fossa navicularis (black and white stars).

The assessment of the fusion of the sphenoid-occipital synchondrosis was done on coronal T1-W or T2-W images (**Figure 2.4**). In 2 individuals it was challenging to discriminate between stage 1 and 2, however fusion had started. In 3 children fusion had begun but there was no associated pituitary bulging. These cases were considered included in the 10 years-puberty group.

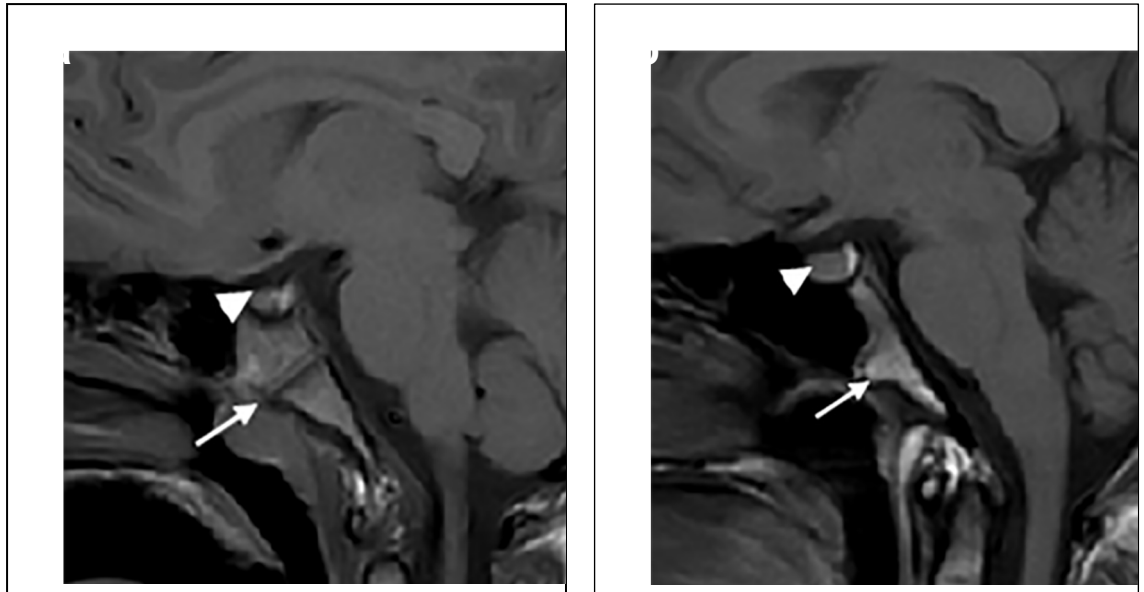


Figure 2.4: T1-W sagittal images in a 7-year old female (a) and a 14-year old female (b). In a, the pre-pubertal appearance of the pituitary gland with its flat upper aspect (arrowhead) and unfused sphenoid-occipital synchondrosis (stage 0, arrow) is seen. In b, the typical post-pubertal bulging of the upper aspect of the pituitary gland is demonstrated and the sphenoid-occipital synchondrosis is fused.

2.3.3.5 Statistical analysis

Statistical analysis was performed using GraphPad Prism software (version 7.04, GraphPad Incorporated company, California). Descriptive statistics were used to describe the data. ADC data was checked for normality (Shapiro-Wilk test), and as all data was not normally distributed, a Kruskal-Wallis test was applied to the rank of the data values in order compare the different samples and to determine whether the medians of the cohorts differ using the rank of the data values.

A Pearson's correlation coefficient examined the relationship between ADC and age.

2.4 RESULTS

2.4.1 Patients' characteristics

60 children who fulfilled the inclusion criteria and were categorized as follows:

5-9 years old:	8 F + 7 M
10 years old to pre-puberty:	7 F + 8 M
Post-pubertal girls:	15 F
Post Pubertal boys:	15 M

2.4.2 ROI sizes

The number of voxels included in each case ranged from 21 to 182 and was significantly different among the groups (5-9 years, mean \pm std = 78.8 \pm 30.8; pre-pubertal aged 10 years and older, mean \pm std = 57.1 \pm 12.4; post-pubertal females, mean \pm std = 40.5 \pm 7.2; post-pubertal males, mean \pm std = 39.5 \pm 14.7; $p < 0.0001$) (**Table 2.3**).

ROI size was smaller in the older children, as the clival marrow was more difficult to identify on the high b-value images, which may have also reduced the

variability of the measurement as reflected by the standard deviation.

	Stage 0	Stage 1	Stages 2 & 3	
	Age: 5-9 y	Age: 10 y to pre-puberty	Post-puberty	
Male	7	8	0	Stage 2 Stage 3 15 0
Female	8	7	Stage 2 Stage 3 10 5	0
Total number of participants	15	15	15	15
Mean voxels in the clival ROI	77.8 ± 31	57.1 ± 12	40.5 ± 7	39.5 ± 15

Table 2.3: Number of voxels in the clival ROI by age group

2.4.3 Normal ADC values

2.4.3.1 Median and mean ADC values in the population

	ADC		
	5-9 years	10 years - puberty	All post-puberty
MEDIAN	77.3	72.3	55.7
Range	44.5, 136.6	50.5, 108.5	37.5, 76.8
IQR	43.5 ± 17.3	35.5 ± 9.1	34.1 ± 17.5
MEAN	77.1 ± 20.1	72 ± 16.9	58.1 ± 15.6
Range	46.3, 136.3	53, 102	36.2, 103.7

Table 2.4: Median and mean ADC values in the clival ROI by age

ADC values were similar between the pre-pubertal groups for both median and mean values and significantly reduced after puberty (cf 2.4.5, **Figure 2.5 a and b**) both with p values of .0001 (**Table 2.5**). Specifically, pre-pubertal mean ADC values for the whole population decreased from 74.6 ± 18.4 pre-puberty to 58.2 ± 15 after it, whilst ADC median values were 74.8 ± 18.2 and 55.7 ± 11.8 , pre- and post-puberty, respectively. There did not appear to be an increase in homogeneity of marrow post-puberty as IQR was similar (**Table 2.5**).

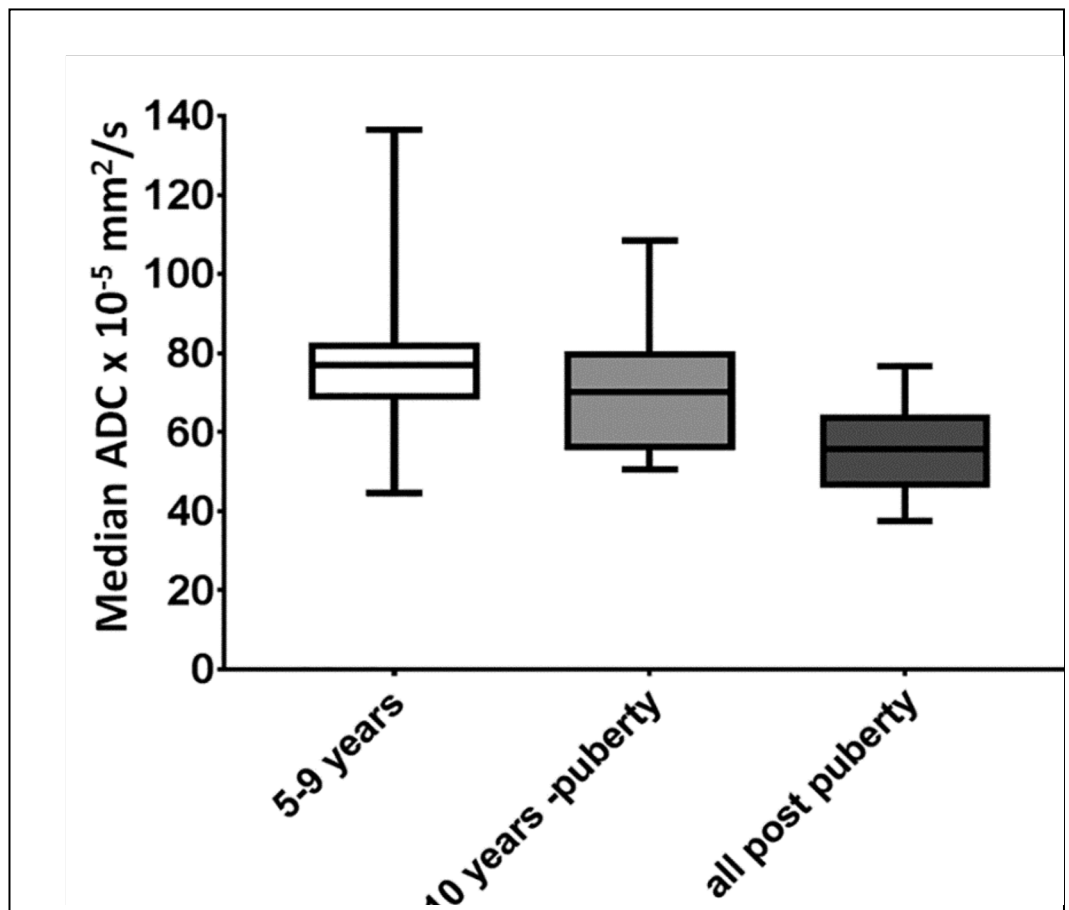


Figure 2.5 a: Boxplots of median ADC by age group

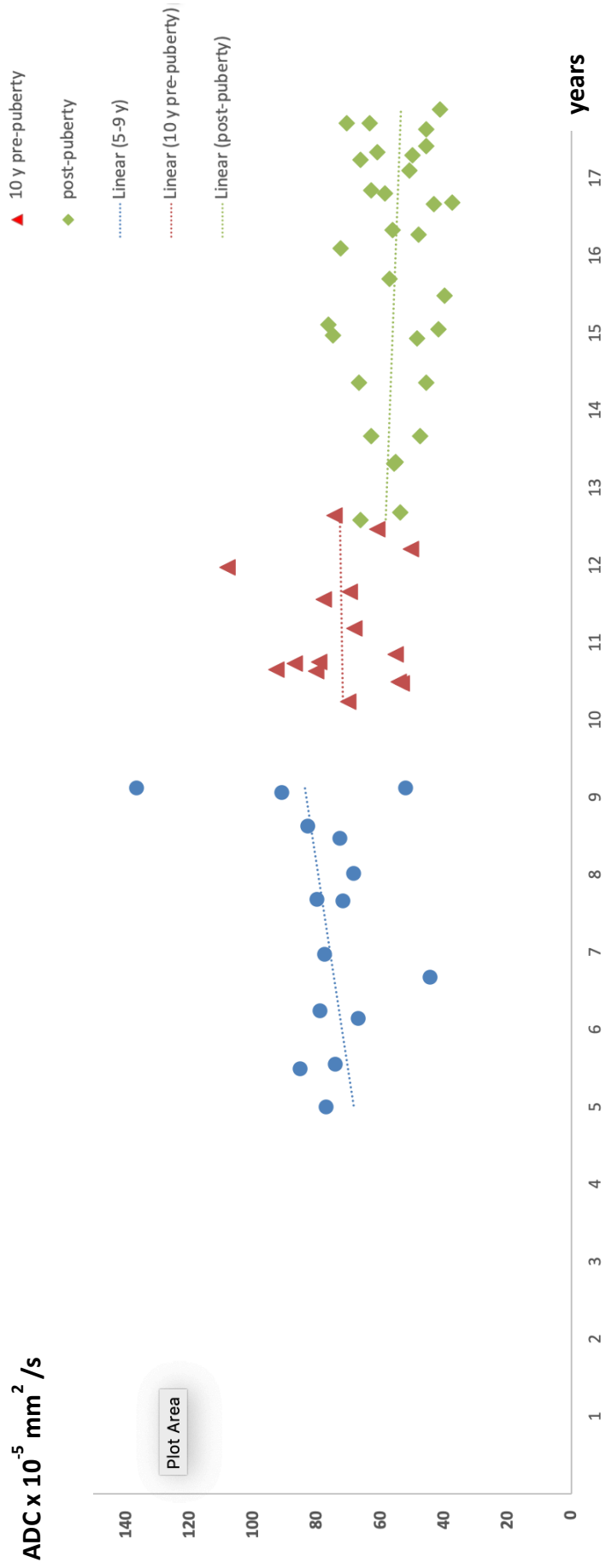


Figure 2.5 b: Scatter plot of median ADC by age group

ADC x 10⁻⁵ mm²/s			
	All pre-pubertal (n = 30)	All post-pubertal (n = 30)	P values (Mann-Whitney U test)
MEAN	74.6 ± 18.4	58.2 ± 15.6	0.0001
C25	54.1 ± 16.8	39.9 ± 10.3	0.0001
MEDIAN	74.8 ± 18.2	55.7 ± 11.8	0.0001
C75	93.6 ± 24.1	74 ± 22.7	0.0002
IQR	39.5 ± 14.2	34.1 ± 17.5	0.2

Table 2.5: Median, mean, and centile ADC values for the pre- and post-pubertal cohorts with the relative statistical significance of the IQR comparison.

2.4.3.2 Comparison of centile ADC values in the population

		ADC X 10⁻⁵ mm²/s			
		10th centile	25th centile	75th centile	90th centile
5-9 years	Mean ± SD	39 ± 16.9	55 ± 19.6	98.5 ± 28.1	114.6 ± 29.2
	Range	16.3 - 79.4	30.5 - 113.6	60.7 - 178.1	74.4 - 185.9
10 year- puberty	Mean ± SD	34 ± 15	53.1 ± 14.2	88.6 ± 18.8	105.5 ± 26.5
	Range	1.7 - 62.8	35.1 - 79.2	63.3 - 123.3	70.6 - 161.6
Post- puberty	Mean ± SD	27.5 ± 9.5	39.9 ± 10.3	74 ± 22.7	91.9 ± 43.1
	Range	13.6 - 43.3	22.3 - 61.2	48.3 - 162.3	55.3 - 254.7

Table 2.6: Distribution of histogram parameters by age group.

2.4.4 Variation with age

Age ranged from 5.0 to 17.9 years (median 12.4 years). There was a significant negative correlation between age and ADC for the whole cohort ($r = -0.48$ for median and -0.42 for mean values, $p = 0.0001$ and 0.0008 respectively). There was also a significant negative correlation between age and ADC for females ($r = -0.5$ for median and -0.4 for mean values, $p = 0.005$ and 0.03 respectively) and for males ($r = -0.53$ for median and -0.48 for mean values, $p = 0.002$ and 0.008 respectively). Regression plots are illustrated in **Figure 2.6**.

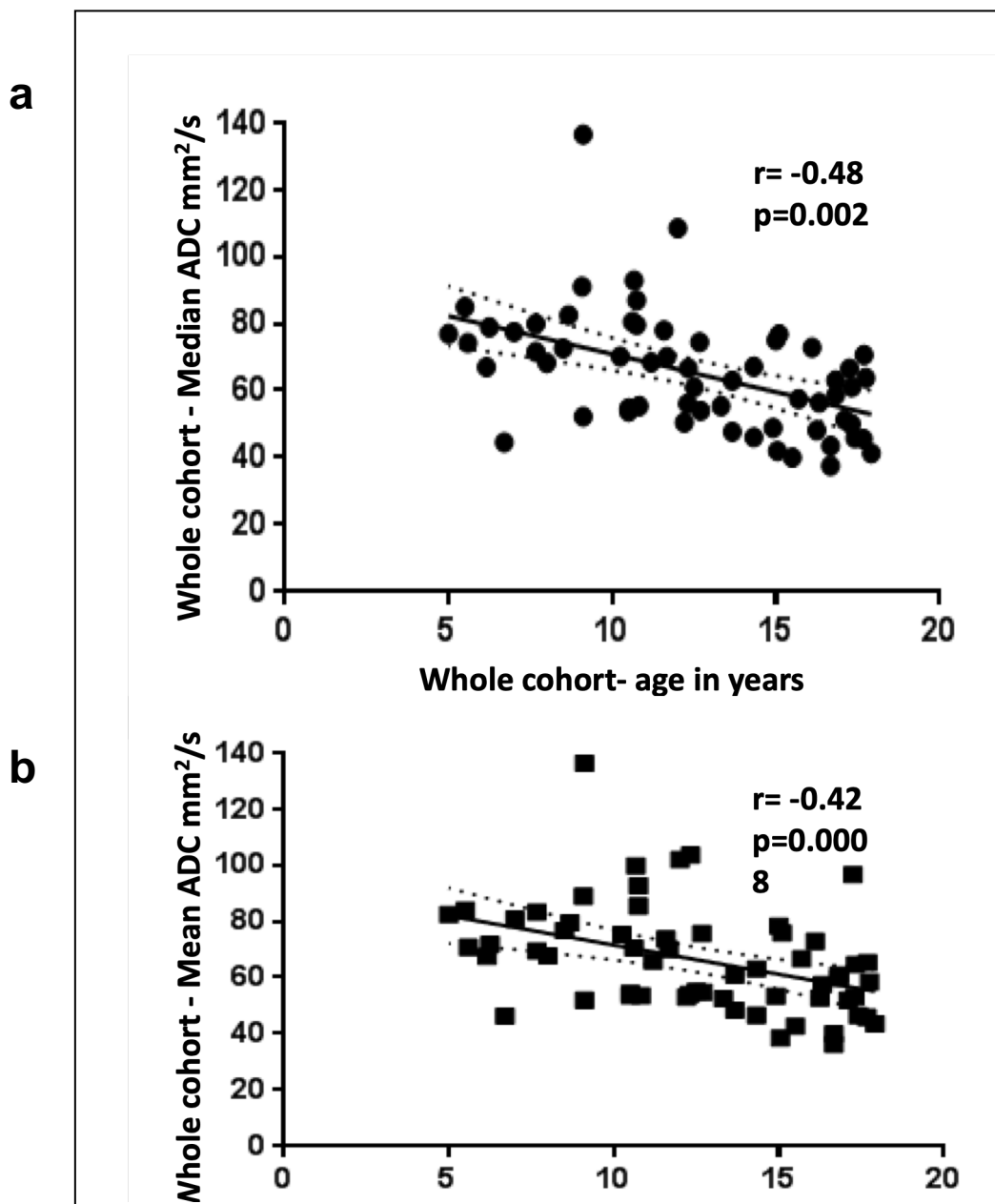
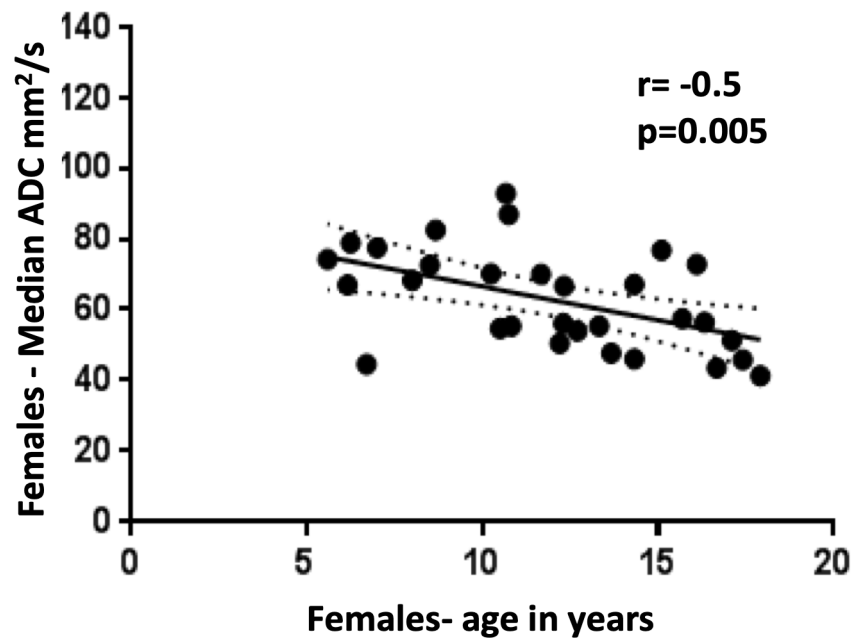


Figure 2.6: Correlation of ADC with age: Median and Mean ADC for the whole cohort (a and b, respectively), females (c and d, respectively) and males (e and f, respectively). There is a significant correlation with age for all categories.

c



d

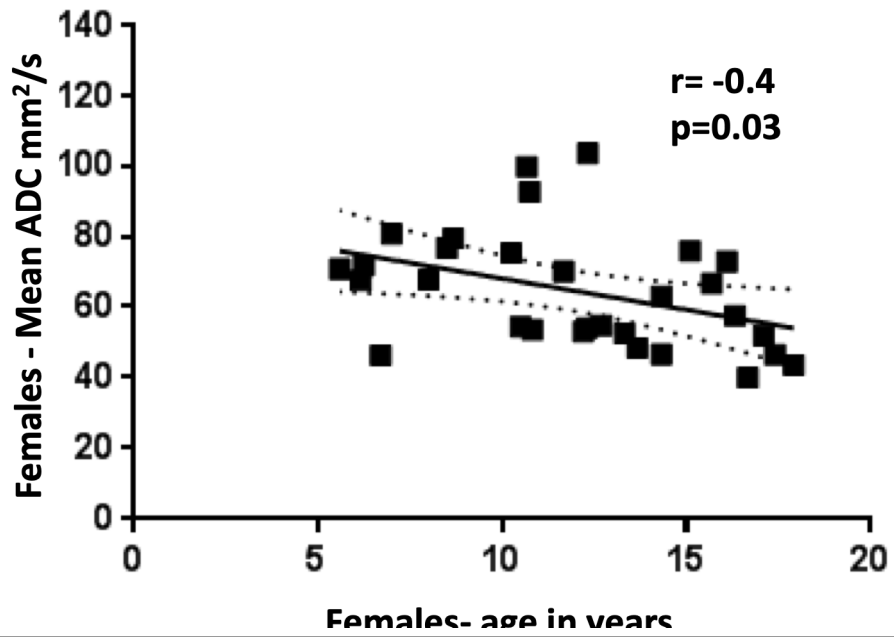


Figure 2.6: Correlation of ADC with age: Median and Mean ADC for the whole cohort (a and b, respectively), females (c and d, respectively) and males (e and f, respectively). There is a significant correlation with age for all categories.

e



f

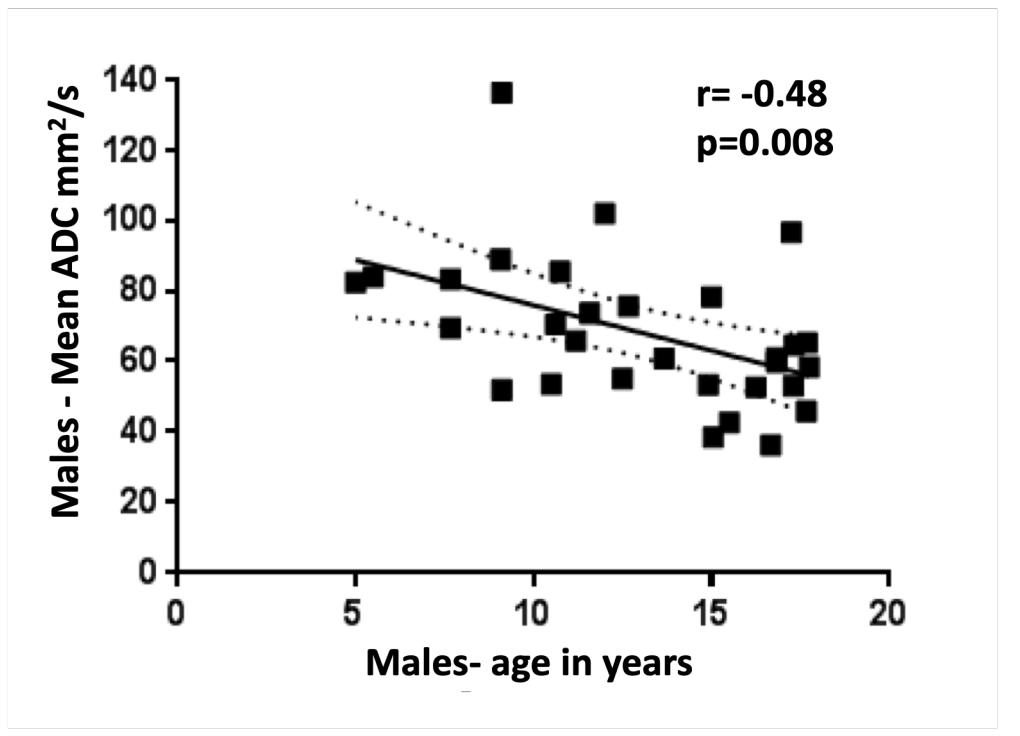


Figure 2.6: Correlation of ADC with age: Median and Mean ADC for the whole cohort (a and b, respectively), females (c and d, respectively) and males (e and f, respectively). There is a significant correlation with age for all categories.

2.4.5 Variation with pubertal status

Age of the post-pubertal cohort ranged from 12.3 to 17.9 years; it was lower in females (median age 15.1 years, range 12.3 to 17.9 years), compared to males (median age 16.8 years, range 13.7 to 17.8 years).

There was a significant difference between mean, median and centile ADC values before and after puberty for the whole population (**Table 2.6**). There was a shift of the ADC histogram to the left post-puberty (**Figure 2.7**) as evidenced by the significant difference in centile values across the population. Again, this was not reflected in an increased homogeneity of values as the interquartile range did not change.

	All pre-pubertal	All post-pubertal	<i>p-value</i>
	ADC X10 ⁻⁶ mm ² /s		
	Mean ± std		
Mean	74.6 ± 18.4	58.2 ± 15.6	0.0001
C10	36.5 ± 15.9	27.5 ± 9.5	0.01
C25	54.1 ± 16.8	39.9 ± 10.3	0.0001
C50	74.8 ± 18.2	55.7 ± 11.8	0.0001
C75	93.6 ± 24.1	74.0 ± 22.7	0.0002
C90	110.0 ± 27.8	91.9 ± 43.1	0.0009
IQR	39.5 ± 14.2	34.1 ± 17.5	0.2

Table 2.7: Mean, median and centile ADC values in pre-pubertal versus post-pubertal subjects.

Example cases are illustrated in **Figures 2.8** and **2.9**.

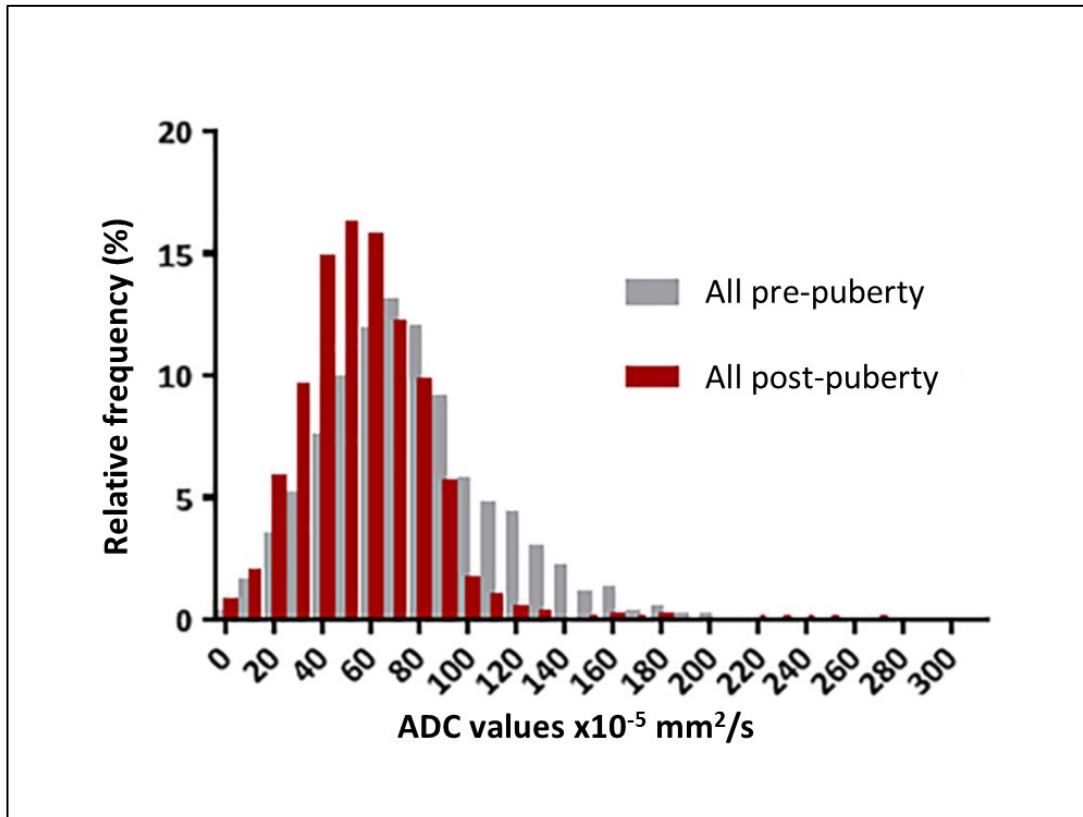


Figure 2.7: Histogram plots for the whole population pre- and post-puberty. There is a left shift in the histograms post-puberty.

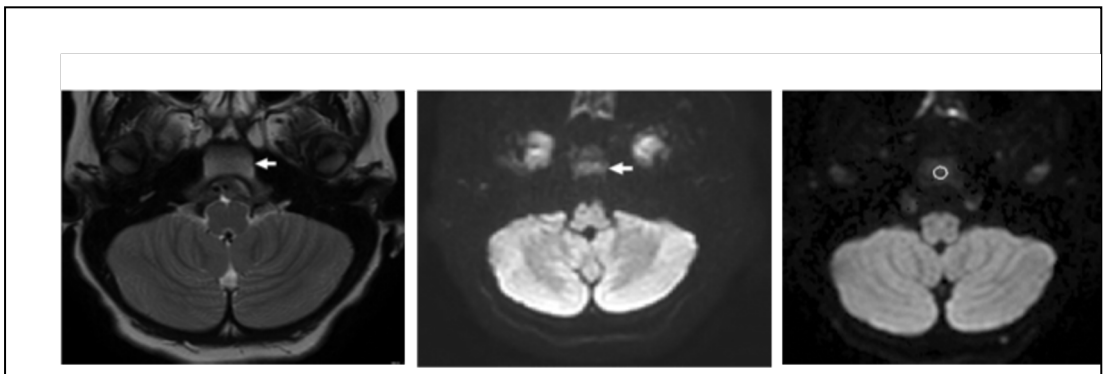


Figure 2.8: Axial T2-W (a), Diffusion weighted (b) and ADC map (c) in a 5.5-year-old pre-pubertal male. Intermediate signal-intensity within the marrow of the clivus is noted in (a) with corresponding high signal intensity in (b). ADC of the hypercellular marrow in (c) is $84.0 \pm 22.2 \text{ mm}^2/\text{s}$.

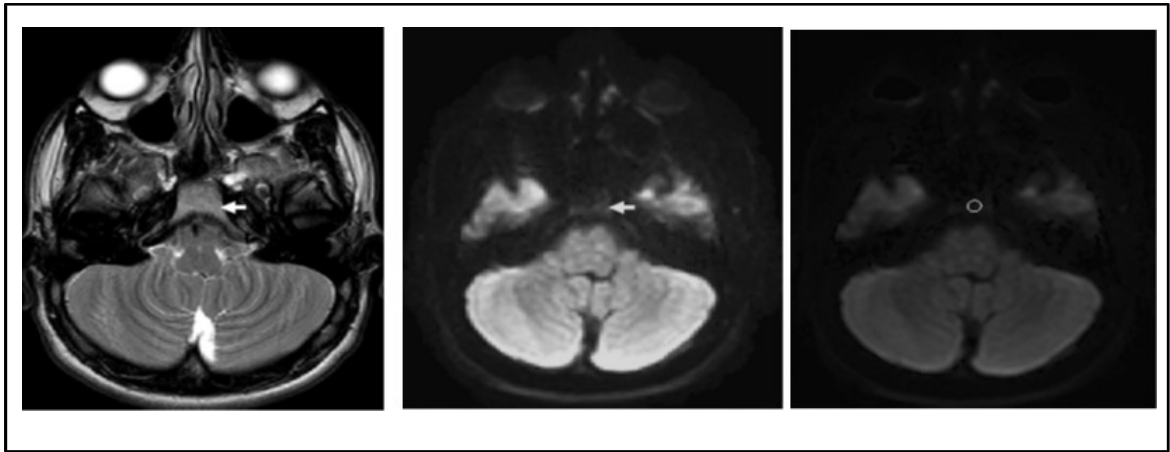


Figure 2.9: Axial T2-W (a), Diffusion weighted (b) and ADC map (c) in a 16.8-year-old post-pubertal male. High signal equivalent to that of fat is noted in the marrow of the clivus in (a) with corresponding low signal intensity on the fat-suppressed diffusion-weighted image in (b). Low ADC ($38.4 \pm 15.9 \text{ mm}^2/\text{s}$) of the fat replaced marrow is evident in (c).

2.4.6 Variation with gender

Pre-puberty, there were no significant differences in mean and median ADC in females vs males ($p= 0.3$ for mean, 0.1 for median and >0.05 at all centile values) (**Table 2.7**).

The pre and post puberty differences seen for the whole cohort also held true for females alone and males alone (**Figure 2.10**) with striking reductions in mean and median ADC and a left shift of histogram centile values (**Figure 2.11**). Differences between the whole cohort comparison pre and post-puberty and the same comparison done by gender (females alone and males alone) were evident, for example the lack of significance between the C90 values for females and the C10 values for males.

	Female pre-pubertal ADC x 10 ⁻⁶ mm ² /s Mean ± std	Female post- pubertal ADC x 10 ⁻⁶ mm ² /s Mean ± std	p- value	Male pre-pubertal ADC x 10 ⁻⁶ mm ² /s Mean ± std	Male post- pubertal ADC x 10 ⁻⁶ mm ² /s Mean ± std	p- value
Mean	70.7 ± 14.8	58.5 ± 16.3	0.04	78.6 ± 21.3	57.8 ± 15.5	0.005
C10	36.9 ± 11.1	28 ± 9	0.03	36.1 ± 20	27.0 ± 10.2	0.15
C25	51.2 ± 11.9	40.2 ± 9.1	0.01	56.9 ± 20.7	39.6 ± 11.7	0.004
C50	69.8 ± 13.7	55.9 ± 10.8	0.009	79.9 ± 21.1	55.6 ± 11.7	0.0002
C75	85.4 ± 16.3	74.2 ± 27.3	0.03	101.7 ± 28.1	73.8 ± 18	0.004
C90	104.0 ± 25.3	93.8 ± 48.1	0.06	116.1 ± 29.7	90.1 ± 39.1	0.008
IQR	34.2 ± 11.5	34 ± 22	0.25	44.8 ± 14.9	34.3 ± 11.7	0.06

Table 2.8: Mean, median and centile vales in female and male subjects showing significant differences before and after puberty.

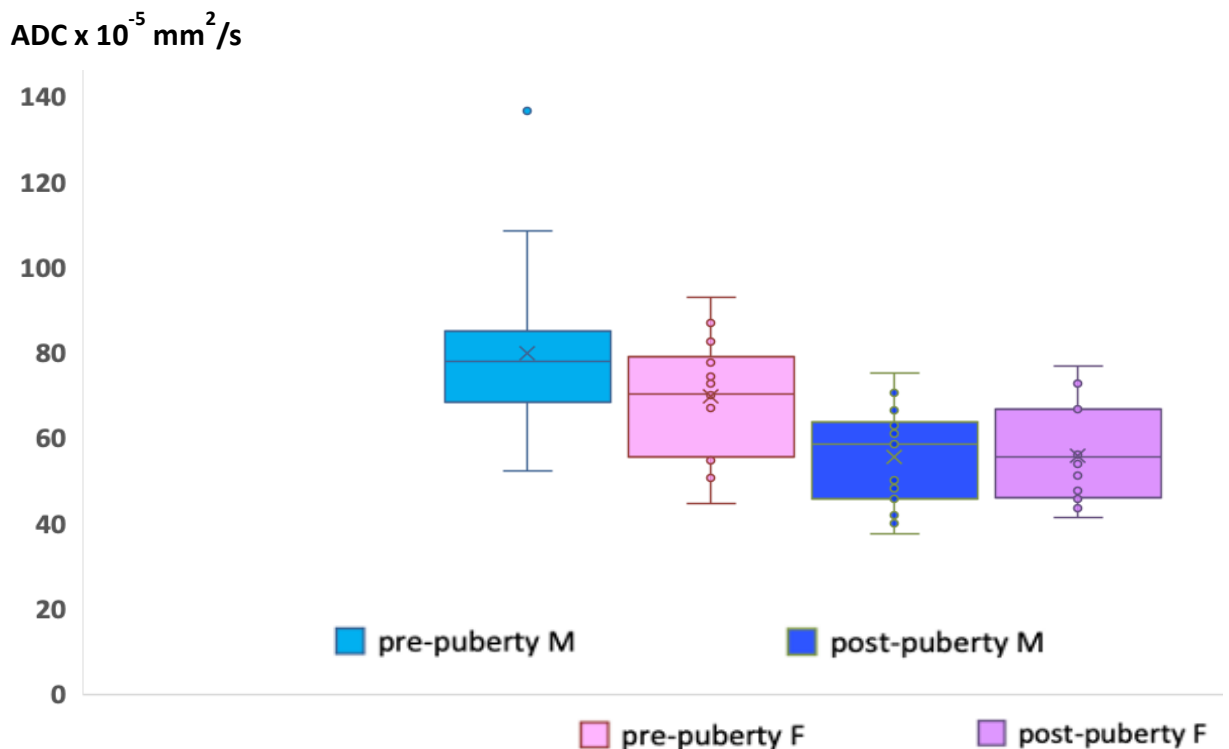


Figure 2.10: Boxplots of pre- and post-pubertal median ADC values in females and males.

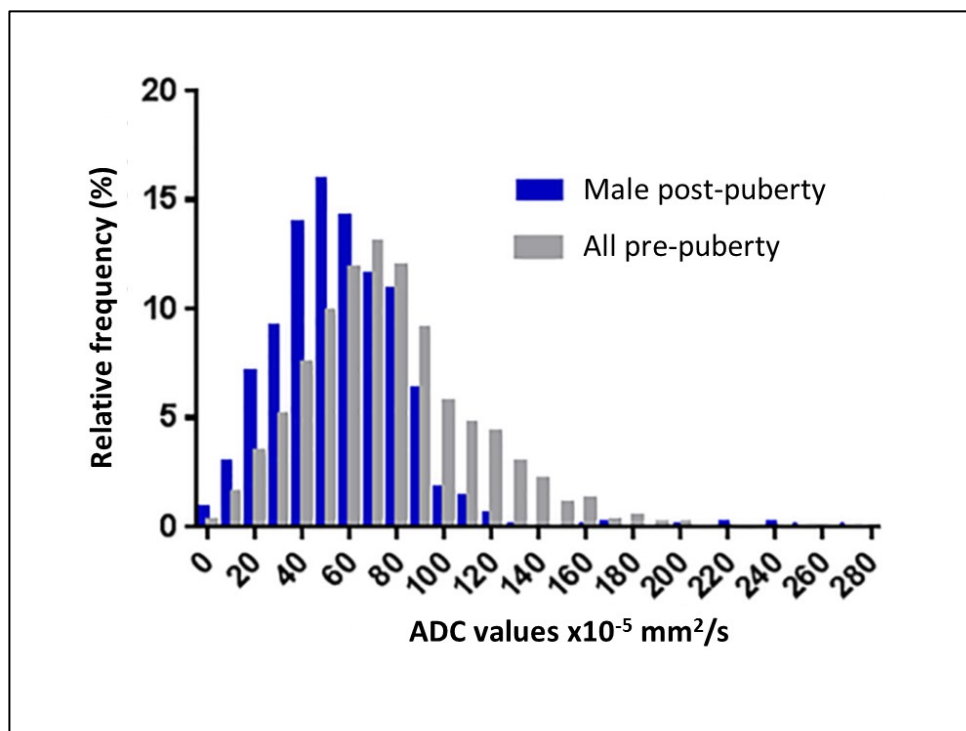
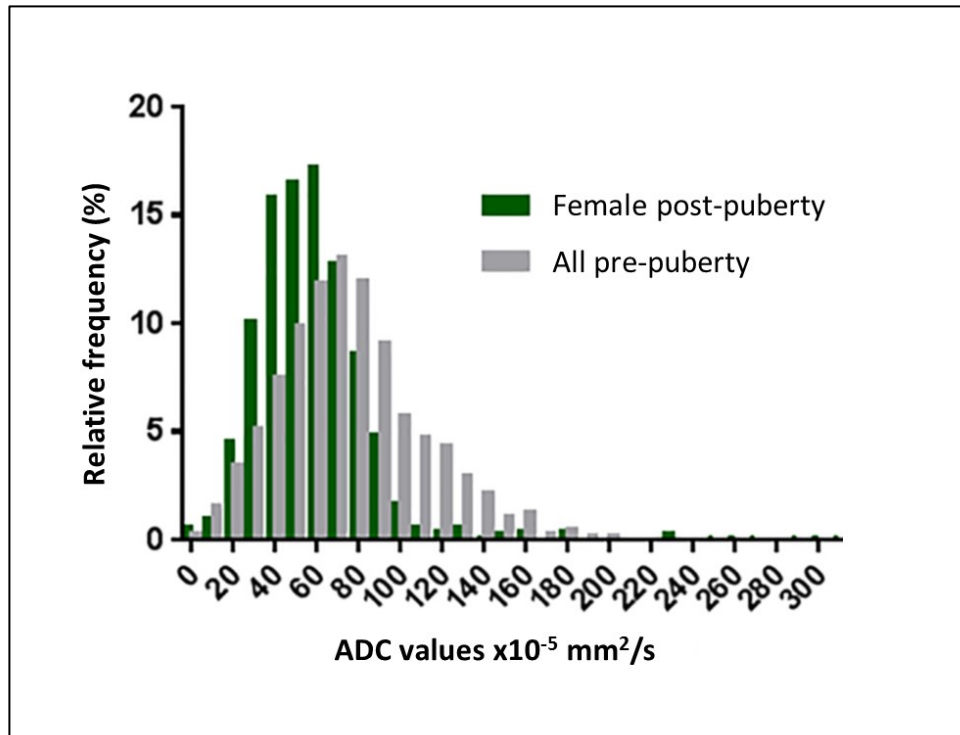


Figure 2.11: Histogram plots for post-pubertal females alone (GREEN) vs all pre-pubertal subjects and males alone (BLUE) vs. all pre-pubertal subjects. There is a left shift in the histograms post-puberty, regardless of gender.

2.5 DISCUSSION

2.5.1 Relationship with age and pubertal status

This is a first report of variation in ADC values in bone marrow in a healthy paediatric population. These have not been previously and univocally demonstrated. Only a few studies are available on focussing on this topic. In my population, there was a trend to a reduction in these values with age, with the 5-9 years old cohort having the highest figures and the male post-puberty group showing the lowest values. A point of particular importance is the robustness of the data in that distribution of values was identical in all four cohorts (5-9 years old, 10 years old – pre-puberty, post-pubertal girls, and post-pubertal boys), as demonstrated by the relative histograms plots (**Figures 2.7 and 2.11**) and by the p values (**Tables 2.5, 2.6, and 2.7**).

A recent publication reporting data in the lumbar spine did not indicate such a change with age as children matured¹¹. Their mean and median ADC values remained between 0.58 and 0.63 x 10⁻³ mm²/s across all age groups (0-2 years, 3-6 years, 7-11 years, 12-14 years, 15-20 years). However, their data did not separate individuals by pubertal status and the distribution of children versus young adults in their cohort is likely to have mostly represented individuals who were chiefly post-pubertal. Post-puberty there is physiological conversion of haematopoietic cells into adipocytes which correlates directly with age,¹² reaching a peak in young adults.

Whilst many reports exist linking sex hormones to cortical bone mass at puberty in both preclinical^{13, 14} and clinical^{15, 16} studies, there is a paucity of data on how the onset of puberty results in measurable changes within the marrow

itself. This has largely been limited by the previous means of studying the bone marrow, which required invasive biopsy and did not interrogate the entire skeleton. The advent of quantitative MRI biomarkers has changed the landscape in this regard^{17, 18} and makes it possible to prospectively derive measurements from bone marrow both within a region or at a whole skeleton level (using whole-body MRI) in order to study changes with normal physiology and with treatment.¹⁹

Marrow adiposity has been inversely related to cortical bone area in young adults²⁰ and to bone mineral content.²¹ However, this step-change at puberty has not been recognised. Although there is extensive evidence linking fat replacement in the marrow of adults to steroid therapy, there is no data linking the increase in marrow fat to the surge of sex steroid hormones at puberty. A recent study in a preclinical mouse model has elegantly demonstrated that leutinizing hormone is involved in haematopoietic stem cell homeostasis. Deletion of the leutinizing hormone growth receptor on haematopoietic stem cells resulted in their continued expansion;²² it may well be that the expression of this receptor particularly at sites within long bones and where haematopoietic function is no longer needed post-puberty is one molecular mechanism driving the replacement of this functionally active tissue with fat.

2.5.2 Region of interest size

Determining a ROI in the skull was challenging. Particularly in the paediatric skull, segmenting out the flat bones introduced too much error when attempting to extract data from a sufficient number of pixels for analysis. A practical approach using the clivus ensured that a 6 mm diameter circular ROI could be obtained on 3 slices so that at least 10 voxels could be included in each scan.

In future, automated segmentation methods may well enable more accurate delineation of the entire skull, which would enable larger scale analyses of this type. In this regard, the Automated Segmentation Task Force formed by a selection of members of the Radiology Research Alliance of the Association of University Radiologists recently published a comprehensive review with a systematic approach by anatomical regions.²³ As expected, CT still plays the main role into the segmentation framework of bones, due to better spatial resolution between the skeleton and adjacent soft tissue structures. Unfortunately, only one study focussed on segmentation of the skull and, although other osseous sites were included in thirty-seven studies, I presume these were mainly done on CT. In the thirty-five MR reports with musculoskeletal applications a wide spectrum of automated segmentation techniques was adopted; the most used methods included hybrid, deformable models, atlas-based, statistical, and graph search, in descending order. First-generation segmentation algorithms — comprising thresholding, region growing, edge detection, and edge tracing — were also enumerated.

2.5.3 Significance of measurements in the clivus

A previous extensive study in 500 subjects, 200 of whom were under 14 years old²³ examined the differences in ADC values by skull location (frontal, temporal, parietal, and occipital) and correlated values with age. Interestingly, the occipital and parietal bones showed a variation with age, with a gradual downward trend between 0 and 30 years, whereas the frontal and temporal bones did not. This is keeping with my findings where the clivus as part of the occipital bone at the skull base shows this change. It indicates that the haemopoietic function of the skull base becomes less important with age as fatty infiltration occurs, while that of the frontal and temporal regions is unaltered into adult life.²⁴ Unfortunately, the values quoted in the study of Li et al. are much higher than in my study, being around $1.0 \times 10^{-3} \text{ mm}^2/\text{s}$. Their data was also acquired at 3 T using b-values of 0 and $750 \text{ s}/\text{mm}^2$. These different technical parameters limit somewhat the comparison between Li's study and mine due to the fact b-values reflect the strength and timing of gradients applied to generate DW images. There is a direct proportion between b-value and the diffusion effects, therefore, the higher the former, the stronger the latter. However, determining ROIs in the flat bones of the skull may well have proved more challenging, particularly in their paediatric subjects.

2.5.4 Relationship of ADC with cellularity

The relationship between bone marrow cellularity and ADC was established more than a decade ago, where a study by Nonomura et al. that examined cellularity in ilium aspirate was correlated with ADC values in 37

adults.²⁵ The 5 children in that study²⁵ did not have bone marrow aspirate performed, but their marrow was considered hypercellular in view of their age (0-3 years). Unfortunately, the b-values used in this study were low (0 and 350 s/mm²), so are likely to reflect perfusional effects rather than true diffusion. This is reflected in absolute values of 0.827 - 0.708 x 10⁻³ for normocellular marrow in children. Unfortunately, also, the absolute cellularity of the aspirates was not quantified, so the relationship between the ADC and cellular “burden” has not been established.

2.5.5 Technical Factors and study limitations

Signal-to-noise ratio is critically important in the reliability of the ADC measurement. This meant that we confined our measurements to ROIs within the clivus. This allowed inclusion of at least 20 voxels in each measurement. It also had the advantage of avoiding sutures within the ROI and having a homogenous area in the centre of the field-of-view from which to derive quantitative data. Other studies of bone marrow in children have not specifically exploited the advantages of measurements within this anatomical area, but overall there is a paucity of bone marrow studies with MRI in children. Those which exist have focussed on larger areas afforded by the vertebrae and iliac bones.²⁶

My study had several limitations. Firstly, it was retrospective and relied on selecting healthy children referred for an MRI brain scan. I attempted to mitigate against errors from inclusion of likely pathologies or treatment related

effects by having very strict inclusion and exclusion criteria. This meant I had to trawl through a large pool of patients. Secondly, only 2 b-values were used in the acquisition and derivation of ADC and one of them was $b=0$. It is now established that elimination of perfusional effects to obtain a true D^* necessitates the lower b-value is $>50 \text{ mm}^2/\text{s}$.²⁷ A third b-value between $50 \text{ mm}^2/\text{s}$ and $1000 \text{ mm}^2/\text{s}$ ensures robustness of the ADC calculation. Unfortunately, this was not available, but my quantified values were similar to other cited literature values.²⁸ Thirdly, I did not directly measure fat-fraction, although this report assumes the relationship between ADC and fat fraction is inverse, so explaining my findings,²⁹ Fourthly, albeit I selected the ROIs within the clivus at the midline in all the cohorts the diameter of the circle varied between 4-6 mm based on the signal-to-noise ratio, as I intentionally avoided to include very noise voxels. Lastly, my assessment of puberty, despite the fact was objective and done on imaging grounds, was not confirmed by blood hormone profiles in these children. Nevertheless, the findings were striking and repeatable when the cohort was additionally divided by gender.

A paper with data from this chapter was published in December 2019
(Appendix 2).

2.6 SUMMARY

The main conclusions of this chapter are:

My null hypothesis is rejected. Particularly, a correlation of ADC with age, puberty, and age exists in children.

Furthermore, this is the first study to document a significant change in marrow ADC related to puberty, using the ADC of marrow in the clivus as a quantitative biomarker.

Lastly, there was no discernible difference by gender.

These data will form the basis for understanding changes that occur in the bone marrow following local and systemic treatments of haematological and non-haematological malignancies described in the following chapters.

2.7 KEY POINTS

- ADC of the clivus bone marrow correlates with age in children; it decreases significantly post-puberty, likely due to replacement of hypercellular marrow with fat.
- There are no gender-related differences in ADC either pre- or post-puberty.

REFERENCES

1. Proytcheva M. Bone marrow evaluation for pediatric patients. *International journal of laboratory hematology*. 2013; 35: 283-9.
2. Chen LT and Weiss L. The development of vertebral bone marrow of human fetuses. *Blood*. 1975; 46: 389-408.

3. Menagh PJ, Turner RT, Jump DB, et al. Growth hormone regulates the balance between bone formation and bone marrow adiposity. *Journal of bone and mineral research : the official journal of the American Society for Bone and Mineral Research*. 2010; 25: 757-768.
4. Blebea JS, Houseni M, Torigian DA, et al. Structural and functional imaging of normal bone marrow and evaluation of its age-related changes. *Seminars in nuclear medicine*. 2007; 37: 185-194.
5. Malkiewicz A and Dzedzic M. Bone marrow reconversion - imaging of physiological changes in bone marrow. *Polish journal of radiology*. 2012; 77: 45-50.
6. Utriainen P, Jaaskelainen J and Voutilainen R. Blood erythrocyte and hemoglobin concentrations in premature adrenarche. *The Journal of clinical endocrinology and metabolism*. 2013; 98: E87-91.
7. Mizoguchi H and Levere RD. Enhancement of heme and globin synthesis in cultured human marrow by certain 5 -H steroid metabolites. *The Journal of experimental medicine*. 1971; 134: 1501-1512.
8. Cristy M. Active bone marrow distribution as a function of age in humans. *Physics in medicine and biology*. 1981; 26: 389-400.
9. Wong AP, Pipitone J, Park MTM, et al. Estimating volumes of the pituitary gland from T1-weighted magnetic-resonance images: effects of age, puberty, testosterone, and estradiol. *NeuroImage*. 2014; 94: 216-21.
10. Alhazmi A, Vargas E, Palomo JM, Hans M, Latimer B and Simpson S. Timing and rate of spheno-occipital synchondrosis closure and its relationship to puberty. *PloS one*. 2017; 12: e0183305.
11. Tschischka A, Schleich C, Boos J, et al. Age-related apparent diffusion coefficients of lumbar vertebrae in healthy children at 1.5 T. *Pediatr. Radiol*. 2018; 48: 1008-1012
12. Zawin JK and Jaramillo D. Conversion of bone marrow in the humerus, sternum, and clavicle: changes with age on MR images. *Radiology*. 1993; 188: 159-164.

13. Izquierdo Ade M, Mishima FD, Carrard VC, Farina M and Nojima Mda C. Effects of induced precocious puberty on cranial growth in female Wistar rats. *European journal of orthodontics*. 2012; 34: 133-140.
14. Yingling VR and Khaneja A. Short-term delay of puberty causes a transient reduction in bone strength in growing female rats. *Bone*. 2006; 38: 67-73.
15. Mahachoklertwattana P, Pootrakul P, Chuansumrit A, et al. Association between bone mineral density and erythropoiesis in Thai children and adolescents with thalassemia syndromes. *Journal of bone and mineral metabolism*. 2006; 24: 146-152.
16. Wang Q, Nicholson PH, Suuriniemi M, et al. Relationship of sex hormones to bone geometric properties and mineral density in early pubertal girls. *The Journal of clinical endocrinology and metabolism*. 2004; 89: 1698-1703.
17. Neubauer H, Evangelista L, Morbach H, et al. Diffusion-weighted MRI of bone marrow oedema, soft tissue oedema and synovitis in paediatric patients: feasibility and initial experience. *Pediatric rheumatology online journal*. 2012; 10:20.
18. Darge K, Jaramillo D and Siegel MJ. Whole-body MRI in children: current status and future applications. *European journal of radiology*. 2008; 68: 289-298.
19. Weber DR, Leonard MB and Zemel BS. Body composition analysis in the pediatric population. *Pediatric endocrinology reviews : PER*. 2012; 10: 130-139.
20. Di Iorgi N, Mo AO, Grimm K, Wren TA, Dorey F and Gilsanz V. Bone acquisition in healthy young females is reciprocally related to marrow adiposity. *The Journal of clinical endocrinology and metabolism*. 2010; 95: 2977-2982.
21. A LN, L JH, Davis M and Casazza K. The relationships among total body fat, bone mineral content and bone marrow adipose tissue in early-pubertal girls. *BoneKEy reports*. 2013; 2: 315.
22. Peng YJ, Yu H, Hao X, et al. Luteinizing hormone signaling restricts hematopoietic stem cell expansion during puberty. 2018; 37.

23. Lenchik L, Heacock L, Weaver A. A, et al. Automated segmentation of tissues using CT and MRI: a systematic review. *Acad Radiol* 2019; 26: 1695-1706
24. Li Q, Pan SN, Yin YM, et al. Normal cranial bone marrow MR imaging pattern with age-related ADC value distribution. *European journal of radiology*. 2011; 80: 471-477.
25. Nonomura Y, Yasumoto M, Yoshimura R, et al. Relationship between bone marrow cellularity and apparent diffusion coefficient. *Journal of magnetic resonance imaging : JMRI*. 2001; 13: 757-760.
26. Herrmann J, Krstin N, Schoennagel BP, et al. Age-related distribution of vertebral bone-marrow diffusivity. *European journal of radiology*. 2012; 81: 4046-4049.
27. Ohno N, Miyati T, Kasai H, et al. Evaluation of perfusion-related and true diffusion in vertebral bone marrow: a preliminary study. *Radiological physics and technology*. 2015; 8: 135-140.
28. Dietrich O, Geith T, Reiser MF and Baur-Melnyk A. Diffusion imaging of the vertebral bone marrow. *NMR in biomedicine*. 2017; 30.
29. Schraml C, Schmid M, Gatidis S, et al. Multiparametric analysis of bone marrow in cancer patients using simultaneous PET/MR imaging: Correlation of fat fraction, diffusivity, metabolic activity, and anthropometric data. *Journal of magnetic resonance imaging: JMRI*. 2015; 42: 1048-1056.

CHAPTER 3 – Investigating the effects of radiation and proton beam therapy on bone marrow: cranial ADC studies

The main purpose of this chapter is to retrospectively investigate the longitudinal effects of conventional radiotherapy with photons (RT) and of the more recent technique adopting protons (PBT) on the ADC values calculated in the marrow of the clivus in a paediatric population affected by intracranial neoplasms.

Furthermore, a comparison between the aforementioned types of treatment with regard to the effects on ADC of the clival marrow will be illustrated.

3.1 INTRODUCTION

Cranial irradiation is used as standard-of care for paediatric brain tumours. The effects of radiation on normal bone marrow in children are, therefore, most easily studied in the skull. RT is used as an adjunctive treatment to primary surgery in the majority of cases. Although paediatric brain tumours come in a variety of forms with varying types, growth patterns, locations, neurological effects and prognosis, the radiation regimens used do not vary substantially. Chemotherapy can also form part of the treatment strategy depending on the tumour type.¹

3.1.1 Paediatric brain tumours

The wide spectrum of histological tumour types, subvariants, and degree of malignant potentiality of paediatric brain tumours is illustrated in **Figure 3.1** and includes benign, borderline, and malignant lesions.

The World Health Organization classification considers the anatomical location, apparent cell of origin, histological features, and grade to facilitate the determination of prognosis, to choose the most appropriate treatment, and to identify patients eligible for clinical trials. In 2016 an official reclassification was published,² which includes genetic, epigenetic, and molecular information in order to predict tumour behaviour and to adopt a more targeted and personalised therapy for each patient.³

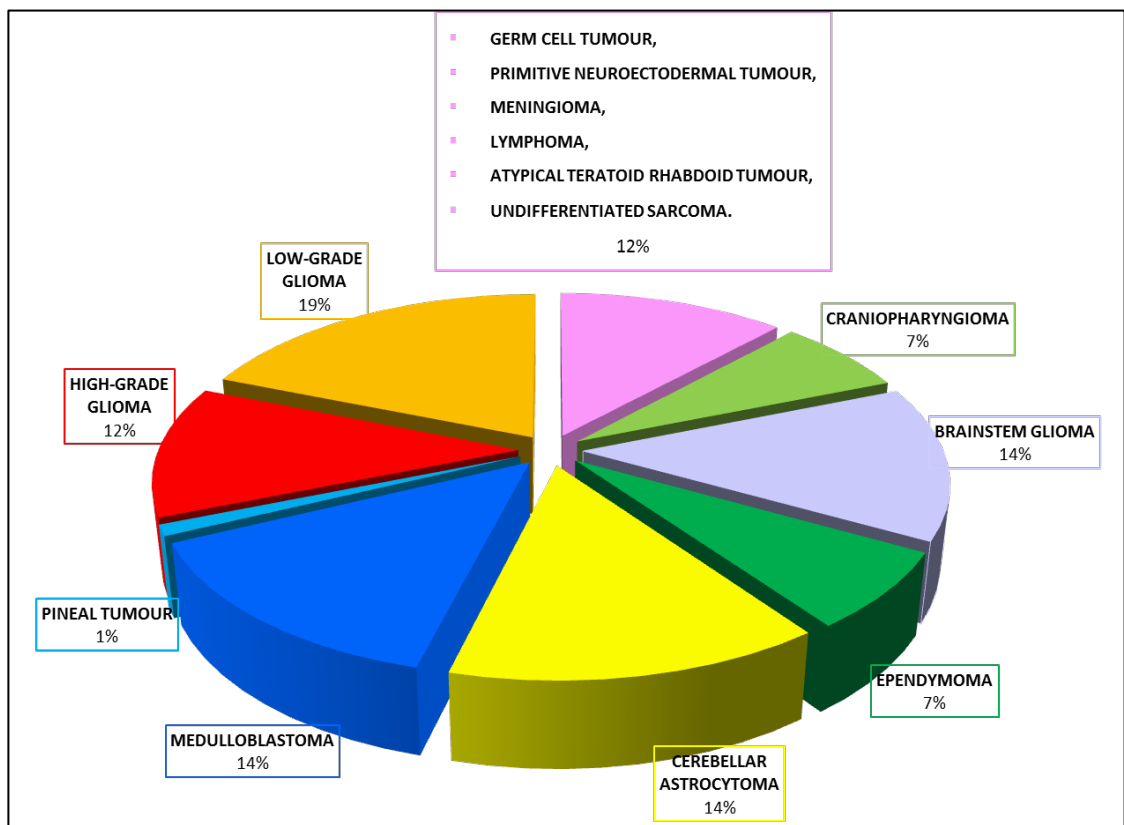


Figure 3.1: Adapted from 'Principles and Practice of Pediatric Oncology' Philip A. Pizzo and David G. Poplak, Lippincott Williams and Wilkins, 6th edition, 2011 – chapter 26 A, pg.718.

3.1.2 Variations in treatment schedules

Low- and high-grade gliomas (including brainstem gliomas) form the majority of neoplasms. Treatment in these cases usually involves surgery, but the age of the child, the grade of tumour, its location and resectability all determine whether RT is utilised instead of or in addition to surgery. Medulloblastomas also form a substantial proportion of patients who require RT following surgery. In benign tumours, such as craniopharyngiomas, that develop anywhere along the infundibular stalk from the floor of the third ventricle to the pituitary gland, radiation to the sellar/suprasellar region can cause significant morbidity (diabetes insipidus, bitemporal hemianopia, and adrenal insufficiency) so that surgical treatment alone is usually preferred. This ranges from drainage of the cystic component to gross total resection, subtotal removal or biopsy only, depending on the size of the tumour and on the extent of disease. Subtotal resection or recurrence with a favourable margin between the optic chiasm and the neoplasm benefits from adjuvant RT and stereotactic radiosurgery in terms of progression-free survival.⁴ Germinomas on the other hand, although rare, are highly responsive to RT, so that this is often the primary treatment modality.⁵

3.1.3 Treatment related toxicity in photon vs. proton beam therapy

3.1.3.1 *Toxicity and bone marrow effects*

Unfortunately, RT comes with toxic side-effects to surrounding normal tissues. An international primary prospective Registry for the Evaluation of Side Effects After Radiation in Childhood and Adolescence (RiSK) database with

standardized documentation of data was initiated in Germany in 2001. Subsequently, over the last decade, a collaboration project (International Project on Prospective Analysis of Radiotoxicity in Childhood and Adolescence, IPPARCA) between the Swedish Working Group for Pediatric Radiation Therapy and RiSK was created to increase the number of cases. This has allowed researchers and clinicians to pool data for toxicity.⁶ Interestingly, the data show that in patients experiencing Grade 3 or 4 acute toxicity (n=315 of 1500 subjects), the biggest source of problems was from effects on bone marrow (63.8%). Maximum chronic toxicity was also from effects on bone marrow (n=663, 18.9%). This highlights bone marrow as a key organ in developing radiation-induced long-term effects.

3.1.3.2 Other common toxicities of cranial irradiation

3.1.3.2.1 Endocrine

The most common radiation-induced endocrinopathies are hypothyroidism and growth hormone deficiency. Fifty percent to 80% of children treated with craniospinal RT for brain tumors will experience growth failure. In addition, precocious puberty, undetected hypothyroidism and poor nutrition have been described.⁷

3.1.3.2.2 Neurocognitive

Childhood cancer survivors exposed to CNS irradiation are at increased risk for neurocognitive deficits. Armstrong et al. have reported associations between region-specific radiation dose and self-reported neurocognitive and health-related quality of life (HRQOL) outcomes in 818 adult survivors of

childhood central nervous system (CNS) malignancies from the Childhood Cancer Survivor Study and shown higher rates of neuropsychological and HRQOL outcomes compared to a sibling control group. Impairment in memory and reduced social functioning were key findings. In particular, irradiation of the temporal region, but not other regions, was significantly associated with memory problems; this was dose dependent.⁸ Irradiation of the temporal region was associated with physical limitations at all radiation levels, poor general health at ≥ 30 to < 50 and ≥ 50 Gy, and poor social functioning at ≥ 50 Gy in a dose-dependent manner.

3.1.3.2.3 Lifetime risk of new cancers

In a paediatric population, where there is a potential long life expectancy, the risk of secondary cancers from radiation therapy is a concern. Despite the excellent dose conformity of intensity modulated RT, adjacent normal tissues inevitably receive some radiation dose. With PBT, this is likely to be smaller, given the much sharper fall-off of beam energy. As it would take in excess of 30 years to monitor the development of secondary cancers as a result of these treatments. Tamura et al.⁹ have modelled the lifetime attributable risk of secondary cancer based on dose distribution data from a 3D radiation treatment planning system. They showed a significant difference between proton beam therapy and IMRT: the cumulative lifetime attributable risk difference was $1.02 \pm 0.52\%$ for cranial irradiation.

3.2 AIM

To examine the effect of conventional radiotherapy and proton beam therapy on apparent diffusion coefficient of normal skull marrow in children treated because of a brain tumour.

3.2.1 Objectives

To establish the reproducibility of the ADC measurement in the bone marrow of the clivus.

To measure early (within 3 months) and late (beyond 3 months) changes in ADC of the bone marrow of the clivus following RT to the head and interpret them in the context of ADC measurement reproducibility.

To measure early (within 3 months) and late (beyond 3 months) changes in ADC of the bone marrow of the clivus following PBT to the head and interpret them in the context of ADC measurement reproducibility.

3.3. METHODS

3.3.1 Measurement reproducibility cohort

Under operational ethical permission (CCR 1406, duration of scan less than 10 minutes) DW-MRI acquisition was run twice — before and after the morphological sequences included in the standard protocol — in 6 children having a brain MRI for clinical purposes. In 4 children DW-MRI was obtained on 2 separate occasions after a 1 to 4-month interval. Scans were done as part of routine follow-up at least 6 months after RT and where no interim treatment was administered.

3.3.2 Photon therapy (RT) cohort

3.3.2.1 Patient selection

This study was approved as a Service Evaluation (662) by The Royal Marsden (**Appendix 1**). Paediatric subjects affected by central nervous system tumours who had RT between March 2006 and July 2017 at The Royal Marsden Hospital were identified. This included 776 individuals. This cohort was refined further based on inclusion and exclusion criteria as below:

3.3.2.1.1 Inclusion criteria

- aged between 5-17 years old
- affected by neurological or intracranial endocrine tumour
- without bony metastatic disease
- conventional RT administered at The Royal Marsden Hospital
- no neoadjuvant or concomitant chemotherapy
- axial pre- and post-RT DW-MRI scans available
- first post-treatment scan within 3 months of completion of treatment

3.3.2.1.2 Exclusion criteria

- patients on any type of medication (including chemotherapy)
- dental brace
- artefacts on DW-MRI (or other main sequences making identification of clivus unreliable)
- bony lesions or illness

113 patients met the first 5 inclusion criteria. These patients were then reviewed by cross-checking all the clinical and demographical information available on the electronic patient record system (**Figure 3.2**). The availability of pre- and post-treatment DW-MRI was established alongside the availability of

an early post-treatment scan within 3 months of completion of treatment. After examining their MR scans on PACS and applying the exclusion criteria (which resulted in 663 exclusions), I identified 12 patients in whom analysable (at least 2 b-values available for generating ADC maps available; some scans from external providers only acquired $b=1000 \text{ s/mm}^2$) pre- and post-DW-MRI sequences were available. These examinations were anonymised and stored on the data storage (XNAT) platform.

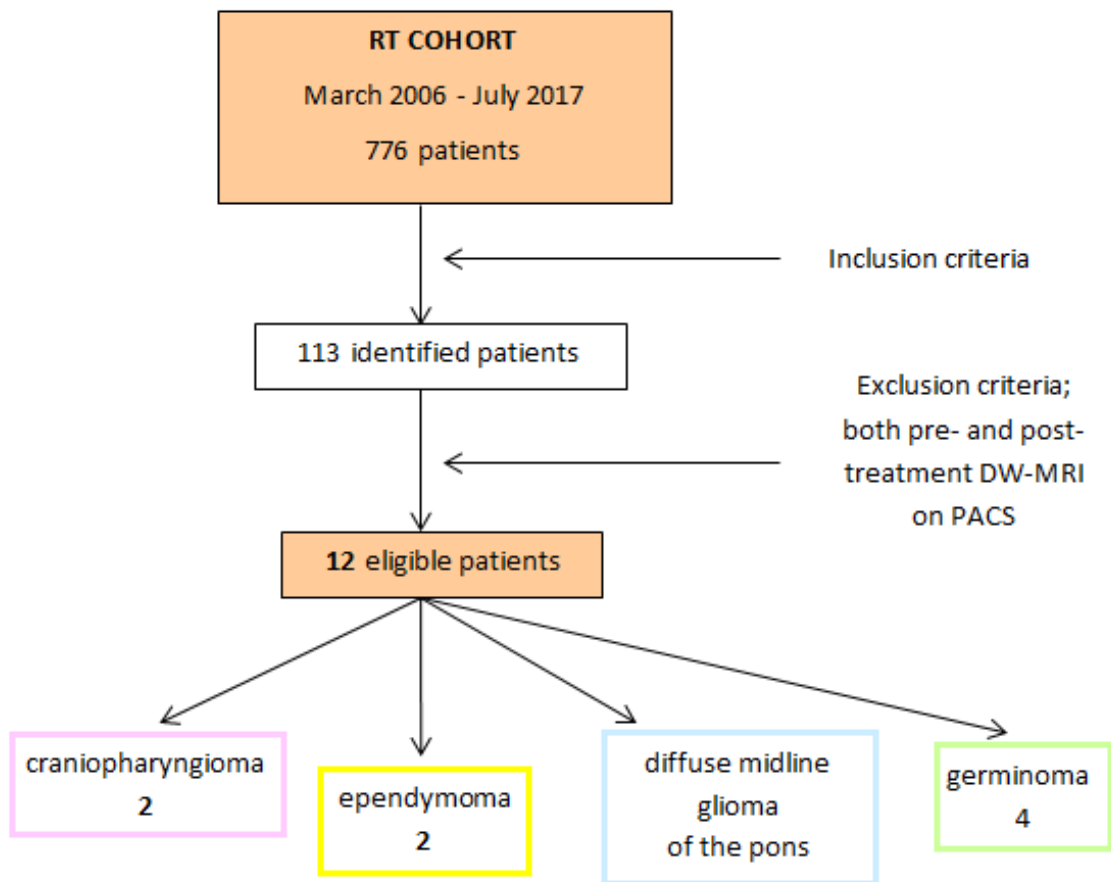


Figure 3.2: Derivation of patients for RT cohort

3.3.2.2 Dose evaluation

Correlation with the DICOM files of the RT plans for the 12 patients included in the cohort was carried out in collaboration with the paediatric

oncology Unit. Pre-treatment CT and MRI scans were reviewed with Dr Enrico Clarke who checked if the clivus was included in the field of treatment and calculated the dose administered.

MR scans were analysed as described in Section 2.3.

3.3.3 Proton beam therapy (PBT) cohort

3.3.3.1 Patient selection

Between 2012 and July 2017, 112 children with neurological/endocrine primary brain tumours were treated with PBT to the brain or intracranial structures courtesy of the Proton Overseas Programme (treatment performed in Jacksonville, Florida or Oklahoma City, Oklahoma). These cases were identified retrospectively from The Royal Marsden Hospital Electronic Patient Record as part of a Service Evaluation (**Appendix 1**) by applying the first 5 inclusion criteria as set out below:

3.3.3.1.1 Inclusion criteria

- aged between 5-17 years old
- affected by neurological or intracranial endocrine tumour
- without bony metastatic disease
- PBT administered at the UFHealth Proton Therapy in Jacksonville (FL) or at the ProCure Proton Therapy Centre in Oklahoma City (OK)
- no neoadjuvant or concomitant chemotherapy
- axial pre- and post-PBT DW-MRI scans available

3.3.3.1.2 Exclusion criteria

- patients on any type of medication (including chemotherapy)
- dental brace
- artefacts on DW-MRI (or other main sequences making identification of clivus unreliable)
- bony lesions or illness

After applying the exclusion criteria and reviewing all pre- and post-treatment MR studies on PACS (which resulted in 98 exclusions), I identified 14 eligible patients with DW-MRI scans available before and after treatment; Unfortunately, four of them had external examinations with DW-MRI images acquire

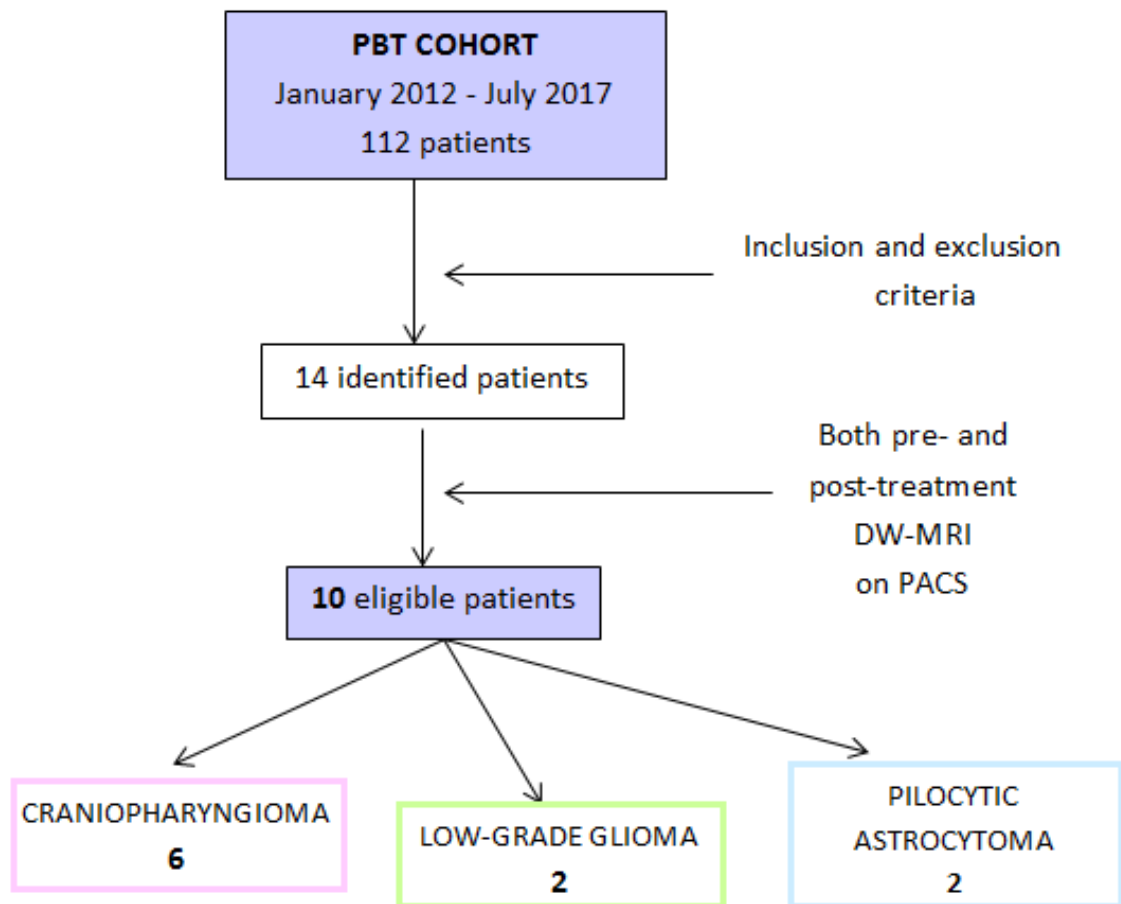


Figure 3.3: Derivation of patients for PBT cohort.

d at $b=1,000 \text{ s/mm}^2$ only. ADC calculation was not possible in these cases. Therefore, a final cohort of 10 children was suitable for analysis.

3.3.3.2 Dose evaluation

The DICOM files with the PBT plans from for the 10 patients were obtained from the 2 external treatment centres. The inclusion of the clivus in the field of treatment was confirmed and the dose which was administered was calculated (Dr Enrico Clarke).

3.3.4 Image acquisition

Children in both cohorts had been scanned at 1.5T (between November 2007 and September 2017).

Axial images were acquired with a slice thickness of 5-6 mm and included T1-W spin echo pre- and post-Gadolinium (Gd) contrast agent, T2-W turbo spin echo, DW-MRI with $b=0$ and $1,000 \text{ s/mm}^2$, and subsequent derivation of an ADC map. Protocol parameters of the free-breath acquired echo-planar 2-dimensional diffusion sequence are illustrated in **Figure 3.4 a** and **b**; particularly, three non-collinear diffusion gradient directions (x, y, and z) were applied.

Coronal images comprised T1-W spin echo pre- and post-Gd administration both with a slice thickness of 3 mm and T2-W post-Gd FLAIR, both with slice thickness of 6 mm, and finally sagittal T1-W spin echo post-Gd with a slice thickness of 5 mm. Imaging examinations were anonymised and data were transferred to the Institute of Cancer Research through the web-platform XNAT, where they are stored.

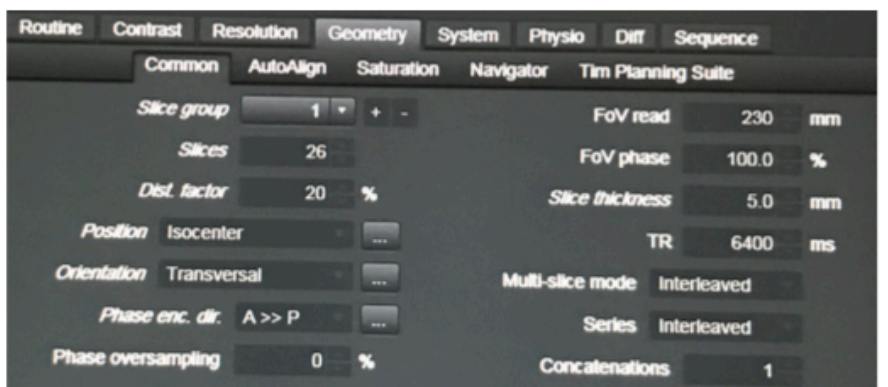
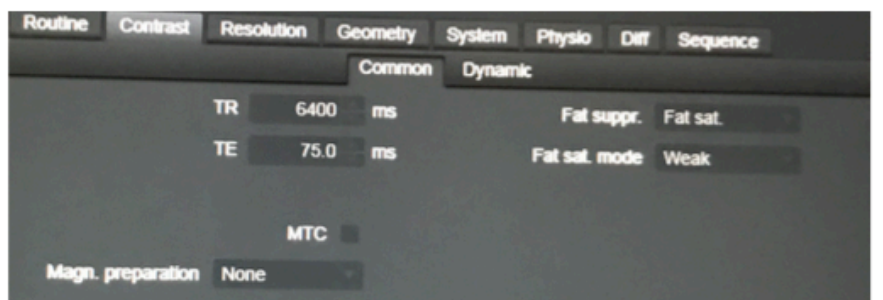
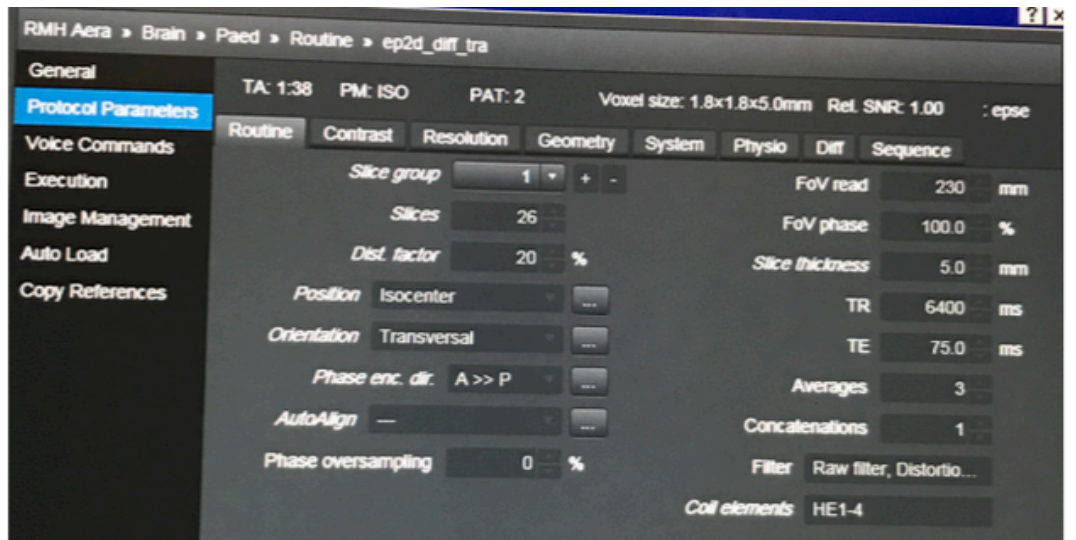


Figure 3.4 a: Protocol parameters of the DW-MRI of the head.

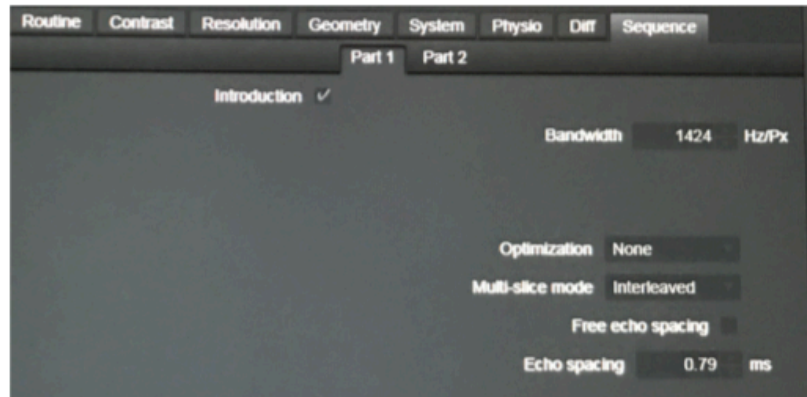
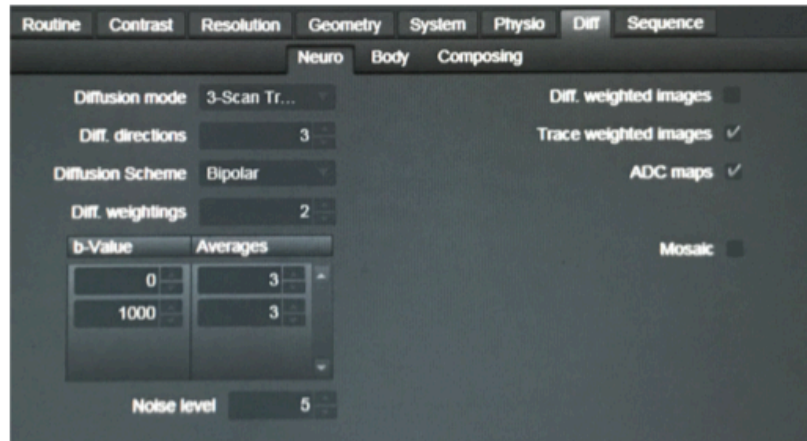
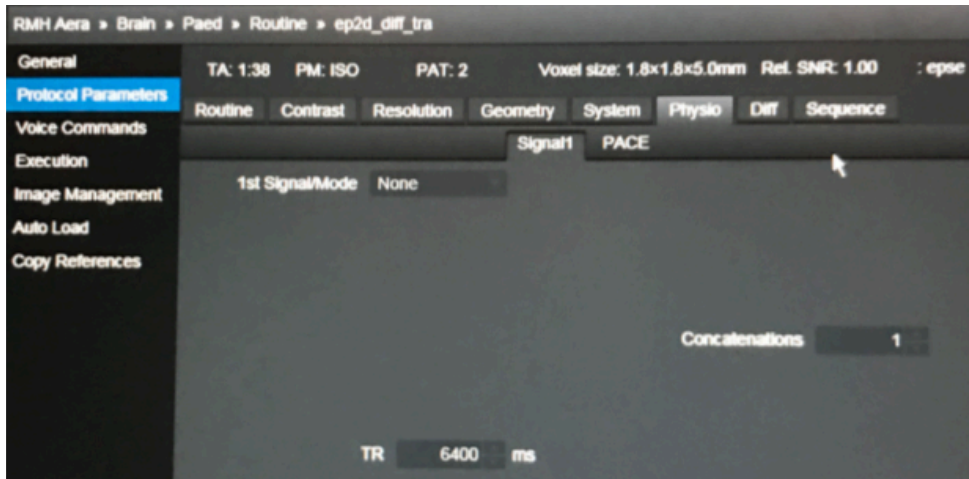


Figure 3.4 b: Protocol parameters of the DW-MRI of the head.

Pt	Baseline scan date	MR Scanner	Treatment completion date	Early post-treatment scan date	MR Scanner	Late post-treatment scan date	MR Scanner
RT COHORT							
1	25 th Mar 2008	Signa Excite	17 th Jul 2008	4 th Sep 2008	Intera	22 nd Jan 2009	Intera
2	24 th Jan 2011	Optima	17 th Jun 2011	22 nd Sep 2011	Aera	30 th May 2012	Avanto
3	12 th Mar 2009	Intera	8 th May 2009	9 th Jul 2009	Intera	1 st Sep 2009	Intera
4	13 th Apr 2010	Avanto*	8 th Jul 2010	6 th Oct 2010	Avanto	/	/
5	14 th Apr 2016	Avanto*	6 th May 2016	29 th Jun 2016	Aera	7 th Oct 2016	Aera
6	23 rd Dec 2015	Avanto*	19 th Feb 2016	23 rd Mar 2016	Avanto	29 th Jun 2016	Avanto
7	19 th Jun 2014	Avanto*	21 st Jul 2014	8 th Sep 2014	Aera	/	/
8	2 nd May 2017	Achieva	24 th May 2017	26 th Jun 2017	Achieva	8 th Sep 2017	Avanto
9	1 st Nov 2007	Signa Excite	15 th Jan 2008	21 st Apr 2008	Intera	/	/
10	12 th May 2015	Aera	9 th Sep 2015	20 th Feb 2015	Aera	19 th Jan 2016	Aera
11	9 th Jun 2010	Avanto*	25 th Aug 2010	1 st Nov 2010	Avanto	/	/
12	25 th Apr 2012	Aera	10 th Aug 2012	4 th Sep 2012	Aera	22 nd Nov 2012	Aera
PBT COHORT							
1	3 rd Aug 2015	Aera	29 th Mar	10 th May	Aera	/	/
2	27 th Sep 2012	Aera	21 st Feb	9 th May 2013	Aera	15 th Aug	Aera
3	4 th May 2016	Avanto*	21 st Sep	1 st Dec 2016	Aera	16 th Mar	Avanto
4	5 th Nov 2015	Avanto	29 th Feb	13 th Apr	Avanto	18 th Jul 2016	Aera
5	12 th Sep 2011	Aera	1 st Feb 2012	26 th Mar	Aera	24 th Jul 2012	Aera
6	21 st Jun 2012	Aera	29 th Aug	1 st Nov 2012	Aera	/	/
7	23 rd Dec 2013	Aera	25 th Mar	4 th Jun 2014	Avanto	22 nd Jul 2014	Avanto
8	23 rd Jan 2013	Aera	17 th Apr	20 th Jun 2013	Aera	/	/
9	5 th Oct 2016	Achieva	28 th Apr	27 th Jun 2017	Aera	10 th Oct	Aera
10	28 th Apr 2014	Avanto*	11 th Aug	17 th Sep	Avanto	21 st Nov	Avanto*

Table 3.1: Relationship of scan timings to end of treatment and scanner used for assessment at each time-point.

3.3.5 Image analysis

3.3.5.1 Method of region of interest delineation

Both axial T2-W images and coronal (T1- or T2-W) were used to identify the exact location of the clivus. The DW-MRI images were correlated with morphological T2-W images. A circular region-of-interest (ROI) of approximately 4-5 mm in diameter was drawn within the clivus, on a midline slice of the $b=1000$ s/mm² diffusion-weighted images using in-house software (Adept®, The Institute of Cancer Research). Data from the entire volume of interest (2 or 3 contiguous slices) were obtained for statistical analysis.

3.3.5.2 ADC calculation

As data was acquired with 2 b-values (0 and 1000 s/mm² routinely acquired in a standard MRI brain scan), ADC was calculated through a monoexponential fit of the data, which resulted in ADC maps (cf. 2.3.3). ADC values on a voxel-by-voxel basis were documented. Aggregate values and descriptive statistics were obtained for each patient. In addition, all data for the entire cohort at each time point were pooled and histograms plotted from which median and centile values were derived representative of each cohort at baseline, early (within 3 months) and late (beyond 3 months) time points.

DWI acquisition	1.5 T Siemens Aera	1.5 T Siemens Avanto						1.5 T Philips Intera	1.5 T Philips Ingenia Achieva	1.5 T GE Signa Excite	1.5 T GE Optima
Hospital	The Royal Marsden	The Royal Marsden	*Kent & Canterbury	*Frimley Park	*East Kent Queen Elizabeth the Queen Mother	*Croydon University	*The Portland	The Royal Marsden	St George's Atkinson Morley	King's College	East Surrey
TR	5,900	3,500	3,100	3,300	3,400	3,900	4,500	3,200	4,300	6,000	8,000
TE	75	75	90	100	100	100	100	90	90	70	100
Slice thickness	5 mm	5 mm									
Readout	Echo-planar										
b-values acquired	0 - 1,000	0 - 1,000	0 - 1,000	0 - 1,000	0 - 500 - 1,000	0 - 500 - 1,000	0 - 1,000	0 - 1,000	0 - 1,000	0 - 1,000	0 - 1,000
b-values utilized for ADC maps	0 - 1,000	0 - 1,000									

Table 3.2 Diffusion-weighted image acquisition protocol for the different scanners used in this study

3.3.5.3 Statistical analysis

Statistical analysis was performed using GraphPad Prism software (version 7.04, GraphPad Incorporated company, California). Bland-Altman plots of difference between measurements versus mean were used to assess the reproducibility of the data by assessing the 95% confidence intervals.

In the treatment effects cohorts, descriptive statistics were used to describe the data. Additionally, ADC data recorded the median, mean, 10th, 25th, 75th, and 90th percentile values. Frequency distributions were used to illustrate the distribution of the mean ADC values before and after treatment.

3.4 RESULTS

3.4.1 Measurement reproducibility

10 patients aged 8-16 years (median 12.9 years) had DW-MRI performed twice to assess reproducibility. 95% confidence intervals of ADC measurements in the reproducibility cohort ranged from -5.5 to +11% (**Figure 3.5**).

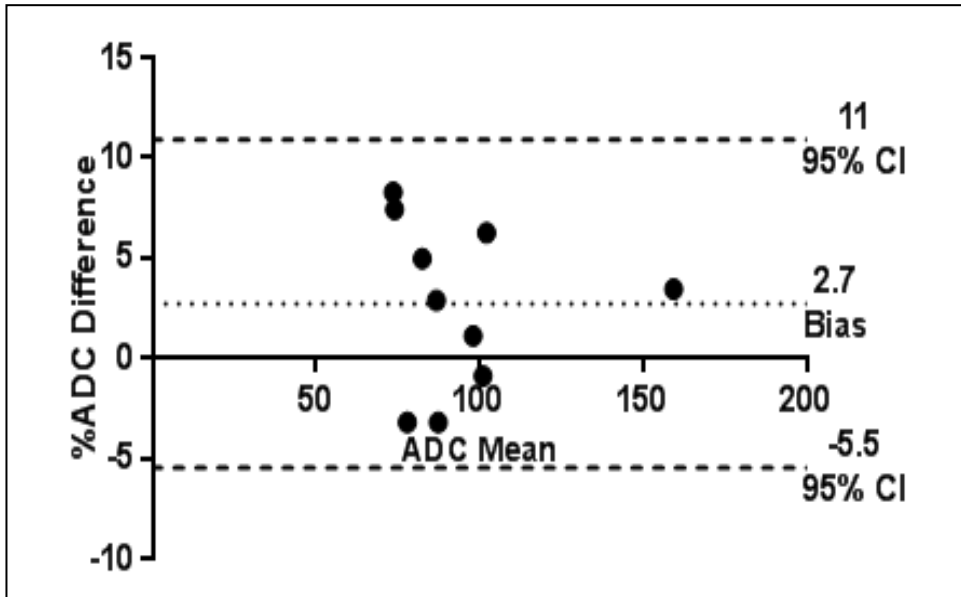


Figure 3.5: Bland-Altman plot showing reproducibility of bone marrow ADC values from the clivus in children.

3.4.2 Photon therapy cohort

3.4.2.1 Patients' characteristics

12 children who fulfilled the inclusion criteria were categorized as follows:

- | | | |
|-----------------------------|------------|-----------|
| 1) craniopharyngioma | 2 patients | 2 F |
| 2) ependymoma | 2 patients | 1 M + 1 F |
| 3) diffuse intrinsic glioma | 4 patients | 2 M + 2 F |
| 4) germinoma | 4 patients | 3 M + 1 F |

3.4.2.2 Regions-of-interest size

The calibre of the circle drawn as a region of interest in the midline of the clivus ranged from 4 to 6 mm. However, a minimum number of 10 voxels was ensured with voxels ranging from 10 to 120 (Pre-treatment median 73, lower quartile 24, upper quartile 115; 1-3 months post-treatment median 26, lower quartile 23, upper quartile 104; 3-6 months post-treatment median 14, lower quartile 10, upper quartile 43).

3.4.2.3 Dose

Table 3.3 lists the radiation dose (minimum, mean, maximum, and total) received by the clivus in each patient during treatment. The clivus of the two patients with craniopharyngioma received 50 Gy, whilst the clivus received 54 Gy in the two patients with ependymoma (one of the latter had been irradiated 3 years earlier where the clivus received 50.1 Gy). In children with diffuse intrinsic pontine/cerebellar glioma, the dose to the clivus was 39 Gy in 3 of 4 cases with one child receiving 54 Gy. In all the four individuals with germinoma the clivus received 40 Gy.

PT	DIAGNOSIS	GENDER	AGE	clivus ROI vol (cm ³)	min dose (cGy)	max dose (cGy)	mean dose (cGy)	sd	treatment completed	prescription	total dose
1	craniopharyngioma & squamous cell carcinoma right temporal lobe	F	7	0.24	4459.0	4974.3	4845.8	102.2	Jul 2008	50Gy/30#	50 Gy
2	craniopharyngioma	F	13	0.24	2764.3	4814.0	4219.3	525.7	Jun 2011	50Gy/30#	50 Gy
3	spinal cord ependymoma	M	8	0.24	312.8	589.8	408.8	90.2	Aug 2006	50.1Gy/30#	104.1 Gy
				0.25	2670.1	4801.2	3427.3	474.4	May 2009	54Gy/30#	
4	recurrent right parietal anaplastic ependymoma	F	11	0.25	79.2	120.6	99.0	13.6	Oct 2014	54Gy/30#	54 Gy
5	diffuse intrinsic pontine glioma	F	5	0.25	851.5	883.8	870.8	8.5	May 2016	9Gy/3#	39 Gy
					2844.4	2990.4	2919.1	35.0		+ 30Gy/10#	
6	diffuse astrocytoma invading pons and left cerebellum	M	9	0.22	3974.8	5368.4	4981.7	295.2	Feb 2016	54Gy/30#	54 Gy
7	diffuse intrinsic pontine glioma	F	10	0.20	3593.0	3898.3	3792.2	58.5	Jul 2014	39Gy/13#	39 Gy
8	diffuse intrinsic pontine glioma	M	11	0.25	916.8	923.3	920.9	1.5	May 2017	9Gy/3#	39 Gy
					2872.9	2962.6	2930.1	19.8		+ 30Gy/10#	
9	suprasellar germinoma	M	10	0.20	1526.6	2279.7	1992.6	252.9	Jan 2008	24Gy/15#	40 Gy
					660.0	1502.9	1131.7	242.7		+16Gy/10#	
10	germinoma of pituitary stalk	F	11	0.25	2157.8	2343.2	2274.5	60.3	Sep 2015	24Gy/15#	40 Gy
					1401.5	1580.9	1530.2	45.1		+ 16Gy/10#	
11	left thalamic germinoma	M	17	0.25	2269.3	2351.6	2311.9	19.9	Aug 2010	24Gy/15#	40 Gy
					312.9	349.1	332.3	7.6		+16Gy/10#	
12	germinoma septum pellucidum	M	17	0.24	1072.6	2237.3	1902.4	313.6	May 2012	24Gy/15#	40 Gy
					101.5	329.2	165.3	63.7		+ 16Gy/10#	

Table 3.3: Radiation dose to the clivus colour coded by tumour type.

NB: The split dose in the prescription column indicates the dose to the whole brain and the boost dose to the neoplasm.

3.4.2.4 Longitudinal treatment effects with radiotherapy (RT) on ADC of clivus

All patients were treated at The Royal Marsden Hospital. All twelve patients had at least one post-treatment scan including DW-MRI; 8 out of 12 had also a second MRI examination. Post-treatment follow-up scans were at a median of 1.6 months after the end of treatment (lower quartile 1.1, upper quartile 1.8 months) for the earlier time point and 4.3 months (lower quartile 3.6, upper quartile 6.1 months) for the later time-point.

On baseline scans mean ADC values fluctuated between 70.6 ± 23.1 s/mm² and 155.6 ± 57.3 s/mm². On the first post-treatment assessment, mean ADC values ranged from 89.2 ± 17.9 s/mm² (1.1 months after completion of radiotherapy) to 274.4 ± 78.7 s/mm² (0.8 months after completion of radiotherapy, **Table 3.2**). In the 8 patients who had follow-up MRI at 3-6 months, mean ADC values ranged between 64 ± 26.3 s/mm² (6.4 months after RT) and 159.4 ± 51.4 s/mm² (3.8 months after RT, **Table 3.2**).

Although the patients in the RT cohort underwent MR examinations of the head on different scanners (**Table 3.1**), key technical parameters — all had echo-planar readout, b values utilised for the ADC maps were always 0 and 1,000 s/mm², TR was mostly around 4,000 and $70 < TE < 100$ — were identical or similar (**Table 3.2**). Moreover, the intra-observer reproducibility with a variability of $\leq 10\%$ ensures that a longitudinal evaluation of the post-treatment marrow ADC trend can be performed.

8 out of 12 children treated with RT showed an increase in mean ADC values on the first post-treatment scan of $>11\%$ (median 39.2% lower quartile, LQ 23.9%, upper quartile, UQ 54.5%); no decreases below measurement

reproducibility were seen. ADC then fell in 4 out 8 patients who had a second follow-up (5 months), but continued to rise in 2, stable in 2 (**Figure 3.6**). Histogram shifts are shown in **Figure 3.7**. Centile values for individual patients in **Table 3.5** show that data from individual subjects mirrored the histogram shifts of the aggregated data from the whole cohort.

Pt	Diagnosis	Gender	Age	Baseline ADC mean \pm SD	1-3 month time-point ADC (mean \pm SD)	% ADC change from baseline at time-point 1	Time interval from end of RT (months)	3-6 month time-point ADC (mean \pm SD)	Time interval from end of RT (months)	% ADC change from baseline at time-point 2
1	craniopharyngioma & right temporal squamous cell carcinoma	F	7	74 \pm 40.8	94.2 \pm 49.8	27	1.8	64 \pm 26.3	6.4	-13
2	craniopharyngioma	F	13	99.8 \pm 42.3	/	/	/	97.1 \pm 33.1	-3	3.2
3	spinal cord ependymoma	M	8	80.1 \pm 22.2	151.7 \pm 85.1	89	2	159.4 \pm 51.4	3.8	99
4	recurrent right parietal anaplastic ependymoma	F	11	105.4 \pm 32.4	/	/	/	116.6 \pm 35.6	10	2.9
5	diffuse midline glioma of the pons	F	5	108.1 \pm 45	112.8 \pm 15.6	4	1.7	132.7 \pm 19.8	5	23
6	diffuse astrocytoma invading pons and left cerebellum	M	9	106.5 \pm 31.3	164.5 \pm 29.6	54	1.1	145.4 \pm 56.3	4.3	37
7	diffuse midline glioma of the pons	F	10	100.3 \pm 33	139.6 \pm 25.3	28	1.6	/	/	/
8	diffuse midline glioma of the pons	M	11	72 \pm 19	89.2 \pm 17.9	24	1.1	120.9 \pm 14.9	3.5	68
9	suprasellar germinoma	M	10	155.6 \pm 57.3	/	/	/	185.8 \pm 18.4	19	3.2
10	germinoma of the pituitary stalk	F	11	84.9 \pm 24.7	102.3 \pm 41.3	20	1.4	77.5 \pm 38.2	4.3	-9
11	left thalamic germinoma	M	17	70.6 \pm 23.1	101.8 \pm 21.4	44	2.2	/	/	/
12	germinoma of the septum pellucidum	M	17	84 \pm 31.9	274.6 \pm 78.7	227	0.8	121.7 \pm 18.4	3.4	45

Table 3.4 Longitudinal changes in ADC at baseline and at subsequent follow-up after RT. Colour coding in the left column indicates tumours within the same histological group.

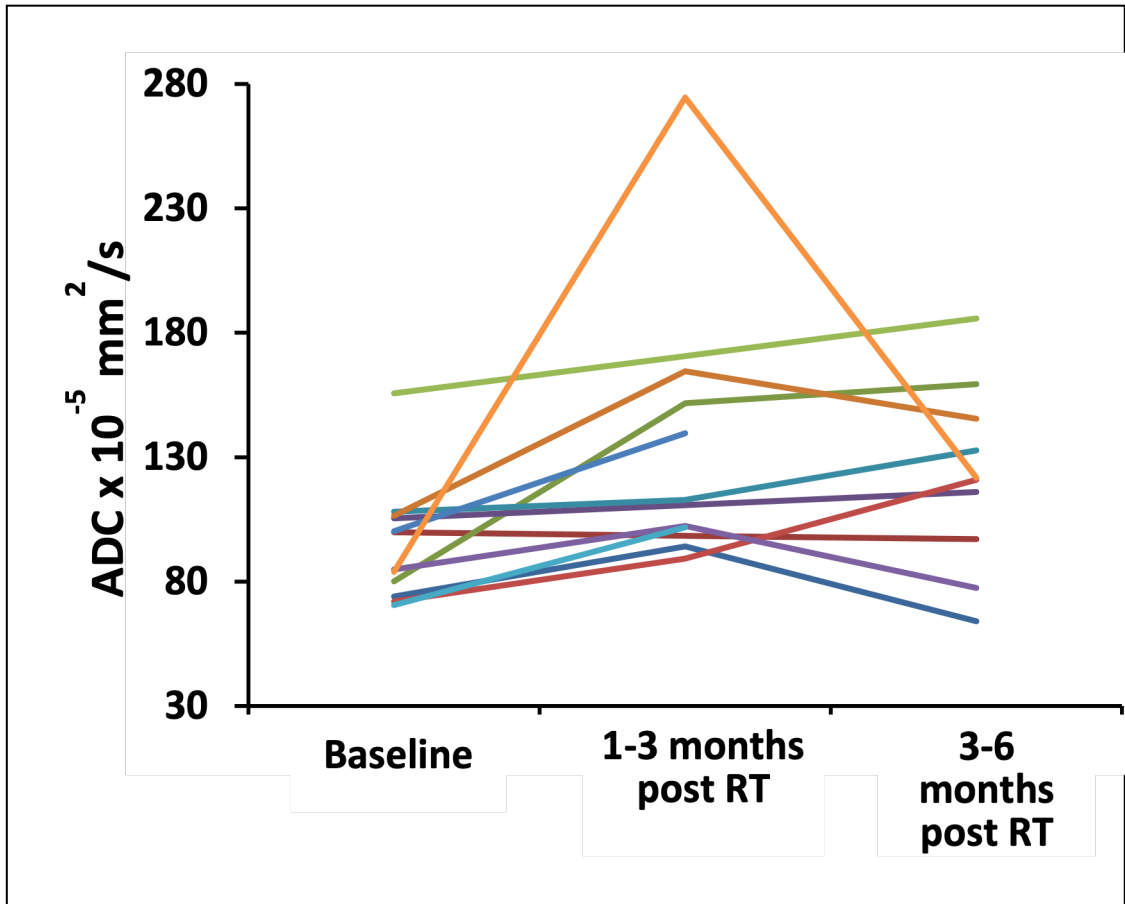


Figure 3.6: Longitudinal patterns of ADC change in skull marrow in children who received RT.

An early rise in ADC was noted in 8 out of 12 children at 1-3 months, which reduced in half of them by 3-6 months, whilst continued to rise in 2 patients and remained stable in the other 2.

Return to below baseline values was seen in 3 of 8 subjects.

Unfortunately, no late MR follow-up was available for two children (ocean boat and sky blue lines, respectively).

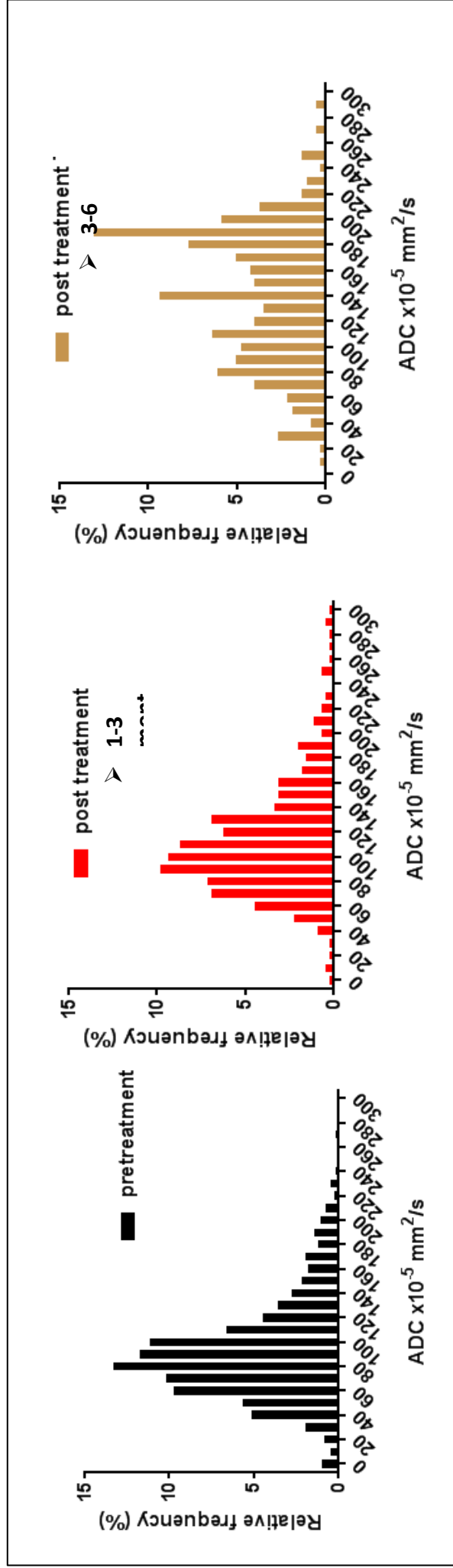


Figure 3.7: Histogram distributions of ADC values before and after RT. There is an early right shift of the histogram, with increasing spread of the values and move to a bimodal distribution.

Pt	10 th centile ADC			25 th centile ADC			Median ADC			75 th centile ADC			90 th centile ADC		
	Pre-RT	1-3 m post-RT	3-6 m post-RT	Pre-RT	1-3 m post-RT	3-6 m post-RT	Pre-RT	1-3 m post-RT	3-6 m post-RT	Pre-RT	1-3 m post-RT	3-6 m post-RT	Pre-RT	1-3 m post-RT	3-6 m post-RT
1	36.1	14.8	26.7	42.5	65.8	44.2	66.3	92.6	71.4	89.1	119.4	79.6	123.8	158.4	90.9
2	52.7	66.8	23.4	75.1	76	67.1	90.5	92.4	80.6	119.7	100.4	100	149.5	132	140
3	66.4	72	/	77.5	92.1	/	104.6	113.4	/	120.4	128.8	/	140.3	144.5	/
4	45.7	81.9	88.9	66	119.9	122.6	83.2	160.6	153.2	96.5	190.9	188.7	103.4	231.7	228.9
5	57.7	84.3	/	81.5	131.4	/	95.6	145.8	/	120	156.8	/	141.3	160.9	/
6	90.9	102.2	102.2	101	115.9	115.9	112.3	138.6	138.6	123.6	145.8	145.8	127.9	151.8	151.8
7	46.2	64.3	95.8	62.3	74.1	110.3	72.3	90.2	121	83.2	102.7	130.3	95.7	114.4	137.8
8	63.7	128.8	69.3	87.5	137.7	106.8	108.4	160.6	132.4	126.4	191.1	182.5	144.9	196.4	186.9
9	39.2	72,5	/	55.1	84.5	/	74	100	/	84.1	118.4	/	101.8	131.8	/
10	57.8	159.7	/	141.6	178.2	/	171	186.8	/	194.7	195.7	/	209.1	207.2	/
11	53.6	51.3	23.4	61.3	72.3	51.8	89.2	105.3	74.7	98.1	127.9	93	114	147.7	100.6
12	41.9	126.3	96.7	64	232.2	100.5	87.1	320	129.9	101	320	135.3	113	320	141.9

Table 3.5: Centile values for individual patients before, 1-3 months and 3-6 months after RT

3.4.3 Proton beam therapy (PBT) cohort

3.4.3.1 *Patient characteristics*

Ten children aged 5-17 years who fulfilled the inclusion criteria had the following diagnoses:

5) craniopharyngioma	6 patients	4 M + 2 F
6) low-grade glioma	2 patients	2 M
7) pilocytic astrocytoma	2 patients	2 F

All patients were treated referred to The Royal Marsden and treated in the USA, nine at Nemous Children's Clinic, in Jacksonville, and one at ProCure Proton Therapy Centre, in Oklahoma City.

The treatment was interrupted (temporarily discontinued in January 2016) in patient 1, a 9-year-old boy affected by WHO grade 1 adamantinomatous craniopharyngioma due to the cyst enlargement requiring neurosurgical drainage four times. In May 2016 he had seizure, weakness of the right side, severe episodes of dystonia, respiratory distress, poor intestinal absorption, and diabetes insipidus; he died in May 2017 from renal failure. All the other patients survived the proton therapy and are still alive.

3.4.3.2 *Regions-of-interest size*

The size of the ROI on each slice ranged from 4 to 6 mm. A minimum number of 10 pixels was ensured with pixels ranging from 15 to 159 (Pre-treatment median=28, LQ=23, UQ=101; 1-3 months post-treatment median=31, LQ=23, UQ=73; 3-6 months post-treatment median=15, LQ=15, UQ=17).

3.4.3.3 *Dose*

Table 3.6 lists the dose of protons (minimum, mean, maximum, and total) received by the clivus in each patient during the treatment. The clivus of

six patients affected by craniopharyngioma received between 39.4 and 55.1 Gy administered in 30 fractions, whilst the mean dose of protons of two children with low-grade ranged between 3.1 and 36.6 Gy. A lower mean dose of protons was received by the clivus in the two individuals with pilocytic astrocytoma (**Table 3.7**).

3.4.3.4 Longitudinal treatment effects with PBT on ADC of clivus

Patients were initially scanned at a median of 2.0 months after the end of treatment; (lower quartile 1.6, upper quartile 2.3 months). 7 out of 10 had also a second later MRI examination at a median of 5.4 months (LQ=3.9 months, UQ=5.8 months).

On baseline scan, mean ADC values fluctuated between 57.4 ± 38.2 s/mm² and 140 ± 38.5 s/mm². On the first post-treatment assessment, mean ADC values ranged from 95 ± 17.5 s/mm² (2 months after completing PBT) to 189.4 ± 72.7 s/mm² (1.2 months after PBT). In the 7 patients who had the second follow-up, mean ADC values ranged from 100.7 ± 31.3 s/mm² (4.6 months after PBT) to 141.7 ± 57 s/mm² (5.8 months after PBT).

	DIAGNOSIS	GENDER	AGE	clivus ROI vol (cm ³)	min dose D99 (cGy)	mean dose (cGy)	max dose DI (cGy)	treatment completed	prescription	proton centre
1	adamantinomatous craniopharyngioma	*M	5	0.23	5419	5469	5496	March 2016	54 CGE / 30 #	FL
2	craniopharyngioma	F	8	0.26	5192	5378	5477	Feb 2013	54 CGE / 30 #	FL
3	cystic adamantinomatous craniopharyngioma	M	9	0.22	5464	5512	5560	Sep 2016	54 CGE / 30 #	FL
4	adamantinomatous craniopharyngioma (WHO grade I)	M	10	0.22	4407	5217	5532	Feb 2016	54 CGE / 30 #	FL
5	craniopharyngioma	M	11	0.23	2692	3942	4890	Feb 2012	54 CGE / 30 #	FL
6	craniopharyngioma (multicystic grade 1)	M	17	0.27	5258	5468	5521	Aug 2012	54 CGE / 30 #	FL
7	low-grade glioma (hypothalamic chiasmatic third ventricular) with hydrocephalus	M	12	0.25	2513	3660	4488	March 2014	53.6 Gy (RBE) / 31 #	OK
8	tectal plate low-grade glioma	M	13	0.23	26	316	955	Apr 2013	54 CGE / 30 #	FL
9	WHO grade I pilocytic astrocytoma infiltrating lateral L thalamus, medial thalami and hypothalamus, invaginating into the 3rd ventricle	F	8	0.22	17	83	189	Apr 2017	54 CGE / 30 #	FL
10	low-grade pilocytic astrocytoma of pons and midbrain	F	12	0.26	3456	4430	4953	Aug 2014	50.4 CGE / 28 #	FL

Table 3.6: PBT dose to the clivus colour coded by tumour type

Pt	Diagnosis	Gender	Age	Baseline ADC mean \pm SD	Time-point 1 ADC (mean \pm SD)	% ADC change from baseline at time-point 1	Time interval from end of PTB (months)	Time-point 2 ADC (mean \pm SD)	Time interval 2 from end of PBT (months)	% ADC change from baseline at time-point 2
1	adamantinomatous craniopharyngioma	M	5	101.9 \pm 58.4	120.1 \pm 33.8	18	1.3	/	/	/
2	craniopharyngioma	F	8	67.9 \pm 22.6	143.4 \pm 19.7	111	2.6	133.3 \pm 27.4	5.8	96
3	cystic craniopharyngioma	F	9	140 \pm 38.5	165.8 \pm 17.6	18	2.3	115.4 \pm 13.8	3.5	-21
4	adamantinomatous craniopharyngioma	M	10	73.7 \pm 17.5	146.6 \pm 105	99	1.5	100.7 \pm 31.3	4.6	37
5	craniopharyngioma	M	11	74.9 \pm 10.1	142.5 \pm 11.9	90	1.8	141.7 \pm 57	5.8	89
6	multicystic craniopharyngioma (grade 1)	M	17	80.7 \pm 17.7	167.4 \pm 20.8	107	2.1	/	/	/
7	hypothalamic chiasmatic third ventricular low-grade glioma	M	12	77.9 \pm 40.3	142.1 \pm 55.5	82	2.3	111.1 \pm 31.5	3.9	43
8	tectal plate low-grade glioma	M	13	109.5 \pm 26.8	135.8 \pm 20.9	24	2.1	/	/	/
9	pilocytic astrocytoma infiltrating thalami and hypothalamus, invaginating into the third ventricle	F	8	57.4 \pm 38.2	95 \pm 17.5	66	2	108.5 \pm 30.2	5.4	89
10	low-grade pons and midbrain pilocytic astrocytoma	F	12	139.4 \pm 101.9	189.4 \pm 72.7	36	1.2	114.5 \pm 34.9	3.3	-18

Table 3.7: Longitudinal changes in ADC at baseline and at subsequent follow-up after PBT

Notwithstanding the MR scans of the head in the PBT cohort were performed on different scanners (**Table 3.1**), essential technical parameters were identical or similar (**Table 3.2**). Additionally, the intra-observer reproducibility with a variability of $\leq 10\%$ ensures that a longitudinal evaluation of the post-treatment marrow ADC trend can be achieved.

Mean ADC increased early after treatment above measurement reproducibility in all 10 cases (median 42.4%, LQ 21.1%, UQ 49.2%); at second follow up (5 months), ADC then decreased in 5 of 7 patients scanned, was stable in 1 and rose further in 1 (**Figure 3.8**).

A summary of histogram shifts of cumulated voxel data from all patients before and at 2 and 5 months after PBT are illustrated in **Figure 3.9**. Individual patient centile values shown in **Table 3.8** mirror the histogram shifts demonstrated by the aggregated voxel data from the entire cohort.

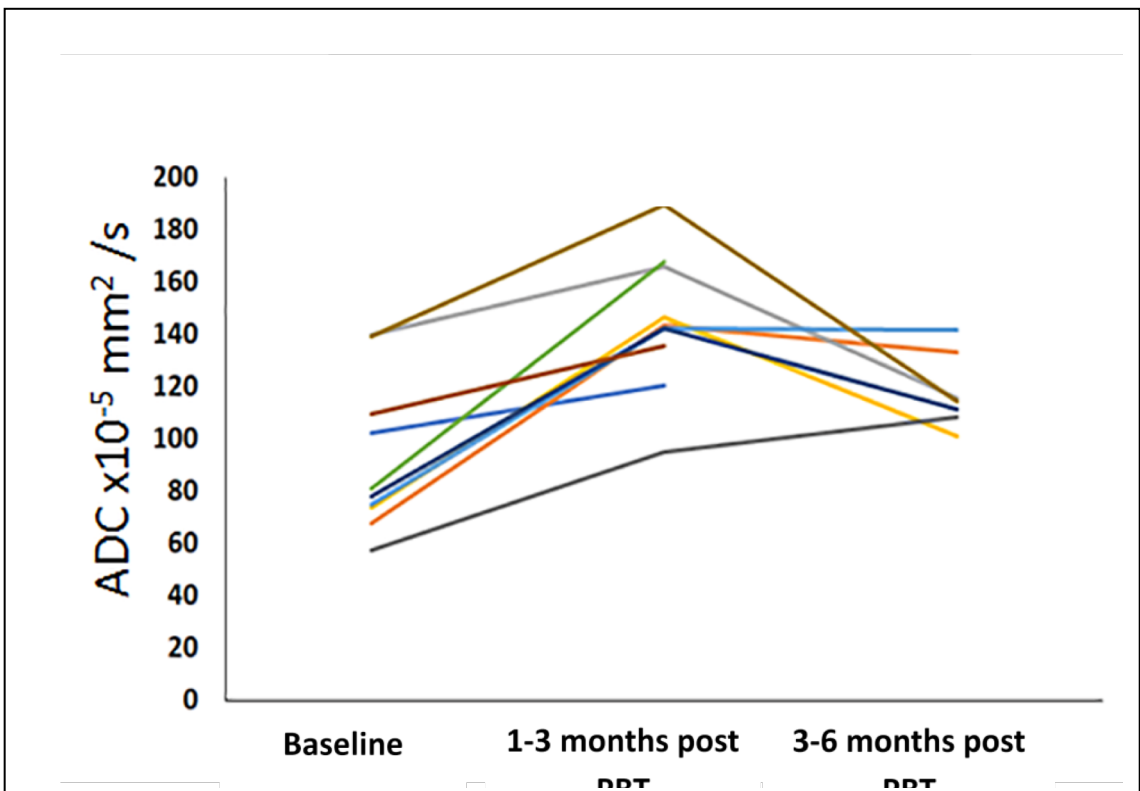


Figure 3.8: Longitudinal patterns of ADC change in skull bone marrow in children who received PBT. An early rise in ADC was noted at 2 months, which reduced at 4 months. Return to below baseline values was seen in 2 of 7 cases.

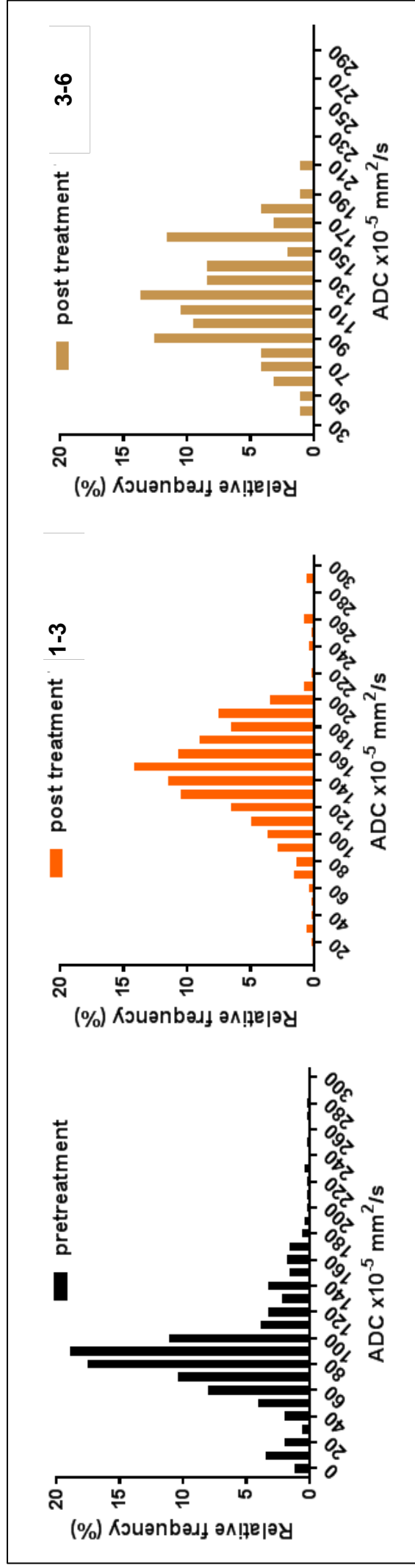


Figure 3.9: Histogram distributions of ADC values before and 1-3 and 3-6 months after PBT. There is an early right shift of the histogram, which later shifts back, but with increasing spread of the values

Pt	10 th centile ADC			25 th centile ADC			Median ADC			75 th centile ADC			90 th centile ADC		
	Pre-PBT	1-3 m post-PBT	3-6 m post-PBT	Pre-PBT	1-3 m post-PBT	3-6 m post-PBT	Pre-PBT	1-3 m post-PBT	3-6 m post-PBT	Pre-PBT	1-3 m post-PBT	3-6 m post-PBT	Pre-PBT	1-3 m post-PBT	3-6 m post-PBT
1	32.9	72.6	/	66.9	86.1	/	88.6	120.1	/	120.4	143	/	131	166.2	/
2	38.7	120.4	93.5	38.7	129.9	108.7	73.2	144.5	142.9	87.2	153.2	155.4	95.7	168.6	160.9
3	78.3	142.4	90.2	117.5	152.6	103	146.9	163.3	115.8	166.7	181.7	123.1	178.9	188.5	127.8
4	49.5	26.2	50.6	61.8	59.8	80	73.4	120.4	106.9	88.2	208.4	126.2	94.4	315.6	133.2
5	59.9	125.3	61.5	66.7	132.7	94.4	74.8	142.9	135.2	81.5	147.8	145.7	82.9	155.5	228.1
6	57.3	135.8	/	66.8	152.2	/	80.6	169.2	/	66.8	184.9	/	105.8	194	/
7	35.3	69.3	73.8	52.3	108.3	92.6	63.3	134.3	103.5	94.8	159.9	117.3	129.9	211.2	159.4
8	84	109.3	/	90.6	117.9	/	96.9	136.6	/	126.9	148.6	/	151	163.6	/
9	64	74.1	86.6	70	83.9	88.1	73.3	90	100.6	79.5	101.9	110.2	88.3	125.5	129.6
10	52.8	100.1	63.4	70.5	111.4	79.7	87.9	167.9	121.9	164.9	258.6	132.2	283.5	285.8	156.6

Table 3.8: Centile values for individual patients before, 1-3 months and 3-6 months after PBT

3.4.4 Comparison RT and PBT cohorts

3.4.4.1 *Timing of follow-up scans*

The median time interval between the end of treatment and the first post-treatment MR scan was <2 months in both cohorts; between the baseline and the second post-treatment scan it was 4.5 months in the RT cohort and 4.6 months for the PBT group. This indicates the time-points for the comparisons were equivalent.

3.4.4.2 *Dose delivered*

The doses delivered to the clivus in the RT and PBT cohorts are tabulated (**Tables 3.9 a and b**). Overall, the range of doses received with RT was much greater (39-54 Gy) with 7 of the 12 patients receiving less than 50 Gy. All patients in the PBT cohort received more than 50 Gy, 8 of 10 received 54 Gy. This comparison is shown in **Figure 3.10**.

pt	RT	overall dose
1	craniopharyngioma	50 Gy
2	craniopharyngioma	50 Gy
3	ependymoma	54 Gy
4	ependymoma	54 Gy
5	diffuse intrinsic pontine glioma	39 Gy
6	diffuse intrinsic pontine glioma	39 Gy
7	diffuse intrinsic pontine glioma	39 Gy
8	diffuse intrinsic pontine glioma invading cerebellum	54 Gy
9	germinoma	40 Gy
10	germinoma	40 Gy
11	germinoma	40 Gy
12	germinoma	40 Gy

Table 3.9 a: Dose delivered to the clivus in patients receiving RT.

pt	PTB	overall dose
1	craniopharyngioma	54 Gy
2	craniopharyngioma	54 Gy
3	craniopharyngioma	54 Gy
4	craniopharyngioma	54 Gy
5	craniopharyngioma	54 Gy
6	craniopharyngioma	54 Gy
7	low-grade glioma	53.6 Gy
8	low-grade glioma	54 Gy
9	ventricular pilocytic astrocytoma invading thalami	54 Gy
10	pilocytic brainstem astrocytoma	50.4 Gy

Table 3.9 b: Dose delivered to the clivus in patients receiving PBT.

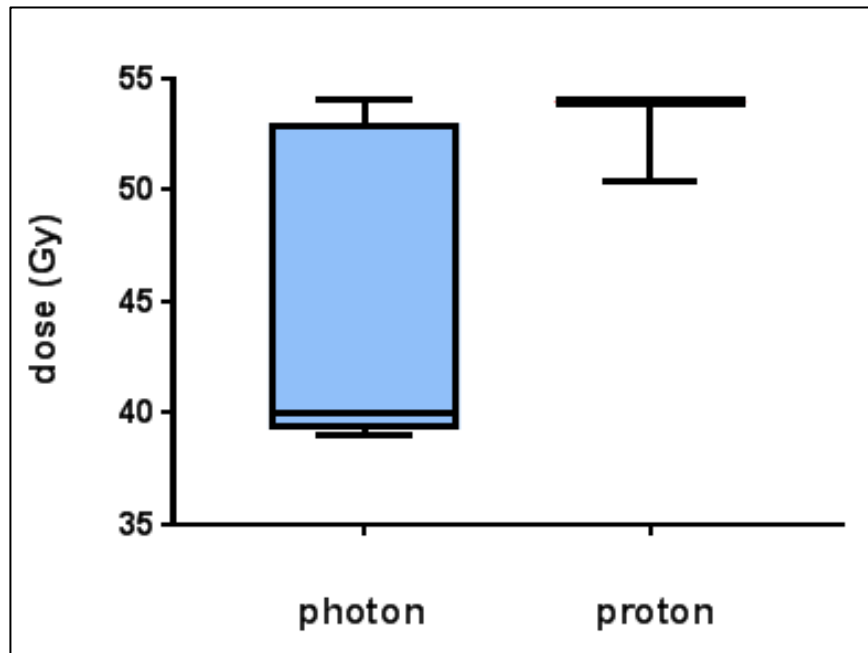


Figure 3.10: Comparison of RT and PBT doses delivered to each of the cohorts.

3.4.4.3 Longitudinal ADC changes with treatment

Comparison of ADC rises with treatment for each cohort are illustrated using frequency distribution histograms of all pixel values from all patients in that cohort at each of the time points. Absolute values (**Figure 3.11 a**) and percentage changes in ADC (**Figure 3.11 b**) show that somewhat larger changes were seen in the proton therapy cohort.

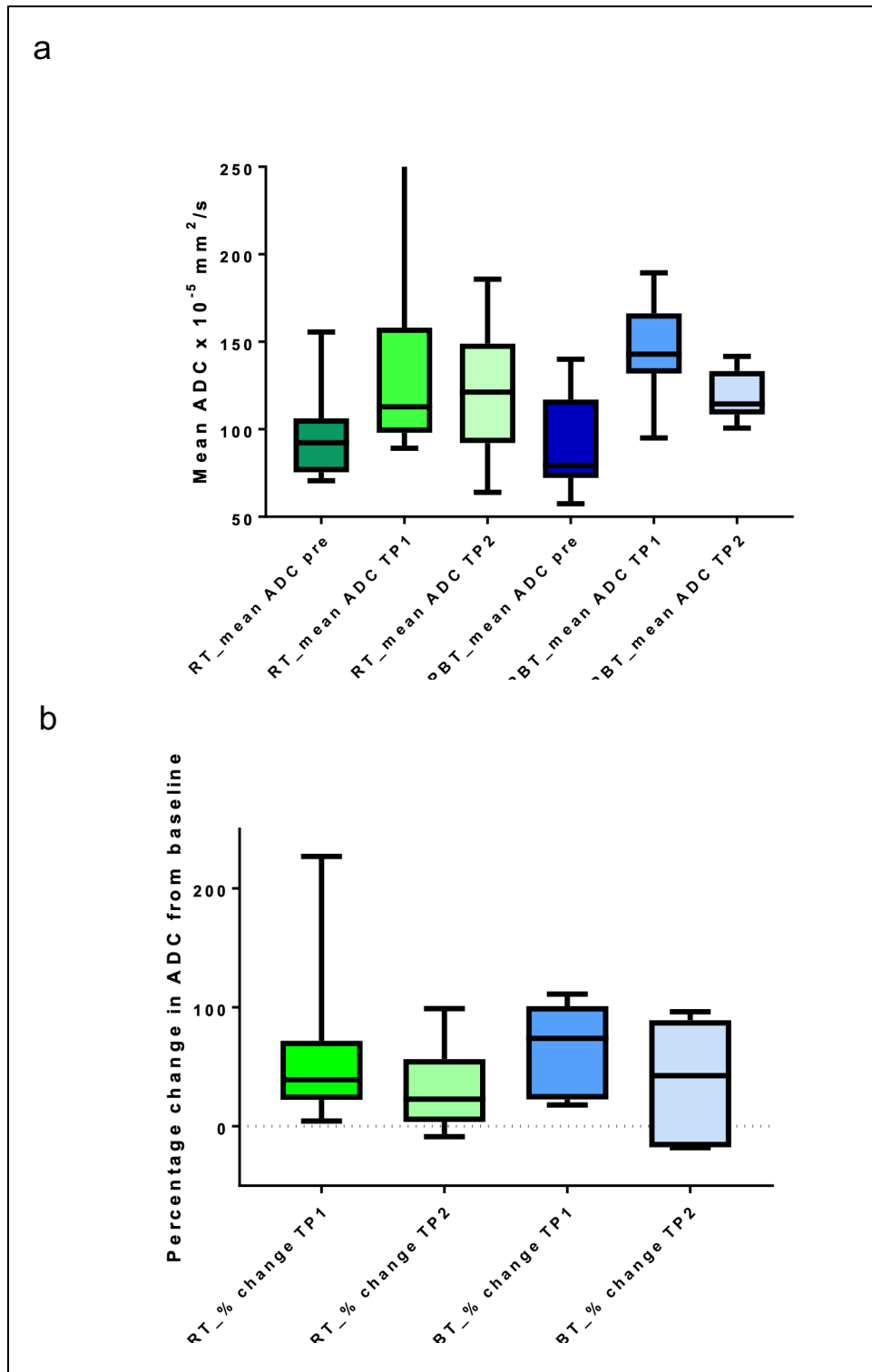


Figure 3.11 a and b: Box and whisker plots showing (a) absolute increases in mean ADC for the whole cohort treated with RT (green fill) and PBT (blue fill) and (b) percentage changes from baseline at the early (TP1, 1-3 months) and late (TP2, 3-6 months) time points.

3.5 DISCUSSION

3.5.1 Nature of the ADC changes post treatment

Both RT and PBT result in acute injury to the tissue in which the energy is deposited. In the normal tissue surrounding the intended target, there is immediate swelling as a result of cell membrane damage, which causes lysis. Resultant inflammatory and immune responses are evoked and contribute to the oedema.¹⁰ High-dose RT has been shown to affect normal tissues included in the RT portal.¹⁰ Early effects typically occur after the first 1–2 weeks after the start of RT.¹¹ They are seen in tissues with rapid cell renewal (epithelial and hematopoietic stem cells), where frequent mitosis is required to maintain organ function.¹⁰ In imaging terms, this disruption of cell membranes reduces the barriers that normally restrict water motion, so that the ADC (which specifically quantifies this molecular motion of water) increases.¹² The degree of change is expected to be related to the size of the injury namely the radiation dose.¹³ The dose delivered to the clivus is influenced by the distance of the target from the clivus. Radiation dose to the clivus in my cohort was highest in patients with craniopharyngiomas, due to its proximity to the target. As there is a sharper fall-off of dose in PBT compared to RT,^{14, 15} the dose to the clivus may well have been lower in PBT than with RT despite the higher dose to the target with PBT. In adults, increasing radiation dose exposure has been associated with increasing fat fraction quantified by MRI in the vertebral body. This was shown to correspond to decrease in peripheral blood counts.¹⁶

The use of DW-MRI for investigating the effects of RT in adults has largely focussed on the effects of radiation on the ADC of the bone metastases themselves and not on the surrounding normal marrow.¹⁷ It is difficult to

interpret my data in context of these findings. In metastatic tissue, the demonstrated increase in ADC is an intended toxic effect indicative of treatment response¹⁸ rather than a bystander effect.

3.5.2 Longitudinal evolution of the ADC changes post treatment

In adults, inflammatory changes have been demonstrated in bone marrow on MRI (increased signal intensity on STIR images and increased enhancement on gadolinium-enhanced images) as early as 7 days after radiation therapy.¹⁹ At 4 weeks after RT, fatty replacement and early fibrosis are common (high signal intensity on T1-W MR images and persistent enhancement).¹⁹ A study in the lumbar spine of adults showed that there was increased signal-intensity during the first 2 weeks of therapy on Short tau inversion recovery (STIR) MRI reflecting almost immediate marrow oedema.²⁰ Six weeks to 14 months after therapy, there was homogenous or heterogenous fat replacement.²¹ PET/MR imaging studies also indicate that irradiated marrow spaces (ie, cervical spine, mandible, bony skull base, ossified laryngeal cartilages) show persistent signs of injury from RT.²² In my study, the fat suppressed DW-MRI sequences I analysed indicated that in children receiving RT or PBT to the brain, changes consistent with oedema were observable at 2 months, and were beginning to settle by 4-6 months, although some children had a persistent rise in ADC. Patient age and radiation dose may well have been responsible for the latter but drawing conclusions from my small numbers of patients is not possible.

Fatty replacement of the irradiated marrow is a well-described late change in adults, due to the increased differentiation of mesenchymal stem cells to adipose cells following radiation.²³ Alterations in the fat component of vertebral marrow has been described as early as 1-2 weeks after initiation of treatment using different MRI sequences^{20, 24} and fatty marrow conversion after 3-4 weeks of radiation insult have been reported from increased signal-intensity on T1-W spin-echo imaging.^{20, 21} Quantification of marrow fat content using a three-point Dixon method has shown that fat replacement over time may impact on the clinical manifestation of myelosuppression.^{16, 23} In this retrospective study, I did not have availability of sequences from which to estimate marrow fat fraction, but future prospective studies could incorporate such measurements.

3.5.3 Clinical impact of the findings

Although the clivus has an important haematopoietic function, it is only a small fraction of the active marrow in children. Therefore, although it has previously been shown in an adult population with pelvic malignancy that haematological toxicity increases with radiation doses to the bone marrow of more than 10 Gy,²⁵ it is unlikely that obliteration of the active marrow in the clivus (or even larger areas of the skull) would lead to haematological toxicity in children with brain tumours. It acts rather as a surrogate tissue for monitoring the effects of radiation on immediately adjacent tissues, such as cranial nerves, that are difficult to evaluate because of their size. Long-term toxicity of cranial irradiation to adjacent normal tissues is substantial: in a single centre series of 50 medulloblastoma patients treated with RT and followed up for 15 years (24

years for 16 surviving patients), 41% of patients who survived five years or more developed grade 3+ toxicity (most commonly hearing impairment requiring intervention (20.5%) and cognitive impairment (18%) prohibiting independent living).²⁶ Cranial nerve palsies have been described following cranial irradiation.²⁷ Although stereotactic radiation delivery reduces the extent of toxicity to neighbouring normal tissues, in future a robust method of measuring toxic effects of radiation in individual subjects that can be derived from imaging data as part of routine follow-up may prove advantageous.

3.5.4 Limitations of the measurement and measurement variability

Measurements of ADC in bone marrow are limited by the fact that on a fat suppressed diffusion-weighted imaging sequence, the SNR is low. This was certainly the case in my data, where the high standard deviations of the mean ADCs cited reflect the wide variation in individual voxel values. Moreover, susceptibility artefact at the skull base from cortical bone and adjacent sinuses is inevitable, particularly in echo-planar based sequences and adds to the error of the measurement.²⁸ Finally, the small size of the anatomic structure being measured meant that data from only a small number of voxels could be extracted. To address these issues, I ensured that I selected scans that were free from visible artefact and in which there was no significant degradation from image noise. This limited the sample size. The variation in scanners and software (normalization factors), meant that objectively selecting patients based on SNR measurements was not feasible or meaningful. Also, I amalgamated the data for the pre- and post-therapy histogram comparisons (using all voxels

from all subjects) to show the pattern of changes following radiation therapy. This reduced the effect of noise from individual patients and illustrated the trends in the data. However, my data was consistent across cohorts and confirms similar data in the adult literature.²⁹ A particular strength of this study was the robustness of the ADC measurements illustrated by the reproducibility cohort. ADC values from bone have been shown to range from 30 to 70 x 10⁻⁵ mm²/s in untreated adults²⁹ with higher cited values in children;³⁰ this agrees with the baseline values in my study.

A major limitation of this study was its retrospective nature. This meant that it was impossible to control the timing at which the follow-up scans were obtained, or to select patients based on radiation dose to clivus, and prospectively record their dose information. It also meant that the imaging studies themselves were non-standardised, and that the b-values used may not have been ideal for ADC derivation. It has previously been shown that use of b=50 or 100 s/mm² as the low b-value removes the effects of faster moving protons from perfusion and provides a better indication of true diffusion.³¹ A third b-value would also have improved the fitting and therefore the ADC quantitation. In a paediatric population, the difficulties around performing such studies prospectively are considerable. Children have a poor acceptance of additional scans for the purposes of research, and ethical issues in carrying these out, despite the lack of ionizing radiation with MRI, remain. For instance, they can more easily than adults withdraw their consent, as demonstrated in the PUMA study (**cf paragraph 5.6.1 and Table 5.1**), due to the fact that they not always completely realise all the benefits to partaking in research, because of their still developing cognitive skills, especially in the youngest child. Also, notwithstanding

nowadays patient information sheets are tailored to participant's age — making the level of English understandable to the diverse range of ages, using also images, and a child-friendly font — it is inevitable that their decision is partially influenced by their parents' opinion as they trust them more than strangers.

Furthermore, in these rare tumours, where patients are geographically remote from the cancer centre, additional visits are not feasible. Despite these difficulties, further work to establish whether ADC measurements in the clivus may be used as a biomarker of radiation injury and relate to long-term toxicities may be worthwhile.

3.6 SUMMARY

The main conclusions of this retrospective study are:

- Longitudinal changes in ADC occur within normal skull marrow following RT and PBT to the brain, therefore, the null hypothesis is rejected. These changes are greater at an early time-point (within 3 months of treatment), but that they gradually diminish. However, longer follow-up would be needed to establish whether the measured imaging changes return to baseline.
- Furthermore, it has not been possible to demonstrate a relationship with dose in these small numbers, particularly because the doses of radiation administered across the cohort were very similar. Surprisingly, slightly greater increases were seen early after treatment in the PBT group, but larger numbers would be needed to show statistically significant differences between patients treated with RT versus PBT.

- The major value of this work has been the establishment of the reproducibility of the ADC measurement in the skull (clivus) of children and the demonstration that measurable ADC changes in normal bone marrow occur following RT and PBT to the brain in a paediatric population.

3.7 KEY POINTS

- It is feasible to measure ADC from the clivus in children with 11% variability (Limits of Agreement).
- Following RT or PBT to the brain, there is an increase above measurement variability in ADC of normal bone marrow within the first 3 months, which subsequently falls.

REFERENCES

1. Geyer JR, Sposto R, Jennings M, et al. Multiagent chemotherapy and deferred radiotherapy in infants with malignant brain tumors: a report from the Children's Cancer Group. *Journal of clinical oncology : official journal of the American Society of Clinical Oncology*. 2005; 23: 7621-7631.
2. Louis DN, Perry A, Reifenberger G, et al. The 2016 World Health Organization Classification of Tumors of the Central Nervous System: a summary. *Acta neuropathologica*. 2016; 131: 803-820.
3. Segal D and Karajannis MA. Pediatric Brain Tumors: An Update. *Current problems in pediatric and adolescent health care*. 2016; 46: 242-250.

4. Reddy GD, Hansen D, Patel A, Lin Y, Jea A and Lam S. Treatment options for pediatric craniopharyngioma. *Surgical neurology international*. 2016; 7: S174-178.
5. Shibamoto Y, Sasai K, Oya N and Hiraoka M. Intracranial germinoma: radiation therapy with tumor volume-based dose selection. *Radiology*. 2001; 218: 452-456.
6. Pixberg C, Koch R, Eich HT, et al. Acute Toxicity Grade 3 and 4 After Irradiation in Children and Adolescents: Results From the IPPARCA Collaboration. *International journal of radiation oncology, biology, physics*. 2016; 94: 792-799.
7. Duffner PK. Long-term effects of radiation therapy on cognitive and endocrine function in children with leukemia and brain tumors. *The neurologist*. 2004; 10: 293-310.
8. Armstrong GT, Jain N, Liu W, et al. Region-specific radiotherapy and neuropsychological outcomes in adult survivors of childhood CNS malignancies. *Neuro-oncology*. 2010; 12: 1173-1186.
9. Tamura M, Sakurai H, Mizumoto M, et al. Lifetime attributable risk of radiation-induced secondary cancer from proton beam therapy compared with that of intensity-modulated X-ray therapy in randomly sampled pediatric cancer patients. *Journal of radiation research*. 2017; 58: 363-371.
10. Stone HB, Coleman CN, Anscher MS and McBride WH. Effects of radiation on normal tissue: consequences and mechanisms. *The Lancet Oncology*. 2003; 4: 529-536.
11. Debnam JM. Imaging of the Head and Neck following Radiation Treatment. *Pathology research international*. 2011; 2011: 607820.
12. Serduc R, van de Looij Y, Francony G, et al. Characterization and quantification of cerebral edema induced by synchrotron x-ray microbeam radiation therapy. *Physics in medicine and biology*. 2008; 53: 1153-1166.
13. Aitasalo K. Bone tissue response to irradiation and treatment model of mandibular irradiation injury. An experimental and clinical study. *Acta otolaryngologica Supplementum*. 1986; 428: 1-54.
14. Lambrecht M, Eekers DBP, Alapetite C, et al. Radiation dose constraints for organs at risk in neuro-oncology; the European Particle Therapy Network

- consensus. *Radiotherapy and oncology : journal of the European Society for Therapeutic Radiology and Oncology*. 2018; 128: 26-36.
15. MacDonald SM, Safai S, Trofimov A, et al. Proton radiotherapy for childhood ependymoma: initial clinical outcomes and dose comparisons. *International journal of radiation oncology, biology, physics*. 2008; 71: 979-986.
 16. Carmona R, Pritz J, Bydder M, et al. Fat composition changes in bone marrow during chemotherapy and radiation therapy. *International journal of radiation oncology, biology, physics*. 2014; 90: 155-163.
 17. Gaeta M, Benedetto C, Minutoli F, et al. Use of diffusion-weighted, intravoxel incoherent motion, and dynamic contrast-enhanced MR imaging in the assessment of response to radiotherapy of lytic bone metastases from breast cancer. *Academic radiology*. 2014; 21: 1286-1293.
 18. Blackledge MD, Collins DJ, Tunariu N, et al. Assessment of treatment response by total tumor volume and global apparent diffusion coefficient using diffusion-weighted MRI in patients with metastatic bone disease: a feasibility study. *PloS one*. 2014; 9: e91779.
 19. Huang W, Yang Y, Sun Z and Zeng X. Early radiation-induced bone marrow injury: serial MR imaging during initial 4 weeks after irradiation. *Academic radiology*. 2009; 16: 733-738.
 20. Blomlie V, Rofstad EK, Skjonsberg A, Tvera K and Lien HH. Female pelvic bone marrow: serial MR imaging before, during, and after radiation therapy. *Radiology*. 1995; 194: 537-543.
 21. Stevens SK, Moore SG and Kaplan ID. Early and late bone-marrow changes after irradiation: MR evaluation. *AJR American journal of roentgenology*. 1990; 154: 745-750.
 22. Varoquaux A, Rager O, Dulguerov P, Burkhardt K, Ailianou A and Becker M. Diffusion-weighted and PET/MR Imaging after Radiation Therapy for Malignant Head and Neck Tumors. *Radiographics : a review publication of the Radiological Society of North America, Inc*. 2015; 35: 1502-1527.
 23. Bolan PJ, Arentsen L, Sueblinvong T, et al. Water-fat MRI for assessing changes in bone marrow composition due to radiation and chemotherapy in

- gynecologic cancer patients. *Journal of magnetic resonance imaging : JMRI*. 2013; 38: 1578-1584.
24. Onu M, Savu M, Lungu-Solomonescu C, Harabagiu I and Pop T. Early MR changes in vertebral bone marrow for patients following radiotherapy. *European radiology*. 2001; 11: 1463-1469.
 25. Liang Y, Bydder M, Yashar CM, et al. Prospective study of functional bone marrow-sparing intensity modulated radiation therapy with concurrent chemotherapy for pelvic malignancies. *International journal of radiation oncology, biology, physics*. 2013; 85: 406-414.
 26. Christopherson KM, Rotondo RL, Bradley JA, et al. Late toxicity following craniospinal radiation for early-stage medulloblastoma. *Acta oncologica (Stockholm, Sweden)*. 2014; 53: 471-480.
 27. Oliff A, Bleyer WA and Poplack DG. Acute encephalopathy after initiation of cranial irradiation for meningeal leukaemia. *Lancet (London, England)*. 1978; 2: 13-15.
 28. lima M, Yamamoto A, Brion V, et al. Reduced-distortion diffusion MRI of the craniovertebral junction. *AJNR American journal of neuroradiology*. 2012; 33: 1321-1325.
 29. Herrmann J, Krstin N, Schoennagel BP, et al. Age-related distribution of vertebral bone-marrow diffusivity. *European journal of radiology*. 2012; 81: 4046-4049.
 30. Nonomura Y, Yasumoto M, Yoshimura R, et al. Relationship between bone marrow cellularity and apparent diffusion coefficient. *Journal of magnetic resonance imaging : JMRI*. 2001; 13: 757-760.
 31. Ohno N, Miyati T, Kasai H, et al. Evaluation of perfusion-related and true diffusion in vertebral bone marrow: a preliminary study. *Radiological physics and technology*. 2015; 8: 135-140.

CHAPTER 4 – Investigating the effects of chemotherapy on bone marrow: lumbosacral spine ADC studies

The main purpose of this chapter is to retrospectively explore the longitudinal effects of conventional chemotherapy on the ADC values calculated in the marrow of the lumbosacral vertebrae in a paediatric population affected by abdominopelvic primary neoplasms.

4.1 INTRODUCTION

In paediatric abdominopelvic malignancy, a variety of treatment recommendations are made based on international guidelines. Commonly, neoadjuvant chemotherapy to shrink the mass is followed by debulking surgery where possible. Radiotherapy (RT or PBT) may be added later to sterilise the surgical bed in order to decrease the incidence of recurrent disease. Furthermore, when a tumour mass is inoperable due to its life-threatening anatomical location or to extensive disease, children are offered a new drug combination or a clinical trial, usually using experimental drugs (including immunotherapy). Therefore, chemotherapy plays a pivotal role in the management of paediatric abdomino-pelvic tumours.

4.1.1 Paediatric abdominopelvic tumours

One third of childhood malignancies are solid abdominopelvic lesions.

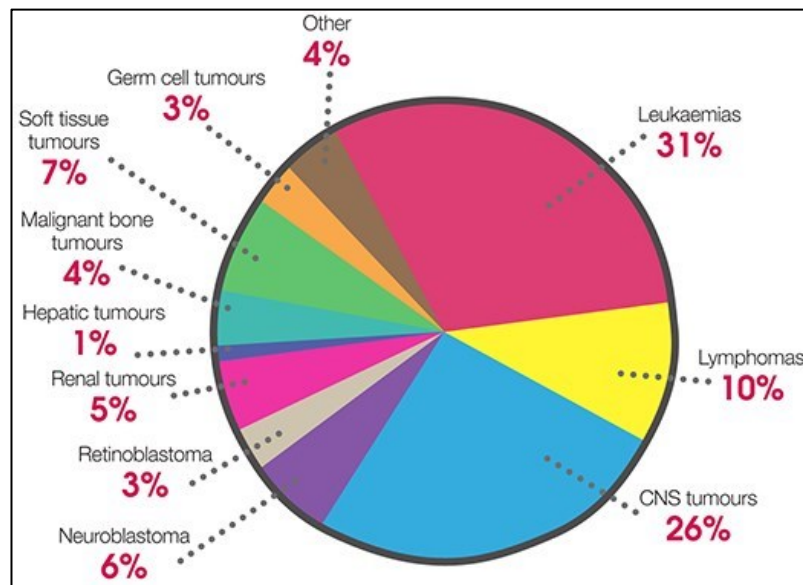


Figure 4.1: Main types of childhood cancer: children aged 0-14, United Kingdom 2001 to 2010. Based on data provided by National Registry of Childhood Tumours.

Wilms' tumour and neuroblastoma are the commonest neoplasms and present as retroperitoneal mass lesions.¹ Abdominal and pelvic rhabdomyosarcomas also occur.² Mesenteric and gastrointestinal tumours are more commonly benign than malignant. Burkitt's lymphoma is the haematological cancer involving the bowel loops.¹ Germ cell tumours encompass a wide range of complex lesions (mature and immature teratoma with possible associated gliomatosis peritonei, ovarian dysgerminoma, and yolk sac tumour) which may also have extragonadally manifestations.³ Hepatoblastoma occurs in infants, deriving from embryonic and foetal hepatocytes with a mesenchymal component, treated with transplant when the mass is too extensive for a conventional excision.⁴ Pancreatoblastoma is a highly rare tumour occurring in the first decade presenting as a mass associated with non-specific symptoms.⁵ Included among tumours originating from soft tissues, fibromatosis is a low-grade benign disease developing from aponeuroses of muscles which may have a local aggressive behaviour.⁶ Thus,

abdominopelvic tumours in children comprise a broad spectrum of entities (**Figure 4.1**)⁷ and so require treatment with a range of systemic therapies with potential effect on neighbouring normal tissues, particularly those with a high proliferative rate, such as normal paediatric bone marrow.

Table 4.1 lists the range of paediatric abdominopelvic tumours by anatomical site that may require systemic therapy.

Anatomical site	Malignant tumour
ADRENAL GLAND	Neuroblastoma Adrenal carcinoma Pheochromocytoma
KIDNEY	Wilms' tumour Nephroblastomatosis Mesoblastic nephroma Multilocular cystic renal tumour Cystic nephroma Cystic partially differentiated neuroblastoma Clear cell sarcoma Primitive neuroectodermal tumor Rhabdoid tumour Lymphomatous nephromegaly Renal cell carcinoma Renal medullary carcinoma (Angiomyolipoma)
LIVER	Hepatoblastoma Hepatocellular carcinoma Embryonal sarcoma Malignant mesenchymal tumour Angiosarcoma Leiomyosarcoma
GALL BLADDER	Leiomyosarcoma
GASTROINTESTINAL TRACT	Burkitt's lymphoma/Non-Hodgkin's lymphoma
LOWER GENITOURINARY TRACT	Rhabdomyosarcoma of the urinary bladder
REPRODUCTIVE SYSTEM	Ovarian germ cell tumour Rhabdomyosarcoma of the vagina Rhabdomyosarcoma of the prostate Paratesticular rhabdomyosarcoma
RETROPERITONEUM AND PELVIS	Rhabdomyosarcoma Neuroblastoma Desmoplastic small round cell tumour Germ cell tumour Hodgkin's lymphoma Non-Hodgkin's lymphoma
SPLEEN	Hodgkin's lymphoma Non-Hodgkin's lymphoma Acute or chronic leukaemia Histiocytosis

Table 4.1: Paediatric abdominopelvic tumours treated with chemotherapy.

4.2.1 Toxicity induced by chemotherapy

Toxicity related to chemotherapy drugs depends on a wide spectrum of factors, comprising the types of agents used (usually a combination is administered), the route of administration (intravenous, oral), the dose, the number of cycles, the patient's age, and the presence of comorbidities.

Based on the time of occurrence since the commencement of chemotherapy, two types of toxicity may occur: acute or late effects. It is the later effects that compromise bone marrow that are investigated in this work.

4.1.2.1 Acute toxicity induced by chemotherapy

Acute toxicity occurs within days of starting therapy and are related to pulmonary and abdominal effects. Pneumonia is common, especially fungal pneumonia due to immunosuppression. Acute abdominal toxicities include colitis, benign pneumatosis intestinalis, small bowel obstruction, sinusoidal occlusive syndrome, pancreatitis, haemorrhagic cystitis, and fungal infection (mucositis).

4.1.2.2 Late effects induced by chemotherapy

Late effects vary with agent used.

4.1.2.2.1 Effects of chemotherapy on bone

This may affect the cortical (mineral) or the marrow component. Effects on bone mineral include osteoporosis and osteonecrosis with corticosteroids and reduced mineral density with antimetabolites. In the marrow, several agents promote myeloid transformation and acute myeloid leukaemia has been described with epipodophyllotoxins and anthracyclines.

4.1.2.2.2 Effects of chemotherapy on other tissues

Renal toxicity is widely seen (especially with alkylating agents and heavy metals), hepatic toxicity is associated with the antimetabolite agents and pulmonary toxicity with alkylating agents and anti-tumour antibiotics. Neurotoxicity is also common with heavy metals (ototoxicity, peripheral sensory neuropathy), antimetabolites (neurocognitive deficits, leukoencephalopathy) and plant alkaloids (Peripheral sensory or motor neuropathy and Raynaud's phenomenon).

Rarely, chemotherapy induces hormonal toxicities. With the alkylating agents, testicular hormonal dysfunction and impaired spermatogenesis have been reported in males, whilst ovarian hormone deficiencies and reduced ovarian follicular pool may occur in females. Other endocrine disorders (central adrenal insufficiency, growth hormone deficiency, hyperprolactinemia, hypopituitarism, precocious puberty, thyroid problems), alimentary disorders, educational issues, emotional issues also occur in children on chemotherapy. The Children's Oncology Group wrote the Long-term follow-up guidelines for survivors of childhood, adolescent, and young adult cancer in October 2018: any type of cancer treatment provokes adverse psychosocial and quality of life effects, mental health disorders, risky behaviours, psychosocial disability due to pain, fatigue, and sleep problems.

4.2 AIM

To examine the effect of conventional chemotherapy on apparent diffusion coefficient of lumbosacral spine marrow in children treated because of an abdominal or pelvic tumour.

4.2.1 Objectives

- To establish the reproducibility of the ADC measurement in the lumbosacral vertebral bone marrow.
- To measure early (within 3 months) and late (beyond 3 months) changes in ADC of the lumbosacral vertebral bone marrow following chemotherapy in children with abdomino-pelvic tumours and interpret them in the context of ADC measurement reproducibility.

4.3 METHODS

4.3.1 Measurement reproducibility cohort

In 10 children off-treatment having spine MRI for clinical follow-up purposes, the DW-MRI acquisition was run twice at the beginning and end of the examination (before and after the morphological sequences included in the standard protocol). This was done under operational ethical permission (CCR 1406, duration of scan less than 10 minutes). It was not possible to do a “coffee-break” study in this paediatric population as is widely acceptable for reproducibility scans in adults by repeating the examination after a 10 min break and re-positioning the patient in the scanner. In an additional 4 subjects who

had two abdomino-pelvic MRI scans with DW-MRI as part of follow-up within a 6-month period, and who had no intervening treatment in the preceding 6 months, scans done on two separate occasions were used to assess reproducibility.

4.3.2 Chemotherapy cohort

4.3.2.1 Patient selection

Paediatric subjects affected by abdominal or pelvic neoplasms who had two abdomen and pelvis MRI scans pre- and post-chemotherapy including DW-MRI as part of the protocol acquisition were studied. This was approved as a Service Evaluation (756) by The Royal Marsden Hospital (**Appendix 1**).

Children who had chemotherapy at The Royal Marsden Hospital between January 2014 and July 2018 were identified.

4.3.2.1.1 Inclusion criteria

- aged between 5-17 years old
- affected by abdominal or pelvic tumour
- without bony metastatic disease
- chemotherapy administered at The Royal Marsden Hospital
- no previous or concomitant RT or PBT to the spine
- axial pre- and post-treatment DW-MRI scans available

4.3.2.1.2 Exclusion criteria

- patients on any type of medication (apart from chemotherapy)
- bony lesions or illness
- artefacts on DW-MRI and/or other main sequences

63 patients met the inclusion criteria. However, this list was refined by cross-checking all the clinical and demographical information available on the electronic patient record system (**Figure 4.1**) and, after reviewing the MR scans on PACS and applying the exclusion criteria, I identified 11 patients in whom analysable pre- and post-DW-MRI sequences were available. Patients with external MR examinations where DW-MRI had been acquired with $b = 1,000$ s/mm^3 only were unsuitable for ADC calculation. Analysable examinations were anonymised and stored on the XNAT platform.

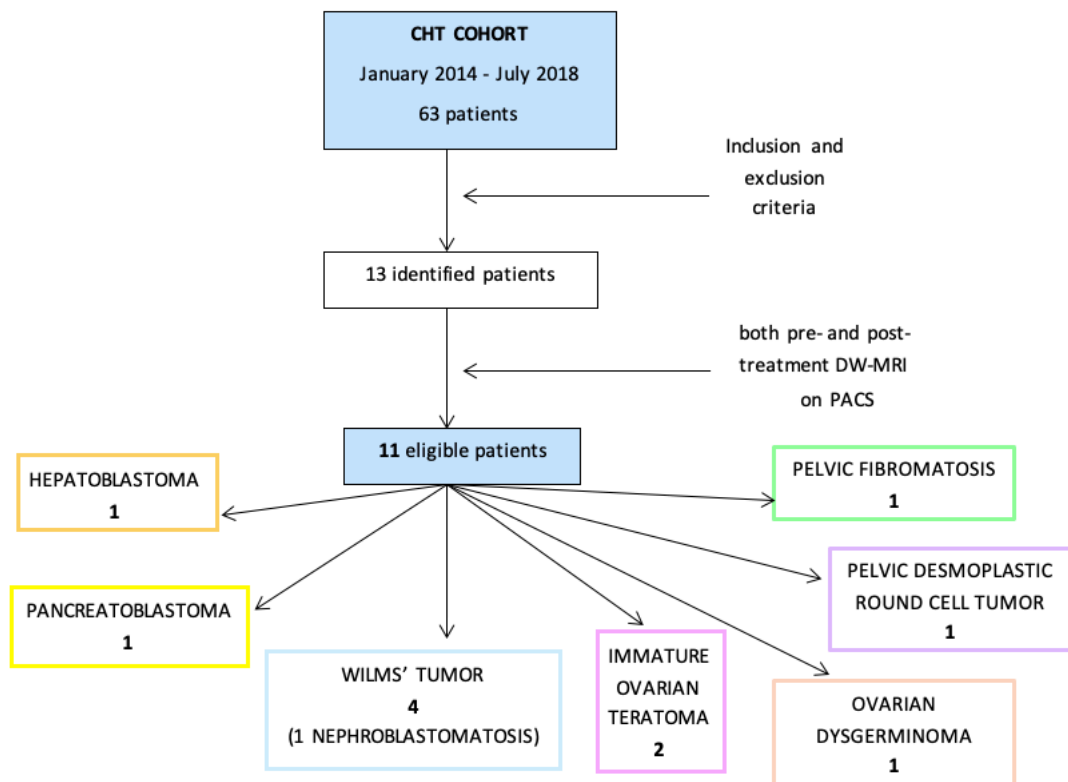


Figure 4.2: Derivation of patients for retrospective analysis of effects of chemotherapy of bone marrow in the lumbosacral spine.

4.3.3 Derivation of patients for chemotherapy cohort

4.3.3.1 Combination of drug evaluation

For these 11 patients included in the cohort the specific agents administered, the overall dose, and number of cycles was recorded. The timings of the imaging scans in relation to chemotherapy completion are given in **Table 4.2**.

Pt	Baseline scan date	MR Scanner	CHT completion date	Early post-CHT scan date	MR Scanner	Late post-CHT scan date	MR Scanner
1	28 th Mar 2012	Aera	26 th Jun 2012	3 rd Oct 2012	Avanto	11 th Jan 2013	Aera
2	16 th Aug 2013	Avanto	21 st Nov 2013	/	/	20 th Mar 2014	Aera
3	20 th Jun 2017	Aera*	13 th Oct 2017	26 th Oct 2017	Avanto	/	/
4	25 th Oct 2016	Signa	29 th Dec 2017	16 th Jan 2018	Aera	18 th Dec 2018	Aera
5	3 rd Oct 2017	Aera	12 th Oct 2017	23 rd Oct 2018	Aera	/	/
6	29 th Jan 2015	Avanto*	13 th Jun 2015	13 th Jul 2015	Aera	3 rd Jul 2015	Aera
7	27 th Mar 2018	Aera	18 th May 2018	7 th Jun 2018	Aera	/	/
8	24 th Aug 2015	Aera	14 th Oct 2016	7 th Jan 2017	Aera	10 th Apr 2017	Aera
9	25 th Feb 2016	Skyra**	2 nd Oct 2017	20 th Oct 2017	Avanto	/	/
10	29 th Apr 2015	Optima	18 th Dec 2015	5 th Jan 2016	Aera	/	/
11	28 th Oct 2015	Avanto	15 th Mar 2016	16 th Jun 2016	Aera	15 th Aug 2016	Aera

Table 4.2: Relation of scan timings to treatment and scanner used for assessment at each time-point. *External examinations; **3 T scanner.

4.3.4 Imaging analysis

Children in the cohort had been scanned at 1.5 T — twenty-nine out of thirty examinations — predominantly on a Siemens Magnetom Avanto (nineteen patients) or Aera (six subjects) scanner at The Royal Marsden; one examination was imported from St George's Hospital – Signa HDtx GE; one was performed on Magnetom Avanto at Great Ormond Street Hospital (GOSH) for Children, and one was obtained at Addenbrooke's Hospital at Cambridge – Optima MR450w, GE) (**Tables 4.2 and 4.3**). The solely study performed on a 3 T scanner (Siemens Magnetom Skyra) was the imported baseline MR of patient 9 affected by pelvic desmoplastic round cell tumour who underwent her post-treatment study on a 1.5 T Avanto scanner at The Marsden.

The Royal Marsden Hospital protocol of breath-hold acquisition included coronal T1- and T2-W TSE (thickness of 4 mm), axial T2-W TSE (at 5 mm), coronal T2-W TRUFI triggered (at 3.5 mm), post-Gadolinium T1-W coronal (at 4 mm) and axial (at 5 mm). Free breath acquisition, whilst, comprised coronal T2-W TRUFI triggered (at 5 mm), T1-W in-phase coronal triggered (at 5 mm), T2-W TSE axial triggered (at 4 mm), T1-W in-phase axial triggered (at 4 mm). In both types of acquisition, EPI 2D DW-MRI was acquired at 6 mm with b values of 0, 100, 500, and 750 s/mm² (n=8). Diffusion-weighted protocols for all scanners are detailed in **Table 4.3**. The most frequently used protocol for an individual scanner where there is variability is given in red. The majority of scans were performed in-house (25 out of 30) with 19 on the Aera and 6 on the Avanto. However, implications of the different acquisition protocols should be taken into account when analysing the results. In fact, apart from the echo-planar readout which was applied to all examinations and the TE the range of which was very

narrow (60-70 for all the scans, apart from one in which 90 was used), TR ranged from 2,700 (1 scan) and 8,500 with the majority of the studies (25) shifted towards the upper limit (5,100-8,500). Unfortunately, the spectrum of the b values adopted was much wider than the other technical parameters. However, almost in all scans analysed (26 out 30) a low b value (50-100 s/mm²) was included which prevented the influence of blood perfusion when ADC maps were calculated.

Imaging examinations were anonymised and data were transferred to the Institute of Cancer Research through the password-protected web-platform XNAT, where they are currently stored.

DW-MRI acquisition	1.5T Siemens Aera (RMH)	1.5T Siemens Aera (RSC)	1.5T Siemens Avanto (RMH)	1.5T Siemens Avanto (GOSH)	1.5T GE Signa (SGH)	1.5T GE Optima (Adnbr)	3T Siemens Skyra (WH)
Number of scans	19	1	6	1	1	1	1
TR (ms)	5100-8500	5500	5100-8000	2700	7000	3600	6000
TE (ms)	70 (60, infants)	60	70	90	70	60	60
Slice thick (mm)	6 (5, infants)	6	5	6	7	10	5
Readout	Echo-planar	Echo-planar	Echo-planar	Echo-planar	Echo-planar	Echo-planar	Echo-planar
b-values (mm²/s) acquired	0, 100, 500, 750 (0,900 in 2012; 100, 600, 1050 in 2013)	50, 400, 800	100, 600, 1050 (0, 50, 600, 900, 1050 in 2012; 0, 100, 750 in 2013)	0, 1000	0, 700	0, 600	0, 600
b-values for ADC maps	all	all	all	all	all	all	all

Table 4.3: Diffusion-weighted protocols on different scanners at different locations. The most frequently used protocol for an individual scanner where there is variability is given in red. The majority of scans were performed in-house (25 out 30) with 19 on the Aera and 6 on the Avanto. (RMH=Royal Marsden Hospital, RSC=Royal Sussex County Hospital, GOSH=Great Ormond Street Hospital, SGH=St George's Hospital, Adnbr=Addenbrooke's Hospital, WH=William Harvey Hospital).

4.3.4.1 Method of region-of-interest delineation

Both axial and coronal T2-W images were used to identify the lumbosacral vertebrae and the DW images were correlated with morphological T2-W images. Circular regions of interest of approximately 8-10 mm in diameter were drawn within L3, L4, L5, and S1 on a midline slice of the highest b value DW images using in-house software (Adept[®], The Institute of Cancer Research, **Figure 4.3**). Data from the entire volume of interest were obtained for statistical analysis.

4.3.4.2 ADC calculation

All studies included at least two b-values. The scanners utilised for each patient at each time-point are listed in **Table 4.2** and any variations in protocol are recorded in **Table 4.3**. In all the cases, ADC was calculated through a monoexponential fit of the data, creating traditional maps (cf. 2.3).

4.3.4.3 Statistical analysis

Statistical analysis was performed using GraphPad Prism software (version 7.04, GraphPad Incorporated company, California). In the reproducibility cohort, Bland-Altman plots of difference between measurements versus mean were used to assess the reproducibility of the data by assessing the 95% confidence intervals.

In the treatment effects cohorts, descriptive statistics were used to describe the data. Additionally, ADC data recorded the median, mean, 10th, 25th, 75th, and 90th percentile values. Frequency distributions were used to illustrate the distribution of the mean ADC values before and after treatment. As data at baseline and at the first post-treatment time-point were normally

distributed (Shapiro-Wilk test), the change between baseline and this time-point used a paired t-test. There were too few data at the later time-point after completing chemotherapy for statistical analysis, so observational conclusions alone were made.

Pt	gender	age (y)	mean ADC first time	SD ADC first time	mean ADC second time	SD ADC second time	mean ADC1 & ADC2	difference ADC values	$\Delta\%$
1	M	16	49.8	11.9	49	11.9	49.4	-0.8	1.6
2	F	12	39.1	15	39.6	15.7	39.35	0.5	1.2
3	F	14	46.7	9.3	47.5	8.4	47.1	0.8	1.7
4	M	8	67.7	12.2	68.1	12.7	67.9	0.4	0.6
5	F	14	47.8	11.6	48.9	9.9	48.35	1.1	2.3
6	F	6	81.5	8.5	80.2	9.3	80.85	-1.3	1.6
7	F	11	53.1	18.3	48.7	14.1	50.9	4.4	8.6
8	F	3	69.8	19.2	72.4	21	71.1	2.6	3.6
9	M	12	55.2	13.8	56	15.4	55.6	0.8	1.4
10	M	15	51.5	8.7	49.8	6.1	50.65	-1.7	3.3

Pt	gender	age (y)	mean ADC first time	SD ADC first time	mean ADC second time	SD ADC second time	Time difference (weeks)	mean ADC1 & ADC2	difference ADC values	$\Delta\%$
11	F	3	100.6	48.6	111	45.5	8.1	105.8	10.4	10.3
12	F	3	62.5	10.8	82	12.6	9.7	72.3	19.5	31.2
13	M	3	99.3	57	88.4	38.7	10.3	93.9	-10.9	-11
14	F	7	56.4	15.4	59.1	8.9	28	57.8	2.7	4.8

Table 4.4: ADC values at 2 time points in 10 patients imaged twice at the beginning and end of the same examination and in 4 patients imaged on separate occasions at a median of 10 weeks apart.

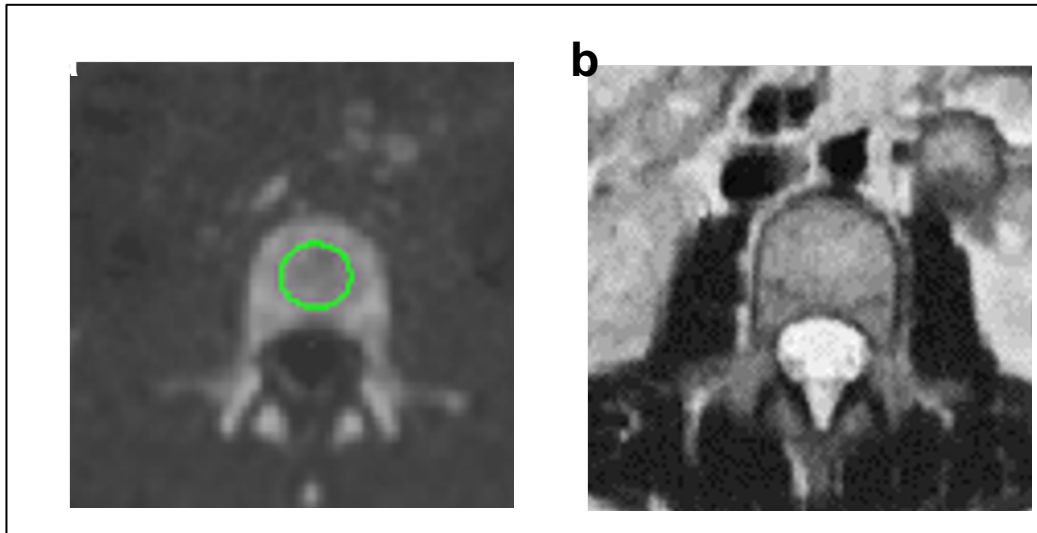


Figure 4.3: Diffusion-weighted axial image ($b= 1050 \text{ s/mm}^2$ through the lumbar spine of a 14 year-old girl (a) with corresponding T2-W image (b) showing circular region-of interest outlined in vertebral marrow (green circle).

4.4 RESULTS

4.4.1 Measurement reproducibility

In the 14 patients aged 3-16 years (median 8 years) who had DW-MRI performed twice to assess reproducibility, the 10 done within the same MRI examination showed very similar ADC values at the beginning and end of the examination. As expected, the ADC variability was much greater when scans acquired on different occasions (median of 10 weeks apart) were considered (**Table 4.4**). Bland-Altman plots were constructed using data from all 14 patients and showed 95% confidence intervals of -23.4% to +19.3% for median ADC and -19.5% to +15.8% for mean ADC (**Figure 4.4**).

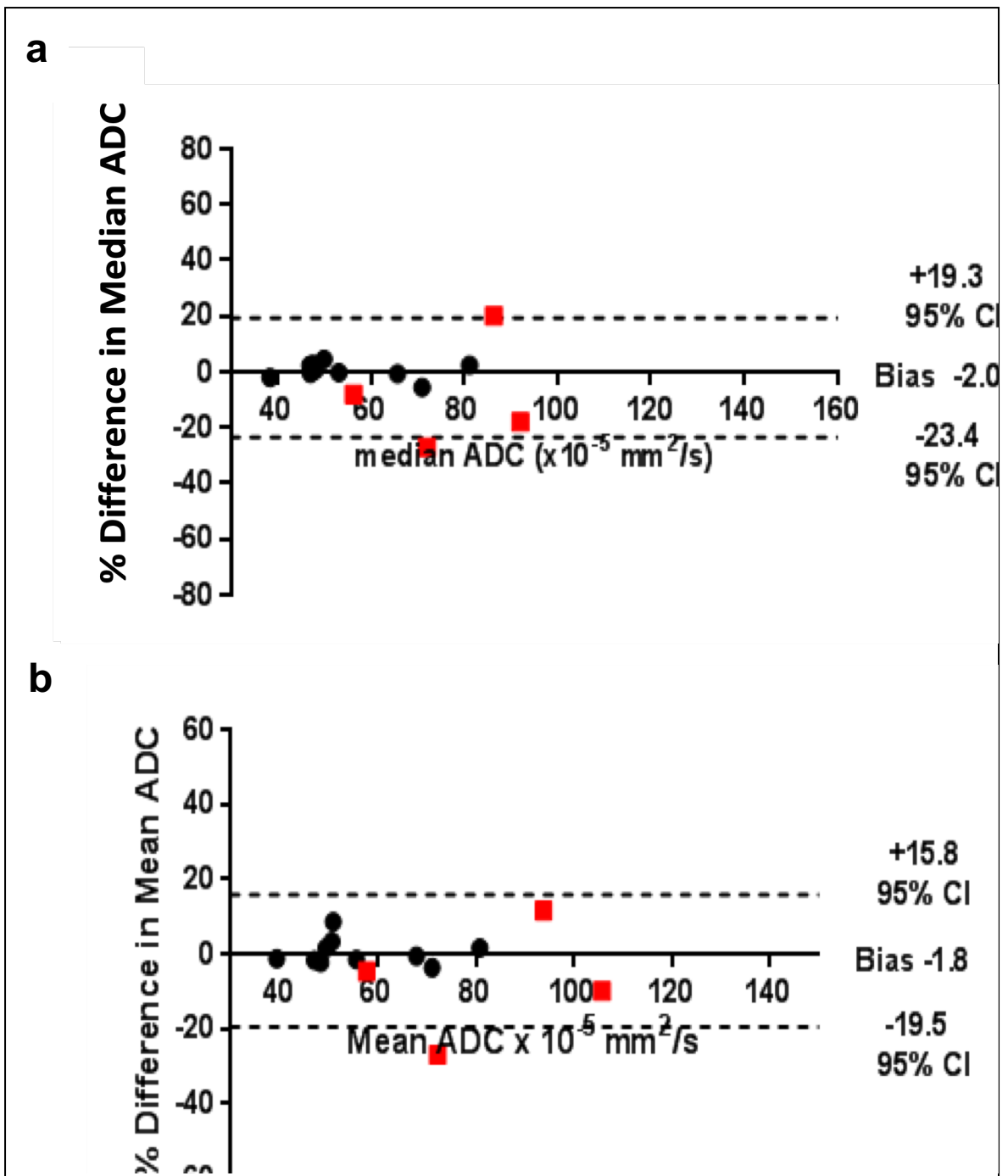


Figure 4.4: Bland-Altman plots showing variability of bone marrow median (a) and mean (b) ADC values from the lumbosacral spine in children. The patients scanned on different days are given in the square red symbols. The black circles denote variability when DW-MRI is repeated within the same examination.

Pt	Diagnosis	Gender	Age (y)	duration chemotherapy (days)	Drugs
1	immature ovarian teratoma with gliomatosis peritonei	F	15	57	etoposide, carboplatin, bleomycin
2	immature right ovarian teratoma with gliomatosis peritonei	F	11	47	etoposide, carboplatin, bleomycin
3	ovarian dysgerminoma	F	12	86	etoposide, carboplatin, bleomycin
4	left nephroblastomatosis	M	2	350	actinomycin, vincristine
5	right Wilms' tumour	F	2	79	actinomycin, vincristine
6	left Wilms' tumour	F	2	123	doxorubicin, cyclophosphamide, etoposide
7	left Wilms' tumour	F	6	56	actinomycin, vincristine
8	pelvic fibromatosis	F	8	381	vinblastine, methotrexate
9*	pelvic desmoplastic round cell tumour	F	16	73	actinomycin, vincristine, ifosfamide, doxorubicin
10*	hepatoblastoma	M	13	37	paclitaxel
11	pancreatoblastoma	F	14	198	cisplatin, doxorubicin, carboplatin, fluorouracil

Table 4.5: Patient characteristics and combination of anticancer drugs received, conjointly and the duration of whole treatment. * Patients who died.

4.3.2 Chemotherapy cohort

4.3.2.1 Patients' characteristics

11 children who fulfilled the inclusion criteria were categorized as given in **Table 4.5**.

All patients were treated at The Royal Marsden Hospital. The timeframe for the post-treatment scan ranged from 37 to 350 days (**Table 4.5**). Patient 7 who was treated for > 1 year did not have late time-point measurements included in this analysis. All patients survived the treatment. However, two patients deceased afterwards (patient 9 with multiply relapsed hepatoblastoma metastatic to lungs and mediastinal lymph nodes died of toxicity induced by pembrolizumab, and patient 10 died of progressive disease) whilst the others are still alive.

4.3.2.2. Combination of agents

The drugs administered were standard chemotherapeutic agents for use in that cancer type. They were used in varying combinations and dose adjusted to the child's age and weight. Platinum based agents in combination with etoposide or vincristine or vinblastine were most commonly used (**Table 4.5**)

4.3.2.3 Region-of-interest size

The calibre of the circle drawn as a region of interest in the midline of the vertebrae L3, L4, L5 and S1 ranged from 8 to 10 mm. Voxels numbers in the regions-of-interest were: pre-treatment median 150, lower quartile 45, upper quartile 160; 1-3 months post-treatment median 277, lower quartile 171, upper quartile 340; 4-12 months post-treatment median 244, lower quartile 201, upper quartile 440).

4.4.2.4 Longitudinal ADC changes with treatment

All patients were treated at The Royal Marsden Hospital. All patients had at least one post-treatment scan including DW-MRI; 6 out of 10 had also a second MRI examination. Post-treatment follow-up scans were at median of 0.9 months (lower quartile 0.6, upper quartile 2.9 months, [mean 1.7 ± 1.3 months])

after completion of chemotherapy for the earlier time point (n=10) and 5.9 months (lower quartile 5.0, upper quartile 6.9 months, [mean 6.8 ± 3.0 months]) after completion of chemotherapy for the later time-point (n=6).

On baseline scan mean ADC values fluctuated between 59.6 ± 12.2 mm^2/s and $122.7 \pm 51.4 \times 10^{-5}$ mm^2/s . On the first post-treatment assessment, mean ADC values ranged from 53.8 ± 9.6 to $85.4 \pm 39 \times 10^{-5}$ mm^2/s and at the second post-treatment assessment from 53 ± 9.3 to $90 \pm 56.8 \times 10^{-5}$ mm^2/s (**Table 4.6**).

Pt	Diagnosis	Gender	Age (y)	Baseline mean ADC \pm SD	1-3 month post-CHT ADC (mean \pm SD)	% ADC change from baseline at time-point 1	Time from end of CHT time-point 1 (months)	4-12 months post-CHT ADC (mean \pm SD)	Time from end of CHT time-point 2 (months)	% ADC change from baseline at time-point 2
1	immature ovarian teratoma with gliomatosis peritonei	F	15	70.7 \pm 25.3	55.1 \pm 5.7	3.5	-22.1	55 \pm 6.6	7.1	-21.9
2	immature right ovarian teratoma with gliomatosis peritonei	F	11	73.1 \pm 20.4	/	/	/	58 \pm 5.9	4.4	-21.3
3	ovarian dysgerminoma	F	12	107.3 \pm 49	85.4 \pm 39	0.5	-20.4	/	/	/
4	nephroblastomatosis left	M	2	68.4 \pm 10.9	77.8 \pm 20.7	0.6	13.7	61 \pm 9.8	12.6	-11.4
5	right Wilms' tumour	F	2	69.8 \pm 19.2	82.7 \pm 9.6	2.6	18.5	/	/	/
6	left Wilms' tumour	F	2	120.5 \pm 51.9	71.5 \pm 38.2	1.1	-40.7	90 \pm 56.8	4.9	-25.2
7	left Wilms' tumour	F	6	81.5 \pm 8.5	61.2 \pm 12.5	0.7	-24.9	/	/	/
8	pelvic fibromatosis	F	8	87.8 \pm 63.6	65.8 \pm 13.7	3	-25.1	65 \pm 16.4	6.4	-25.5
9	pelvic desmoplastic round cell tumour	F	16	59.6 \pm 12.2	59.7 \pm 7.6	0.6	0.17	/	/	/
10	hepatoblastoma	M	13	122.7 \pm 51.4	75.9 \pm 51.4	0.6	-38.1	/	/	/
11	pancreatoblastoma	F	14	63.3 \pm 21.4	53.8 \pm 9.6	3.3	-15	53 \pm 9.3	5.5	-16.9

Table 4.6 Longitudinal changes in ADC at baseline and at subsequent follow-up after chemotherapy. ADC decreased after 1-3 months and subsequently stabilised at this level at the later time-point.

7 out of 10 children treated with chemotherapy showed a decrease in mean ADC values on the first post-treatment scan of 15-40% (median -21.2 % lower quartile, LQ -25%, upper quartile, UQ -3.6%) that was significant (p=0.04, paired t-test).; 1 patient had no imaging at this time-point. Six of these exceeded the 95% CI of measurement variability. ADC then fell further or stabilised in 5 of 6 patients who had a second follow-up between 4-12 months), with a small rise in 1 case (**Figures 4.5 a, b, c** and **4.6 a, b, c**). Data from 2 individual patients during administration of long-term chemotherapy are plotted in **Figure 4.7** and illustrate individual variations in pattern of response during the course of chemotherapy. Histogram shifts for the whole cohort at 1-3 months and 4-12 months post chemotherapy are shown in **Figure 4.8**. Median and centile data for individual patients is given in **Table 4.7**.

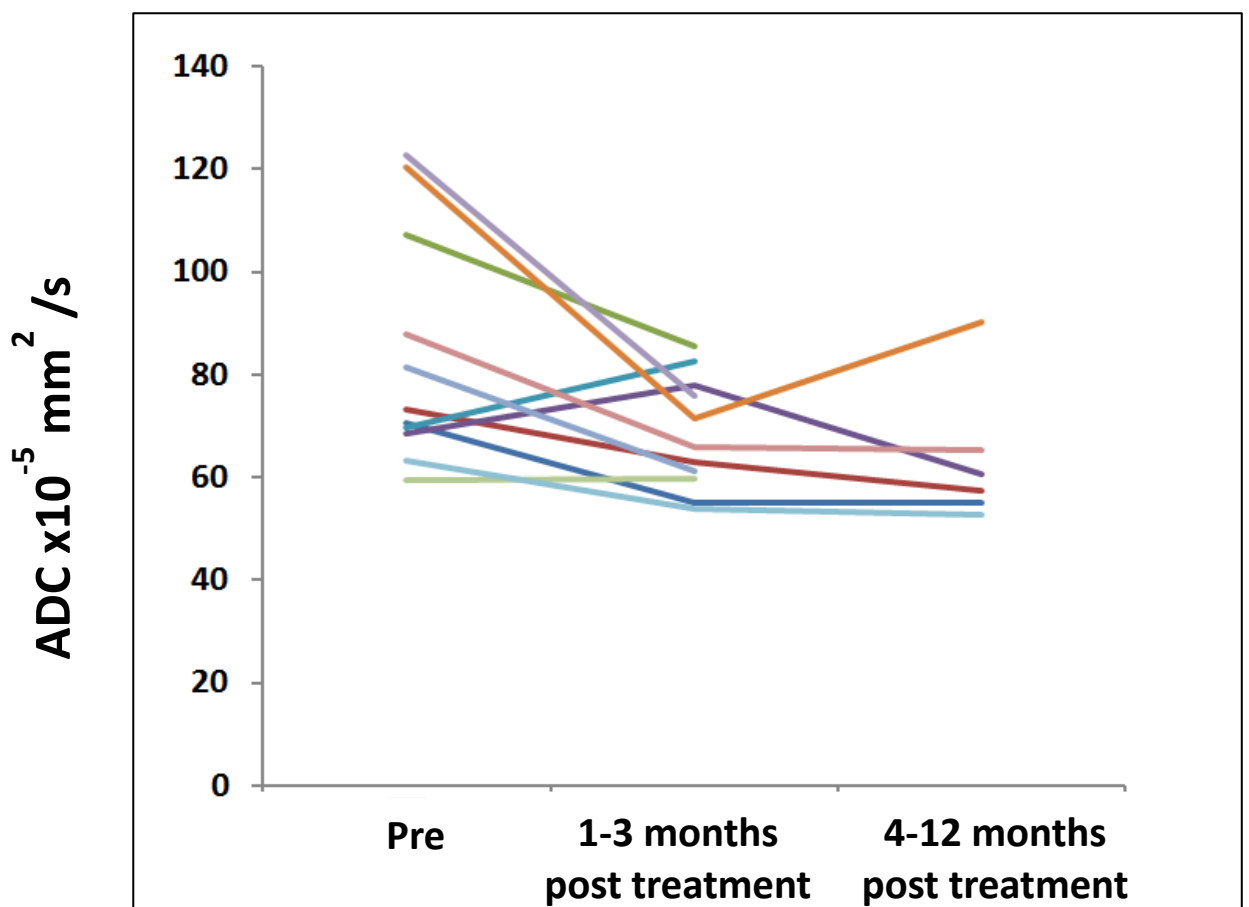


Figure 4.5 a: Longitudinal patterns of ADC change in the lumbosacral marrow in children treated with chemotherapy. A fall in ADC was noted at 1-3 months, which was sustained at 4-12 months. Only 2 cases showed an early rise in ADC, one of which then fell to below baseline values.

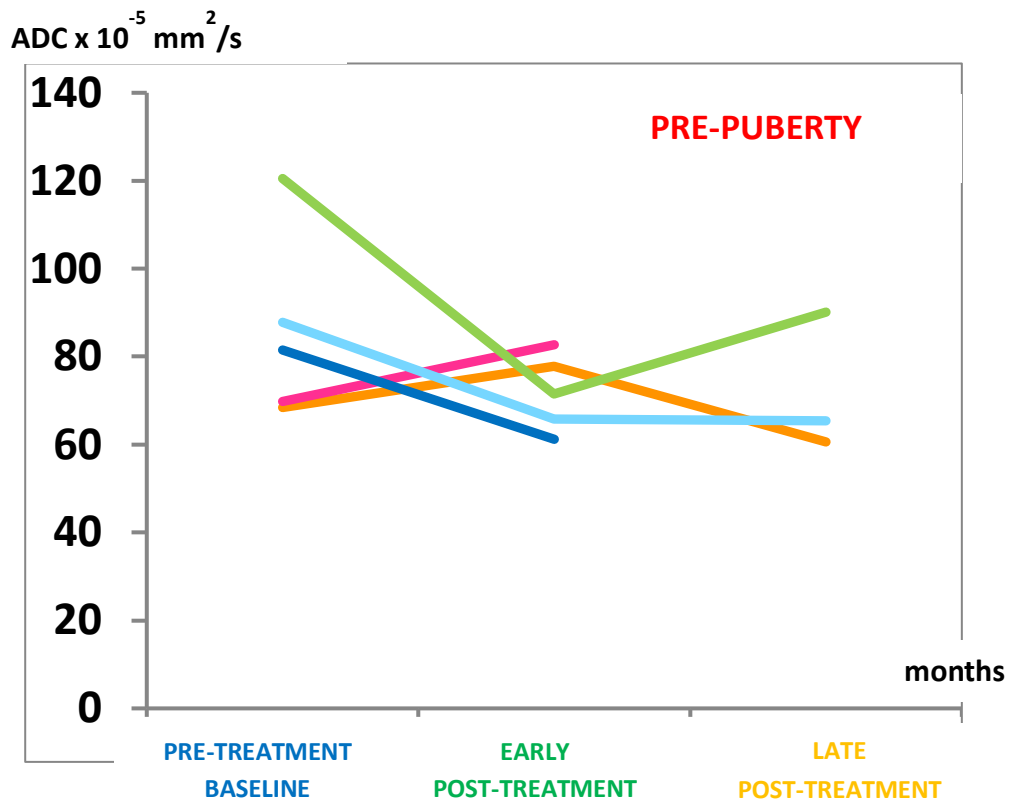


Figure 4.5 b: Longitudinal patterns of ADC change in lumbosacral marrow in pre-pubertal children (patients: 4, 5, 6, 7, and 8) affected by Wilms' tumour and pelvic fibromatosis treated with chemotherapy.

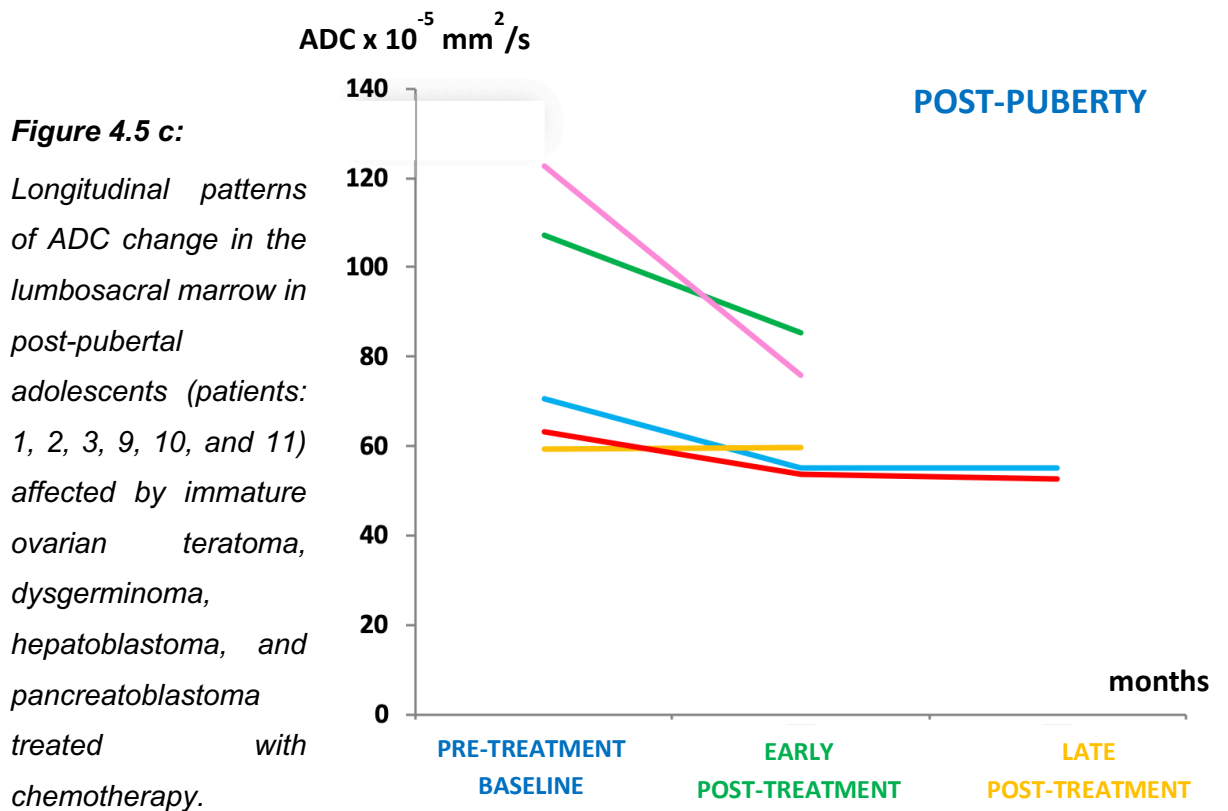


Figure 4.5 c: Longitudinal patterns of ADC change in the lumbosacral marrow in post-pubertal adolescents (patients: 1, 2, 3, 9, 10, and 11) affected by immature ovarian teratoma, dysgerminoma, hepatoblastoma, and pancreatoblastoma treated with chemotherapy.

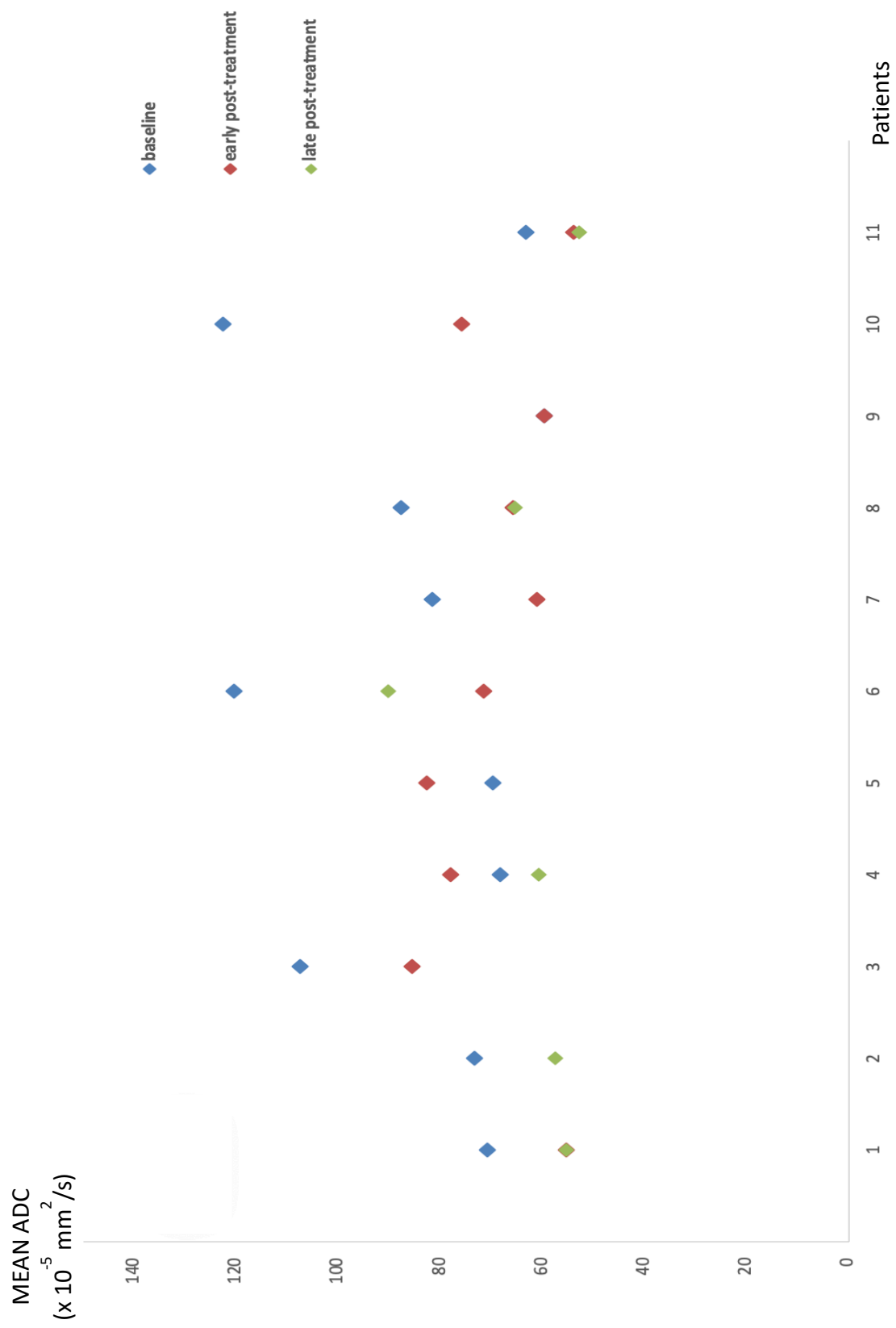


Figure 4.6 a: Scatter plot illustrating mean ADC values pre-treatment, at early (1-3 months) and late (4-12 months) post treatment follow-up.

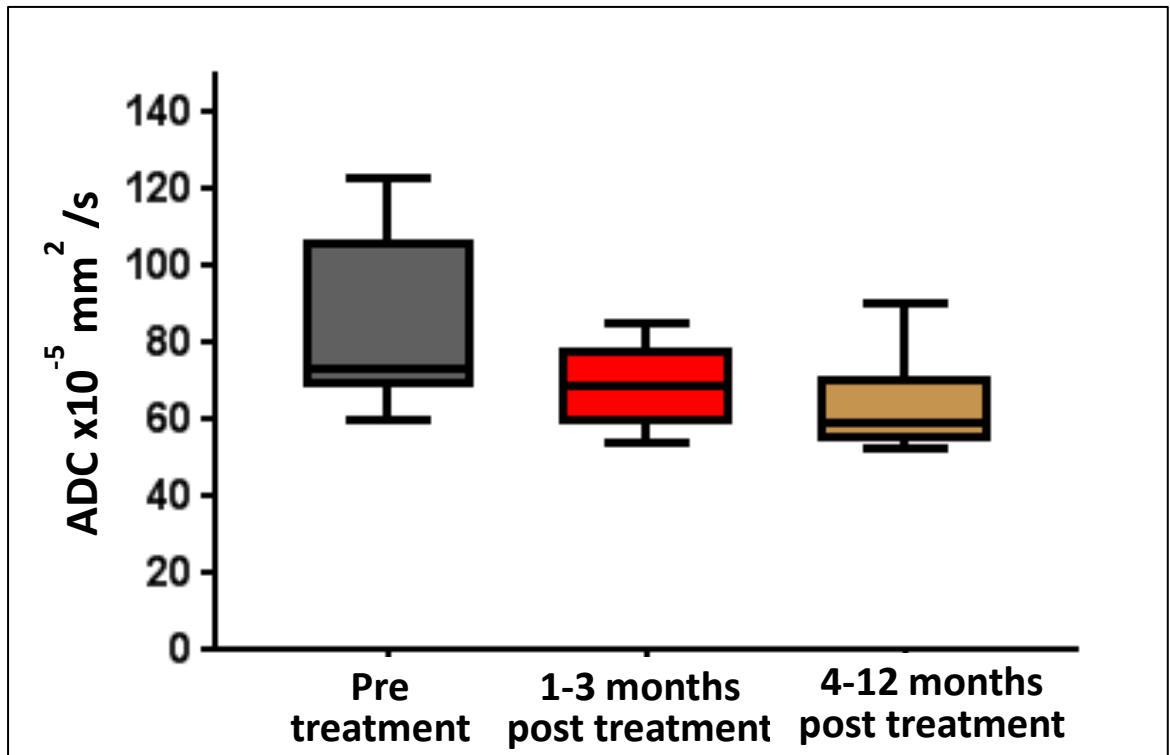


Figure 4.6 b: Box and whisker plots showing median, quartiles and ranges of ADC values pre-treatment and at 1-3 and 4-12 months post treatment. The initial reduction in ADC was significant ($p=0.04$)

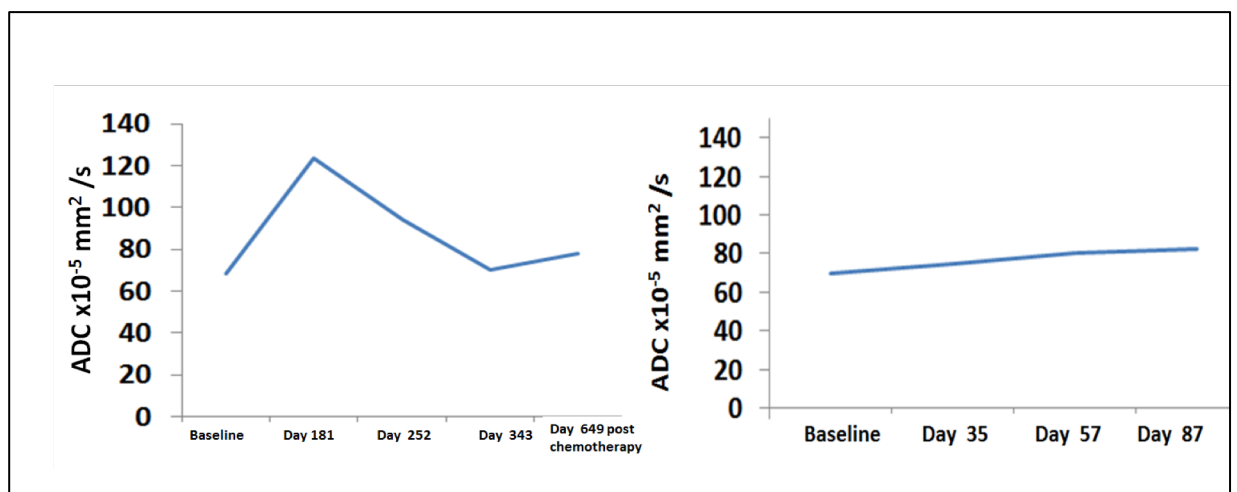


Figure 4.7: Longitudinal ADC changes during chemotherapy in 2 separate individuals over time, show a spike pattern of response in one (patient 5 with Wilms' tumour who received further chemotherapy, actinomycin and vincristine) and a much more gentle rise in the other (patient 8, affected by pelvic fibromatosis receiving methotrexate and vinblastine).

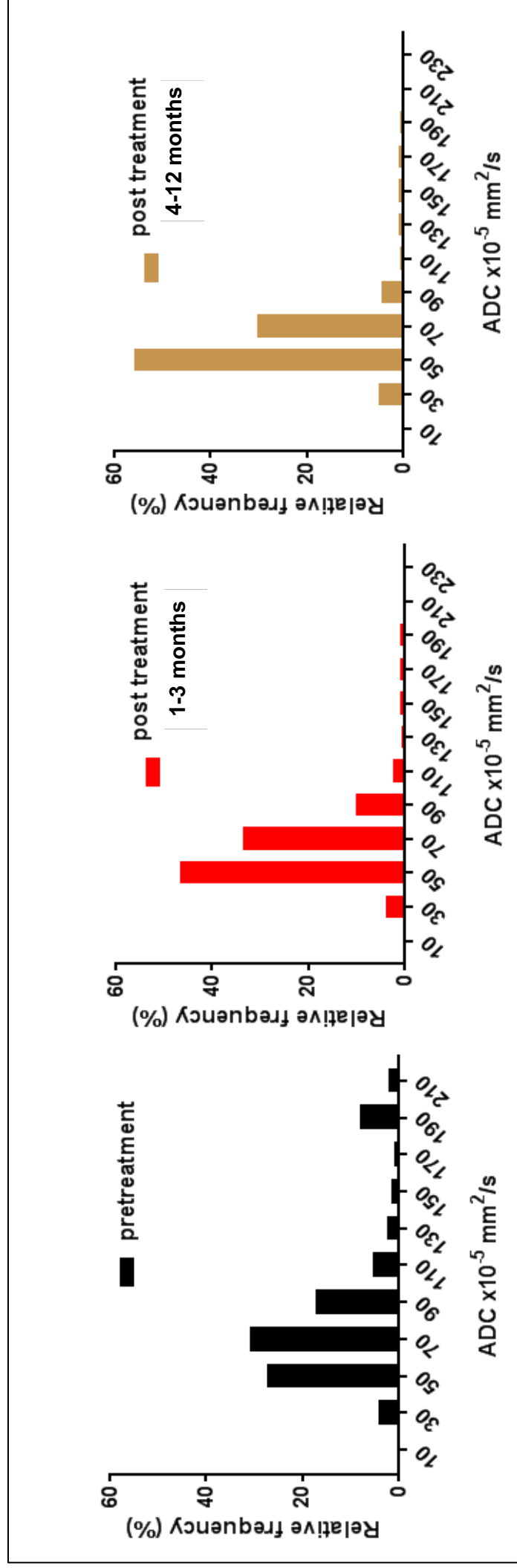


Figure 4.8: Histogram distributions of ADC values before and after chemotherapy. The ADC values are more widely distributed at baseline, but within 3 months they are predominantly lower. This pattern remains stable without further change over time, as evidenced by the very similar histogram distribution of values at the later time-point.

Pt	10 th centile ADC			25 th centile ADC			Median ADC			75 th centile ADC			90 th centile ADC		
	Pre-CHT	1-3 m post-CHT	3-6 m post-CHT	Pre-CHT	1-3 m Post-CHT	3-6 m post-CHT	Pre-CHT	1-3 m post-CHT	3-6 m post-CHT	Pre-CHT	1-3 m post-CHT	3-6 m post-CHT	Pre-CHT	1-3 m post-CHT	3-6 m post-CHT
1	47.4	48	46.4	52.5	51.6	50.6	58.5	55.1	54.8	79.6	58.6	59.6	117	62	63.5
2	47.8	/	50.3	57.7	/	53.5	69.3	/	57.1	86.8	/	61.2	97.9	/	65.5
3	59.4	53	/	67.5	60.3	/	84.6	70.7	/	151	97.6	/	174.3	147.1	/
4	55.3	53.8	49.2	60	58.1	54	66.8	73.7	59.7	76.5	98.8	66.1	83.1	107.1	72
5	44.4	71.7	/	54.4	75.9	/	69	81	/	83.5	88.1	/	95.7	95.9	/
6	59.6	29	27.9	64.4	42.5	41.6	137.2	64.1	73.7	147.9	81.4	139.4	195.1	139.1	173.9
7	70.4	46.4	/	75.7	52.4	/	82.2	60.2	/	86.1	70	/	91.2	78.8	/
8	38.8	46.9	42.3	46.5	56.2	53.7	56.8	66.1	66.4	90.3	76.6	76.4	197.7	83.8	83.8
9	44.9	50.8	/	51.6	55.1	/	59.2	59.2	/	64.5	63.3	/	64.5	69.5	/
10	72.7	40.2	/	79	48.8	/	91.7	57	/	189.4	73.7	/	194.1	171.1	/
11	36.9	41	40.8	46.4	47.5	46.5	62.6	53.7	51.8	77.8	59.7	58.1	96	66	66.2

Table 4.7: Median and centile values for individual patients before, 1-3 months and 4-12 months after completion of chemotherapy

4.4.2.5 Changes in peripheral blood post chemotherapy

Variations in haemoglobin and white count at the same time-points as the imaging where available are given in **Table 4.8**. Across the cohort, there were no substantial change in these measures at these time-points.

Pt	Peripheral blood results					
	Haemoglobin g/L			White cell count x 10 ⁹ /L		
	Baseline	Post-CHT T-P 1	Post-CHT T-P 2	Baseline	Post-CHT T-P 1	Post-CHT T-P 2
1	128	/	120	4.8	/	4.9
2	132	/	133	6.6	/	6.1
3	103	115	/	6	2.6	/
4	119	94	/	8	4.7	/
5	95	103	/	9	7.7	/
6	90	99	110	4.8	4.9	11.6
7	112	92	/	10.2	4.7	/
8	118	/	/	9.5	/	/
9	97	159	/	6.5	4.3	/
10	105	98	/	4.1	4.2	/
11	120	111	115	8.5	4.6	7.2

Table 4.8: Peripheral blood haemoglobin and white cell counts for individual patients at equivalent time-points to imaging data. There was no substantial variation from baseline apart from patient 9 who experienced significant liver toxicity to chemotherapy and died shortly after the early post-treatment measurement. Reference values for haemoglobin for children aged 2-6 are 110-140 g/L and for those aged 6-12 are 115 to 155 g/L. For white cell count for children aged 2-6 are 5-15 x 10⁹/L and for those aged 6-12 are 5-13 x 10⁹/L. Above this adult reference ranges apply: haemoglobin 120-150 g/L for females, 130-170 g/L for males and white cell count 4-10 x10⁹ /L.

4.5 DISCUSSION

4.5.1 Nature of the ADC changes post treatment

The use of ADC as a response biomarker for studying the effect of chemotherapy on bone marrow in adult haematological malignancies is well established.^{8, 9} In these studies, emphasis has been on delineating abnormal areas within bone marrow and following the changes with treatment: a significant increase in ADC of responding lesions, vs non-responding lesions has been demonstrated,¹⁰ which is in keeping with findings from other solid tumours. In myeloma, where there is widespread bone marrow involvement and assessment of the whole skeleton is the norm, the increase in ADC also has been shown to be significant in responders compared to no responders.¹¹

There is a paucity of data on ADC changes in *normal* bone marrow following chemotherapy. The general myelosuppressive effect of chemotherapy on bone marrow has long been established, and decreased marrow functioning has been reported for up to several years after chemotherapy;¹² effects are monitored via peripheral blood counts. These do not necessarily reflect changes in bone marrow composition. In a more recent study of patients treated with chemoradiotherapy for cervical cancer, the effect of chemoradiotherapy was documented in normal pelvic bone marrow and showed a significant increase in true diffusion but not in ADC (where the perfusional elements of the low b-values are included in the calculation) in patients experiencing haematological toxicity compared to those who did not.¹³ However, these effects are likely to have reflected the pelvic *radiation* dose, and there were no longitudinal measurements made, nor any indication on whether the changes were reversible on follow-up. The degree and the time course of bone marrow

suppression (nadir, time to marrow recovery) are known to vary among different chemotherapeutic drugs.¹² My study in a paediatric population documents ADC changes from chemotherapy at early and late time-points, where no current literature exists.

As demonstrated with other tissues, the factors affecting the ADC values in bone marrow include tissue perfusion, extracellular and intracellular movement of water molecules, and diffusion of water molecules across cell membranes.¹⁴ Yellow bone marrow has a lower DW-MRI signal intensity because of its lower water content compared to red bone marrow; its lower ADC value reflects the hydrophobicity of fat, its relatively low perfusion and proton density.¹⁵ It is therefore likely that the influence of chemotherapy is more distinct in bone regions that have a physiologically higher red marrow fraction;¹⁶ in adults this is in the proximal skeleton where up to 60% of the entire red marrow is located. My data are limited to the lumbar spine, which has a high red marrow content in paediatric and adult populations, so the changes measured are likely to be in regions with high potential for haematological toxicity.

4.5.2 Longitudinal evolution of the ADC changes post treatment

Even in adults, documentation of the longitudinal effects of chemotherapy on normal bone marrow with imaging is limited. However, it has been demonstrated that there is a trend towards higher fat content of the proximal skeleton (spine and pelvis) in patients who had chemotherapy in their medical history, irrespective of the time interval between chemotherapy and imaging examination. This suggests that chemotherapy might have long-term effects on the composition of bone marrow.¹⁷ Other studies with longitudinal

data in adults have inevitably included radiation therapy as a concomitant treatment, confounding the results.¹⁸ These have indicated that mid-treatment changes in fat fraction of bone marrow were evident in patients with known myelotoxic regimens, but not in those causing less marrow suppression, and that these changes were sustained at the end of treatment. As the less myelotoxic treatments often were radiation only, without chemotherapy, it is clear that the addition of chemotherapy induces these changes. However, it does not indicate the effect of chemotherapy alone.

A study by Gerard et al¹⁹ was the first to document the longitudinal changes in bone marrow in patients with haematological malignancy treated with chemotherapy. As this preceded the current establishment of diffusion-weighted techniques in bone marrow, they used a modified Dixon chemical shift imaging technique to quantify longitudinal changes in bone marrow fat that occurred during induction chemotherapy in patients with acute leukaemia. Imaging was done at relatively low field-strength (0.6T) and 47 imaging studies were obtained in 11 patients over the course of treatment. Quantitative measures of fat fractions and water and fat component T1 and T2 relaxation times showed sequential increases in fat fractions among responding patients (n=9), consistent with biopsy-confirmed clinical remission. In two patients who later relapsed, sharp decreases in fat fractions were noted. In two patients who failed to regenerate normal marrow, unchanging, low fat fractions were seen. Water component T1 values reflected post-therapeutic changes in the hematopoietic elements. They concluded that quantitative chemical shift imaging was useful in assessing treatment response in acute leukaemia during early bone marrow regeneration and, later, in ascertaining remission or

relapse. Unfortunately, in this clinical scenario, where peripheral blood assessments are simple, cheap and easily tolerated, the need for imaging assessments has not been realised. In an era of increasingly complex chemotherapeutic regimens, however, where early marrow damage to otherwise normal marrow in non-haematological malignancy may not be evident early in peripheral blood, and where marrow aspirates are poorly tolerated, the use of imaging follow-up may be more acceptable and useful.

4.5.3 Clinical impact of the findings

Several studies both adult and paediatric of response to chemotherapy exist in the literature. However, the focus of the measurement has always been on the tumour itself rather than on surrounding normal tissues. A small trial of chemotherapy in osteosarcomas showed that children who received chemotherapy prior to surgery had a greater increase in tumour ADC than those who did not.²⁰ A separate study showed that post-chemotherapy increases in ADC related to larger necrosis in osteoblastic but not in chondroblastic osteosarcomas.²¹ A detailed study utilizing data from the Childhood Cancer and Leukaemia group database investigated and compared the robustness and suitability of several diffusion change metrics for assessment of treatment response on highly heterogeneous clinical paediatric data.²² The effects that different ROI selection, registration technique, and threshold selection had on functional diffusion map metrics were documented. Functional diffusion maps represent a recent method among the imaging biomarkers used in neuro-oncology which adopts a statistical approach for segmenting heterogeneous neoplasms by applying a defined threshold of ADC change following

treatments. Namely, it quantifies gradual ADC changes in the same voxels of the tumour measured in the same patient over a series of follow-up MR examinations. These authors presented the ADC data as ratios (post to pre chemotherapy ADC measurements) or normalised ratios to white matter, rather than as a percentage increase. They showed that normalised ADC ratios in brain tumours increased significantly in responders compared to non-responders (as defined by Response Assessment in Neuro-Oncology, RANO criteria). However, all measurements were made in the tumour itself, so again there is no data on changes within normal surrounding tissues. Although my data is from a small retrospective series and is relatively poorly controlled, it shows that measurement of ADC in normal bone marrow is not only feasible, but that changes are measurable beyond the levels of reproducibility following chemotherapy and that this may well be a viable way of assessing potential marrow toxicity to novel agents within clinical trials before changes in blood counts are evident.

4.5.4 Limitations of the measurement and measurement variability

The retrospective nature of this study represents a major limitation. As a result of this, it was not possible to standardise the timing of acquisition of the follow-up scans, nor to select patients based on the same tumour type and consequently the identical combination of drugs, dose, and number of cycles of treatment. Unfortunately, this also implied that the sequences included in the imaging protocol were not always standardised (although the majority of diffusion-weighted images were acquired with the same b values and slice of thickness, there were data from a variety of scanners with a different protocol in

terms of b values and slice thickness). Moreover, the b-values used may not have been ideal for ADC derivation. Inclusion of b=0 has been recognised as adding to the variability of the measurement, particularly as the low b-values may introduce the longer path lengths travelled by protons in the microvasculature. Removing the effects of perfusion is now widely practised in ADC quantitation, where a low b-value of 50 or 100 s/mm² is advocated.²³ Unfortunately, in this retrospective analysis, I did not have the option of optimising the acquisition protocol or refining the analysis to achieve the most accurate results for ADC. Going forward in prospective trials, the use of b=50 or 100 s/mm² should be mandated where quantitation is intended.

4.6 SUMMARY

The main conclusions of this chapter are:

Obtaining reproducibility data in children is challenging. As there are relatively few repeat or follow-up paediatric abdominal MR examinations done on patients who are not on treatment, it was difficult to obtain repeat abdomino-pelvic scans in a population with identical age range without interval intervention that could be analysed for ADC measurement reproducibility.

Furthermore, although in comparison to brain studies, variation in the ADC measurement was higher, the reductions in ADC following chemotherapy exceeded measurement variability in the majority of cases. These might be due to either increase in the intracellular fluid component or to reduction of the extracellular space, for instance,

caused by cytotoxic oedema — as a result of cell swelling as a consequence of either cell death or failure of transmembrane ion pumps — or owing to fragmentation of the cellular components leading to increase in the viscosity in the intra- or extracellular compartments. A combination of these phenomena occurring simultaneously might also represent a valid possibility.

The changes post-chemotherapy predominantly showed a decrease in ADC by 3 months, which was then sustained without further change beyond that time-point. The stability of the data in individual patients indicates that the findings are likely to be reliable.

The acute rise in ADC seen with patients on RT/PBT and chemotherapy was not evident after treatment completion.

4.7 KEY POINTS

- ADC quantitation in the lumbar spine of children can have a measurement variability of up to 25% (Limits of Agreement).
- At 1-3 months after completion of chemotherapy there is a reduction in ADC in vertebral marrow beyond measurement variability in 70% of cases which is sustained when measured at 4-12 months post-treatment.

REFERENCES

1. Renz DM and Mentzel HJ. [Imaging of abdominal tumors in childhood and adolescence : Part II: relevant intra-abdominal and retroperitoneal tumor entities]. *Der Radiologe*. 2018; 58: 673-686.
2. Levy AD, Manning MA and Miettinen MM. Soft-Tissue Sarcomas of the Abdomen and Pelvis: Radiologic-Pathologic Features, Part 2-Uncommon Sarcomas. *Radiographics : a review publication of the Radiological Society of North America, Inc*. 2017; 37: 797-812.
3. Heo SH, Kim JW, Shin SS, et al. Review of ovarian tumors in children and adolescents: radiologic-pathologic correlation. *Radiographics : a review publication of the Radiological Society of North America, Inc*. 2014; 34: 2039-2055.
4. Roebuck DJ, Aronson D, Clapuyt P, et al. 2005 PRETEXT: a revised staging system for primary malignant liver tumours of childhood developed by the SIOPEL group. *Pediatric radiology*. 2007; 37: 123-32; quiz 249-250.
5. Chung EM, Travis MD and Conran RM. Pancreatic tumors in children: radiologic-pathologic correlation. *Radiographics : a review publication of the Radiological Society of North America, Inc*. 2006; 26: 1211-1238.
6. Elkaoui H, Bounaim A, Ait Ali A, Zentar A and Sair K. [Pelvic fibromatosis]. *Presse medicale (Paris, France : 1983)*. 2016; 45: 538-540.
7. Main types of childhood cancer: children aged 0-14 years. United Kingdom 2001 to 2010. *Based on data provided by National Registry of childhood Tumours*.
8. Abdulqadhr G, Molin D, Astrom G, et al. Whole-body diffusion-weighted imaging compared with FDG-PET/CT in staging of lymphoma patients. *Acta radiologica (Stockholm, Sweden : 1987)*. 2011; 52: 173-180.
9. Gu J, Chan T, Zhang J, Leung AY, Kwong YL and Khong PL. Whole-body diffusion-weighted imaging: the added value to whole-body MRI at initial diagnosis of lymphoma. *AJR American journal of roentgenology*. 2011; 197: W384-391.
10. Sun M, Cheng J, Zhang Y, Wang F, Meng Y and Fu X. Application value of diffusion weighted whole body imaging with background body signal suppression in monitoring the response to treatment of bone marrow

- involvement in lymphoma. *Journal of magnetic resonance imaging : JMRI*. 2016; 44: 1522-1529.
11. Giles SL, Messiou C, Collins DJ, et al. Whole-body diffusion-weighted MR imaging for assessment of treatment response in myeloma. *Radiology*. 2014; 271: 785-794.
 12. Mauch P, Constine L, Greenberger J, et al. Hematopoietic stem cell compartment: acute and late effects of radiation therapy and chemotherapy. *International journal of radiation oncology, biology, physics*. 1995; 31: 1319-1339.
 13. Lee EYP, Perucho JAU, Vardhanabhuti V, et al. Intravoxel incoherent motion MRI assessment of chemoradiation-induced pelvic bone marrow changes in cervical cancer and correlation with hematological toxicity. *Journal of magnetic resonance imaging : JMRI*. 2017; 46: 1491-1798.
 14. Federau C, Meuli R, O'Brien K, Maeder P and Hagmann P. Perfusion measurement in brain gliomas with intravoxel incoherent motion MRI. *AJNR American journal of neuroradiology*. 2014; 35: 256-262.
 15. Shah R, Stieltjes B, Andrulis M, et al. Intravoxel incoherent motion imaging for assessment of bone marrow infiltration of monoclonal plasma cell diseases. *Annals of hematology*. 2013; 92: 1553-1557.
 16. Rose BS, Liang Y, Lau SK, et al. Correlation between radiation dose to (1)(8)F-FDG-PET defined active bone marrow subregions and acute hematologic toxicity in cervical cancer patients treated with chemoradiotherapy. *International journal of radiation oncology, biology, physics*. 2012; 83: 1185-1191.
 17. Schraml C, Schmid M, Gatidis S, et al. Multiparametric analysis of bone marrow in cancer patients using simultaneous PET/MR imaging: Correlation of fat fraction, diffusivity, metabolic activity, and anthropometric data. *Journal of magnetic resonance imaging : JMRI*. 2015; 42: 1048-1056.
 18. Carmona R, Pritz J, Bydder M, et al. Fat composition changes in bone marrow during chemotherapy and radiation therapy. *International journal of radiation oncology, biology, physics*. 2014; 90: 155-163.
 19. Gerard EL, Ferry JA, Amrein PC, et al. Compositional changes in vertebral bone marrow during treatment for acute leukemia: assessment with quantitative chemical shift imaging. *Radiology*. 1992; 183: 39-46.

20. Degnan AJ, Chung CY and Shah AJ. Quantitative diffusion-weighted magnetic resonance imaging assessment of chemotherapy treatment response of pediatric osteosarcoma and Ewing sarcoma malignant bone tumors. *Clinical imaging*. 2018; 47: 9-13.
21. Wang J, Sun M, Liu D, et al. Correlation between apparent diffusion coefficient and histopathology subtypes of osteosarcoma after neoadjuvant chemotherapy. *Acta radiologica (Stockholm, Sweden : 1987)*. 2017; 58: 971-976.
22. Rodriguez Gutierrez D, Manita M, Jaspán T, Dineen RA, Grundy RG and Auer DP. Serial MR diffusion to predict treatment response in high-grade pediatric brain tumors: a comparison of regional and voxel-based diffusion change metrics. *Neuro-oncology*. 2013; 15: 981-989.
23. Winfield JM, Collins DJ, Priest AN, et al. A framework for optimization of diffusion-weighted MRI protocols for large field-of-view abdominal-pelvic imaging in multicenter studies. *Medical physics*. 2016; 43: 95.

CHAPTER 5 – Summary and Future Work

5.1 *HOW TO MEASURE THE BONE MARROW IN CHILDREN: challenges in assessing variability and need for multicentre trials*

In the assessment of any quantitative measurement a variety of factors will affect the measurement's variability. This work has attempted to establish the variability of ADC's derived from clival bone marrow and lumbar spine of children. To do such a study prospectively is ethically questionable if a child required sedation or anaesthesia to tolerate the scan. In this regard, no child out sixty was sedated or anaesthetised in the non-oncological cohort (**Chapter 2**); conversely, one out twelve (a 5-year-old female with diffuse pontine glioma) and one out ten (a 5-year-old male with adamantinous craniopharyngioma) were sedated in the RT and PBT cohorts, respectively (**Chapter 3**), and three out evelen patients affected by unilateral nephroblastomatosis (1) and Wilms' tumour (2) were anaesthetised since all of them were 2 years old.

I, therefore, undertook to derive these data from retrospective images. However, as these children had been referred for brain scans because of potential neurological complaints, exclusion of children with potential pathologies was essential and left very few numbers for analysis. This was somewhat easier in the brain than in the spine, because diffusion-weighted imaging forms part of the standard protocol for MRI brain assessment. Moreover, acquisition parameters are largely more standardised, and this reflects the relatively tight reproducibility of mean and median ADC values (**cf Figure 3.4**). In the spine, repeating the ADC measurement at the beginning and end of the examination gave very little variation as expected (**cf Figure 4. 4**) but in 4 cases where the

DWI was done on different occasions with a different scanners and protocols without any standardisation, 95% CI were approaching 50% (**cf Figure 4.4**). This further emphasises the need for standardisation of quantitative imaging biomarkers.

Oncological diseases in children fortunately are rare. In order to amass a body of data, therefore, it has always been necessary to work in multicentre, multinational consortia to generate the required evidence for best practice. Working in large consortia and pooling data from individual centres has therefore become an essential requirement for trials in paediatric oncology. Many consortia exist, focussed around specific disease entities for example the European Consortium for Innovative therapies for Children with Cancer (ITCC,¹,² dealing with delivery of drugs and anaesthetics (GAS consortium,³) but there are few such consortia in imaging,^{4, 5} where standards are set for a paediatric population. This places an increased demand for standardisation of methodology used to generate such data in paediatric centres. Particularly in imaging where data may be acquired on multiple vendor platforms and the acquisition and analysis protocols are likely to be driven by individual operator preferences at each centre, it is key to establish at the onset the benchmarks for data acquisition and analysis within clinical trials. If quantitative methods such as diffusion-weighted imaging are to be used, strict quality assurance and quality control procedures need to be in place so that data can be meaningfully pooled to yield valid results.⁶ Preliminary tests with phantoms in all the centres involved in a specific prospective study using magnets with the same strength and the same type of coils should ensure that key technical parameters — such as signal-to-noise ratio, brightness, geometric accuracy, slice of thickness,

signal intensity uniformity, high-contrast spatial resolution, and low-contrast object detectability — are, if not identical, at least very similar.

5.2 WHEN TO MEASURE THE BONE MARROW IN CHILDREN: Response Assessments and their timing in the face of multimodality treatment

The work described in Chapters 3 and 4 interrogating the effect of radiation therapy, proton therapy and chemotherapy was retrospective, which meant that the time lines for follow-up were not standardised.

Despite this, there were trends in the data, showing that with RT and PT increases in ADC occurred early after treatment and that they subsequently diminished. This is likely to be related to the immediate response of tissue to acute injury caused by these ionizing radiations. Cell lysis and oedema are early responses to acute injury⁷ and are likely to be responsible for the early increases in ADC.

With chemotherapy the systemic exposure to agents that cause cell death by disrupting cell cycle or cellular metabolism does not pose such an immediate toxic insult and the timing of response appeared slower and more sustained. Unfortunately, the chemotherapy regimens used varied across the cohort, which was inevitable in a retrospective study across multiple tumour types. This is likely to have caused a lot of variability in the response: this has been shown in adults where the precise chemotherapy administered with pelvic radiation had differing degrees of haematological toxicity.⁸ More than the age range of the population, the organs affected, the technical parameters related to the different scanners, the timepoints of the MR examinations during the follow-

up, the combination of drugs and the number of cycles, the largest source of variability was undoubtedly the different tumour types; in fact, the intrinsic cellularity and the solid/cystic component ratio at baseline conjointly with the consequent architectural changes owing to the treatment effect make the sample heterogenous. It is well demonstrated that even the same neoplasm might present with a broad spectrum of aggressivity, histological subtypes, and grading — which often correlates with the amount and speed of tumour marker secretion — resulting in a different dose, combination or cycles number of anticancer drugs. Also, as the cohort I studied was small, chemotherapy-related variability may well have masked the overall trends in the data. My null hypothesis — conventional chemotherapy does not cause effects on ADC of the lumbosacral marrow — can be rejected since p value (0.04) is less than α (0.05) or type I error, related to false positive results. β (or type 2 error, related to false negative results), commonly and arbitrary set at 0.2, is used to calculate the power that is the probability to detect the effect in the sample and corresponding to $1 - \beta$ (which equals 0.8). Ideally, such a study would be carried out prospectively in children affected by the same tumour type — including analogous histological grading — within a defined age, group receiving a similar (if not identical) combination of agents with equal relative dose (based on the patient's weight and age) and number of cycles, and all being imaged within a narrow time window of treatment completion. Therefore, the conclusions drawn in Chapter 4 represent an attempt to analysis a trend from the available data, taking into account the aforementioned sources of variability.

A crucial aspect of meaningful use of ADC measurements to assess normal tissue toxicity in the clinic is to obtain data at multiple time-points and

look at trends in individual patients. Having established the limits of agreement for such measurements it would be possible to ascertain whether local radiation regimes or specific chemotherapeutic agents were causing any undue regional or systemic bone marrow effects over time. Information from blood counts reflects what is going on in the skeleton as a whole rather than at a regional level and is not so informative in this regard. Even with systemic toxins such as chemotherapy, the use of bone marrow imaging may provide information on the timing and long-term sequelae of such therapies and hence allow 'rescue' measures to be put in place as and when needed. A prospective study measuring ADC midway through neoadjuvant chemotherapy in adolescents with osteosarcoma indicated that the ADC midway through chemotherapy was significantly higher in those that showed histological response versus those that did not, but that the differences between the responding and non-responding neoplasms was not evident when comparing ADCs obtained at the end of chemotherapy.⁹ Although these measurements were in the tumour rather than in surrounding normal bone marrow, it may well be that the optimal time for ADC measurements is not at the end but during a treatment, to capture a peak ADC change. Even in adults, the data on normal bone marrow changes with chemotherapy are poorly documented, and no definitive data on this topic monitoring changes with ADC exists. Preclinical data focuses on the tumour itself rather than on normal bone marrow. In children, where haematopoietic marrow forms a greater proportion of the total marrow mass and, therefore, the potential for haematological toxicity is high, having a measure of early toxicity that is non-invasive and that can be derived from the images at the same time

as the data for response assessment of the tumour itself, would be a major step forward in monitoring bone marrow toxicity.

5.3 WHERE TO MEASURE THE BONE MARROW IN CHILDREN: regional variations in response in the maturing skeleton-local vs whole skeleton measurements

The selection of sites for my bone marrow measurements was determined by the available paediatric populations undergoing diffusion-weighted MRI at multiple time points as part of their clinical imaging. The one area where this is routinely done is in paediatric brain imaging, hence the choice of skull for making the measurements in Ch 2 (determining ADC measurements by age group) and in Ch 3 (examining the effects of radiation therapy and proton therapy on bone marrow). The skull is also a good site for selection because it is a major hematopoietic bone. Unfortunately, its flat nature means that segmentation of bone marrow is not only difficult, but error prone due to partial volume effects from neighbouring bony cortex and scalp fat. I, therefore, selected the clivus where it was possible to draw a region of interest reliably within bone marrow. This had to be done on axial images as the diffusion-weighted images were acquired in this way, but future work utilising clivus marrow when performed prospectively may be better served by sagittal diffusion-weighted imaging where delineation of the clivus would be easier.

For the chemotherapy cohort diffusion-weighted imaging is performed for patients with abdominal tumours, hence the choice of the lumbar spine for my measurements. This afforded a large area in which to place a region of interest

more reliably, so it was surprising that in the 4 cases where ADC measurement variability was studied by comparing values obtained from 2 separate scans that the results were so variable. In addition to protocol variation, differences in positioning leading to partial volume effects from neighbouring intervertebral disc on axial images may have been factors contributing to this variation. This raises questions around whole skeleton imaging with autosegmentation as areas for development.

5.4 POTENTIAL UTILITY OF ADC IN BONE MARROW TRANSPLANTATION

Whole body DW-MRI (WB DW-MRI) has now been implemented for routinely evaluating skeletal disease in oncology in adults. The high sensitivity, speed and quantitative capability have addressed an unmet need in imaging primary and secondary malignancies. Combined with anatomical imaging, WB DW-MRI now forms a tool that has been tailored to detect both focal and diffuse disease, to quantify burden and response as well as assessing mechanical complications.¹⁰ This blend of anatomical and functional imaging has recently been recommended by the International Myeloma Working Group for work-up of solitary bone plasmacytoma or smouldering multiple myeloma.¹¹ In adults, WB DWI can provide information on differences between normal and diseased bone marrow architecture for the entire skeleton in a 25-minute time-frame [Giles, 2015]. This has led to feasibility studies for staging and follow-up of malignancies in children but not in the context of bone marrow disease.^{12, 13}

5.5 FUTURE POTENTIAL FOR WHOLE BODY DWI FOR ASSESSING CHILDHOOD LEUKAEMIA

Although leukaemia accounts for 31% of all childhood cancer,^{14, 15} it is not currently routinely investigated with WB DW-MRI. The relative proportions of tumour, red marrow and yellow marrow alter with age and with treatment, and make interpretation of images challenging.¹⁰

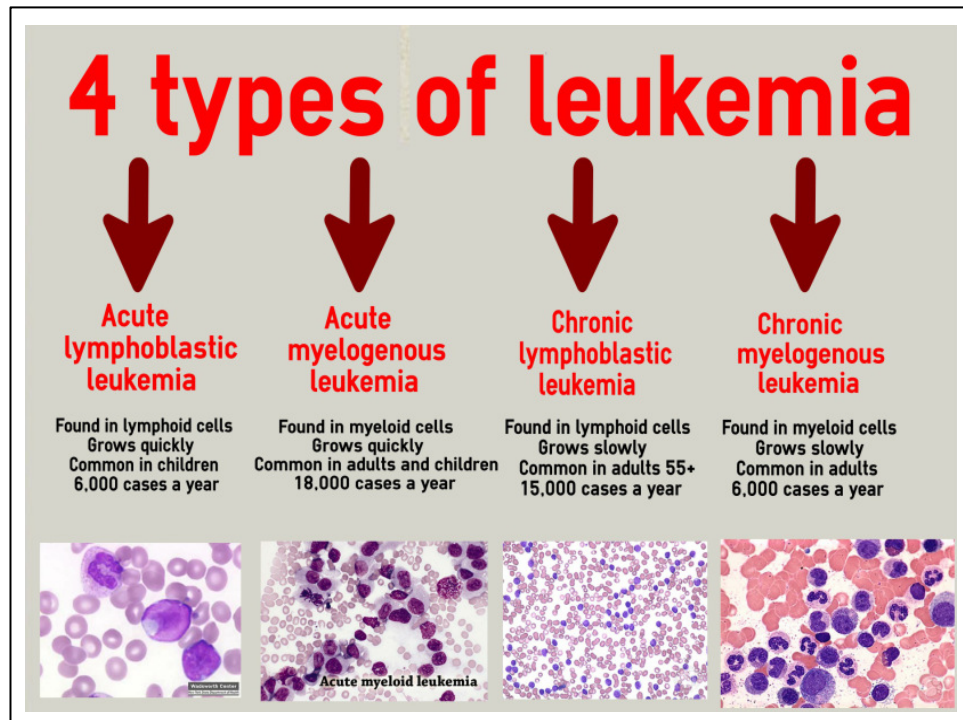


Figure 5.1: Types of leukaemia; from MedicineNet.com and the American Society of Hematology

According to ALLR3 treatment guidelines,¹⁶ children diagnosed with high-risk relapsed acute lymphoblastic leukaemia (ALL) are planned for allogeneic haemopoietic stem cell transplantation (HSCT) after high-dose chemotherapy and total bone irradiation. In children with high risk or relapsed acute myeloid leukaemia (AML) high-dose chemotherapy alone is administered prior to HSCT.¹⁷

Haemopoietic engraftment usually occurs a median of 2 to 3 weeks following HSCT if the donor is a sibling or after 3 weeks when the donor is unrelated;

engraftment is marked by an increase in white blood cell count. In future, change in ADC at time of engraftment not only may aid assessment of successful engraftment but indicate the extent of ongoing support and immunosuppression required, and predict longer term outcome.

5.5.1 Preliminary work

Initial work aiming to develop an adequate DWI scanning protocol with regard to parameters best suited to robust ADC delineation in an acceptable time frame (<10 min of additional scan time) have been optimized in a small cohort of children undergoing clinical MR scans at 1.5 T scanners since January 2017. Ethical permission for this is currently operational (CCR1406).

Reproducibility in bone marrow MRI has already been proved in adults in both healthy volunteers and patients with myeloma. ADC measurements (applying $b=50$ and 900 s/mm²) have been shown to be repeatable in segmented marrow volumes; a paired t test between the two observations indicates no significant difference between subject measurements for both cohorts. Furthermore, the measurement was also consistent with intraclass correlation coefficient of 0.981 and 0.991 for intraobserver and interobserver comparisons, respectively.¹⁸

5.6 PUMA STUDY

A prospective research study entitled Quantitative magnetic resonance imaging of bone marrow in a paediatric population with leukaemia – PUMA (Paediatric osseoUs Marrow Assessment) has been approved by the Health

Research Authority (South West - Central Bristol Research Ethics Committee) on 21st February 2018 and opened to recruitment afterwards. The full protocol is given in **Appendix 2**.

Pt	Gender	Age (y)	Disease	Date consent	Date baseline MR scan	Completion		Withdrawal		Note
						Occurred	Date	Reason	Date	
1	F	6	Philadelphia-positive ALL	15 th Mar 2018	13 th Apr 2018	/	/	Engraftment syndrome on day 5 post allogeneic bone marrow transplant	19 th Apr 2018	/
2	F	12	ALL	29 th Mar 2018	/	/	/	Withdrawn consent	19 th Apr 2018	/
3	F	10	ALL	19 th Apr 2018	/	/	/	Unfit to lay down in the scanner	13 th Jul 2018	/
4	M	7	ALL	25 th Jul 2018	/	/	/		27 th Jul 2018	/
5	F	10	Relapsed B-cell ALL	7 th Feb 2019	8 th Feb 2019	yes	5 th Mar 2019	/	/	/
6	M	11	Relapsed B-cell ALL	28 th Mar 2019	/	/	/	Unwell due to severe skin infection (acute graft-versus-host disease, stage 3, grade 1)	25 th Apr 2019	Died at Great Ormond Street Hospital for Children on 1 st Aug 2019 of respiratory distress due to prolonged metabolic acidosis and multiorgan failure

Table 5.1 Recruitment status to PUMA study

5.6.1 Recruitment status

From March 2018 to date 6 patients have been consented and recruited. However, four children withdrew before the baseline MR examination and one child scanned did not have the second scan due to engraftment syndrome 5-day post-transplant. So far only one patient completed the research study. Therefore, no data for the analysis are currently available.

The slow enrolment was caused by the fact that two co-investigators left the Trust after February 2018 (the Paediatric Bone Marrow Transplant Fellow and the statistician) and replaced by new colleagues after a gap and a transition period in the team. Furthermore, the consent was asked approximately one month before the baseline was performed when they relatively well; in between these patients underwent high-dose chemotherapy and total bone irradiation which made them fragile and not fit enough to lay down in the MR scanner. Thirdly, being paediatric individuals they change their mind more easily than adults, therefore, they are less reliable in terms of consent.

5.6.2 Future work on PUMA

An extent of the term of PUMA study to allow target recruitment — which remains unchanged at 12 — to be achieved was requested and obtained on 17th December 2018. Its new closure is due on 31st December 2020. Hopefully, recruitment should be completed by then and data regarding lumbosacral marrow ADC values of pre- and post-transplant DWI-MR scans analysed.

REFERENCES

1. Georger B, Chisholm J, Le Deley MC, et al. Phase II study of gemcitabine combined with oxaliplatin in relapsed or refractory paediatric solid malignancies: An innovative therapy for children with Cancer European Consortium Study. *European journal of cancer (Oxford, England : 1990)*. 2011; 47: 230-238.
2. Chisholm JC, Merks JHM, Casanova M, et al. Open-label, multicentre, randomised, phase II study of the EpSSG and the ITCC evaluating the addition of bevacizumab to chemotherapy in childhood and adolescent patients with metastatic soft tissue sarcoma (the BERNIE study). *European journal of cancer (Oxford, England : 1990)*. 2017; 83: 177-184.
3. Davidson AJ, Disma N, de Graaff JC, et al. Neurodevelopmental outcome at 2 years of age after general anaesthesia and awake-regional anaesthesia in infancy (GAS): an international multicentre, randomised controlled trial. *Lancet (London, England)*. 2016; 387: 239-250.
4. Meeus EM, Zarinabad N, Manias KA, et al. Diffusion-weighted MRI and intravoxel incoherent motion model for diagnosis of pediatric solid abdominal tumors. *Journal of magnetic resonance imaging : JMRI*. 2018; 47: 1475-1486.
5. Manias KA, Gill SK, MacPherson L, Foster K, Oates A and Peet AC. Magnetic resonance imaging based functional imaging in paediatric oncology. *European journal of cancer (Oxford, England : 1990)*. 2017; 72: 251-265.
6. deSouza NM, Winfield JM, Waterton JC, et al. Implementing diffusion-weighted MRI for body imaging in prospective multicentre trials: current considerations and future perspectives. *European radiology*. 2018; 28: 1118-1131.
7. Spence AM, Geraci JP and Cent RR. Irradiation and BCNU effects in the stroma in a rat transplanted glioma model: analysis of cerebral tumor bed effect. *Neuropathology and applied neurobiology*. 1985; 11: 229-244.
8. Bazan JG, Luxton G, Kozak MM, et al. Impact of chemotherapy on normal tissue complication probability models of acute hematologic toxicity in

- patients receiving pelvic intensity modulated radiation therapy. *International journal of radiation oncology, biology, physics*. 2013; 87: 983-991.
9. Baunin C, Schmidt G, Baumstarck K, et al. Value of diffusion-weighted images in differentiating mid-course responders to chemotherapy for osteosarcoma compared to the histological response: preliminary results. *Skeletal radiology*. 2012; 41: 1141-1149.
 10. Messiou C and Kaiser M. Whole body diffusion weighted MRI--a new view of myeloma. *British journal of haematology*. 2015; 171: 29-37.
 11. Dimopoulos MA, Hillengass J, Usmani S, et al. Role of magnetic resonance imaging in the management of patients with multiple myeloma: a consensus statement. *Journal of clinical oncology : official journal of the American Society of Clinical Oncology*. 2015; 33: 657-664.
 12. Siegel MJ, Acharyya S, Hoffer FA, et al. Whole-body MR imaging for staging of malignant tumors in pediatric patients: results of the American College of Radiology Imaging Network 6660 Trial. *Radiology*. 2013; 266: 599-609.
 13. Nievelstein RA and Littooi AS. Whole-body MRI in paediatric oncology. *La Radiologia medica*. 2016; 121: 442-453.
 14. Main types of childhood cancer: children aged 0-14 years. United Kingdom 2001 to 2010. *Based on data provided by National Registry of childhood Tumours*.
 15. Children's cancers incidence by type
 16. ALLR3: An International Collaborative Trial for Relapsed and Refractory Acute Lymphoblastic Leukaemia (phase III, ongoing).
 17. MyeChild01 protocol: International Randomised Phase III Clinical Trial in Children with Acute Myeloid Leukaemia - Incorporating an Embedded Dose Finding Study for Gemtuzumab Ozogamicin in Combination with Induction Chemotherapy, 2015.
 18. Giles SL, Messiou C, Collins DJ, et al. Whole-body diffusion-weighted MR imaging for assessment of treatment response in myeloma. *Radiology*. 2014; 271: 785-794.

APPENDIX 1 **Service Evaluation 662 proposal form**

- Service Evaluations are now administered through Research and Development (R&D)
- **Statistician involvement is MANDATORY** and Forms MUST be accompanied by either scanned versions with signatures **in section 2** or emails from both the statistician and Unit Head of Department approving the proposal before submission **before Clinical Review can be arranged**
- If a patient or public questionnaire is included, the Form, Questionnaire and a Patient Information Sheet must be forwarded to the Patient and Public Involvement (PPI) Lead for review. A Patient Information Sheet Template can be found on the Intranet in Clinical R&D\All Documents\Service Evaluation.
- Please complete this form as a 'Word' document and return a copy by e-mail attachment to 'Service Evaluation' (Service.Evaluation@rmh.nhs.uk)
- Data collection MUST NOT commence until WRITTEN approval from the CCR (Committee for Clinical Review) Reviewer has been given to the project, by Research and Development
- Refer to the guidance document on the Clinical Research & Development (R&D) site on the trust intranet for full guidance on the submission process, including design of Clinical Report Forms (data collection tools) and spreadsheets.
- Please send all queries to Service.Evaluation@rmh.nhs.uk

Shaded boxes are for Statistics office use only.

Service Evaluation Title: Quantitative magnetic resonance imaging of bone marrow in a			
Is this required for an MSc Sc?	MD(Res)	If Yes, date M.Sc report required	/
Other Sites involved: Yes	UK	Data collection: Retrospective	
Applicant Division:	Division of Radiotherapy and Imaging		
Applicant Name:	Dr Erika Pace	Contact No: 6102	
Designation:	Clinical Research Fellow in Radiology	Unit/Dept.: Department of Radiology	
Email address:	Erika.Pace@icr.ac.uk		
Planned Start Date:	December 2016	Date final report anticipated: December 2017	
Does the proposer plan to leave the RM before the expected report date?	No		
Co- Investigator(s) (List all)	Nandita deSouza, Julia Chisholm, Henry Mandeville		
Data Manager (Name)	Erika Pace		
Is a questionnaire involved?	No	Is this a patient or staff questionnaire?	/
'Other' questionnaire	/		
Name of Patient and Public Involvement (PPI) reviewer if patient questionnaire:	/		
Does SE have cost implications?	No		

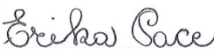
Section 2.

Statistical support provided by	Karen Thomas	
I approve the above methodology (Signed) Statistician		30 th August 2017
⌘ Period for data retention	Related to trial / research? Yes - <i>If Yes please pass SE data to QA team secretary for retention.</i>	

Approval By Head of Unit / Dept

This applicant has agreed to complete this service evaluation and to report the results back to the CCR in a timely fashion. If the proposer leaves the Royal Marsden before completing and reporting the project results back to the CCR, the handover arrangements detailed on page 1 of this form (or if unanticipated, subsequently separately notified to Service.Evaluation@rmh.nhs.uk) will apply, and I confirm my agreement to these handover arrangements.

Head of Unit / Dept Name:	MRI Unit, Sutton Professor Nandita deSouza	30 th August 2017
Head of Unit/Dept Signature:		
Note: ** All countersignatures MUST be obtained either electronically or in handwriting <i>before</i> submission and a fully countersigned copy submitted to the Service.Evaluation@rmh.nhs.uk in electronic format.		

Applicant Declaration and signature	I confirm that I have completed the following actions prior to submitting this proposal to the Committee for Clinical Research (CCR) for clinical review : i) obtained the involvement of a named trust/ICR statistician, who has reviewed and approved the proposal ii) sought and obtained approval for this evaluation from the clinical audit lead for my Unit / Department or Sutton & Merton Community Services, who has seen and signed a copy of this proposal iii) sought and obtained approval for this evaluation from my Head of Department who has seen and signed a copy of this proposal iv) have made/ will make arrangements that if I leave the Royal Marsden before this SE project is reported, the project (including all data), will be handed over to a suitable staff member (agreed by my Head of Department) to complete and report back to the Committee for Clinical Research.	
* Applicant Declaration and	Please see declaration and SIGN and DATE this form, after the Clinical Audit Lead and Head of Department. (See the end of the form, below).	
Signed (Applicant)		30 th August 2017

*Note: The applicant is the person who is primarily responsible for the project design, data collection and reporting of the completed project.

⌘ Note: Freedom of Information Act 2000 – Retention of Service evaluation data

Data should be retained for 5 years after the results and action plan have been agreed with the relevant Unit/ Department and reported to CCR and to IGRM.

However, if the SE data are related to ongoing research e.g. following extraction from a research data set – the SE data should be retained for the same period of time as the related research data set or for five years, whichever is the longer.

The following template can be used as a starting point for service evaluations. Text in blue has been written as a guide to completing the template – all the blue text should be replaced with your own text as appropriate to your study. The completed protocol should act as a blueprint or 'recipe book' to conducting your evaluation: that is, a reasonably well-informed person should be able to use the protocol (and only the protocol) as a set of instructions which are comprehensive enough to enable them to carry out the study from start to finish.

NOTE: All Sections of the following pages are MANDATORY for completion

LAY SUMMARY

A novel biomarker in oncological imaging,¹ the apparent diffusion coefficient (ADC), has emerged, derived from diffusion-weighted magnetic resonance imaging (DW-MRI), which is based on quantification of the diffusivity of water molecules within a tumour.² In adult bone marrow it improves lesion detection and the assessment of treatment response.³ ADC values are inversely correlated with tumour cellularity and may be used as prognostic indicators of bone marrow involvement.⁴ Because it avoids radiation exposure and intravenous contrast agents,⁵ DW-MRI is appealing in the field of paediatric oncology for the assessment of bone marrow disease.⁶ However, ADC values will vary by patient age, puberty and gender⁷ as well as previous radiation exposure and the reproducibility of the measurement in children is unknown. This service evaluation aims to establish reproducibility of ADC by age, gender, pubertal status and previous radiation exposure.

Background Information

Within the adult population, the usefulness of the DW-MRI for the assessment of bone marrow both in healthy and affected individuals has been demonstrated.⁸ The International Myeloma Working Group has recently introduced whole body DW-MRI into the management pathway for patients with myeloma, due to its capability to quantify both burden of disease and the response to treatment.⁴

Although feasibility studies have explored DW-MRI for staging and follow-up of malignancies in children, it has not been used in the context of bone marrow disease.⁹

This Service Evaluation will be undertaken as part of an MD(Res) degree. I wish to establish the values of ADC and their variability in a paediatric population by age, gender, pubertal status and previous radiation exposure by analysing retrospectively the skull bone marrow of patients who have previously had brain or spine MRI and in whom DWI was routinely performed as part of the examination.

SE Aims

To develop repeatability estimates for measuring paediatric bone marrow on DW-MRI and establish ranges of values by age, gender, pubertal status, previous radiation exposure for skull and spine. This will be done by evaluating the bone marrow on DW-MR scans of head and spine previously carried out in children for clinical purposes.

SE Objectives:

1. To establish the repeatability of the ADC measurements in skull of children;
2. To determine differences in values for the ADC and fat fraction in normal bone marrow by age, gender and pubertal status;
3. To examine the effect of radiotherapy on the ADC of skull marrow.

SE design

Cross-sectional comparison of ADC in children. Patients will be analysed in categories by age, gender, pubertal status, radiation exposure and anatomical location.

This pilot single study includes Royal Marsden in- and outpatients, therefore, most of them will have an MR scan done in our unit, in Sutton. Whether the images are acquired elsewhere, the scans will be imported onto our PACS.

Eligibility for inclusion in the SE

Irrelevant; this data is collected for clinical purposes.

Planned methodology

Data Collection between	March 2006 to date
Data source to be used	Electronic Patient Records, Picture Archiving and Communication System, Multidisciplinary Team Meetings agenda, The Royal Marsden Information System, Radiotherapy Database.

Statistical considerations

Endpoints

Comparison of ADC values of the bone marrow of the skull and spine in:

- 10 girls aged 5-10 years;
- 10 boys aged 5-10 years;
- 10 girls post-menarche;
- 10 boys post-puberty.

Sample size

Male/female patients between 4 and 18 years old undergoing MR scans for clinical purposes will be included. We roughly estimate there to be 40 individuals.

Analysis methods

Bone marrow will be segmented in selected regions of interest in the skull and spine.

Median, mean and percentile ADC values of the chosen regions of interest will be calculated. For the data showing a normal distribution, an unpaired t-test will be employed for analysis. Otherwise, non-parametric test Wilcoxon-Mann U test will be used.

For the repeatability study, Bland-Altman plot will be used to assess the variability.

Histograms analysis of the ADC of the segmented skeleton will be used for analysis of longitudinal studies.

Study organisation

Patients will be identified through the monthly MR scans booking lists owned by the Department of Radiology, and by interrogating the hospital information system.

Data of the eligible paediatric patients (regarding demographics, clinical history, diagnosis, treatments...) will be collected in spreadsheets.

Study organisation: Who does what.

Dr Erika Pace will assess eligibility of children, collect and enter data. She will also draw regions of interest on MR images and analyse data.

Radiographers will anonymise the MR scans and upload them on the software platform. Ms Karen Thomas will have the responsibility for overseeing statistical analyses.

Prof deSouza will have overall responsibility for the study and will conduct in accordance within the Research Governance Framework. She will be responsible for data storage.

Drs Julia Chisholm and Henry Mandeville will be notified by Dr Erika Pace about the suitable paediatric MR scans the latter will include in the evaluation.

Data storage and data handling

Data will be stored, filed and handled in accordance with the Data Protection Act and

Good Clinical Practice. All patients' identification will be removed prior to any activity involving electronic transfer of data. Identification numbers will be used instead of subjects' names.

Electronic storage of information is on one of the Royal Marsden computer system servers. Digital confidential data will be saved on databases whose access requires a password known only to restricted personnel involved in the conduction of the study.

Patients' anonymised MR images will be uploaded on the software platform XNAT accessible only to EP and NdS, who own a personal account.

Physical data (paper records, patient information sheets, assent/consent forms, and case report forms) will be stored in a casefile kept within a file cabinet in locked offices within the MRI Unit of the Royal Marsden in Sutton, which is access controlled. Clinicians involved in the care of the patient and the co-investigators will have access to the data, under the custodianship of Dr Erika Pace.

References

1. O'Connor JP, Aboagye EO, Adams JE, et al. Imaging biomarker roadmap for cancer studies. *Nature reviews Clinical oncology*. 2017; 14: 169-186.
2. Koh DM and Collins DJ. Diffusion-weighted MRI in the body: applications and challenges in oncology. *AJR American journal of roentgenology*. 2007; 188: 1622-1635.
3. Perez-Lopez R, Lorente D, Blackledge MD, et al. Volume of Bone Metastasis Assessed with Whole-Body Diffusion-weighted Imaging Is Associated with Overall Survival in Metastatic Castration-resistant Prostate Cancer. *Radiology*. 2016; 280: 151-160.
4. Messiou C and Kaiser M. Whole body diffusion weighted MRI--a new view of myeloma. *British journal of haematology*. 2015; 171: 29-37.
5. Kyriazi S, Morgan V, Collins D and deSouza N. (2009) Echo planar diffusion-weighted MRI of the abdomen and pelvis: comparison of free-breathing monopolar and bipolar spin-echo sequences in assessing image quality and apparent diffusion coefficients. *Proc Intl Soc Mag Reson Med* 17.
6. Voss SD. Pediatric oncology and the future of oncological imaging. *Pediatric radiology*. 2011; 41 Suppl 1: S172-185.
7. Chan BY, Gill KG, Rebsamen SL and Nguyen JC. MR Imaging of Pediatric Bone Marrow. *Radiographics : a review publication of the Radiological Society of North America, Inc*. 2016; 36: 1911-1930.
8. Giles SL, deSouza NM, Collins DJ, et al. Assessing myeloma bone disease with

whole-body diffusion-weighted imaging: comparison with x-ray skeletal survey by region and relationship with laboratory estimates of disease burden. *Clinical radiology*. 2015; 70: 614-621.

9. Nievelstein RA and Littooi AS. Whole-body MRI in paediatric oncology. *La Radiologia medica*. 2016; 121: 442-453.

APPENDIX: ADD LIST OF DATA ITEMS FOR COLLECTION

Data list

- Patient demographics:
 - date of birth,
 - gender,
 - pubertal status.

- Clinical history:
 - type of diagnosis,
 - date of diagnosis.

- Treatment-related:
 - date of commencement and end of photon/proton therapy,
 - treatment protocol,
 - field of irradiation,
 - dose.



Original Article

Variation of the apparent diffusion coefficient of skull bone marrow by age group, pubertal status, and gender in a pediatric population

Acta Radiologica
0(0) 1–9
© The Foundation Acta Radiologica
2019
Article reuse guidelines:
sagepub.com/journals-permissions
DOI: 10.1177/0284185119894217
journals.sagepub.com/home/acr

Erika Pace^{1,2}, Andrew D MacKinnon^{2,3} and
Nandita M deSouza^{1,2}

Abstract

Background: Bone marrow composition varies with stage of development.

Purpose: To assess differences in apparent diffusion coefficient (ADC) derived from clivus bone marrow in healthy children by age, pubertal status, and gender as a benchmark when monitoring local and systemic treatment-induced effects.

Material and Methods: Non-oncological pediatric patients (30 pre-pubertal [15 girls, 15 boys] and 30 post-pubertal [15 girls, 15 boys]) with previous normal magnetic resonance imaging (MRI) of the brain including diffusion-weighted magnetic resonance imaging (DW-MRI; 1.5-T Philips Achieva-Ingenua, b-values 0 and 1000s/mm²) were studied. A 4–6 mm diameter region of interest (ROI), drawn within the clivus on two or three DW-MRI slices, yielded mean and centile ADC values. Pubertal status was recognized from imaging appearances of the pituitary gland and from fusion of the sphenoid-occipital synchondrosis. Correlations between ADC and age were assessed (Pearson's coefficient). Mann-Whitney U tests compared ADC by age, pubertal status, and gender.

Results: Age and ADC were significantly negatively correlated (median ADC $r = -0.48$, mean ADC $r = -0.42$, $P = 0.0001$ and 0.0008 , respectively) which held true when divided by gender. Mean and median ADC differed significantly before and after puberty for the whole population ($P = 0.0001$ and 0.0001 , respectively). There was a left shift of the ADC histogram after puberty with significant differences in centile values. ADC differences before and after puberty remained when divided by gender (girls: $P = 0.04$ and 0.009 , respectively; boys: $P = 0.005$ and 0.0002 , respectively).

Conclusion: ADC of clivus bone marrow correlates with age in children. ADC decreases significantly after puberty, likely due to replacement of hypercellular marrow with fat. There are no gender-related differences in clivus bone-marrow ADC before or after puberty.

Keywords

Diffusion-weighted magnetic resonance imaging, apparent diffusion coefficient, bone marrow, puberty, gender, pediatric

Date received: 20 August 2019; accepted: 18 November 2019

Introduction

Bone marrow composition varies with biological and physiological requirements at different stages of development (1). Hematopoietic cells appear within the medullary cavities of bones at around 14 weeks of gestation (2). By birth, the bone marrow represents the principal anatomical location of hematopoiesis. The marrow space occupied by hematopoietic cells diminishes from 90% at birth to approximately 50% at the age of 30 years and 30% at the age of 70 years as it

¹CRUK Imaging Centre, The Institute of Cancer Research, Sutton, UK

²The Royal Marsden Hospital, Department of Radiology, Sutton, UK

³Department of Neuroradiology, Atkinson Morley Regional Neuroscience Centre, St George's University Hospitals NHS Foundation Trust, London, UK

Corresponding author:

Nandita M deSouza, The Institute of Cancer Research and The Royal Marsden Hospital, Downs Road, Sutton, Surrey SM2 5PT, UK.
Email: nandita.desouza@icr.ac.uk

becomes progressively replaced by fat (3,4). The relative proportion of marrow hematopoietic components versus fat components also classically depends on the type of bone (long, short, flat, and irregular). Until puberty, the entire skeleton remains hematopoietically active, but by the age of 18 years, the production of blood cells persists only in the vertebrae, ribs, sternum, skull, pelvis, proximal humeral, and femoral epiphyses, while bones in other osseous locations undergo fatty infiltration (5). An indication of the proportion of cellular versus fatty component of the bone marrow in children would be informative on the proliferative state of the bone marrow and on changes that occur as a result of therapy.

Diffusion-weighted magnetic resonance imaging (DW-MRI) uses non-ionizing radiation without administration of extrinsic contrast agents to characterize tissues. Its quantified metric, the apparent diffusion coefficient (ADC), has been strongly linked to cell density of tissues (6). Moreover, the sequence uses a fat suppression pulse, so that fat interspersed within tissue results in a reduction in ADC. Although there is no direct quantification of fat, lower ADC values have been used as a surrogate for the appearance of fat within bone marrow of the axial and appendicular skeleton in several studies in adults (7,8). There are limited data on ADC values in normal, healthy children (9), but no studies to date have documented differences in cellular versus fat components of bone marrow in children by age, pubertal status, and gender.

This work retrospectively studied bone marrow in the skull because DW-MRI forms a routine part of brain imaging in children. The flat shape of the skull bones meant that region of interest (ROI) delineation in the skull was best done in the clivus. This area of the skull base represents one of the thickest bones within the cranium, making ROI in multiple adjacent slices with an interval of 5 mm feasible. Additionally, its mid-line location means that the clivus is routinely included in the field of irradiation as a treatment for brain tumor, making it ideally placed for the measurement of treatment-related ADC changes in future studies. The aim of the present study was to assess the differences in ADC derived from the bone marrow of the clivus in a healthy pediatric population by age, pubertal status, and gender.

Material and Methods

Patient selection

Non-oncological pediatric patients who previously had brain MRI for clinical purposes and in whom DW-MRI was routinely performed as part of the examination were studied. The study was approved

by the Institutional Review Board and the need for written consent was waived.

Inclusion and exclusion criteria chosen were to allow the retrospective selection of a cohort of pediatric patients (aged 5–17 years) with normal MRI brain scans ($n=60$) with DWI that was artefact-free. Electronic patient records were assessed to confirm clinical presentation and any follow-up diagnosis. Indications for MRI were headaches, transient neurological symptoms, syncopal episodes, and possible seizures (but with normal electroencephalogram). Patients with any condition that might affect the bone marrow (infection, bone lesions at any site, systemic diseases, oncological diagnosis, or on medication) were excluded. Of 1140 children identified on the database over a two-year period (1 March 2016 to 31 March 2018), 60 individuals met these stringent exclusion criteria, all of whom were included in the analysis.

Image acquisition

All children had been scanned on a 1.5-T Philips Achieva-Ingenu upgraded to d-stream (digital rf) platform. Their examinations were anonymized and transferred to a research imaging repository at The Institute of Cancer Research through a secure web-based data analysis platform. Axial single-shot echo-planar diffusion-weighted images (b -values = 0 and 1000 s/mm^2) were routinely acquired as part of the standard MRI brain scan. The voxel resolution was $0.9375 \times 0.9375 \times 4$ mm. Axial T2-weighted (T2W) spin-echo (SE) and fluid-attenuated inversion recovery (FLAIR), as well as sagittal T1-weighted (T1W) SE and coronal T2W SE images were acquired in each case. In individuals aged >16 years, the sagittal T1W SE was replaced by T2W SE. These images were part of a standard anatomical protocol for brain imaging and were not optimized for bone marrow study; they were not utilized in this study.

Image analysis

T2W images were used to identify the exact location of the clivus. The axial DW images were then correlated with morphological T2W images. A circular ROI of 4–6 mm in diameter was drawn within the clivus on the DW images (EP, pediatric radiologist with two years of experience) using in-house software (Adept[®], The Institute of Cancer Research, UK). Care was taken to include the maximum number of pixels from clival marrow while avoiding contamination from surrounding bony cortex (Fig. 1). In 58 cases, this was possible on two central slices; in two cases, ROIs were possible in three adjacent slices. To avoid including artefacts, the ROIs were drawn within the clivus at the level of

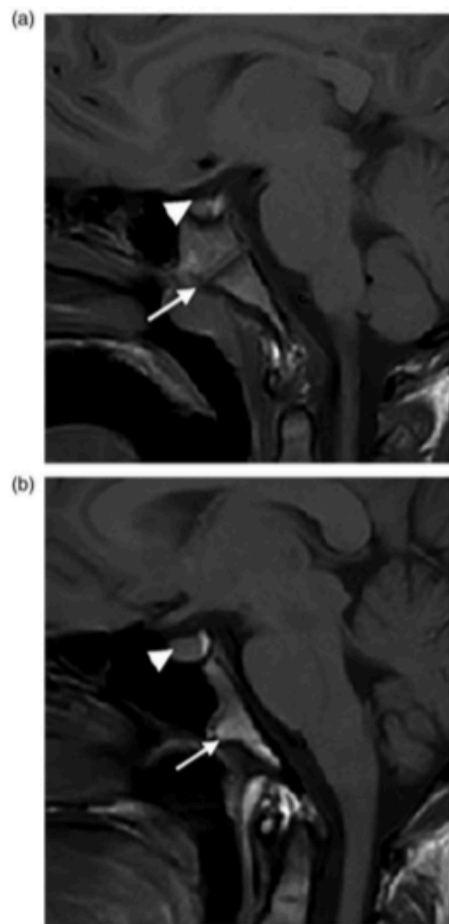


Fig. 1. Sagittal T1W midline images through the clivus in a seven-year-old girl (a) and a 16-year-old girl (b). (a) The superior aspect of the pituitary is flat (arrowhead) and the synchondrosis is unfused (Stage 0, arrowhead). (b) The superior aspect of the pituitary bulges upward (arrowhead) and the synchondrosis is fused (arrow).

the fossa navicularis. Use of the high b-value image for ROI definition rather than the ADC map ensured reliable placement within the high signal of clivus marrow. Each patient measurement to review images, plan ROI placement and extract and tabulate the ADC values took approximately 15 min. To determine inter-observer variability of the measurement, a second observer (NdS, MR radiologist with 25 years of experience, non-specialist in pediatric neuroradiology) independently drew an ROI within the clivus on a single central slice of the DW images in a randomly selected subset of 20 individuals (five from each group). Data from the entire volume of the ROIs were extracted and the ADC calculated on a voxel-by-voxel basis using a mono-exponential fit of the data.

Table 1. Staging system for pubertal status based on sphenoid-occipital synchondrosis closure on imaging (adapted from Alhazmi et al. (11)).

Stage		
0	Unfused	Completely open with no evidence of fusion between the basilar portion of the occipital and the sphenoid, no bone present in the gap
1	Fusing endocranially	<50% the length of the synchondrosis is fused proceeding endo- to ectocranially
2	Fusing ectocranially	>50% the length of the synchondrosis is fused; the ectocranial (inferior) border remains unfused
3	Complete fusion	Completely fused with the appearances of normal bone throughout; a fusion scar may be present

This yielded a range of ADC values for each individual from which median, mean, 10th, 25th, 75th, and 90th percentiles were derived. Traditional ADC maps were also created.

Recognition of pubertal status was radiological in the 10–17-year-old age group. Puberty was determined from the imaging appearances of the anterior pituitary gland (convex bulging above the sella superiorly) together with sphenoid-occipital synchondrosis fusion (Fig. 1). At puberty, there is physiological enlargement of the anterior pituitary gland, often more notable in girls, when the gland develops a convex superior border and often bulges just out of the sella. The appearance of the anterior pituitary gland was assessed on both sagittal (T1W images if aged < 16 years and T2 if older as per adult MR routine protocol) and coronal T2W images (10). In addition, the maturation stage of sphenoid-occipital synchondrosis closure was assessed on the sagittal MR images (Table 1). Its relationship to puberty has been described in a recent study and proposed on computed tomography. Stages 0 and 1 were considered pre-pubertal and stages 2 and 3 post-pubertal (11).

Data Analysis

Statistical analysis was performed using Excel and GraphPad Prism software (version 7.04, GraphPad, San Diego, CA, USA). Descriptive statistics were used to describe the data. Data were checked for normality (D'Agostino and Pearson normality test), although the data from female patients were normally distributed and those from male patients were not. Therefore, a Mann-Whitney U test was used to compare groups.

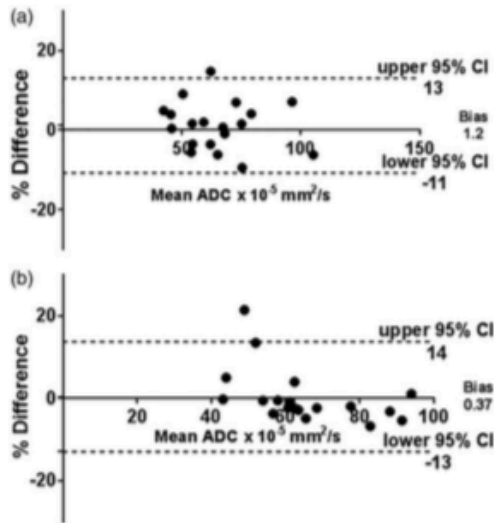


Fig. 2. Bland-Altman plots (difference between two measurements vs. their mean) showing the variability of the ADC median values (a) and ADC mean values (b) from clivus marrow when derived by two independent observers. Data were obtained in a subset of 20 randomly selected patients (five from each group). All 95% CIs representing the limits of agreement were less than $\pm 15\%$.

A Pearson's correlation coefficient examined the relationship between ADC and age.

Results

Of the 60 children who met the selection criteria, there were 15 aged 5–9 years (eight girls, seven boys), 15 pre-pubertal aged ≥ 10 years (seven girls, eight boys), 15 post-pubertal girls, and 15 post-pubertal boys.

The number of voxels included in each case was in the range of 21–182 and was significantly different among the groups (5–9 years: mean \pm SD = 78.8 ± 30.8 ; pre-pubertal aged ≥ 10 years: mean \pm SD = 57.1 ± 12.4 ; post-pubertal girls: mean \pm SD = 40.5 ± 7.2 ; post-pubertal boys: mean \pm SD = 39.5 ± 14.7 ; $P < 0.0001$).

Inter-observer variability (95% limits of agreement) was in the range of -11 to $+13\%$ for median ADC values and -13 to $+14\%$ for mean ADC values (Fig. 2).

Variation with age

The age range of patients was 5.0–17.9 years (median age = 12.4 years). There was a significant negative correlation between age and ADC for the whole cohort ($r = -0.48$ for median and -0.42 for mean values, $P = 0.0001$ and 0.0008 , respectively). There was also a significant negative correlation between age and ADC for girls ($r = -0.5$ for median and -0.4 for mean values, $P = 0.005$ and 0.03 , respectively) and for boys ($r = -0.53$ for median and -0.48 for mean values,

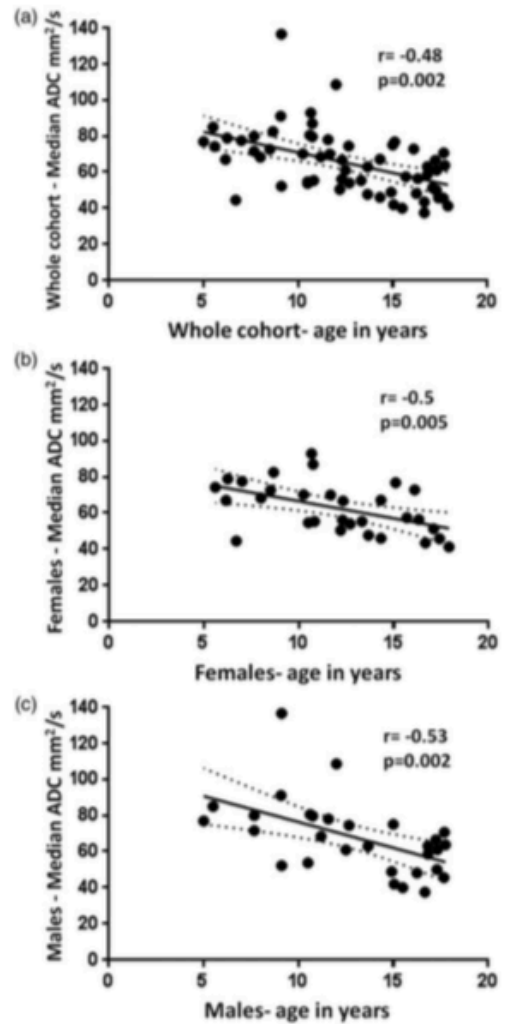


Fig. 3. Scatter plots showing the negative correlation of the ADC with age in (a) the whole cohort; (b) girls alone; and (c) boys alone.

$P = 0.002$ and 0.008 , respectively). Regression plots for median values are illustrated in Fig. 3.

Variation with pubertal status

Age of the pubertal cohort was in the range of 12.3–17.9 years; it was lower in girls (median age = 15.1 years; age range = 12.3–17.9 years) compared to boys (median age = 16.8 years; age range = 13.7–17.8 years).

There was a significant difference between mean and median ADC values before and after puberty for the whole population (Table 2, Fig. 4), which was greater than the 95% limits of agreement for inter-observer variability. There was a shift of the ADC histogram to the left after puberty (Fig. 5a) as evidenced by the

Table 2. Pre- and post-pubertal mean and centile values of ADC showing significant differences with pubertal status.

	All pre-pubertal (n = 30) ADC × 10 ⁻⁵ mm ² /s	All post pubertal (n = 30)	P value (Mann–Whitney U test)
Mean	74.6 ± 18.4	58.2 ± 15.6	0.0001
C25	54.1 ± 16.8	39.9 ± 10.3	0.0001
C50	74.8 ± 18.2	55.7 ± 11.8	0.0001
C75	93.6 ± 24.1	74.0 ± 22.7	0.0002
IQR	39.5 ± 14.2	34.1 ± 17.5	0.2

Values are given as mean ± SD.
ADC, apparent diffusion coefficient; IQR, interquartile range.

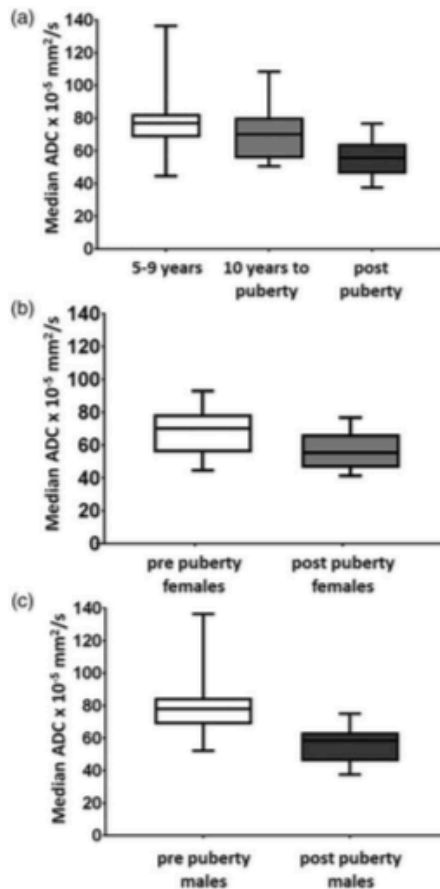


Fig. 4. Box and whisker plot comparing ADC of 5–9-year-olds, 10 years to puberty, and all post-pubertal individuals (a), between pre- and post-pubertal girls (b) and pre- and post-pubertal boys (c).

significant difference in centile values across the population. This is illustrated in exemplar cases before (Fig. 6) and after (Fig. 7) puberty. However, this was not reflected in an increased homogeneity of values as the interquartile range did not change (Table 2).

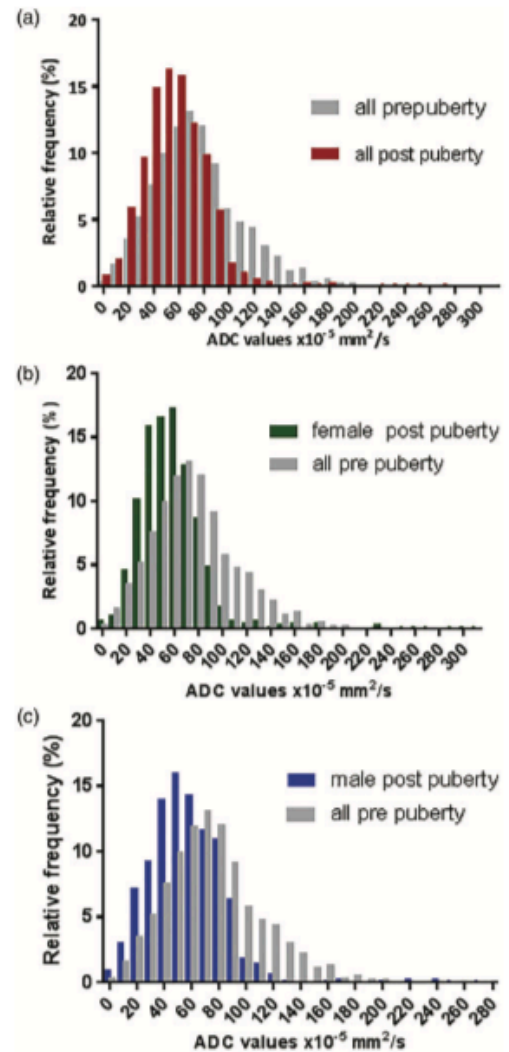


Fig. 5. Histogram plots for the whole population before and after puberty (a) and for post-pubertal girls alone vs. all pre-pubertal individuals (b) and boys alone vs. all pre-pubertal individuals (c). There is a left shift in the histograms after puberty, regardless of gender.

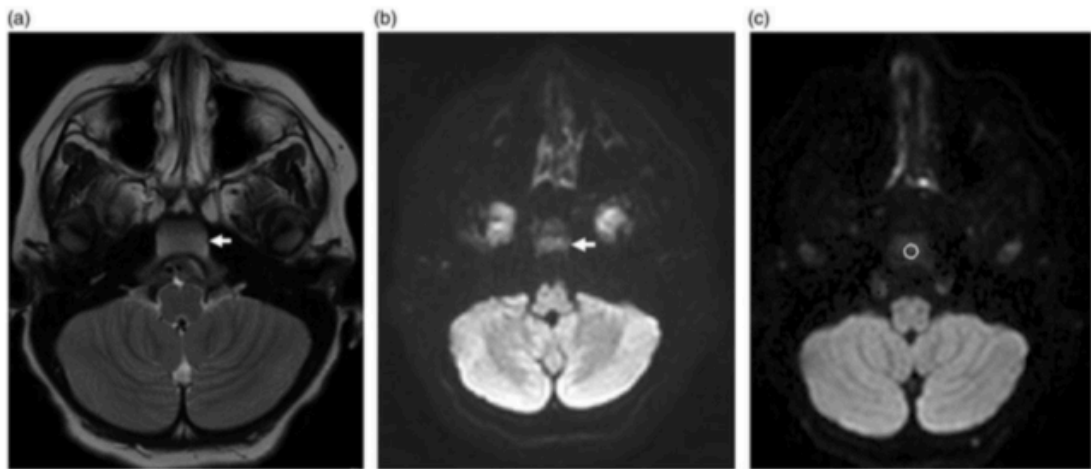


Fig. 6. Axial T2W (a), diffusion-weighted (b), and ADC map (c) in a 5.5-year-old pre-pubertal boy. Intermediate signal intensity within the marrow of the clivus is noted (a) with corresponding high signal intensity (b). (c) ADC of the hypercellular marrow is $84.0 \pm 22.2 \text{ mm}^2/\text{s}$.

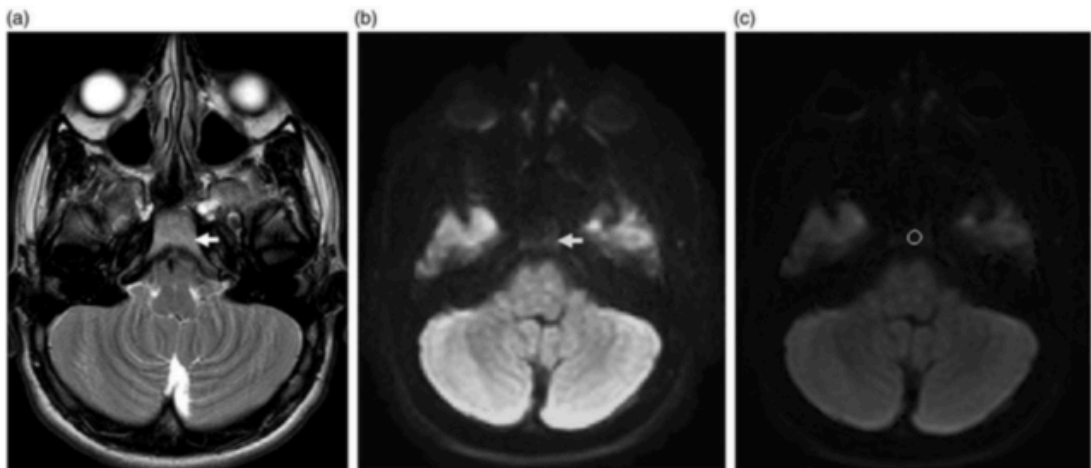


Fig. 7. Axial T2W (a), diffusion-weighted (b), and ADC map (c) in a 16.8-year-old post-pubertal boy. High signal equivalent to that of fat is noted in the marrow of the clivus (a) with corresponding low signal intensity on the fat-suppressed DW image (b). (c) Low ADC ($38.4 \pm 15.9 \text{ mm}^2/\text{s}$) of the fat replaced marrow is evident.

Variation with gender

Before puberty, there were no significant differences in mean or median ADC in girls versus boys ($P = 0.3$ for mean, 0.1 for median, and >0.05 at all centile values).

The pre- and post-puberty differences seen for the whole cohort also held true for girls alone and boys alone (Table 3, Fig. 4) with striking reductions in mean and median ADC and a left shift of histogram centile values (Fig. 5b and c). Differences between the whole cohort comparison before and after puberty and the same comparison done by gender (girls alone

and boys alone) were evident, e.g. the lack of significance between the 90th centile values for girls and the 10th centile values for boys. However, these differences are likely to relate to the smaller patient numbers when divided by gender rather than representing true differences.

Discussion

This is a first report of variation in ADC values in bone marrow with age, pubertal status, and gender in a healthy pediatric population. A large study of 500

Table 3. Mean and centile values of ADC before and after puberty by gender, showing that the reductions in ADC after puberty were present in both girls and boys.

	Pre-pubertal girls (n = 15) ADC $\times 10^{-5}$ mm ² /s	Post-pubertal girls (n = 15) ADC $\times 10^{-5}$ mm ² /s	P value (Mann–Whitney U test)	Pre-pubertal boys (n = 15) ADC $\times 10^{-5}$ mm ² /s	Post-pubertal boys (n = 15) ADC $\times 10^{-5}$ mm ² /s	P value (Mann–Whitney U test)
Mean	70.7 \pm 14.8	58.5 \pm 16.3	0.04	78.6 \pm 21.3	57.8 \pm 15.5	0.005
C25	51.2 \pm 11.9	40.2 \pm 9.1	0.01	56.9 \pm 20.7	39.6 \pm 11.7	0.004
C50	69.8 \pm 13.7	55.9 \pm 10.8	0.009	79.9 \pm 21.1	55.6 \pm 11.7	0.0002
C75	85.4 \pm 16.3	74.2 \pm 27.3	0.03	101.7 \pm 28.1	73.8 \pm 18.0	0.004
IQR	34.2 \pm 11.5	34.0 \pm 22.0	0.25	44.8 \pm 14.9	34.3 \pm 11.7	0.06

Values are given as mean \pm SD.

ADC, apparent diffusion coefficient; IQR, interquartile range.

individuals in seven groups had the 6–14-year age group categorized as one and did not interrogate the effects of puberty on the bone marrow (12). While many reports exist linking sex hormones to cortical bone mass at puberty in both preclinical (13,14) and clinical (15,16) studies, there is a paucity of data on how the onset of puberty results in measurable changes within the marrow itself. This has been limited by the previous means of studying bone marrow, which required invasive biopsy and did not interrogate the entire skeleton. The advent of quantitative MRI biomarkers has changed the landscape in this regard (17,18) and makes it possible to prospectively derive measurements from bone marrow both within a region or at a whole skeleton level (using whole-body MRI) in order to study changes with normal physiology and with treatment (19).

We report a significant correlation of ADC with age. A recent publication reporting data in the lumbar spine did not indicate such a change with age as children matured (9). Their mean and median ADC values remained between 0.58 and 0.63 $\times 10^{-3}$ mm²/s across all age groups. However, their data did not separate individuals by pubertal status and the distribution of children versus young adults in their cohort is likely to have represented individuals who were chiefly post-pubertal.

It is well established that cancellous bone decreases and bone marrow fat content increases with age. This physiological replacement of hematopoietic cells with adipocytes correlates directly with age (20), reaching a peak in young adults. Marrow adiposity has been inversely related to cortical bone area in young adults (21) and to bone mineral content (12). However, this step-change at puberty has not been recognized. Although there is extensive evidence linking fat replacement in the marrow of adults to steroid therapy, there are no data linking the increase in marrow fat to the surge of sex steroid hormones at puberty. A recent study in a preclinical mouse model has elegantly

demonstrated that leutinizing hormone is involved in hematopoietic stem-cell homeostasis (22); it may well be that the expression of this receptor particularly at sites within long bones and where hematopoietic function is no longer needed after puberty is one molecular mechanism driving the replacement of this functionally active tissue with fat.

The factors governing the relative amounts of hematopoietic and fatty components was elegantly hypothesized by Gurevitch et al. (23) where a dependence on the number of pluripotent mesenchymal stem cells (that differentiate to support both osteogenesis and hematopoiesis) was recognized. They hypothesized that as these cells are bound to endosteal and trabecular surfaces, they were numerous in growing tubular and cancellous bone, but once maturity was reached, they were far less numerous in tubular bones than in cancellous bone, because of the smaller internal bone surface area in the former. After maturity, therefore, mesenchymal stem cells in tubular bones favor support of a critical osteogenic function while in cancellous bone where they are more numerous, they retain a hematopoietic support function because of continued direct contact with hematopoietic cells. In the absence of hematopoietic cells, they change into fat-accumulating cells (24) so that fat fraction increases. T1 measurements have been used to estimate fat fraction (25). Although this was not possible in this retrospective study, it would be of interest to quantify regional bone marrow fat changes in the skeleton with the onset of puberty.

The relationship between bone marrow cellularity and ADC was established more than a decade ago, where a study that correlated cellularity in ilium aspirate was correlated with ADC values in 37 adults and children (26). The five young children in Nonomura et al.'s study did not have bone marrow aspirate performed, but their marrow was considered hypercellular in view of their age (0–3 years). Unfortunately, the b-values used in this study were low (0 and

350 s/mm²), so are likely to represent perfusional effects rather than true diffusion. This is reflected in the relatively high absolute values of 0.827 and 0.708×10^{-3} for normocellular marrow in the adults in their cohort. Unfortunately, also, the absolute cellularity of the aspirates was not quantified, so the relationship between the ADC and cellular "burden" has not been established.

Determining a ROI in the flat bones of a pediatric skull is challenging. Using the clivus ensured that a 4–6 mm diameter circular ROI could be obtained on two or three slices so that at least 21 voxels could be included in each scan. In future, automated segmentation methods may well enable more accurate delineation of the entire skull, which would enable larger scale analyses of this type. A previous extensive study in 500 individuals, 200 of whom were aged < 14 years (27), examined the differences in ADC values by skull location and correlated values with age. Interestingly, the occipital and parietal bones showed a variation with age, with a gradual downward trend between 0 and 30 years, whereas the frontal and temporal bones did not. This is in keeping with the findings in our study where the clivus as part of the occipital bone at the skull base shows this change. It indicates that, as with the tubular bones, the hemopoietic function of the skull base becomes less important with age, while that of the frontal and temporal regions is unaltered into adult life (27).

Signal-to-noise ratio is critically important in the reliability of the ADC measurement. ROIs within the clivus allowed inclusion of at least 21 voxels and had the advantage of avoiding sutures with a homogenous area from which to derive quantitative data. Other studies of bone marrow in children have focused on larger areas afforded by the vertebrae and iliac bones (9). Nevertheless, the values we obtained here are in keeping with those from these other studies.

Our study had several limitations. First, it was retrospective and relied on selecting healthy children with normal MRI brain scans. We attempted to mitigate against errors from inclusion of likely pathologies or treatment-related effects by having very strict inclusion and exclusion criteria. We interrogated a large pool of > 1000 children scanned over a two-year period to derive these patient numbers for investigation. In future, exploiting data from image biobanks may be possible. Second, only two b-values were used in the acquisition for derivation of ADC and one of them was b = 0. It is now established that elimination of perfusional effects to obtain a true D* necessitates that the lower b-value is > 50 mm²/s (28). A third b-value in the range of 50–1000 mm²/s ensures robustness of the ADC calculation. Although this was not available, our quantified values were similar to other

cited literature values (29). Third, we did not directly measure fat fraction, although this report assumes the relationship between ADC and fat fraction is inverse, thus explaining our findings (7). Fourth, our assessment of puberty, although objective and done on imaging grounds, was not confirmed by blood hormone profiles in these children. Although a prospective longitudinal study before and after puberty as verified by hormone profiles is the ideal, this is difficult to justify. It would, however, establish definitively whether there was a linear correlation of ADC with age or a step-change at puberty. Our data show a negative correlation of ADC with age and illustrates the range of normal values, but the sample size is too small to differentiate a linear decrease of ADC with age from a step-change at puberty. Finally, measuring ADC reproducibility would have been ideal, but as our cohort were children with minimal symptoms, a second/follow-up MRI scan was not justified. Measurement of ADC in adult populations has indicated that it is a robust measurement in normal bone marrow (30), and that the differences reported in this study are greater than the published limits of agreement.

In conclusion, this study shows a correlation of ADC with age in children. Moreover, it is the first study to document a significant change in marrow ADC related to puberty, using the ADC of marrow in the clivus as a quantitative biomarker. There were no discernible differences by gender. These data will form the basis for understanding changes that occur in the bone marrow following local and systemic treatments of hematological and non-hematological malignancies.

Acknowledgements

We gratefully acknowledge assistance from Jonathan Rhodes (Superintendent Neuroradiographer, Department of Neuroradiology, St George's Hospital, London, UK); Simon Doran (Senior Staff Scientist, Cancer Imaging Centre, The Institute of Cancer Research, Sutton, UK); James D'Arcy (Computer Officer, Division of Radiotherapy and Imaging, Magnetic Resonance Unit, Sutton, UK) and Matthew Orton (Staff Scientist, Division of Radiotherapy and Imaging, Magnetic Resonance Unit, Sutton, UK).

Declaration of conflicting interests


The author(s) declared no potential conflicts of interest with respect to the research, authorship, and/or publication of this article.

Funding

The author(s) received the following financial support for the research, authorship, and/or publication of this article: CRUK and EPSRC support to the Cancer Imaging Centre at ICR and RMH in association with MRC and Department

of Health C1060/A10334, C1060/A16464 and NHS funding to the NIHR Biomedical Research Centre and the Clinical Research Facility in Imaging.

ORCID iD

Nandita M deSouza  <https://orcid.org/0000-0003-4232-476X>

References

1. Proytcheva M. Bone marrow evaluation for pediatric patients. *Int J Lab Hematol* 2013;35:283–289.
2. Chen LT, Weiss L. The development of vertebral bone marrow of human fetuses. *Blood* 1975;46:389–408.
3. Blebea JS, Houseni M, Torigian DA, et al. Structural and functional imaging of normal bone marrow and evaluation of its age-related changes. *Semin Nucl Med* 2007;37:185–194.
4. Malkiewicz A, Dziedzic M. Bone marrow reconversion - imaging of physiological changes in bone marrow. *Pol J Radiol* 2012;77:45–50.
5. Cristy M. Active bone marrow distribution as a function of age in humans. *Phys Med Biol* 1981;26:389–400.
6. Hillengass J, Bauerle T, Bartl R, et al. Diffusion-weighted imaging for non-invasive and quantitative monitoring of bone marrow infiltration in patients with monoclonal plasma cell disease: a comparative study with histology. *Br J Haematol* 2011;153:721–728.
7. Schraml C, Schmid M, Gatidis S, et al. Multiparametric analysis of bone marrow in cancer patients using simultaneous PET/MR imaging: Correlation of fat fraction, diffusivity, metabolic activity, and anthropometric data. *J Magn Reson Imaging* 2015;42:1048–1056.
8. Messiou C, Giles S, Collins DJ, et al. Assessing response of myeloma bone disease with diffusion-weighted MRI. *Br J Radiol* 2012;85:e1198–203.
9. Herrmann J, Krstin N, Schoennagel BP, et al. Age-related distribution of vertebral bone-marrow diffusivity. *Eur J Radiol* 2012;81:4046–4049.
10. Wong AP, Pipitone J, Park MTM, et al. Estimating volumes of the pituitary gland from T1-weighted magnetic-resonance images: effects of age, puberty, testosterone, and estradiol. *Neuroimage* 2014;94:216–221.
11. Alhazmi A, Vargas E, Palomo JM, et al. Timing and rate of sphenoid-occipital synchondrosis closure and its relationship to puberty. *PLoS One* 2017;12:e0183305.
12. A LN, L JH, Davis M, et al. The relationships among total body fat, bone mineral content and bone marrow adipose tissue in early-pubertal girls. *Bonekey Rep* 2013;2:315.
13. Izquierdo Ade M, Mishima FD, Carrard VC, et al. Effects of induced precocious puberty on cranial growth in female Wistar rats. *Eur J Orthod* 2012;34:133–140.
14. Yingling VR, Khaneja A. Short-term delay of puberty causes a transient reduction in bone strength in growing female rats. *Bone* 2006;38:67–73.
15. Mahachoklertwattana P, Pootrakul P, Chuansumrit A, et al. Association between bone mineral density and erythropoiesis in Thai children and adolescents with thalassemia syndromes. *J Bone Miner Metab* 2006;24:146–152.
16. Wang Q, Nicholson PH, Suuriniemi M, et al. Relationship of sex hormones to bone geometric properties and mineral density in early pubertal girls. *J Clin Endocrinol Metab* 2004;89:1698–1703.
17. Neubauer H, Evangelista L, Morbach H, et al. Diffusion-weighted MRI of bone marrow oedema, soft tissue oedema and synovitis in paediatric patients: feasibility and initial experience. *Pediatr Rheumatol Online J* 2012;10:20.
18. Darge K, Jaramillo D, Siegel MJ. Whole-body MRI in children: current status and future applications. *Eur J Radiol* 2008;68:289–298.
19. Weber DR, Leonard MB, Zemel BS. Body composition analysis in the pediatric population. *Pediatr Endocrinol Rev* 2012;10:130–139.
20. Zawin JK, Jaramillo D. Conversion of bone marrow in the humerus, sternum, and clavicle: changes with age on MR images. *Radiology* 1993;188:159–164.
21. Di Iorgi N, Mo AO, Grimm K, et al. Bone acquisition in healthy young females is reciprocally related to marrow adiposity. *J Clin Endocrinol Metab* 2010;95:2977–2982.
22. Peng YJ, Yu H, Hao X, et al. Luteinizing hormone signaling restricts hematopoietic stem cell expansion during puberty. *EMBO J* 2018;37:e98984.
23. Gurevitch O, Slavin S, Feldman AG. Conversion of red bone marrow into yellow - Cause and mechanisms. *Med Hypotheses* 2007;69:531–536.
24. Hayashi K, Kagawa K, Awai M, et al. The role of marrow architecture and stromal cells in the recovery process of aplastic marrow of lethally irradiated rats parabiosed with healthy litter mates. *Scan Electron Microsc* 1986;(Pt. 4):1489–1499.
25. Le Ster C, Lasbleiz J, Kannengiesser S, et al. A fast method for the quantification of fat fraction and relaxation times: Comparison of five sites of bone marrow. *Magn Reson Imaging* 2017;39:157–161.
26. Nonomura Y, Yasumoto M, Yoshimura R, et al. Relationship between bone marrow cellularity and apparent diffusion coefficient. *J Magn Reson Imaging* 2001;13:757–760.
27. Li Q, Pan SN, Yin YM, et al. Normal cranial bone marrow MR imaging pattern with age-related ADC value distribution. *Eur J Radiol* 2011;80:471–477.
28. Ohno N, Miyati T, Kasai H, et al. Evaluation of perfusion-related and true diffusion in vertebral bone marrow: a preliminary study. *Radiol Phys Technol* 2015;8:135–140.
29. Dietrich O, Geith T, Reiser MF, et al. Diffusion imaging of the vertebral bone marrow. *NMR Biomed* 2017. doi: 10.1002/nbm.3333.
30. Messiou C, Collins DJ, Morgan VA, et al. Optimising diffusion weighted MRI for imaging metastatic and myeloma bone disease and assessing reproducibility. *Eur Radiol* 2011;21:1713–1718.

Contents Page

Research Staff Details

Study Summary

Protocol Synopsis

0. Flow Chart

1. Hypothesis

2. Aims

3. Background

4. Preliminary Work

5. Study Design

Endpoints

Primary

Secondary

Inclusion/Exclusion Criteria

Inclusion Criteria

Exclusion Criteria

8. Methodology

9. Data Acquisition

Data Analysis

Segmenting Regions of Interest

Analysis Methods and Statistical Considerations

Sample Size

Data Collection

11. Study organisation / Trial Monitoring and Management Strategy

- Governance ICR

12. Safety Reporting

Regulatory & Ethics Committee Approval

Ethical Considerations

Informed Consent

Patient Confidentiality

14. Data Handling and Record Keeping

15. Financing, Indemnity, and Insurance

16. Publication Policy

17. Abbreviations

18. References

Research Staff Details:

Chief Investigator:

Professor Nandita deSouza,
Radiologist,
CRUK Cancer Imaging Centre,
The Institute of Cancer Research (ICR)
and The Royal Marsden NHS Foundation Trust (RMH) Downs Road, Sutton, Surrey
SM2 5PT
Tel: 020 8661 3289
Fax: 020 8661 0846
Email: Nandita.desouza@icr.ac.uk

Co- Investigators:

Dr Erika Pace, Radiologist,
CRUK Cancer Imaging Centre,
The Institute of Cancer Research
and The Royal Marsden NHS Foundation Trust Downs Road, Sutton, Surrey
SM2 5PT
Tel: 020 8661 6101
Fax: 020 8661 0846
Email: Erika.Pace@icr.ac.uk

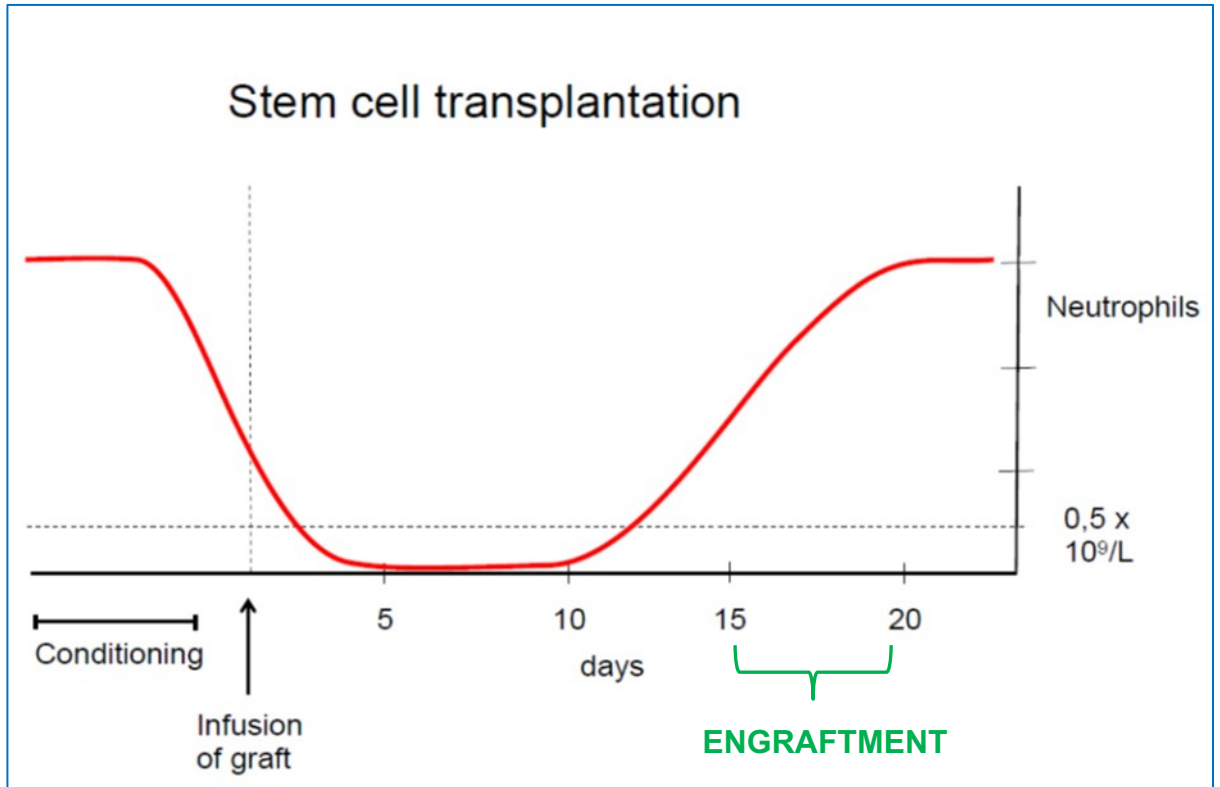
Dr Sucheta Vaidya Paediatric Oncologist,
The Royal Marsden NHS Foundation Trust Downs Road, Sutton, Surrey
SM2 5PT
Tel: 020 8661 3617
Email: Sucheta.Vaidya@rmh.nhs.uk

Statistician:

Ms Karen Thomas Senior Statistician,
The Royal Marsden NHS Foundation Trust Downs Road, Sutton, Surrey
SM2 5PT
Tel: 020 8661 3641
Email: Karen.Thomas@rmh.nhs.uk

1.0 STUDY SUMMARY

Title	Quantitative magnetic resonance imaging of bone marrow in a paediatric population with leukaemia	
Aims	<p>To establish whether ADC of bone marrow after transplantation at the point of engraftment* (as defined by peripheral blood white cell count) increases above previously established limits of agreements (repeatability).</p> <p>To define the range of ADC change in patients with successful engraftment of paediatric bone marrow.</p>	
Trial Design	Pilot single centre study assessing biomarker change post bone marrow transplant	
Main Eligibility Criteria	<p>All patients with proven acute lymphoblastic or myeloblastic leukaemia planned for bone marrow transplantation</p> <p>Cooperative paediatric individuals and young adults (5-24-years-old) not requiring general anaesthesia or sedation for the purpose of MRI</p> <p>Able to lie flat throughout the scan</p>	
Treatment	Bone marrow transplant as per standard patient care, no change for trial purposes	
Endpoints	Primary	Percentage of children who achieve a change in ADC of their bone marrow with engraftment that is greater than previously established limits of agreement (repeatability) of the measurement under the currently underway service evaluation project SE662.
	Secondary	<p>Heterogeneity of ADC distribution within lumbar spine & pelvis before and after engraftment</p> <p>Correlation between ADC change and white blood cell count</p> <p>Comparison of baseline ADC between patients with treated ALL and treated AML</p>



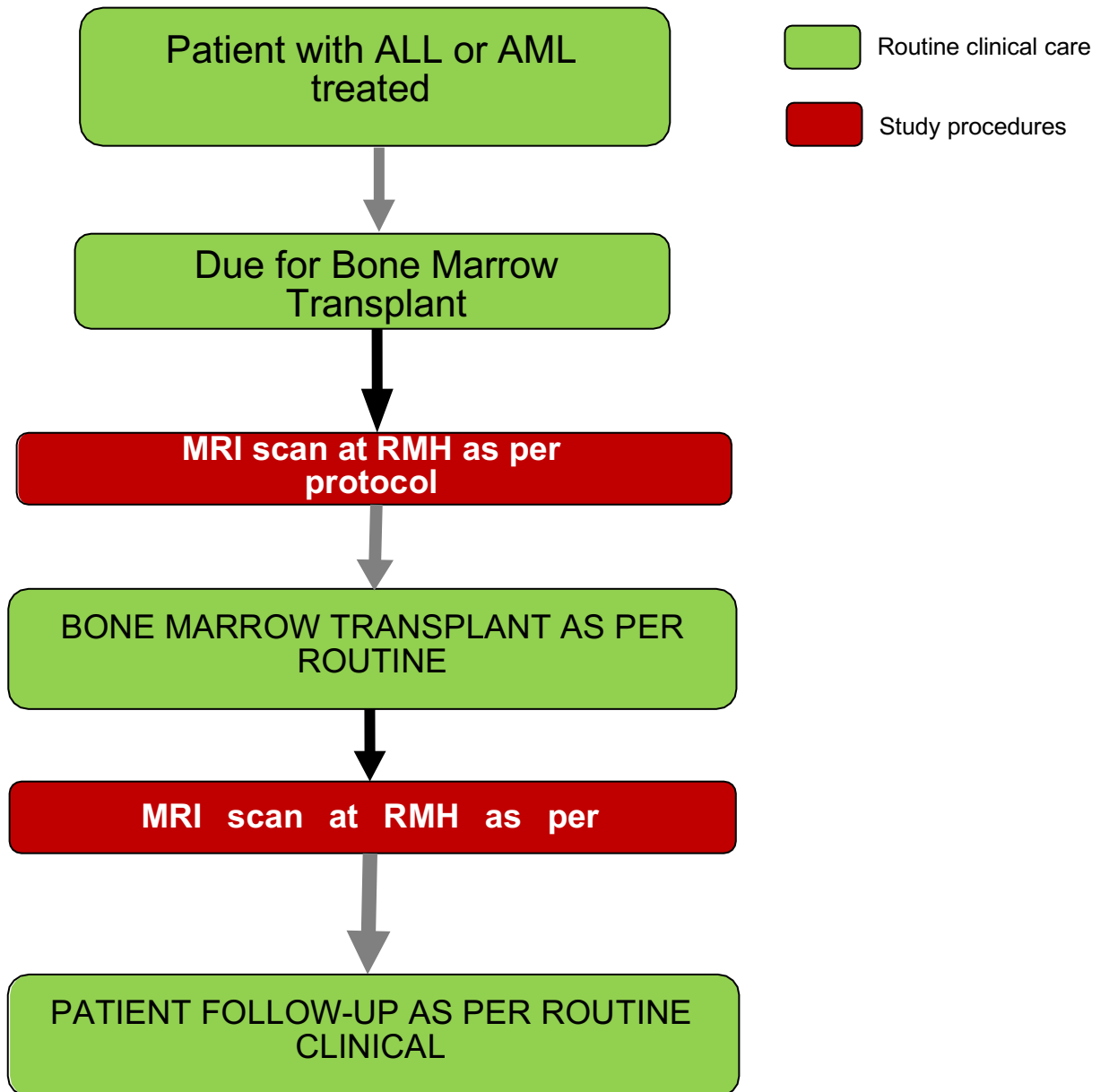
From the European Group for Blood and Marrow Transplantation, 2011

***NEUTROPHIL ENGRAFTMENT** defined as the first of 2 or 3 consecutive days when the absolute neutrophilic count was equal to or greater than $0.5 \times 10^9/l$. This usually occurs 2 weeks after bone marrow transplantation.

PLATELET ENGRAFTMENT defined as the first day of an unsupported platelet count equal to or greater than $20 \times 10^9/l$, a minimum of 7 days after the last platelet transfusion.

PROTOCOL SYNOPSIS

Flow Chart



1. Hypothesis

Following allogenic haemopoietic stem cell transplantation, changes in bone marrow ADC are measurable at the point of engraftment and in conjunction with peripheral blood counts may provide a future biomarker of successful clinical outcome.

2. Aims

- To establish whether ADC of bone marrow after transplantation at the point of engraftment (as defined by peripheral blood white cell count) increases above previously established limits of agreements (repeatability).
- To define the range of ADC change in paediatric patients with successful engraftment of haemopoietic stem cells following transplantation.

3. Background

The apparent diffusion coefficient (ADC) derived from diffusion-weighted magnetic resonance imaging (DW-MRI) has emerged as a potential novel biomarker in oncological imaging. By quantifying the diffusivity of water molecules within a tumour, this technique improves lesion detection and the assessment of treatment response.^{1, 2} Changes in the ADC values are inversely correlated with tumour cellularity.³ Because it avoids radiation exposure and intravenous contrast agents,⁴ DW-MRI is appealing in the field of paediatric imaging, but more work is needed to determine its utility in paediatric bone marrow disease.⁵

Whole body DW-MRI (WB DW-MRI) has now been implemented for routinely evaluating skeletal disease in oncology in adults. The high sensitivity, speed and quantitative capability have addressed an unmet need in imaging primary and secondary malignancies. Combined with anatomical imaging, WB DW-MRI now forms a tool that has been tailored to detect both focal and diffuse disease, to quantify burden and response as well as assessing mechanical complications.⁶ This blend of anatomical and functional imaging has recently been recommended by the International Myeloma Working Group for work-up of solitary bone plasmacytoma or smouldering multiple myeloma.⁷ In adults, WB DWI can provide information on differences between normal and diseased bone marrow architecture for the entire skeleton in a 25 minute time frame.⁸ This has led to

feasibility studies for staging and follow-up of malignancies in children but not in the context of bone marrow disease.^{9, 10}

Although leukaemia accounts for 31% of all childhood cancer,^{11, 12} it is not currently routinely investigated with WB DW-MRI. The relative proportions of tumour, red marrow and yellow marrow alter with age and with treatment, and make interpretation of images challenging.⁶ Also, in adults, the signal characteristics of normal bone marrow have been shown to differ according to the gender; hyperintensity is more frequently detected in women than in men and ADC is significantly higher.¹³ According to ALLR3 treatment guidelines,¹⁴ children diagnosed with high risk relapsed acute lymphoblastic leukaemia (ALL) are planned for allogeneic haemopoietic stem cell transplantation (HSCT) after high-dose chemotherapy and total bone irradiation. In children with high risk or relapsed acute myeloid leukaemia (AML) high-dose chemotherapy alone is administered prior to HSCT.¹⁵ Haemopoietic engraftment usually occurs a median of 2 to 3 weeks following HSCT if the donor is a sibling or after 3 weeks when the donor is unrelated; engraftment is marked by an increase in white blood cell count. In future, change in ADC at time of engraftment not only may aid assessment of successful engraftment but indicate the extent of ongoing support and immunosuppression required, and predict longer term outcome.

4. Preliminary work

Initial work aiming to develop an adequate DWI scanning protocol with regard to parameters best suited to robust ADC delineation in an acceptable time frame (<10 min of additional scan time) have been optimized in a small cohort of children undergoing clinical MR scans at 1.5 T scanners since January 2017. Ethical permission for this is currently operational (CCR1406).

Reproducibility in bone marrow MRI has already been proved in adults by Christina Messiou et al. in both healthy volunteers and patients with myeloma. They showed that ADC measurements (applying $b=50$ and 900 s/mm^2) were repeatable in segmented marrow volumes; a paired t test between the two observations indicates no significant difference between subject measurements for both cohorts. Furthermore,

the measurement was also consistent with intraclass correlation coefficient of 0.981 and 0.991 for intraobserver and interobserver comparisons, respectively.¹⁶ Prior to this study, the variation in quantitative DW-MRI within a paediatric population according to gender, age, puberty, and anatomic location within the skeleton in patients undergoing clinical MRI scans will be done to inform measurement repeatability. Namely, about 1,150 MR scans of the brain performed at St. George's Hospital in a non-oncological paediatric population were reviewed for as part of a service evaluation project (SE662) approved from The Royal Marsden. Limits of agreement will be obtained assessing MR studies performed at in children without known leukaemia, lymphoma or bony (primary/secondary) neoplasm/other disease, without any previous surgery and radiotherapy involving the clivus and both mandibular condyles. Less than 70 provisional potential suitable exams where the bone marrow of the skull appeared normal have already been selected by Dr Erika Pace. Dr Andrew MacKinnon, a consultant neuroradiologist working at both sites, has started reviewing them and so far confirmed the eligibility for 18 patients. Therefore, considering the whole procedure (determine the final cohort, anonymization of the scans, downloading from St. George's Hospital PACS, uploading onto XNAT system at The Royal Marsden/Institute of Cancer Research, download on ICR computer, drawing region of interest using Adept, generating spreadsheet with data), we should be able to have this data by the end of November 2017.

5. Study Design

This is a pilot imaging study investigating change in ADC at a single time point post-transplantation in patients.

6. Endpoints

Primary

- Percentage of children who achieve a change in ADC of their bone marrow with engraftment that is greater than previously established limits of agreement (reproducibility) of the measurement.

Secondary

- Heterogeneity of ADC distribution within lumbar spine & pelvis before and after engraftment
- Correlation between ADC change and white blood cell count
- Comparison of baseline ADC between patients with treated ALL and treated AML

7. Inclusion/ Exclusion Criteria

Inclusion Criteria

1. All patients with relapsed or high risk acute lymphoblastic or myeloblastic leukaemia planned for haemopoietic stem cell transplantation
2. Cooperative paediatric individuals and young adults (5-24-years-old) not requiring general anaesthesia or sedation for the purpose of MRI
3. Able to lie flat throughout the scan

Exclusion Criteria

1. Non cooperative patients
2. Ferromagnetic implants, contraindicating MRI
3. Claustrophobia
4. Unable to lie flat throughout the scan
5. Uncertain histological diagnosis
6. Musculoskeletal disorders
7. Metabolic disorders
8. Lack of signed parental consent and patient's verbal approval

All participants, if older than 18 years, or their parent, when the patient is younger, will complete an MRI safety questionnaire with the radiographers prior to being scanned.

Subject Withdrawal Criteria

- Poor quality of MR images.
- Interrupted scans.
- Lack of post-transplantation MR scan.

8. Methodology

A pilot paediatric cohort of 12 patients with ALL or AML, aged 5-25 years old, will be studied before and after haemopoietic stem cell transplantation.

Patients with either of the two types of acute leukaemia will be included. This means that some will have transplantation after induction chemotherapy alone, whilst others will also have total bone irradiation. ALL can benefit more frequently from transplantation after induction chemotherapy with or without total bone irradiation before transplantation. Participating in this study will not affect that treatment decision.

After written informed consent from patients or their parents/legal guardian (when younger than 18 years), participants will be invited to have two MR scans.

Dr Erika Pace will liaise with the clinical team regarding patients' wellness to attend the scans and to schedule them.

A baseline magnetic resonance scan with diffusion-weighted images and without contrast administration will be performed at the end of the neoadjuvant treatment (chemotherapy with/without radiation depending on the type of leukaemia).

A second scan will be performed at 2 weeks after bone marrow transplantation when an engraftment is expected. Studies will be reported and electronically recorded on the Radiology Information System where they will be accessible to clinicians via the electronic patients' record.

Standard serum parameters of disease and engraftment such as white blood cell count and platelets, will be assessed by the paediatric team at the above mentioned time points to determine the outcome of the transplantation.

The Haematology-Oncology Unit at The RM undertakes roughly 20 allogeneic stem cell transplants for acute leukaemias each year. Dr Erika Pace is the co-dedicated radiologist for the RMH Paediatric Leukaemia and Solid Tumour MDT allowing efficient identification of patients and transmission of results. As RMH is the network referral center for autografting, all newly diagnosed and relapsed leukaemic patients are discussed at the weekly multidisciplinary team meeting. Recruitment will commence once ethical approval has been obtained.

9. Data Acquisition

MRI acquisition (two identical scans, one at baseline and the other after the transplantation at the moment of the likely engraftment) will include T1-weighted, T2-weighted and DW axial sequences through L3-S1 and through the bony pelvis.

National Radiological Protection Board guidelines will be adopted. No contrast agent administration is required, so participants do not have to alter their lifestyle. They must be able to tolerate lying flat throughout the duration of the scan. No sedation or general anaesthesia will be provided as only cooperative children will be recruited. However, four play-specialists work in the Paediatric Unit at The RM; therefore, they may be involved with the preparation before the scans when a participant is quite young (for instance, 5-6 years old).

10. Data Analysis

The primary endpoint of the study is to assess the change in ADC following bone marrow transplantation at the point of engraftment in paediatric patients with leukaemia. We will establish the percentage of children who achieve a change in ADC of their bone marrow with engraftment that is greater than the limits of agreement of repeatability of the measurement, established from previous historical data.

Segmenting Regions of Interest

Regions of interest encompassing L3-S1 vertebral bodies and the whole iliac bones will be segmented on axial images of the baseline scan and on the post-transplant scan done 2 weeks after the transplantation when the engraftment is expected to occur. This will be based on peripheral blood white cell count.

Statistical analysis: Karen Thomas, Erika Pace.

Analysis Methods and Statistical Considerations

Mean ADC of spinal and pelvic marrow pre and post-transplant will be recorded in 12 patients. Changes will be described graphically using scatterplots of pre and post treatment values and histograms and waterfall plots of absolute and percentage

change. Baseline ADC and post-treatment change will be summarised using descriptive statistics (mean, standard deviations, median and quartiles).

This pilot study implies all descriptive endpoints.

The primary endpoint of the study is to assess the degree of success of the bone marrow transplantation in paediatric patients with leukaemia from an imaging point of view. The percentage with a 95% confidence interval of children who achieve a change in the mean of ADC of their whole imaged (lumbosacral and pelvic regions) bone marrow with engraftment which is greater than limits of agreement of repeatability of the measurements.

For the **secondary endpoints**:

- Heterogeneity of ADC distribution within lumbar spine & pelvis before and after engraftment: this will be evaluated for each patient in each scan (mean ADC for each ROI) and summarised with histograms and descriptive statistics.
- Correlation between ADC change and white blood cell count at the point of engraftment, when an increase of white cell blood count is expected, will be calculated using Pearson or Spearman's correlation coefficient, as appropriate.
- Comparison of baseline ADC between patients with treated ALL and treated AML: descriptive statistics (standard deviation, mean, and histograms) will be used to summarise distribution of mean ADC in subgroups of patients defined by diagnosis.

Sample size

This is a pilot study and so the sample size (12 patients) has been chosen for largely pragmatic reasons, considering that on average 20 paediatric bone marrow transplantation procedures are yearly carried at The Royal Marsden. A 95% confidence interval for the primary endpoint can thus be calculated with maximum width 58%.

Prof. deSouza will have overall responsibility for the study and will conduct in accordance within the Research Governance Framework. She will be responsible for data storage.

Data will be transferred internally to Research Development Support Unit/the statistician for statistical analysis overseen by Karen Thomas.

Digital confidential data will be saved on spreadsheets whose access requires a password known only to a restricted number of people (investigator and some co-investigators). Patients' anonymised MR images will be upload on XNAT, a software platform accessible only to people (as above) owning a personal account. Whilst, printed documents (such as case report forms, patient/parents/legal guardian sheet, assent/consent form) will be stored in a boxfile kept within a locked file cabinet in Dr Erika Pace's office (The Royal Marsden, Sutton, East Wing, Ground Floor, Room 142) throughout the duration of the study and moved to the trial co-ordinator's office once the study has been closed.

Data Collection:

Male and female inpatients below the age of 25 years old.

At each imaging time point we will record:

DWI: pattern of disease; total number of lesions; whole marrow ADC metrics.

Disease on DWI is defined as areas of restricted diffusion evident at high b value and confirmed on the ADC map.

Standard markers: white blood cell count, platelets.

11. Study Organisation/ Trial Monitoring and Management Strategy

Completion of Case Report Forms at the time of registration (baseline) and after the second MR scan will be filled by Dr. Erika Pace, radiographers and trial co-ordinator.

Governance ICR:

The Institute of Cancer Research is the sponsor of this study and has responsibility for ensuring appropriate ethics committee opinion and authorisations are obtained.

The Chief Investigator, Prof Nandita deSouza, will have overall responsibility for the study and will conduct it in accordance with the Research Governance Framework for Health and Social Care and the principals of Good Clinical Practice.

Monitoring of study progress will be performed Dr Erika Pace (co-investigator).

Consent will be performed by Dr Erika Pace, the paediatric team (Dr Sucheta Vaidya and their colleagues interested in leukaemia and bone marrow transplantation), radiographers, and Prof Nandita deSouza, as per delegation log.

All participants or their parents will complete an MRI safety questionnaire with the radiographers prior to being scanned.

The imaging protocols will be maintained by radiographers and physicists.

The MRI scans will be reviewed by radiology staff and made available to the clinical units in the standard way.

Statistician, Karen Thomas, will be involved in this study (especially in the database design) and will work with the investigators to ensure the quality and completeness of the data.

Data Analysis will be performed by: Karen Thomas, and Dr Erika Pace.

Trial co-ordinator (Tiffany Rushen) will be responsible for study administration including progress reporting, amendments and notification of study closure in accordance with ethical and research and developmental approval procedures.

Patient Screening. In the absence of contraindications to MRI the patients will be invited to participate by referring haematologists interested in paediatric bone marrow transplantation, paediatric oncologists (Dr Sucheta Vaidya) or by the following imaging staff following discussion with the referring colleague: Dr Erika Pace, MRI research radiographers, Prof. deSouza. Patients will be given a patient information sheet.

Participation or refusal to participate will not affect the patient's management.

Patient Withdrawal: patients may withdraw at any point.

Study Completion: last patient, last visit.

Patients will be followed up clinically.

End of Trial Definition: subject participation will run from the time of recruitment to second scan post bone marrow transplantation.

12. Safety Reporting

No adverse events are expected in this imaging study. All participants, or their parents on their behalf, will complete an MRI safety questionnaire with the radiographers prior to being scanned.

An adverse event as a result of MRI scanning would be excessive radiofrequency exposure leading to tissue heating. This parameter is closely monitored prior to and during the MRI scan. Patient complaints of itching or burning will be recorded.

13. Regulatory and Ethics Committee Approval

Ethical Considerations

The study will be carried out in accordance with the Declaration of Helsinki (1996), and local R&D and Ethics Committee approval will be sought. It is the responsibility of the Chief Investigator to obtain a favorable ethical opinion prior to recruiting patients and to conduct the study in accordance with the conditions of ethical approval.

Informed Consent

Written informed consent will be obtained from each patient by the Chief Investigator or designated representative.

It is the responsibility of the Chief Investigator to give each patient, prior to inclusion in the trial, full and adequate verbal and written information regarding the objective and procedures of the trial and the possible risks involved. Sufficient time will be allowed for the patient to decide on trial entry and they will be informed about their right to withdraw from the trial at any time.

The written patient information sheet, which will be given to each patient before enrolment, is an approved patient information sheet according to national guidelines.

Patient Confidentiality

Patient confidentiality will be maintained in accordance with the Data Protection Act 1998 and local confidentiality code of practice and data protection policy and procedure.

14. Data Handling and Record Keeping

Data will be handled within the data protection act and in accordance with good clinical practice. The investigators will permit trial related audits, providing direct access to the source data and documents.

Quality control and assurance of the MRI protocols and acquisition will be maintained by physicists and the radiographers.

Anonymised data will be kept in Excel format in a secure server maintained by Dr Erika Pace.

Record keeping will be managed by Dr Erika Pace and radiographers.

Dr Erika Pace will be responsible for study administration, including progress reporting, amendments and notification of study closure in accordance with ethical and research and developmental approval procedures.

As the South West – Central Bristol Research Ethics Committee suggested, the general practitioner of the participant will not be informed about the study as no change will be made to the patient's treatment.

Prof. Nandita deSouza will have overall responsibility for the study and will conduct it in accordance with the Research Governance Framework for Health and Social Care and the principals of Good Clinical Practice. She will be responsible for data storage.

15. Financing, Indemnity, and Insurance

The scans are funded by a CRUK imaging centre grant held by Profs deSouza and Leach (2013-2018).

The study is investigator designed and led and meets the criteria for R&D support as outlined in the Statement of Partnership on Non-Commercial Research and Developmental in the NHS in England.

NCRN (or regional equivalent) network resources should be made available for this study and NIHR portfolio adoption will be applied for.

Indemnity is provided by the usual NHS indemnity arrangements.

The Institute of Cancer Research is sponsoring this study.

16. Publication Policy

Presentations, audits, and publications require authorisation by the principal investigator, who is responsible for the intellectual property.

The International Committee of Medical Journal Editors (ICMJE) requires clinical trials to be entered onto a recognised registry before recruitment of the first patient, in order for the trial to be published in an ICMJE journal. This study will be registered on www.clinicaltrials.gov.

17. Abbreviations

ALL	acute lymphoblastic leukaemia
AML	acute myeloid leukaemia
ADC	apparent Diffusion Coefficient
BMT	bone marrow transplantation
DW-MRI	diffusion weighted imaging magnetic resonance
HSCT	haemopoietic stem cell transplantation
WB-DWI	whole body diffusion-weighted imaging

References

1. Padhani AR, Liu G, Koh DM, et al. Diffusion-weighted magnetic resonance imaging as a cancer biomarker: consensus and recommendations. *Neoplasia (New York, NY)*. 2009; 11: 102-125.
2. Afaq A, Andreou A and Koh DM. Diffusion-weighted magnetic resonance imaging for tumour response assessment: why, when and how? *Cancer imaging : the official publication of the International Cancer Imaging Society*. 2010; 10 Spec no A: S179-188.
3. Koh DM and Collins DJ. Diffusion-weighted MRI in the body: applications and challenges in oncology. *AJR American journal of roentgenology*. 2007; 188: 1622-1635.
4. Kyriazi S, Morgan V, Collins D and deSouza N. (2009) Echo planar diffusion-weighted MRI of the abdomen and pelvis: comparison of free-breathing monopolar and bipolar

- spin-echo sequences in assessing image quality and apparent diffusion coefficients. *Proc Intl Soc Mag Reson Med* 17.
5. Voss SD. Pediatric oncology and the future of oncological imaging. *Pediatric radiology*. 2011; 41 Suppl 1: S172-185.
 6. Messiou C and Kaiser M. Whole body diffusion weighted MRI--a new view of myeloma. *British journal of haematology*. 2015; 171: 29-37.
 7. Dimopoulos MA, Hillengass J, Usmani S, et al. Role of magnetic resonance imaging in the management of patients with multiple myeloma: a consensus statement. *Journal of clinical oncology : official journal of the American Society of Clinical Oncology*. 2015; 33: 657-664.
 8. Giles SL, deSouza NM, Collins DJ, et al. Assessing myeloma bone disease with whole-body diffusion-weighted imaging: comparison with x-ray skeletal survey by region and relationship with laboratory estimates of disease burden. *Clinical radiology*. 2015; 70: 614-621.
 9. Siegel MJ, Acharyya S, Hoffer FA, et al. Whole-body MR imaging for staging of malignant tumors in pediatric patients: results of the American College of Radiology Imaging Network 6660 Trial. *Radiology*. 2013; 266: 599-609.
 10. Nievelstein RA and Littoij AS. Whole-body MRI in paediatric oncology. *La Radiologia medica*. 2016; 121: 442-453.
 11. Main types of childhood cancer: children aged 0-14 years. United Kingdom 2001 to 2010. . *Based on data provided by National Registry of childhood Tumours*
 12. Children's cancers incidence by type
 13. Cui FZ, Cui JL, Wang SL, et al. Signal characteristics of normal adult bone marrow in whole-body diffusion-weighted imaging. *Acta radiologica (Stockholm, Sweden: 1987)*. 2016; 57: 1230-1237.
 14. ALLR3: An International Collaborative Trial for Relapsed and Refractory Acute Lymphoblastic Leukaemia (phase III, ongoing).
 15. MyeChild01 protocol: International Randomised Phase III Clinical Trial in Children with Acute Myeloid Leukaemia - Incorporating an Embedded Dose Finding Study for Gemtuzumab Ozogamicin in Combination with Induction Chemotherapy, 2015.
 16. Giles SL, Messiou C, Collins DJ, et al. Whole-body diffusion-weighted MR imaging for assessment of treatment response in myeloma. *Radiology*. 2014; 271: 785-794.